Title

The Role of Glutamine in Primed Human Pluripotent Stem Cell Fate

Permalink

https://escholarship.org/uc/item/7cw5t8t6

Author

Lu, Vivian

Publication Date

2022

Peer reviewed|Thesis/dissertation

UNIVERSITY OF CALIFORNIA

Los Angeles

The Role of Glutamine in Primed Human Pluripotent Stem Cell Fate

A dissertation submitted in partial satisfaction of the

requirements for the degree of Doctor of Philosophy in

Molecular and Medical Pharmacology

by

Vivian Lu

2022

ABSTRACT OF THE DISSERTATION

The Role of Glutamine in Primed Human Pluripotent Stem Cell Fate

by

Vivian Lu

Doctor of Philosophy in Molecular and Medical Pharmacology

University of California, Los Angeles, 2022

Professor Donald B. Kohn, Co-Chair

Professor Michael A. Teitell, Co-Chair

Human pluripotent stem cells can self-renew indefinitely or be induced to differentiate into the three embryonic germ lineages: endoderm, mesoderm, and ectoderm. Multiple studies show that reconfiguring metabolic pathway activities influences the fate of pluripotent stem cells through metabolite-regulated changes in intracellular signal transduction pathways and the epigenome. Through these and potentially additional mechanisms, the conversion of available nutrients into metabolite fluxes and steady-state levels can tip the balance between pluripotent stem cell self-renewal and differentiation, although which nutrients and metabolites favor specific cell fate decisions are largely unidentified.

Glutamine participates in a wide variety of cellular processes beyond biomass and energy-producing reactions in pluripotent and adult-type stem cells. We showed that endoderm, mesoderm, and ectoderm all consume abundant glutamine supplied in cell culture media. Additionally, exogenous glutamine withdrawal biased spontaneous human pluripotent stem cell

differentiation toward ectoderm and away from mesoderm. However, a mechanism for this nutrient-directed cell fate bias was, until recently, unknown.

We uncovered that while all three germ lineages are capable of *de novo* glutamine synthesis, only ectoderm generates sufficient glutamine to sustain cell viability and differentiation, clarifying lineage fate restrictions observed with glutamine withdrawal. While exogenous glutamine is dispensable for ectoderm, complete glutamine starvation obliterates this lineage, suggesting a critical role for glutamine in ectoderm specification. We uncovered that glutamine fulfillment of mTORC1 activation, but not biosynthetic demands and protein translation, is critical for initiating ectoderm fate commitment. Glutamine acts as a signaling molecule to activate mTORC1 signaling in ectoderm that supersedes lineage-specifying cytokine induction. In contrast, glutamine in mesoderm and endoderm serves as the preferred precursor of α-ketoglutarate without a direct role in cell fate signaling. Our findings show that a nutrient acts as a signaling molecule to control cell fate, raising a question about whether the nutrient environment functions directly in cell differentiation during development.

For these reasons, we hypothesize that intracellular glutamine may help coordinate differentiation of the three embryonic germ layers. Differing patterns of nutrient availability occur during early embryonic germ lineage differentiation. Interestingly, transcriptome analysis of a gastrulation-stage human embryo shows unique glutamine enzyme-encoding gene expression patterns may also distinguish germ lineages *in vivo*.

In summary, these findings reveal critical roles for metabolic regulation and nutrient signaling during early embryonic development.

The dissertation of Vivian Lu is approved.

Kathrin Plath

Heather R. Christofk

Donald B. Kohn, Committee Co-Chair

Michael A. Teitell, Committee Co-Chair

University of California, Los Angeles

2022

DEDICATION

This dissertation is dedicated to my parents, Lindy Phung and Tung Lu, for their unconditional love and support, thank you for everything. To my paternal grandmother, Ai Muoi Lam "ma-ma", who is no longer of this world but continues to inspire me to achieve great things. To my maternal grandmother, Moi Nhi Lay "po-po", for helping to raise me. To my mentor, Mike Teitell, for believing in me before I believed in myself. And to my partner Nick Barbieri, for being my best friend and biggest cheerleader.

TABLE OF CONTENTS

LIST OF FIGURES AND TABLES

LIST OF ABBREVIATIONS

PSC	Pluripotent stem cell
hPSC	Human pluripotent stem cell
iPSC	Induced pluripotent stem cell
mESC	Mouse embryonic stem cell
Gln	Glutamine
Glu	Glutamate
Glc	Glucose
GLS (1/2)	Glutaminase 1 / 2
GS	Glutamine synthetase
mTORC1	Mammalian or mechanistic target of rapamycin complex 1
TCA cycle	Tricarboxylic acid cycle
ETC	Electron transport chain
Acetyl-CoA	Acetyl coenzyme A
α-KG	Alpha-ketoglutarate
PDH	Pyruvate dehydrogenase
PDK	Pyruvate dehydrogenase kinase
OCT4	Octamer-binding transcript factor 4 (also known as POU5F1)
SOX2	SRY (sex determining region Y)-box 2
SOX17	SRY-box 17
PAX6	Paired box protein 6
TBXT	T-box transcription factor T (also known as BRACHYURY)
HAND1	Heart and neural crest derivatives expressed protein 1

ACKNOWLEDGEMENTS

I am immensely grateful to the many individuals who have supported and guided me throughout not only graduate school, but also life. First, I want to thank my Ph.D. advisor, Dr. Michael Teitell, for teaching me to trust my mind. Mike provided a rigorous but nurturing training environment to learn without fear of failure. The intellectual freedom Mike allowed brought out the creativity and grit in me that I never knew existed. Next, I want to thank my Ph.D. thesis committee, Dr. Donald Kohn, Dr. Kathrin Plath, and Dr. Heather Christofk for keeping me on track and providing crucial feedback on my work.

Thank you to past and present members of the Teitell Lab for making the lab feel like home. I am grateful to Irena Roy, Alejandro Torres, Jr., Alex Napior, Amy Carver, Amy Vandiver, Jason Hong, Fasih Ahsan, Alex Sercel, Alex Patananan, Lynnea Waters, and Diane Kim for their exceptional kindness and support. I am especially grateful to Irena Roy for her collaboration and friendship in good and bad times. Additionally, thank you to my graduate school cohort and friends for experiencing this marathon with me, especially Lisa Ta, Nebula (Jiaying) Han, and Zhiyuan Mao.

Thank you to my dear friends Chris Hughes, Will McKay, Tonia Nguyen, Veda Vuligonda and of course my best friend and the sister I never had Megan Walding, who have kept me grounded throughout my studies. Special thanks to my partner Nick Barbieri, for always pushing me to be the best version of myself and building a beautiful life with me.

Lastly, I want to thank my family for their continuous love and support. Special thanks to my parents, Tung Lu and Lindy Phung, for instilling in me the hard work, mental fortitude, and moral foundation necessary to achieve my goals. Everything I have accomplished I owe to you two.

EDUCATION

Ph.D. Candidate in Molecular and Medical Pharmacology   2016-Present
University of California, Los Angeles
GPA: 3.90 NIH F31 NRSA Recipient
Thesis Advisor: Michael A. Teitell, M.D., Ph.D.

B.A. in Biological Sciences, Minor in Health Care Studies   2012-2016
University of Southern California
GPA: 3.87 Magna Cum Laude, Phi Beta Kappa, Discovery Scholar

PUBLICATIONS

Lu V*, Zeidan AR*, Mi KL, Norman RB, Patel ZS, Huff JL. Commonalities Between Aging and Adverse Outcomes of Radiation Exposure on the Brain. *In Preparation (with NASA).*

Lu V, Doan M, Roy IJ, Torres Jr. A, Teitell MA. Use of Chemically Defined, Nutrient-Balanced Media for Germ Lineage Differentiation of Primed Human Pluripotent Stem Cells. *STAR Protocols. In Review.*

Lu V, Roy IJ, Torres Jr. A, Joly JH, Ahsan FM, Graham NA, Teitell MA. (2022). Glutamine-Dependent Signaling Controls Pluripotent Stem Cell Fate. *Developmental Cell*, 57, 610–623.e1–e8. DOI: 10.1016/j.devcel.2022.02.003. PMID: 35216682.

Lu V*, Roy IJ*, Teitell MA. (2021). Nutrients and the Fate of Pluripotent Stem Cells. *Cell Metabolism*, 33(11), 2108-2121. DOI: 10.1016/j.cmet.2021.09.013. PMID: 34644538.

Lu V*, Dahan P*, Ahsan FM, Patananan AN, Roy IJ, Torres Jr. A, Nguyen RMT, Huang D, Braas, D, Teitell MA. (2019). Mitochondrial Metabolism and Glutamine are Essential for Mesoderm Differentiation of Human Pluripotent Stem Cells. *Cell Research,* 29(7), 596–598. DOI: 10.1038/s41422-019-0191-2. PMID: 31189991.

Lu V & Teitell MA. (2019). Alpha-ketoglutarate: a 'magic' metabolite in early germ cell development. *The EMBO Journal,* 38(1): e100615. DOI: 10.15252/embj.2018100615. PMID: 30275267.

Dahan P*, **Lu V***, Nguyen RMT, Kennedy SAL, Teitell MA. (2018). Metabolism in pluripotency: Both driver and passenger? *Journal of Biological Chemistry*, 294(14):5420-5429. DOI: 10.1074/jbc.TM117.000832. PMID: 29463682.

Zhang J, Zhao J, Dahan P, **Lu V**, Zhang C, Li H, Teitell MA. (2018). Metabolism in Pluripotent Stem Cells and Early Mammalian Development. *Cell Metabolism*, 27(2), 332-338. DOI: 10.1016/j.cmet.2018.01.008. PMID: 29414683.

Okita K, Morales AM, Dean AC, Johnson MC, **Lu V**, Farahi J, Mandelkern MA, London ED. (2018). Dopamine Striatal Dopamine D1-type Receptor Availability: No Difference from Control but Association with Cortical Thickness in Methamphetamine Users. *Molecular Psychiatry*, 23(5):1320-1327. DOI: 10.1038/mp.2017.172. PMID: 28894300.

PRESENTATIONS

Lu V, Roy IJ, Torres Jr. A, Joly JH, Ahsan FM, Graham NA, Teitell MA. (2022). Pluripotent Stem Cell Fate is Controlled by a Glutamine Signal. Cell Symposia: Metabolites in Signaling and Disease. Lisbon, Portugal.

Tu WB, Nakano H, **Lu V**…Plath K. (2022). The Impact of Tryptophan Metabolite Signaling on Cell Fate Decisions. Cell Symposia: Metabolites in Signaling and Disease. Lisbon, Portugal.

Lu V, Zeidan AR, Norman RB, Patel ZS, Huff JL. (2022). Common Pathways in the Irradiated and Aging Brain: Mitochondrial Dysfunction at the Crossroads. NASA Human Research Program Investigators' Workshop. Virtual.

Lu V, Norman RB, Patel ZS, Huff JL. (2021). Space Radiation and Mitochondrial Metabolism. NASA Langley Research Center Intern Research Symposium. Virtual.

Lu V, Roy IJ, Teitell, MA. (2020). Mitochondrial Metabolism and Glutamine Are Essential for Mesoderm Differentiation of Human Pluripotent Stem Cells. Tumor Metabolism Keystone Symposia*. Banff, Alberta, Canada. *Abstract accepted, cancelled due to COVID-19.

Lu V, Roy IJ, Teitell, MA. (2019). The Role of Acidification in Human Pluripotent Stem Cell Differentiation. ISSCR Annual Meeting. Los Angeles, CA.

Lu, V, Roy, IJ, Dahan, P, and Teitell, MA. (2019). The Role of pH in Pluripotent Stem Cell Differentiation. Stem Cells B2B- Bench to Bedside, 15th BSCRC Stem Cell Symposium. Los Angeles, CA.

Lu V, Teitell, MA. (2018). Acidic pH in Pluripotent Stem Cell Differentiation. UCLA Molecular Pharmacology Retreat. Huntington Beach, CA.

Lu V, Teitell, MA. (2018). The Role of pH in Pluripotent Stem Cell Differentiation. 'From Stem Cells to Human Development' Meeting. Dorking, Surrey, UK.

Lu V, Teitell, MA. (2017). Uncovering Bioenergetic Mechanisms that Control Pluripotent Stem Cell Differentiation. UCLA Molecular Pharmacology Retreat. Huntington Beach, CA.

Lu V, Sternberg PW. (2015). Investigating and characterizing neuropeptide gene *flp-8* on developmental fate and behavior in *Caenorhabditis elegans.* Caltech Summer Seminar. Pasadena, CA.

GRANTS & FELLOWSHIPS

Ruth L. Kirschstein Predoctoral NRSA (F31HD097960). NIH	2019-2022
Dissertation Year Fellowship. *Awarded, declined due to funding surplus*. UCLA	2021-2022
Dr. Ursula Mandel Fellowship. UCLA	2019-2020
Broad Stem Cell Training Program - Rose Hills Foundation Scholarship. UCLA	2018-2019
Student Opportunities for Academic Research. USC	2016
Amgen Scholars Fellowship Award. Caltech	2015
Rose Hills Undergraduate Research Fellowship. USC	2014
Provost's Undergraduate Research Fellowship. USC	2014
Student Opportunities for Academic Research. USC	2013
Summer Undergraduate Research Fund. USC	2013

AWARDS

Awardee. Graduate Programs in Bioscience Fellowship Incentive Program.	2019-2022
Awardee. Keystone Symposia on Metabolic Decisions Scholarship.	2021
Awardee. Rose Hills Foundation Science & Engineering Graduate Scholarship.	2018-2019
Awardee. Amgen Scholars Alumni Travel Award.	2018
Honorable Mention–Best Student Presentation. SCAS Annual Meeting.	2014
Awardee. University of Southern California Trojan League of Los Angeles Scholarship.	2014
Honoree. Phi Kappa Phi National Honor Society—Sophomore Scholars Recognition.	2013
Awardee. Rose Hills Scholarship for Science and Engineering.	2013-2016
Awardee. University of Southern California Dornsife College Dean's List.	2012-2016

CHAPTER 1:

Introduction

HUMAN PLURIPOTENT STEM CELLS

The modern era of regenerative medicine began over two decades ago with the successful isolation and culture of embryonic stem cells (ESCs) from a human blastocyst (Thomson et al., 1998). A decade later, the promise of pluripotent stem cells (PSCs) grew with the discovery that the combination of four factor variations (cMyc, Oct3/4, Sox2, Klf4 or *OCT4*, *SOX2*, *NANOG*, *LIN28*) could convert adult human fibroblasts into "induced" pluripotent stem cells (iPSCs) in a process known as reprogramming (Takahashi et al., 2007; Yu et al., 2007). The defining characteristics of PSCs are their ability to self-renew indefinitely or differentiate into the primary germ lineages, endoderm, mesoderm, and ectoderm, upon induction with specific cues. In this thesis, pluripotent/self-renewing stem cells are cells expressing core pluripotency transcription factors (OCT4, NANOG, SOX2, and others), and differentiation is the loss of these core pluripotency transcription factors coupled with the expression of lineage-specifying biomarkers (Yeo and Ng, 2013). Additionally, two functional features of PSCs are (1) blastocyst chimerism, which is the capacity to re-enter development in a host embryo, and (2) teratoma formation, which is the ability to spontaneously generate the three germ layers (De Los Angeles et al., 2015).

Intrinsic plasticity in cell identity, in conjunction with its reproduction of certain features of early mammalian development *ex vivo*, enables the promise of PSCs for applications in tissue engineering, regenerative medicine, and early embryo development studies. However, to date, this promise has not been fully realized due to stochastic genetic lesions, reprogramming factors, and residual pluripotency that all increase the risk of tumorigenicity manifesting as both malignant transformation and benign teratoma formation (Lee et al., 2013; Yamanaka, 2020). Additionally, heterogeneity in morphology, growth rate, gene expression profiles, and differentiation potential among PSC lines presents another challenge in downstream applications. Genetic background variation, rather than cell origin, is a major contributing factor

for transcriptional and epigenetic differences among PSC lines, as genetically matched human PSCs (hPSCs) and human iPSCs (hiPSCs) are molecularly and functionally equivalent (Choi et al., 2015). Studies have also reported varying differentiation capacity linked to epigenetic variation among PSC lines (Koyanagi-Aoi et al., 2013; Nishizawa et al., 2016). Accordingly, this thesis takes a different approach in optimizing PSC differentiation strategies by identifying and manipulating distinct metabolic requirements during differentiation. The following findings will ultimately inform more precise control of directed tri-lineage hPSC differentiation and reveal novel metabolic or pharmacological factors to optimize regenerative cell therapies.

METABOLISM AND STEM CELL FATE DETERMINATION

PSCs are highly proliferative, employing aerobic glycolysis to meet the biosynthetic and energetic demands required for rapid growth and division. Mitochondrial respiration and oxidative phosphorylation (OXPHOS) are downregulated in PSCs, which possess active but immature-looking mitochondria (Folmes et al., 2011; Zhang et al., 2011; Zhou et al., 2012). For many years, these metabolic features of PSCs were seen as passive consequences associated with the pluripotent cell state, but several lines of evidence have demonstrated the active, facilitating role of metabolic rewiring in pluripotent state transitions. For example, a shift from OXPHOS to glycolytic metabolism is required for somatic cell reprogramming (Zhou et al., 2012). Indeed, glycolytic gene expression occurs early in reprogramming and precedes the induction of pluripotent and self-renewal genes (Folmes et al., 2012; Folmes et al., 2011; Mathieu et al., 2014; Prigione et al., 2014). Furthermore, promotion of glycolytic pathway effectors increased, while inhibition of glycolytic enzyme activity decreased, reprogramming efficiency (Folmes et al., 2011). These findings indicated that glycolytic flux upregulation and OXPHOS downregulation are regulatory pre-requisites, rather than passive responses, for the de-differentiation process.

Upon the discovery that glycolytic metabolism is a controlling feature of pluripotent induction, additional reports emerged on metabolic regulation on other aspects of PSC fate decisions (Carey et al., 2015; Folmes et al., 2011; Moussaieff et al., 2015; Shiraki et al., 2014; Shyh-Chang et al., 2013; TeSlaa et al., 2016; Varum et al., 2011). An important theme during this era was the discovery that metabolic intermediates generated from glycolysis, tricarboxylic acid (TCA) cycle, and one-carbon mentalism can serve as reactants in epigenome, chromatin, and gene expression alterations. These metabolites include alpha ketoglutarate (α-KG) (Carey et al., 2015; TeSlaa et al., 2016), succinate (TeSlaa et al., 2016), acetyl-CoA (Moussaieff et al., 2015), methionine/threonine (Shiraki et al., 2014; Shyh-Chang et al., 2013), ascorbate (Chen et al., 2013; Eid and Abdel-Rehim, 2016; Esteban et al., 2010; Hore et al., 2016), and nicotinamide adenine dinucleotide (NAD+) (Calvanese et al., 2010; Fang and Li, 2021; Lees et al., 2020). Thus, in coordination with specific cell differentiation cues (such as BMP, Wnt, and SMAD signaling pathway induction or inhibition), metabolism enables and reinforces PSC cell fate decisions via metabolite-responsive fate-specifying transcription programs, enzyme-mediated chromatin changes, and/or nutrient-sensitive signaling (Baksh and Finley, 2021).

Until about half a decade ago, consensus in the field was that as PSCs differentiate into more specialized mature cells, a metabolic shift from aerobic glycolysis to OXPHOS is generally required. However, early hPSC differentiation into the three germ layers does not exhibit this indiscriminate shift in metabolic phenotype. In 2017, a study reported endoderm cells exhibit relatively moderate OXPHOS, mesoderm cells induce high-level OXPHO, and ectoderm cells maintain elevated glycolysis (Cliff et al., 2017). Additional studies indicated that a tightly regulated metabolic continuum exists across the range of ESC and ESC-derived states (from early lineage to terminal cell differentiation) that is context and cell-type specific (Chi et al., 2020; Cornacchia et al., 2019; Lu et al., 2019; Oburoglu et al., 2014; Tohyama et al., 2013). These findings implied potential for even more control over PSC differentiation by taking

advantage of early cell-type specific metabolic dependencies to guide or enrich for cells of interest (Tohyama et al., 2016; Tohyama et al., 2013). Here specifically, manipulation of only glutamine revealed the ability to control tri-lineage differentiation efficiency, viability, and enrichment.

GLUTAMINE

Glutamine is the most abundant amino acid in plasma and muscle and a major carrier of nitrogen (Cruzat et al., 2018). Classically, glutamine is known as a non-essential amino acid (NEAA), meaning the body is able to endogenously synthesize sufficient amounts for nitrogen balance or biosynthesis. This classification has since been reconsidered for contexts in which endogenous production is insufficient, such as during embryo/fetal development, where glutamine is a "conditionally essential" amino acid (Lacey and Wilmore, 1990; Wernerman, 2008; Wu, 2010). Glutamine contributes to effectively every essential metabolic requirement of rapidly proliferating cells, including: serving as TCA cycle and mitochondrial metabolism fuel, generating glutathione to detoxify oxidative stress, producing biosynthetic macromolecules nucleotides, amino sugars, NEAAs, and proteins, as well as activating nutrient-sensitive cell signaling pathways (DeBerardinis and Cheng, 2010; Watford, 2015; Yang et al., 2017).

The functional roles of glutamine can be classified into three main categories – nitrogen donor, carbon donor, and signaling molecule. While glucose, the other major nutrient, is only able to serve as a carbon donor, glutamine uniquely acts as both a carbon and nitrogen donor. Glutamine is an obligate nitrogen donor, meaning to be oxidized, glutamine must donate its amide (γ nitrogen) group to form glutamate, which then loses its amine group (α nitrogen) to form TCA cycle metabolite α-KG (Wise and Thompson, 2010). This process, known as glutaminolysis, is orchestrated by glutaminase (GLS1/GLS2), while the reverse reaction is

5

enabled by glutamine synthetase (GS) conversion of glutamate and ammonia to glutamine. Deamination of glutamine to glutamate frees up the amide group to serve as a precursor to purines, pyrimidines, glucosamine, NAD+, ammonia, and asparagine (Yang et al., 2017). As a carbon donor, glutamine can provide the carbon backbone for α-KG, a key TCA metabolite and epigenome co-factor. Additionally, in hypoxic or defective mitochondria conditions, glutamine can directly supply carbons for citrate production and subsequent fatty acid synthesis via the reductive carboxylation process (Metallo et al., 2011). Finally, unmetabolized glutamine plays a key function in the activation of intracellular signaling pathways, namely, the mechanistic target of rapamycin complex 1 (mTORC1). Glutamine activation of mTORC1 occurs through Rag GTPase-dependent activation via exogenous leucine and arginine exchange, or by Rag GTPase-independent activation via direct glutamine interaction with Arf1 GTPase (Jewell et al., 2015; Meng et al., 2020; Saxton and Sabatini, 2017). In sum, glutamine plays key roles in biomass/energy generation, cell maintenance, and signaling through its inherent biochemical and biophysical properties.

GLUTAMINE AND STEM CELLS

Along with glucose, glutamine has endured remarkable longevity in research interest for its role in tumor cell metabolism, dating back to the 1950s (DeBerardinis and Cheng, 2010; Eagle, 1955). In the past decade, this interest has expanded to PSC metabolism and fate, with reports showing promising results on using context-specific glutamine deprivation as a strategy to enrich for differentiated cells of interest. For instance, short-term glutamine withdrawal eliminated cells with high glutamine dependence and enriched for mouse ESCs (mESCs) and hPSCs with high expression of pluripotent transcription factors OCT4 and SOX2 (Vardhana et al., 2019). In contrast, long-term glutamine deprivation coupled with differentiation cues eliminated PSCs to enrich for hPSC-derived cardiomyocytes (Tohyama et al., 2016) or enhance the angiogenic capacity of endothelial cells (Marsboom et al., 2016). These reports indicate

6

manipulating the timing and context of exogenous glutamine availability enables control over whether PSCs or non-pluripotent cells are removed from the cell population.

In 2019, we showed that long-term glutamine deprivation during spontaneous 21-day hPSC differentiation inhibited mesoderm but promoted ectoderm lineage development. This was an exciting finding as it indicated glutamine presence can bias and skew differentiation potentiation in the absence of lineage-specifying cytokines and chemokines. These data initiated a fundamental question on whether specification into the three embryonic germ layers differentially required glutamine availability (Lu et al., 2019), which would provide further insight on the impact of metabolism on the coordination of early mammalian development. This thesis documents the active roles of metabolism in pluripotency and differentiation, the similarities in metabolism between PSCs and early mammalian development, the application of chemically defined nutrient-equivalent tri-lineage differentiation culture media, and the roles of extracellular and intracellular glutamine availability on downstream PSC fate decisions.

CHAPTER SUMMARIES

Chapter 2 of this thesis is a comprehensive review of the driving role of metabolic flux and metabolite concentration on pluripotency and differentiation regulation. This chapter provides updated context for seminal findings in the stem cell metabolism field and identifies the key open questions for future investigations. This review article was previously published as a Review article in *Journal of Biological Chemistry* in 2018 by the laboratory of Dr. Michael Teitell. It was selected for a special virtual issue on "Pluripotency regulation and differentiation" in 2019.

Chapter 3 of this thesis discusses the influence of metabolism on gene expression in embryos, their *ex vivo* models (PSCs), and primordial germ cell differentiation through epigenome modification. This chapter reviews published evidence revealing the context-dependent

7

coordination of intracellular signaling, histone modifications, and gene expression in developing, quiescent, and malnourished embryos and in early germ cell development. The first part of this chapter, entitled "Metabolism in Pluripotent Stem Cells and Early Mammalian Development," was previously published as a Review article in *Cell Metabolism* in 2018 by the laboratories of Drs. Jin Zhang and Michael Teitell. This article was special featured in the "Cell Press Selections Stem Cell Metabolism: Fate Regulation and Disease Modeling" Reprint Compendium. The second part of this chapter, entitled "Alpha-ketoglutarate: a "magic" metabolite in early germ cell development," was previously published as a News and Views commentary article in *The EMBO Journal* in 2018 by the laboratory of Dr. Michael Teitell.

Chapter 4 of this thesis is a detailed protocol for the maintenance of hPSCs and subsequent differentiation into the three embryonic germ lineages (endoderm, mesoderm, and ectoderm). This chapter provides a robust and validated method for preparing chemically defined, nutrient-balanced differentiation culture medium to enable customizable experimental conditions. This work has been submitted as a manuscript to the journal *STAR Protocols* and is currently in revision.

Chapter 5 of this thesis is a comprehensive literature review on the role of unmetabolized nutrients in PSC cell fate decisions through nutrient-sensitive intracellular signaling, cell enrichment, and context-dependent mechanisms of action. This chapter synthesizes impactful questions of high research interest and highlights the lack of detailed work on these robust, reproducible observations. This work was previously published as a Perspective article in *Cell Metabolism* in 2021 by the laboratory of Dr. Michael Teitell.

Chapter 6 of this thesis demonstrates that deprivation of extracellular glutamine is able to bias hPSC fate decisions during spontaneous non-directed differentiation—a process that generates

all three germ layers without lineage-specifying cytokines under control conditions. While all three embryonic germ layers utilize extracellular glutamine as the major carbon contributor to the TCA cycle, only certain lineages are dependent on glutamine. Specifically, during the formation of hPSC-derived embryoid bodies, endodermal/mesodermal cell potentiation is inhibited while ectodermal cell potentiation is slightly promoted by the lack of glutamine. This work initiated a fundamental question on whether glutamine availability is a core cell type-specific requirement during early mammalian development. This research article was published as a Letter to the Editor in *Cell Research* in 2019 by the laboratory of Dr. Michael Teitell.

Chapter 7 of the thesis elucidates the critical role of glutamine in the differentiation capacity, cell fate, and viability of all three germ layers. This work is the direct continuation of Chapter 6, enabling deeper insight into the distinct glutamine dependencies exhibited by each lineage cell type. In brief, endoderm/mesoderm cells are dependent on extracellular glutamine to provide the carbon skeleton for α-KG generation. While these cell types are capable of generating endogenous glutamine upon extracellular glutamine deprivation via GS, these levels are insufficient to support cell survival. In contrast, upon extracellular glutamine deprivation, ectoderm cells are capable of synthesizing sufficient intracellular glutamine levels to sustain glutamine-dependent mTORC1 signaling and enable ectoderm specification to occur. Importantly, these requirements are specific and irreplaceable by other mTORC1-sensed amino acids and/or glutamine-derived metabolites, clarifying core functions for non-metabolized nutrients in developmental regulation. This work was published as an Article in *Developmental Cell* in 2022 by the laboratory of Dr. Michael Teitell.

REFERENCES

Baksh, S.C., and Finley, L.W.S. (2021). Metabolic Coordination of Cell Fate by alpha-Ketoglutarate-Dependent Dioxygenases. Trends Cell Biol *31*, 24-36.

Calvanese, V., Lara, E., Suarez-Alvarez, B., Abu Dawud, R., Vazquez-Chantada, M., Martinez-Chantar, M.L., Embade, N., Lopez-Nieva, P., Horrillo, A., Hmadcha, A.*, et al.* (2010). Sirtuin 1 regulation of developmental genes during differentiation of stem cells. Proc Natl Acad Sci U S A *107*, 13736-13741.

Carey, B.W., Finley, L.W., Cross, J.R., Allis, C.D., and Thompson, C.B. (2015). Intracellular alpha-ketoglutarate maintains the pluripotency of embryonic stem cells. Nature *518*, 413-416.

Chen, J., Guo, L., Zhang, L., Wu, H., Yang, J., Liu, H., Wang, X., Hu, X., Gu, T., Zhou, Z.*, et al.* (2013). Vitamin C modulates TET1 function during somatic cell reprogramming. Nat Genet *45*, 1504-1509.

Chi, F., Sharpley, M.S., Nagaraj, R., Roy, S.S., and Banerjee, U. (2020). Glycolysis-Independent Glucose Metabolism Distinguishes TE from ICM Fate during Mammalian Embryogenesis. Dev Cell.

Choi, J., Lee, S., Mallard, W., Clement, K., Tagliazucchi, G.M., Lim, H., Choi, I.Y., Ferrari, F., Tsankov, A.M., Pop, R.*, et al.* (2015). A comparison of genetically matched cell lines reveals the equivalence of human iPSCs and ESCs. Nat Biotechnol *33*, 1173-1181.

Cliff, T.S., Wu, T., Boward, B.R., Yin, A., Yin, H., Glushka, J.N., Prestegaard, J.H., and Dalton, S. (2017). MYC Controls Human Pluripotent Stem Cell Fate Decisions through Regulation of Metabolic Flux. Cell Stem Cell *21*, 502-516 e509.

Cornacchia, D., Zhang, C., Zimmer, B., Chung, S.Y., Fan, Y., Soliman, M.A., Tchieu, J., Chambers, S.M., Shah, H., Paull, D.*, et al.* (2019). Lipid Deprivation Induces a Stable, Naive-to-Primed Intermediate State of Pluripotency in Human PSCs. Cell Stem Cell *25*, 120-136 e110.

Cruzat, V., Macedo Rogero, M., Noel Keane, K., Curi, R., and Newsholme, P. (2018). Glutamine: Metabolism and Immune Function, Supplementation and Clinical Translation. Nutrients *10*.

De Los Angeles, A., Ferrari, F., Xi, R., Fujiwara, Y., Benvenisty, N., Deng, H., Hochedlinger, K., Jaenisch, R., Lee, S., Leitch, H.G.*, et al.* (2015). Hallmarks of pluripotency. Nature *525*, 469-478.

DeBerardinis, R.J., and Cheng, T. (2010). Q's next: the diverse functions of glutamine in metabolism, cell biology and cancer. Oncogene *29*, 313-324.

Eagle, H. (1955). Nutrition needs of mammalian cells in tissue culture. Science *122*, 501-514.

Eid, W., and Abdel-Rehim, W. (2016). Vitamin C promotes pluripotency of human induced pluripotent stem cells via the histone demethylase JARID1A. Biol Chem *397*, 1205-1213.

Esteban, M.A., Wang, T., Qin, B., Yang, J., Qin, D., Cai, J., Li, W., Weng, Z., Chen, J., Ni, S.*, et al.* (2010). Vitamin C enhances the generation of mouse and human induced pluripotent stem cells. Cell Stem Cell *6*, 71-79.

Fang, Y., and Li, X. (2021). Sirtuins in metabolic and epigenetic regulation of stem cells. In Sirtuin Biology in Cancer and Metabolic Disease, pp. 25-37.

Folmes, C.D., Dzeja, P.P., Nelson, T.J., and Terzic, A. (2012). Metabolic plasticity in stem cell homeostasis and differentiation. Cell Stem Cell *11*, 596-606.

Folmes, C.D., Nelson, T.J., Martinez-Fernandez, A., Arrell, D.K., Lindor, J.Z., Dzeja, P.P., Ikeda, Y., Perez-Terzic, C., and Terzic, A. (2011). Somatic oxidative bioenergetics transitions into pluripotency-dependent glycolysis to facilitate nuclear reprogramming. Cell Metab *14*, 264-271.

Hore, T.A., von Meyenn, F., Ravichandran, M., Bachman, M., Ficz, G., Oxley, D., Santos, F., Balasubramanian, S., Jurkowski, T.P., and Reik, W. (2016). Retinol and ascorbate drive erasure of epigenetic memory and enhance reprogramming to naive pluripotency by complementary mechanisms. Proc Natl Acad Sci U S A *113*, 12202-12207.

Jewell, J.L., Kim, Y.C., Russell, R.C., Yu, F.X., Park, H.W., Plouffe, S.W., Tagliabracci, V.S., and Guan, K.L. (2015). Metabolism. Differential regulation of mTORC1 by leucine and glutamine. Science *347*, 194-198.

Koyanagi-Aoi, M., Ohnuki, M., Takahashi, K., Okita, K., Noma, H., Sawamura, Y., Teramoto, I., Narita, M., Sato, Y., Ichisaka, T.*, et al.* (2013). Differentiation-defective phenotypes revealed by large-scale analyses of human pluripotent stem cells. Proc Natl Acad Sci U S A *110*, 20569-20574.

Lacey, J.M., and Wilmore, D.W. (1990). Is glutamine a conditionally essential amino acid? Nutr Rev *48*, 297-309.

Lee, A.S., Tang, C., Rao, M.S., Weissman, I.L., and Wu, J.C. (2013). Tumorigenicity as a clinical hurdle for pluripotent stem cell therapies. Nat Med *19*, 998-1004.

Lees, J.G., Gardner, D.K., and Harvey, A.J. (2020). Nicotinamide adenine dinucleotide induces a bivalent metabolism and maintains pluripotency in human embryonic stem cells. Stem Cells *38*, 624-638.

Lu, V., Dahan, P., Ahsan, F.M., Patananan, A.N., Roy, I.J., Torres, A., Jr., Nguyen, R.M.T., Huang, D., Braas, D., and Teitell, M.A. (2019). Mitochondrial metabolism and glutamine are essential for mesoderm differentiation of human pluripotent stem cells. Cell Res *29*, 596-598.

Marsboom, G., Zhang, G.F., Pohl-Avila, N., Zhang, Y., Yuan, Y., Kang, H., Hao, B., Brunengraber, H., Malik, A.B., and Rehman, J. (2016). Glutamine Metabolism Regulates the Pluripotency Transcription Factor OCT4. Cell Rep *16*, 323-332.

Mathieu, J., Zhou, W., Xing, Y., Sperber, H., Ferreccio, A., Agoston, Z., Kuppusamy, K.T., Moon, R.T., and Ruohola-Baker, H. (2014). Hypoxia-inducible factors have distinct and stage-specific roles during reprogramming of human cells to pluripotency. Cell Stem Cell *14*, 592-605.

Meng, D., Yang, Q., Wang, H., Melick, C.H., Navlani, R., Frank, A.R., and Jewell, J.L. (2020). Glutamine and asparagine activate mTORC1 independently of Rag GTPases. Journal of Biological Chemistry *295*, 2890-2899.

Metallo, C.M., Gameiro, P.A., Bell, E.L., Mattaini, K.R., Yang, J., Hiller, K., Jewell, C.M., Johnson, Z.R., Irvine, D.J., Guarente, L.*, et al.* (2011). Reductive glutamine metabolism by IDH1 mediates lipogenesis under hypoxia. Nature *481*, 380-384.

Moussaieff, A., Rouleau, M., Kitsberg, D., Cohen, M., Levy, G., Barasch, D., Nemirovski, A., Shen-Orr, S., Laevsky, I., Amit, M.*, et al.* (2015). Glycolysis-mediated changes in acetyl-CoA and histone acetylation control the early differentiation of embryonic stem cells. Cell Metab *21*, 392-402.

Nishizawa, M., Chonabayashi, K., Nomura, M., Tanaka, A., Nakamura, M., Inagaki, A., Nishikawa, M., Takei, I., Oishi, A., Tanabe, K.*, et al.* (2016). Epigenetic Variation between Human Induced Pluripotent Stem Cell Lines Is an Indicator of Differentiation Capacity. Cell Stem Cell *19*, 341-354.

Oburoglu, L., Tardito, S., Fritz, V., de Barros, S.C., Merida, P., Craveiro, M., Mamede, J., Cretenet, G., Mongellaz, C., An, X.*, et al.* (2014). Glucose and glutamine metabolism regulate human hematopoietic stem cell lineage specification. Cell Stem Cell *15*, 169-184.

Prigione, A., Rohwer, N., Hoffmann, S., Mlody, B., Drews, K., Bukowiecki, R., Blumlein, K., Wanker, E.E., Ralser, M., Cramer, T.*, et al.* (2014). HIF1alpha modulates cell fate reprogramming through early glycolytic shift and upregulation of PDK1-3 and PKM2. Stem Cells *32*, 364-376.

Saxton, R.A., and Sabatini, D.M. (2017). mTOR Signaling in Growth, Metabolism, and Disease. Cell *168*, 960-976.

Shiraki, N., Shiraki, Y., Tsuyama, T., Obata, F., Miura, M., Nagae, G., Aburatani, H., Kume, K., Endo, F., and Kume, S. (2014). Methionine metabolism regulates maintenance and differentiation of human pluripotent stem cells. Cell Metab *19*, 780-794.

Shyh-Chang, N., Locasale, J.W., Lyssiotis, C.A., Zheng, Y., Teo, R.Y., Ratanasirintrawoot, S., Zhang, J., Onder, T., Unternaehrer, J.J., Zhu, H.*, et al.* (2013). Influence of threonine metabolism on S-adenosylmethionine and histone methylation. Science *339*, 222-226.

Takahashi, K., Tanabe, K., Ohnuki, M., Narita, M., Ichisaka, T., Tomoda, K., and Yamanaka, S. (2007). Induction of pluripotent stem cells from adult human fibroblasts by defined factors. Cell *131*, 861-872.

TeSlaa, T., Chaikovsky, A.C., Lipchina, I., Escobar, S.L., Hochedlinger, K., Huang, J., Graeber, T.G., Braas, D., and Teitell, M.A. (2016). alpha-Ketoglutarate Accelerates the Initial Differentiation of Primed Human Pluripotent Stem Cells. Cell Metab *24*, 485-493.

Thomson, J.A., Itskovitz-Eldor, J., Shapiro, S.S., Waknitz, M.A., Swiergiel, J.J., Marshall, V.S., and Jones, J.M. (1998). Embryonic stem cell lines derived from human blastocysts. Science *282*, 1145-1147.

Tohyama, S., Fujita, J., Hishiki, T., Matsuura, T., Hattori, F., Ohno, R., Kanazawa, H., Seki, T., Nakajima, K., Kishino, Y.*, et al.* (2016). Glutamine Oxidation Is Indispensable for Survival of Human Pluripotent Stem Cells. Cell Metab *23*, 663-674.

Tohyama, S., Hattori, F., Sano, M., Hishiki, T., Nagahata, Y., Matsuura, T., Hashimoto, H., Suzuki, T., Yamashita, H., Satoh, Y*., et al.* (2013). Distinct metabolic flow enables large-scale purification of mouse and human pluripotent stem cell-derived cardiomyocytes. Cell Stem Cell *12*, 127-137.

Vardhana, S.A., Arnold, P.K., Rosen, B.P., Chen, Y., Carey, B.W., Huangfu, D., Fontaine, C.C., Thompson, C.B., and Finley, L.W.S. (2019). Glutamine independence is a selectable feature of pluripotent stem cells. Nat Metab *1*, 676-687.

Varum, S., Rodrigues, A.S., Moura, M.B., Momcilovic, O., Easley, C.A.t., Ramalho-Santos, J., Van Houten, B., and Schatten, G. (2011). Energy metabolism in human pluripotent stem cells and their differentiated counterparts. PLoS One *6*, e20914.

Watford, M. (2015). Glutamine and glutamate: Nonessential or essential amino acids? Anim Nutr *1*, 119-122.

Wernerman, J. (2008). Clinical use of glutamine supplementation. J Nutr *138*, 2040S-2044S.

Wise, D.R., and Thompson, C.B. (2010). Glutamine addiction: a new therapeutic target in cancer. Trends Biochem Sci *35*, 427-433.

Wu, G. (2010). Functional amino acids in growth, reproduction, and health. Adv Nutr *1*, 31-37.

Yamanaka, S. (2020). Pluripotent Stem Cell-Based Cell Therapy-Promise and Challenges. Cell Stem Cell *27*, 523-531.

Yang, L., Venneti, S., and Nagrath, D. (2017). Glutaminolysis: A Hallmark of Cancer Metabolism. Annu Rev Biomed Eng *19*, 163-194.

Yeo, J.C., and Ng, H.H. (2013). The transcriptional regulation of pluripotency. Cell Res *23*, 20-32.

Yu, J., Vodyanik, M.A., Smuga-Otto, K., Antosiewicz-Bourget, J., Frane, J.L., Tian, S., Nie, J., Jonsdottir, G.A., Ruotti, V., Stewart, R*., et al.* (2007). Induced pluripotent stem cell lines derived from human somatic cells. Science *318*, 1917-1920.

Zhang, J., Khvorostov, I., Hong, J.S., Oktay, Y., Vergnes, L., Nuebel, E., Wahjudi, P.N., Setoguchi, K., Wang, G., Do, A*., et al.* (2011). UCP2 regulates energy metabolism and differentiation potential of human pluripotent stem cells. EMBO J *30*, 4860-4873.

Zhou, W., Choi, M., Margineantu, D., Margaretha, L., Hesson, J., Cavanaugh, C., Blau, C.A., Horwitz, M.S., Hockenbery, D., Ware, C*., et al.* (2012). HIF1alpha induced switch from bivalent to exclusively glycolytic metabolism during ESC-to-EpiSC/hESC transition. EMBO J *31*, 2103-2116.

CHAPTER 2:

Metabolism in Pluripotency: Both Driver and Passenger?

Metabolism in pluripotency: Both driver and passenger?

Perrine Dahan[‡], Vivian Lu[§], Robert M. T. Nguyen[‡], Stephanie A. L. Kennedy[‡¶], and Michael A. Teitell[‡‖**‡‡§§¶¶1]

From the Departments of [‡]Pathology and Laboratory Medicine and [§]Molecular and Medical Pharmacology and [§§]Jonsson Comprehensive Cancer Center, David Geffen School of Medicine, UCLA, Los Angeles, California 90095, the [¶]Department of Biology, California State University at Northridge, Northridge, California 91330, the [‖]California NanoSystems Institute, [**]Department of Bioengineering, and [‡‡]Molecular Biology Institute, UCLA, Los Angeles, California 90095, and the [¶¶]Eli and Edythe Broad Center of Regenerative Medicine and Stem Cell Research, UCLA, Los Angeles, California 90095

Edited by John M. Denu

Pluripotent stem cells (PSCs) are highly proliferative cells characterized by robust metabolic demands to power rapid division. For many years considered a passive component or "passenger" of cell-fate determination, cell metabolism is now starting to take center stage as a driver of cell fate outcomes. This review provides an update and analysis of our current understanding of PSC metabolism and its role in self-renewal, differentiation, and somatic cell reprogramming to pluripotency. Moreover, we present evidence on the active roles metabolism plays in shaping the epigenome to influence patterns of gene expression that may model key features of early embryonic development.

Most investigators view metabolism, which encompasses the synthesis and utilization of macromolecules and energy, as a passive supporter of self-renewal and rapid proliferation in pluripotent stem cells (PSCs)[2] and their differentiated, slower dividing progeny. However, exciting recent studies are changing this perception by showing an active role for metabolism in PSC fate determination.

Metabolism in PSCs and somatic cells

Glycolysis and oxidative phosphorylation

Mammalian cells generate ATP by varying the ratios of glycolysis and oxidative phosphorylation (OXPHOS). Human and mouse PSCs produce energy mainly by the enzymatic conversion of glucose to lactate (1), which contrasts with resting somatic body cells that favor OXPHOS (Fig. 1) (2–5). This difference persists for PSCs made from blastocysts or by somatic cell reprogramming, independent of oxygen availability (6). We interpret this energetic difference as a possible programmed feature of cell state rather than a consequence of relative hypoxia in earliest embryo development. Despite a markedly lower ATP yield per glucose molecule, elevated glycolysis in PSCs, also seen in rapidly dividing cancer cells (Warburg effect), has several key advantages. Increased glycolytic flux fuels the biosynthesis of nucleotides, lipids, and reducing equivalents to support rapid cell replication. Maintaining embryonic integrity, or genomic stability during embryonic development, requires reducing genomic and mitochondrial DNA damage and protein and lipid oxidation from reactive oxygen species (ROS) produced by OXPHOS. A premium for embryonic integrity is also manifest as heightened apoptosis sensitivity in early embryos, germ cells, and PSCs (2, 7, 8). Favoring glycolysis reduces ROS, which, along with augmented antioxidant mechanisms, supports PSC self-renewal until differentiation is triggered with required OXPHOS and ROS elevations (9–11).

Glutamine

Glutamine supports PSC survival and expansion by increasing antioxidant GSH (4) and fueling mitochondrial energy metabolism (12–14). Glutaminolysis generates tricarboxylic acid (TCA) cycle substrates (12) and supports the mitochondrial inner membrane potential ($\Delta\Psi$) required for PSC survival (15). A paradoxically high $\Delta\Psi$ in PSCs compared with PSC-differentiated progeny cells (3, 16, 17), despite low OXPHOS in PSCs, may arise from the hydrolysis of glycolytic ATP by complex V ATP synthase. PSCs show low expression of inhibitory factor 1, which prevents the ATP synthase from running as an ATP hydrolase (2). Because low $\Delta\Psi$ facilitates the induction of apoptotic pathways, enhanced apoptotic sensitivity of PSCs compared with PSC-differentiated progeny is surprising with comparatively heightened $\Delta\Psi$ in PSCs and requires further study.

Lipids

Similar to rapidly dividing cancer cells and antigen-activated lymphocytes, robust lipid biosynthesis occurs in PSCs to replenish membranes and organelles (16). Lipid production also supports somatic cell reprogramming to pluripotency (18, 19). Carbons for lipid building are siphoned from glycolysis and

[2] The abbreviations used are: PSC, pluripotent stem cell; i/h/PSC, induced/human pluripotent stem cell; OXPHOS, oxidative phosphorylation; TCA, tricarboxylic acid; $\Delta\Psi$, mitochondrial inner membrane potential; CPTF, core pluripotency transcription factor; TF, transcription factor; UCP2, uncoupling protein 2; HBP, hexosamine biosynthesis pathway; UDP-GlcNAc, UDP N-acetylglucosamine; OGT, O-GlcNAc transferase; O-GlcNAc, O-linked β-D-N-acetylglucosamine. OGA, O-GlcNAcase; SIRT1, sirtuin 1; NPC, neural progenitor cell; FA, fatty acid; JHDM, Jumonji C-domain containing histone demethylase; TET, ten-eleven-translocase; α-KG, α-ketoglutarate; ESC, embryonic stem cell; mESC, mouse ESC; NNMT, nicotinamide N-methyltransferase; SAM, S-adenosylmethionine; Ac-CoA, acetyl-CoA; HIF, hypoxia-inducible factor.
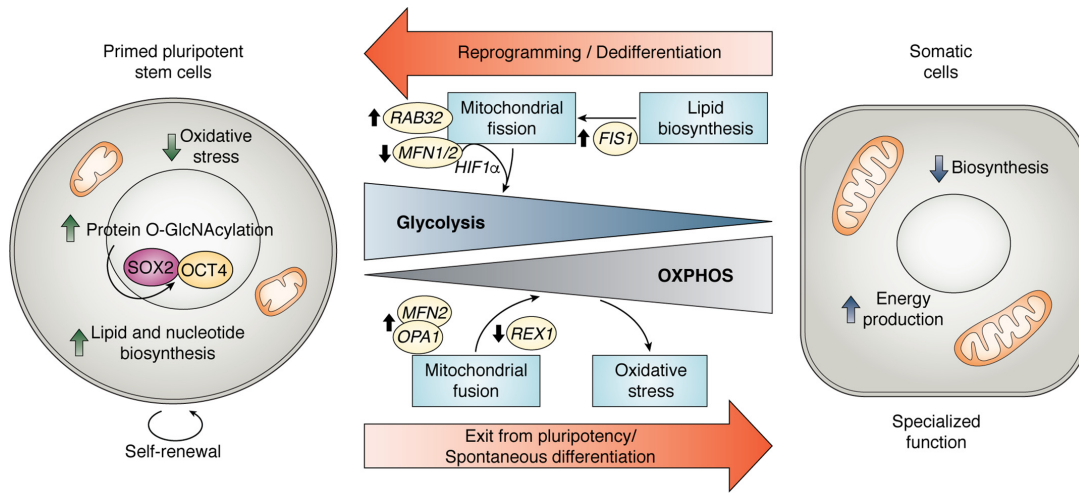
Figure 1. Metabolic transitions between pluripotency and differentiation. The primed pluripotent state is characterized by elevated glycolysis, which associates with a fragmented mitochondrial network. Glycolytic metabolism fuels rapid proliferation and self-renewal while maintaining molecular integrity from decreased oxidative stress. PSC metabolism appears to favor a relatively high level of protein *O*-GlcNAcylated motifs, particularly on SOX2 and OCT4, that are quickly erased upon differentiation. These modifications could also regulate other transcription factors and epigenome remodelers upon pluripotency exit. During PSC-derived generation of somatic cells, such as cardiomyocytes, oxidative metabolism is up-regulated by mitochondrial dynamics via REX1 repression and MFN2 and OPA1 expression. This supports efficient mitochondrial energy production at the expense of macromolecular biosynthesis. The consequence of increased OXPHOS is increased ROS production and oxidative stress, which may serve regulatory roles in differentiation. Conversely, the reprogramming of somatic cells toward pluripotency depends on an early glycolytic shift, and mitochondrial morphology remodeling facilitated by RAB32 kinase and lipid biosynthesis induced FIS1 stabilization. The down-regulation of proteins driving MFN1/2 can promote a glycolytic shift through HIF1α stabilization.

glutaminolysis biochemical pathways (12, 14). Indeed, lipid anabolism promotes PSC identity, notably by regulating mitochondrial dynamics (see below).

Regulation of PSC metabolism

Core pluripotency transcription factors

In embryonic stem cells (ESCs), core pluripotency transcription factors (CPTFs), such as OCT4, interact with the promoters of genes encoding glycolytic enzymes hexokinase 2 and pyruvate kinase M2 (PKM2) to drive transcription and augment glycolytic flux (5, 20, 21). Metabolic coordination by CPTFs indicates an essential role for metabolism in pluripotency.

Regulators of mitochondrial carbon routing

Uncoupling protein 2 (UCP2) is a mitochondrial inner membrane protein expressed in PSCs that limits OXPHOS and ROS production (2). Aberrant re-expression of UCP2 in many types of cancer also inhibits OXPHOS to bias ATP production toward aerobic glycolysis or "Warburg" metabolism (22). UCP2 functions as a carbon substrate transporter. In PSCs, UCP2 expels carbon 4 (C4) intermediate metabolites, including oxaloacetate, malate, and L-aspartate from the TCA cycle and mitochondrial matrix, thereby reducing electron-donating substrates for OXPHOS and ATP production (22). In cancer cells, UCP2 conversely promotes the incorporation of carbons from glutaminolysis into the TCA cycle. Recent studies also show that glutamine supports the TCA cycle more robustly in PSCs than in differentiated cardiomyocyte progeny cells (12). Combined, these studies provide a model for PSCs in which

UCP2 routes glucose-derived carbons into cytosolic biosynthetic pathways and glutamine-derived carbons into the TCA cycle to maintain ΔΨ and low OXPHOS levels. This model is supported by a study that shows glucose provides metabolites only for the first steps (Ac-CoA, citrate, and *cis*-aconitate) of the TCA cycle, whereas glutamine contributes metabolites to later TCA cycle steps as an anaplerotic fuel (Fig. 2) (12).

Another potential carbon routing regulator in PSCs comes from cancer metabolism studies. Cancer cells show robust glucose import and augmented glycolysis to feed biosynthetic reactions. This activity blocks pyruvate oxidation to CO_2 in the mitochondria by repression of the mitochondrial pyruvate carrier (MPC) genes, *MPC1/2* (23). Pyruvate exclusion from mitochondrial oxidation may be a more general stem cell strategy beyond cancer cells that requires further study. Supporting this idea, repression of MPC levels occurs in intestinal and hair-follicle adult stem cells, whereas MPC levels increase with differentiation of intestinal crypt stem-like cells (24, 25).

Mitochondrial network

PSCs show punctate mitochondria with immature inner membrane cristae and evidence of reduced functionality with low OXPHOS (2, 4, 5) and ROS production (14, 26). A granular mitochondrial morphology contrasts with elongated interlacing mitochondrial networks in somatic cells and helps to sustain CPTF expression and prevent expression of differentiation genes (27). Conversely, the REX1 pluripotency-associated transcription factor (TF) causes Ser-616 phosphorylation and activation of the mitochondrial fission regulator DRP1 by CDK1/cyclin B (27). Also, repression of mitochondrial fusion proteins

16
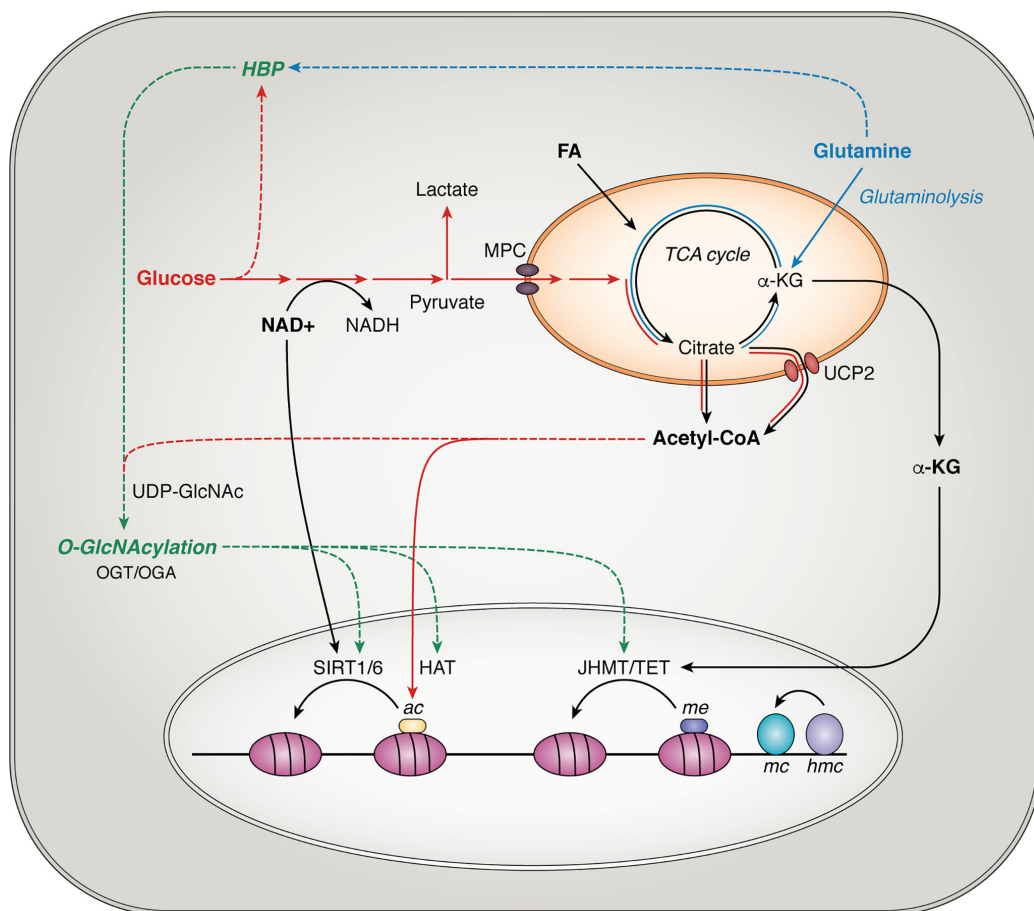
Figure 2. Influence of metabolism on the epigenome in the maintenance of pluripotency. Glycolytic flux regulates the NAD$^+$/NADH ratio, which controls the activities of sirtuin (*SIRT*) histone deacetylases. TCA cycle intermediates exported from the mitochondria include citrate and α-KG. Conversion of cytosolic citrate to Ac-CoA provides a donor for HAT-mediated histone acetylation. α-KG is a cofactor for histone and DNA demethylation reactions by JHDM and TET enzymes, respectively. By-products of glucose and glutamine catabolism supply reactants for *O*-GlcNAc modifications of epigenetic remodeling proteins through the HBP. Highlighted in *red, blue,* and *green* are the metabolic pathways associated with pluripotency, their contribution to TCA cycle metabolite production, and their subsequent influence on the epigenome (*solid lines*). Another potential mechanism for how metabolism can shape transcriptional patterns could be by fueling HBP-derived *O*-GlcNAcylation of proteins driving epigenome remodeling (*dashed line*).

MFN1/2 during somatic cell reprogramming is linked to reduced p53 expression and increased proliferation (26). Together, these studies connect mitochondrial network dynamics with pluripotency and proliferation in PSCs.

Mitochondrial dynamics regulators may influence PSC metabolic flux. A granular mitochondrial morphology supports fatty acid (FA) biosynthesis and promotes glycolytic gene expression (14). Studies show that mitochondrial fission with an immature ultrastructure, rather than function of respiratory chain complexes, supports a glycolytic preference (2, 4, 5). In immortalized fibroblasts, mitochondrial dysfunction and a shift to glycolysis occurs with mitochondrial fission factor overexpression (28). Additionally, MFN1/2 depletion can augment the expression and stabilization of the glycolytic master up-reg-

ulator, hypoxia-inducible factor 1α (HIF1α) (26). These data suggest that network regulators influence both the cell cycle and metabolism in pluripotency. The potential for mitochondrial network morphology to affect the expression of cell fate and metabolism genes requires further investigation. New insights from recent studies on metabolic control of chromatin structure and gene expression (detailed later) provide a potential mechanism for this connection.

Metabolism in pluripotent cell-fate transitions

Metabolic events during iPSC generation

Reprogramming somatic body cells to induced pluripotent stem cells (iPSCs) is a model for cell-fate transitions. iPSC pro-

17

duction provides insight for how metabolism governs pluripotency and self-renewal or differentiation into highly specialized and functional cell types. Stimulating glycolytic flux by modulating pathway regulators or effectors promotes iPSC reprogramming efficiency, whereas impeding glycolysis has the opposite effect (21, 29, 30). Transcriptome and proteome analyses during reprogramming reveal metabolic roles in dedifferentiation. Changes in the expression of metabolic genes that shift OXPHOS to glycolysis precede the induction of pluripotency and self-renewal genes (21, 31–34). An early reprogramming hyper-energetic state, partly mediated by estrogen-related nuclear receptors, shows elevated OXPHOS and glycolysis, with increases in mitochondrial ATP production proteins and antioxidant enzymes (32, 35, 36). An early burst in OXPHOS increases ROS generation and leads to an increase in nuclear factor (erythroid-derived 2)-like 2 (NRF2) activity, which promotes a subsequent glycolytic shift through HIF activation (36). Together, these studies show a progression from a hyper-energetic state to glycolysis during the conversion to pluripotency.

Hypoxia-related pathways in PSC fate transitions

Inducing glycolysis and reducing OXPHOS by modulating p53 and HIFs can influence somatic cell dedifferentiation. p53 inactivation (37–40) and HIF stabilization in low O_2 tension promote reprogramming efficiency (34, 41) and reversible pluripotency re-entry during early differentiation (42). Early in reprogramming, HIF1α and HIF2α are stabilized in normoxia and are notably required for metabolic shift by facilitating the expression of glycolysis-enforcing genes such as the pyruvate dehydrogenase kinase 3 (34). However, enforced HIF2 stabilization is deleterious during the last steps of iPSC generation by inducing tumor necrosis factor–related apoptosis inducing ligand (TRAIL) (34).

Conversely, HIFs and hypoxia-related pathways are also effectors in driving early differentiation depending on environmental context. For instance, hypoxia promotes PSC differentiation into definitive endoderm and retinal or lung progenitors (43, 44). In the context of neurogenesis, low O_2 tension and HIFs propel a neural fate at the expense of other germ lineages in early differentiation of hPSCs. At later stages of neural specification from neural progenitor cells (NPCs), hypoxia promotes glial rather than neuronal fate by an increase in regulating the activity of Lin28 (45). A synergistic combination of HIF1α and Notch signaling promotes hiPSC-derived NPC differentiation into astrocytes through DNA demethylation of the glial fibrillary acidic protein– encoding gene (46). Overall, by promoting glycolysis and changing epigenome modifications associated with cell identity, HIF1α influences cell fate toward either pluripotency or differentiation depending on the environmental context. O_2 tension is an environmental driver that modifies metabolism to enable epigenome remodeling and changes in gene expression to influence cell fate.

Lipid metabolism and mitochondrial dynamics in somatic cell reprogramming

Compared with differentiated cells, iPSCs undergo rewiring of energetic and biosynthetic programs as illustrated by the reduction of mitochondrial oxidative stress pathways and rapid lipogenesis (19). For instance, somatic cell reprogramming efficiency is promoted by an increase in key lipogenic enzymes, such as Ac-CoA carboxylase and FA synthase (18, 19).

The *de novo* FA biosynthesis controls reprogramming and pluripotency through shifts in mitochondrial dynamics. Equilibrium toward mitochondrial fission is driven by lipogenic enzyme (ACC1) inhibition of mitochondrial fission factor (FIS1), ubiquitin–proteasome degradation, and the lipid generation (14). Mitochondrial dynamics is further supported by reduction of MFN1/2 and an increase of the mitochondrial protein kinase A–anchoring protein RAB32 involved in mitochondrial fission synchronization (26, 47). Genetic or pharmacological perturbation of MFN1/2 endorses HIF1α stabilization through ROS production and promotes iPSC generation by indirectly favoring a metabolic transition from OXPHOS to glycolysis (26, 48). These findings hint at an interconnected mechanism triangulating lipid metabolism, mitochondrial fission, and a metabolic shift to glycolysis that favors the PSC state (Fig. 1).

Metabolism in pluripotency exit and early differentiation

Metabolic remodeling during PSC differentiation

Spontaneous nondirected hPSC differentiation shows an opposite metabolic shift compared with somatic cell reprogramming. A gradual increase in lactate production associates with an increase in O_2 consumption, mitochondrial biogenesis, and ROS accumulation (2, 11, 49). This progressive metabolic remodeling is partly mediated by UCP2 repression, which enables complete mitochondrial oxidation of pyruvate leading to an increase in OXPHOS (2). An increase in ROS is a direct consequence of increased OXPHOS and is enforced by repression of major antioxidant defenses (11, 49), suggesting a role for oxidative stress in PSC differentiation. Support for this idea comes from mouse ESC (mESC) cardiac differentiation studies that show ROS augmentation through activation of mitogen-activated protein kinase (MAPK) signaling pathways (9, 10, 50). OXPHOS and ROS are also driven by proteins orchestrating mitochondrial dynamics through REX1 repression (27) and the requirement for MFN2 and OPA1 expression during cardiomyocyte differentiation from mESCs (51).

Metabolites supporting pluripotency exit

Although PSCs and cancer cells have a shared metabolic hallmark, aerobic glycolysis or the Warburg effect, a unique mechanism for how this metabolic shift supports pluripotency exit has recently been proposed. A critical point of divergence is that PSCs strategically utilize glycolysis to produce both lactate and cytosolic Ac-CoA by siphoning glucose-derived citrate from the TCA cycle (Fig. 2). Inhibition or promotion of glycolytic Ac-CoA enhances or delays differentiation, respectively, suggesting that Ac-CoA has a key role during the glycolytic switch in pluripotency exit (52). In PSCs, glycolytic Ac-CoA production is through ATP citrate lyase enzyme activity and may consequently fuel histone acetylation. However, in the 1st h of spontaneous differentiation, repression of this enzyme may assist exit-associated epigenome remodeling by reducing substrate for histone acetylases (52).

18
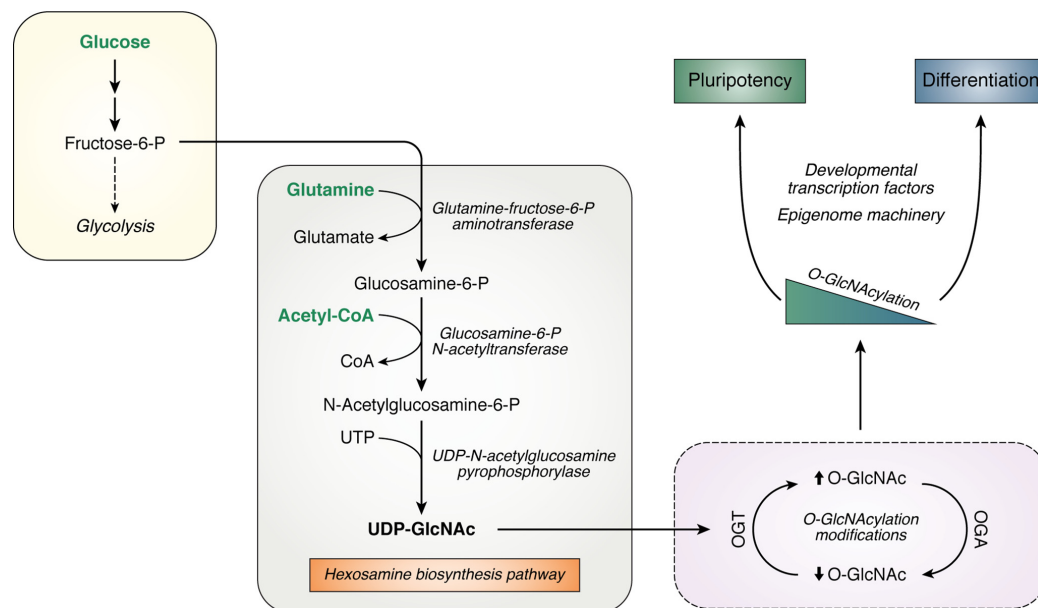
Figure 3. Nutrient-sensing HBP regulates pluripotency and differentiation. A branch of glycolysis fuels the HBP to produce UDP-GlcNAc. Pathway flux depends on levels of macromolecular metabolism, including carbohydrate, lipid, nucleotide, and amino acid biosynthesis. UDP-GlcNAc is a key intermediate for post-translational modification of Ser and Thr residues. The catalytic activity of OGT and OGA determines the level of protein *O*-GlcNAcylation. This modification influences pluripotency and differentiation gene networks via transcriptional and epigenetic machinery.

Metabolic shift kinetics linked with cell fate

In vitro modeling of embryonic tri-lineage differentiation provides insight for metabolic events during early lineage commitment. Substantially diminished glycolytic flux does not occur for all lineages. Sustained high aerobic glycolytic flux is necessary for early ectoderm lineage commitment and expression of ectoderm-specific differentiation genes (53). Conversely, a metabolic shift toward OXPHOS has recently been observed in early mesoderm and endoderm lineage cells and is consistent with an elevated OXPHOS requirement for PSC generation of cardiomyocytes (54). The utilization of other carbon sources and pathway fluxes beyond glucose in early fate outcome remains unexplored.

Hexosamine biosynthesis and fate transitions

The hexosamine biosynthesis pathway (HBP) is a nutrient-sensing pathway that depends on glucose, glutamine, and cytosolic Ac-CoA levels (Fig. 2). HBP branches from glycolysis to produce UDP-GlcNAc as an end product. UDP-GlcNAc is a substrate of *O*-GlcNAc transferase (OGT) for post-translational protein modification by *O*-GlcNAcylation with addition of *O*-linked β-D-GlcNAc (*O*-GlcNAc). The removal of *O*-GlcNAc by *O*-GlcNAcase (OGA) counteracts OGT activity, and this dynamic cycling of protein GlcNAcylation regulates numerous cell processes such as cell cycle, signaling pathways, transcription, and organelle and chromatin dynamics (55).

During development and general differentiation processes, GlcNAcylation is implicated in the regulation of pluripotency and gene silencing (56–62). Manipulation of *O*-GlcNAcylation to elevate *O*-GlcNAc motifs delays mESC differentiation and subsequent generation of cardiomyocytes (56–61). Conversely, a decrease in *O*-GlcNAcylation disrupts self-renewal and reprogramming (57) but promotes differentiation in neuronal cells (63–65). Moreover, CPTFs such as OCT4 and SOX2 harbor an *O*-GlcNAcylation motif that is quickly erased upon differentiation (57). Together, these studies suggest that a high rate of *O*-GlcNAcylation is involved in the maintenance and acquisition of pluripotency, whereas its reduction is linked to pluripotency exit and differentiation. Elevated glucose, glutamine, and Ac-CoA production in PSCs could support enhanced HBP flux to provide substrate for OGT (Fig. 3). CPTF promoter occupancy at the OGA-encoding gene (66, 67) implies a role for protein *O*-GlcNAcylation dynamics in pluripotency. This suggestion is supported by *in vivo* studies showing roles for OGT and OGA during embryogenesis (68–70). Remarkably, high-level *O*-GlcNAcylation was linked with perturbation in glucose homeostasis and neural tube defects in the fetus of diabetic mice (71). Thus, HBP constitutes a direct link between metabolism and protein *O*-GlcNAcylation, with a suggested role in regulating pluripotency dynamics and cell-fate acquisition by regulating TFs and the epigenome remodeling machinery, but this idea requires further study.

Metabolism modulates epigenetic remodeling

Metabolism has key roles for inducing, maintaining, and exiting pluripotency. It is remarkable that major metabolic pathways can influence the activity of multiple epigenome-

modifying enzymes, providing an exciting potential connection to cell-fate plasticity.

TCA cycle–derived metabolites

hPSCs produce cytosolic Ac-CoA from glycolysis, but rapidly lose this activity in early differentiation, which parallels reduced histone acetylation and expression of pluripotency markers coinciding with the expression of early differentiation genes (52). The simultaneous occurrence of these temporal events suggests that a metabolic shift could drive changes in gene expression patterns and cell fate by modulating histone acetylation. A complementary question could be whether metabolism also affects the dynamics of epigenome methylation. One possible connection could be via the TCA cycle metabolites α-ketoglutarate (α-KG) and succinate, respective cofactor and inhibitor for epigenome demethylase remodeling enzymes. α-KG, made from either glucose or glutamine, is a cofactor for Jumonji C-domain containing histone demethylases (JHDM) and ten-eleven–translocase (TET) DNA demethylases that sustain the naïve pluripotent state in mESCs (72). Yet, in the context of early differentiation, increased α-KG levels enhance ectoderm lineage commitment (73), suggesting that metabolism influences chromatin dynamics contextually in pluripotency maintenance or exit.

O-GlcNAcylation

HBP is another potential link between metabolism and epigenome remodeling (Fig. 2). OGT influences DNA methylation and histone modifications by regulating the stabilization, localization, or substrate specificity for specific sets of genes. OGT modifies the epigenome machinery, including TET family enzymes and polycomb group proteins, which are transcriptional repressors that regulate gene expression patterns during embryonic development and differentiation (59). In ESCs, by physically interacting with these proteins, OGT is directed toward the chromatin to influence histone methylation, including H3K4 tri-methylation (H3K4me3), DNA methylation through TET1 interactions, and recruitment of TFs to specific target genes (56–61). Enriched GlcNAc motifs in the catalytic subunit of polycomb complex PRC1 represses neural differentiation genes, whereas this motif is absent on stemness-associated genes, including cell cycle genes (74). Moreover, *O*-GlcNAcylation may be implicated in neural and neuronal cell-fate determination through epigenic modulation by the association of OGT with TET3, resulting in recruitment of NeuroD1 to brain-specific target genes (64). *O*-GlcNAcylation modifications appear to influence the determination of specific neuronal identity. During mESC differentiation, OGA co-localizes with the histone acetyltransferase p300 on the neuropeptide-encoding gene orexin in orexin neurons, whereas OGT co-localizes with histone deacetylase sirtuin 1 (SIRT1) in non-orexin-expressing cells (65). Because of the direct link between HBP and *O*-GlcNAcylation, we propose that metabolic fluctuations induced by specific microenvironmental differentiation drivers, such as hypoxia, could participate in establishing distinct epigenome patterns associated with cell fate and function acquisitions and maintenance.

S-Adenosylmethionine (SAM)

Methyltransferases for histones and DNA depend on the levels of SAM and threonine, which are required for pluripotency. Extracellular threonine in mESCs or methionine in hPSCs are the only amino acids critical for pluripotency and used for SAM production (75, 76). PSCs use internal regulatory systems to maintain intracellular SAM levels that involve p53 and p38 cell cycle and apoptosis regulators (8, 76). mESCs or hPSCs grown in reduced threonine/methionine show spontaneous differentiation and slowed growth (82, 83). Threonine depletion decreases SAM production and influences H3K4me3 levels, suggesting a possible mechanism for how threonine and SAM levels regulate pluripotent cell fate (75).

Ascorbate

Another regulator of histone modifications is ascorbate, the principal form of vitamin C at physiological pH. Ascorbate is an epigenomic regulator of DNA methylation and a modulator of iPSC reprogramming efficiency (77, 78). It is also a cofactor for TET enzymes that catalyze the oxidation of 5-methylcytosine to 5-hydroxymethylcytosine. By contributing to the demethylation of both DNA and histones, ascorbate appears to augment the erasure of epigenetic memory, and in this manner, it enhances stem cell reprogramming (77). Increased ascorbate enhances iPSC generation, which parallels TET1 deficiency in improving reprogramming efficiency. Conversely, TET1 overexpression impairs reprogramming (76). Although TET1 in the absence of ascorbate remains functional, the addition of ascorbate is critical for the epithelial-to-mesenchymal transition during reprogramming to pluripotency (79).

NAD

Cellular NAD level is directly impacted by the metabolic state, such as glycolytic flux, and regulates the activity of NAD$^+$-dependent histone deacetylase sirtuins (Fig. 2), including SIRT1, which is induced in hPSCs (80). SIRT1 controls cell fate by regulating p53-dependent homeobox protein transcription factor NANOG (homeobox protein transcription factor) expression and transcriptional repression of differentiation genes in hPSCs (8, 80, 81). During hESC differentiation, SIRT1 is repressed, leading to acetylation and reactivation of multiple differentiation genes, including *PAX6, TBX3,* and *DLL* (80). Further investigations are required to understand how distinct metabolic shifts during cell-fate conversions influence the NAD$^+$/NADH ratio and, subsequently, how NAD levels impact histone acetylation remodeling events specifically through sirtuin activities.

Metabolism in naïve and primed pluripotency

The pre-implantation blastocyst retains a developmentally unrestricted cell population that differs from its post-implantation counterpart (82). Although the inner cell mass of pre- and post-implantation blastocysts yields ESCs for growth *in vitro* (83, 84), pre-implantation ESCs exist in a naïve or ground pluripotent state, whereas post-implantation ESCs exist in a primed state. Naïve PSCs introduced in the pre-implantation blastocyst can contribute to a chimeric mouse (85), whereas

20

primed PSCs cannot, discerning their distinct developmental potential. Another distinguishing characteristic between these two PSC states is how metabolism fuels the requirements for self-renewal and proliferation. Pre-implantation blastocyst-derived naïve PSCs utilize glycolysis and OXPHOS and then transition to glycolysis dependence in the primed state, despite having functionally mature mitochondria (86). The coordination of TFs Zic3 and Esrrb regulates bivalent metabolism observed in naïve PSCs (87). Naïve PSCs also have a greater glycolytic output compared with primed PSCs (88). Yet, different patterns of glycolysis and OXPHOS could play additional roles beyond supporting higher proliferation in naïve ESCs (89, 90). For instance, an open question is whether dissimilar metabolic profiles between primed and naïve PSCs is implicated in distinct transcriptional patterns and chromatin organization, ultimately influencing respective developmental potentials. This issue will most likely be a relevant topic in the coming years for the field, as illustrated by the studies conveyed below.

Metabolism and the naïve PSC epigenome

Naïve and primed PSCs show structural changes in chromatin structure, including histone and DNA modifications, that have functional consequences in regard to developmental potential through TF expression and suppression of lineage-restrictive genes (91). Although naïve hESCs with properties similar to mESCs have been claimed (85, 89, 90, 92), these cells show some differences in pluripotency markers and functions that probably require more optimized culture and nutrient conditions to improve consistency between species. There is increasing evidence for interactions between the metabolome and epigenome to sustain a global hypo-methylated profile associated with naïve PSCs (93). Mechanistically, glucose- and glutamine-derived TCA cycle metabolite α-KG, acting as a cofactor for JHMD and TET proteins (Fig. 2), sustains the naïve state in mESCs by global hypo-methylation (72). Additionally, as mentioned previously, HBP couples macromolecular metabolism to *O*-GlcNAc modifications on proteins, including epigenetic modifiers (Fig. 3) (94). Cycling of these post-translational modifications by OGT and OGA are required for naïve and primed state induction, maintenance, and differentiation (56, 95). OGT interacts with TET1 enzymes preferentially at transcription start sites, thereby influencing gene expression (58). This may implicate OGT in globally regulating the DNA hypomethylation profile in naïve compared with primed PSCs. As such, the *O*-GlcNAcylation cycle could have a role in the observed differences of X-chromosome inactivation in primed state female ESCs (97). Thus, a potential link between OGT and X-chromosome inactivation may have functional relevance in the context of naïve and primed PSCs (94).

Moreover, naïve to primed epigenetic transitions are partly mediated by nicotinamide *N*-methyltransferase (NNMT), which decreases H3K27me3. By consuming SAM and up-regulating Wnt signaling, NNMT prevents histone methylation in the naïve state (98). In addition to the role of ascorbate in reprogramming (84, 85), a combination of ascorbate and retinol has been shown to enhance naïve state acquisition by increasing TET expression and catalysis (99). In contrast, high ratios of L-proline to ascorbate prevents naïve state maintenance,

although the mechanism(s) by which L-proline induces epigenetic changes has yet to be elucidated (96). Collectively, these studies suggest a role for metabolism in influencing naïve *versus* primed pluripotency dynamics by facilitating chromatin remodeling through multiple specific metabolites.

Conclusions

Accumulating evidence illustrates the influence of metabolism on differentiation plasticity by regulating the epigenetic machinery. Our current understanding provides a foundation for further investigations into links between environmental stimuli and subsequent metabolic adaptations that orchestrate epigenome remodeling events, which ultimately drive cell fate. A key open question is what recruits epigenome remodelers, co-factors, and substrates to specific loci to influence patterns of pluripotent and somatic cell gene expression. Here, we suggest that HBP may have a role by acting at crucial nodes connecting metabolism and epigenome remodeling. Answers to fundamental questions raised here will provide a deeper basis for generating safe and accessible PSC-derived cells for use in regenerative medicine, disease modeling, and drug screening applications in the future.

References

1. Houghton, F. D., Thompson, J. G., Kennedy, C. J., and Leese, H. J. (1996) Oxygen consumption and energy metabolism of the early mouse embryo. *Mol. Reprod. Dev.* **44,** 476–485 CrossRef Medline
2. Zhang, J., Khvorostov, I., Hong, J. S., Oktay, Y., Vergnes, L., Nuebel, E., Wahjudi, P. N., Setoguchi, K., Wang, G., Do, A., Jung, H. J., McCaffery, J. M., Kurland, I. J., Reue, K., Lee, W. N., *et al.* (2011) UCP2 regulates energy metabolism and differentiation potential of human pluripotent stem cells. *EMBO J.* **30,** 4860–4873 CrossRef Medline
3. Chung, S., Dzeja, P. P., Faustino, R. S., Perez-Terzic, C., Behfar, A., and Terzic, A. (2007) Mitochondrial oxidative metabolism is required for the cardiac differentiation of stem cells. *Nat. Clin. Pract. Cardiovasc. Med.* **4,** Suppl. 1, S60–67 CrossRef Medline
4. Prigione, A., Fauler, B., Lurz, R., Lehrach, H., and Adjaye, J. (2010) The senescence-related mitochondrial/oxidative stress pathway is repressed in human induced pluripotent stem cells. *Stem Cells* **28,** 721–733 CrossRef Medline
5. Varum, S., Rodrigues, A. S., Moura, M. B., Momcilovic, O., Easley C. A., 4th., Ramalho-Santos, J., Van Houten, B., and Schatten, G. (2011) Energy metabolism in human pluripotent stem cells and their differentiated counterparts. *PLoS ONE* **6,** e20914 CrossRef Medline
6. Fischer, B., and Bavister, B. D. (1993) Oxygen tension in the oviduct and uterus of rhesus monkeys, hamsters and rabbits. *J. Reprod. Fertil.* **99,** 673–679 CrossRef Medline
7. Madden, D. T., Davila-Kruger, D., Melov, S., and Bredesen, D. E. (2011) Human embryonic stem cells express elevated levels of multiple pro-apoptotic BCL-2 family members. *PLoS ONE* **6,** e28530 CrossRef Medline
8. Setoguchi, K., TeSlaa, T., Koehler, C. M., and Teitell, M. A. (2016) P53 regulates rapid apoptosis in human pluripotent stem cells. *J. Mol. Biol.* **428,** 1465–1475 CrossRef Medline
9. Crespo, F. L., Sobrado, V. R., Gomez, L., Cervera, A. M., and McCreath, K. J. (2010) Mitochondrial reactive oxygen species mediate cardiomyocyte formation from embryonic stem cells in high glucose. *Stem Cells* **28,** 1132–1142 CrossRef Medline
10. Xiao, Q., Luo, Z., Pepe, A. E., Margariti, A., Zeng, L., and Xu, Q. (2009) Embryonic stem cell differentiation into smooth muscle cells is mediated by Nox4-produced H2O2. *Am. J. Physiol. Cell Physiol.* **296,** C711–C723 CrossRef Medline
11. Cho, Y. M., Kwon, S., Pak, Y. K., Seol, H. W., Choi, Y. M., Park, D. J., Park, K. S., and Lee, H. K. (2006) Dynamic changes in mitochondrial biogenesis and antioxidant enzymes during the spontaneous differentiation of hu-

man embryonic stem cells. *Biochem. Biophys. Res. Commun.* **348,** 1472–1478 CrossRef Medline

12. Tohyama, S., Fujita, J., Hishiki, T., Matsuura, T., Hattori, F., Ohno, R., Kanazawa, H., Seki, T., Nakajima, K., Kishino, Y., Okada, M., Hirano, A., Kuroda, T., Yasuda, S., Sato, Y., *et al.* (2016) Glutamine oxidation is indispensable for survival of human pluripotent stem cells. *Cell Metab.* **23,** 663–674 CrossRef Medline

13. Zhang, H., Badur, M. G., Divakaruni, A. S., Parker, S. J., Jäger, C., Hiller, K., Murphy, A. N., and Metallo, C. M. (2016) Distinct metabolic states can support self-renewal and lipogenesis in human pluripotent stem cells under different culture conditions. *Cell Rep.* **16,** 1536–1547 CrossRef Medline

14. Wang, L., Zhang, T., Wang, L., Cai, Y., Zhong, X., He, X., Hu, L., Tian, S., Wu, M., Hui, L., Zhang, H., and Gao, P. (2017) Fatty acid synthesis is critical for stem cell pluripotency via promoting mitochondrial fission. *EMBO J.* **36,** 1330–1347 CrossRef Medline

15. Green, D. R., and Kroemer, G. (2004) The pathophysiology of mitochondrial cell death. *Science* **305,** 626–629 CrossRef Medline

16. Armstrong, L., Tilgner, K., Saretzki, G., Atkinson, S. P., Stojkovic, M., Moreno, R., Przyborski, S., and Lako, M. (2010) Human induced pluripotent stem cell lines show stress defense mechanisms and mitochondrial regulation similar to those of human embryonic stem cells. *Stem Cells* **28,** 661–673 CrossRef Medline

17. Schieke, S. M., Ma, M., Cao, L., McCoy, J. P., Jr., Liu, C., Hensel, N. F., Barrett, A. J., Boehm, M., and Finkel, T. (2008) Mitochondrial metabolism modulates differentiation and teratoma formation capacity in mouse embryonic stem cells. *J. Biol. Chem.* **283,** 28506–28512 CrossRef Medline

18. Wu, Y., Chen, K., Liu, X., Huang, L., Zhao, D., Li, L., Gao, M., Pei, D., Wang, C., and Liu, X. (2016) Srebp-1 interacts with c-Myc to enhance somatic cell reprogramming. *Stem Cells* **34,** 83–92 CrossRef Medline

19. Vazquez-Martin, A., Corominas-Faja, B., Cufi, S., Vellon, L., Oliveras-Ferraros, C., Menendez, O. J., Joven, J., Lupu, R., and Menendez, J. A. (2013) The mitochondrial H(+)-ATP synthase and the lipogenic switch: new core components of metabolic reprogramming in induced pluripotent stem (iPS) cells. *Cell Cycle* **12,** 207–218 CrossRef Medline

20. Kim, H., Jang, H., Kim, T. W., Kang, B. H., Lee, S. E., Jeon, Y. K., Chung, D. H., Choi, J., Shin, J., Cho, E. J., and Youn, H. D. (2015) Core pluripotency factors directly regulate metabolism in embryonic stem cell to maintain pluripotency. *Stem Cells* **33,** 2699–2711 CrossRef Medline

21. Folmes, C. D., Nelson, T. J., Martinez-Fernandez, A., Arrell, D. K., Lindor, J. Z., Dzeja, P. P., Ikeda, Y., Perez-Terzic, C., and Terzic, A. (2011) Somatic oxidative bioenergetics transitions into pluripotency-dependent glycolysis to facilitate nuclear reprogramming. *Cell Metab.* **14,** 264–271 CrossRef Medline

22. Vozza, A., Parisi, G., De Leonardis, F., Lasorsa, F. M., Castegna, A., Amorese, D., Marmo, R., Calcagnile, V. M., Palmieri, L., Ricquier, D., Paradies, E., Scarcia, P., Palmieri, F., Bouillaud, F., and Fiermonte, G. (2014) UCP2 transports C4 metabolites out of mitochondria, regulating glucose and glutamine oxidation. *Proc. Natl. Acad. Sci. U.S.A.* **111,** 960–965 CrossRef Medline

23. Schell, J. C., Olson, K. A., Jiang, L., Hawkins, A. J., Van Vranken, J. G., Xie, J., Egnatchik, R. A., Earl, E. G., DeBerardinis, R. J., and Rutter, J. (2014) A role for the mitochondrial pyruvate carrier as a repressor of the Warburg effect and colon cancer cell growth. *Mol. Cell* **56,** 400–413 CrossRef Medline

24. Flores, A., Schell, J., Krall, A. S., Jelinek, D., Miranda, M., Grigorian, M., Braas, D., White, A. C., Zhou, J. L., Graham, N. A., Graeber, T., Seth, P., Evseenko, D., Coller, H. A., Rutter, J., *et al.* (2017) Lactate dehydrogenase activity drives hair follicle stem cell activation. *Nat. Cell Biol.* **19,** 1017–1026 CrossRef Medline

25. Schell, J. C., Wisidagama, D. R., Bensard, C., Zhao, H., Wei, P., Tanner, J., Flores, A., Mohlman, J., Sorensen, L. K., Earl, C. S., Olson, K. A., Miao, R., Waller, T. C., Delker, D., Kanth, P., *et al.* (2017) Control of intestinal stem cell function and proliferation by mitochondrial pyruvate metabolism. *Nat. Cell Biol.* **19,** 1027–1036 CrossRef Medline

26. Son, M. J., Kwon, Y., Son, M. Y., Seol, B., Choi, H. S., Ryu, S. W., Choi, C., and Cho, Y. S. (2015) Mitofusins deficiency elicits mitochondrial metabolic reprogramming to pluripotency. *Cell Death Differ.* **22,** 1957–1969 CrossRef Medline

27. Son, M. Y., Choi, H., Han, Y. M., and Cho, Y. S. (2013) Unveiling the critical role of REX1 in the regulation of human stem cell pluripotency. *Stem Cells* **31,** 2374–2387 CrossRef Medline

28. Guido, C., Whitaker-Menezes, D., Lin, Z., Pestell, R. G., Howell, A., Zimmers, T. A., Casimiro, M. C., Aquila, S., Ando' S., Martinez-Outschoorn, U. E., Sotgia, F., and Lisanti, M. P. (2012) Mitochondrial fission induces glycolytic reprogramming in cancer-associated myofibroblasts, driving stromal lactate production, and early tumor growth. *Oncotarget* **3,** 798–810 Medline

29. Panopoulos, A. D., Yanes, O., Ruiz, S., Kida, Y. S., Diep, D., Tautenhahn, R., Herrerías, A., Batchelder, E. M., Plongthongkum, N., Lutz, M., Berggren, W. T., Zhang, K., Evans, R. M., Siuzdak, G., and Izpisua Belmonte, J. C. (2012) The metabolome of induced pluripotent stem cells reveals metabolic changes occurring in somatic cell reprogramming. *Cell Res.* **22,** 168–177 CrossRef Medline

30. Zhang, J., Nuebel, E., Daley, G. Q., Koehler, C. M., and Teitell, M. A. (2012) Metabolic regulation in pluripotent stem cells during reprogramming and self-renewal. *Cell Stem Cell* **11,** 589–595 CrossRef Medline

31. Cacchiarelli, D., Trapnell, C., Ziller, M. J., Soumillon, M., Cesana, M., Karnik, R., Donaghey, J., Smith, Z. D., Ratanasirintrawoot, S., Zhang, X., Ho Sui, S. J., Wu, Z., Akopian, V., Gifford, C. A., Doench, J., *et al.* (2015) Integrative analyses of human reprogramming reveal dynamic nature of induced pluripotency. *Cell* **162,** 412–424 CrossRef Medline

32. Hansson, J., Rafiee, M. R., Reiland, S., Polo, J. M., Gehring, J., Okawa, S., Huber, W., Hochedlinger, K., and Krijgsveld, J. (2012) Highly coordinated proteome dynamics during reprogramming of somatic cells to pluripotency. *Cell Rep.* **2,** 1579–1592 CrossRef Medline

33. Prigione, A., Rohwer, N., Hoffmann, S., Mlody, B., Drews, K., Bukowiecki, R., Blümlein, K., Wanker, E. E., Ralser, M., Cramer, T., and Adjaye, J. (2014) HIF1α modulates cell fate reprogramming through early glycolytic shift and upregulation of PDK1–3 and PKM2. *Stem Cells* **32,** 364–376 CrossRef Medline

34. Mathieu, J., Zhou, W., Xing, Y., Sperber, H., Ferreccio, A., Agoston, Z., Kuppusamy, K. T., Moon, R. T., and Ruohola-Baker, H. (2014) Hypoxia-inducible factors have distinct and stage-specific roles during reprogramming of human cells to pluripotency. *Cell Stem Cell* **14,** 592–605 CrossRef Medline

35. Kida, Y. S., Kawamura, T., Wei, Z., Sogo, T., Jacinto, S., Shigeno, A., Kushige, H., Yoshihara, E., Liddle, C., Ecker, J. R., Yu, R. T., Atkins, A. R., Downes, M., and Evans, R. M. (2015) ERRs mediate a metabolic switch required for somatic cell reprogramming to pluripotency. *Cell Stem Cell* **16,** 547–555 CrossRef Medline

36. Hawkins, K. E., Joy, S., Delhove, J. M., Kotiadis, V. N., Fernandez, E., Fitzpatrick, L. M., Whiteford, J. R., King, P. J., Bolanos, J. P., Duchen, M. R., Waddington, S. N., and McKay, T. R. (2016) NRF2 orchestrates the metabolic shift during induced pluripotent stem cell reprogramming. *Cell Rep.* **14,** 1883–1891 CrossRef Medline

37. Marión, R. M., Strati, K., Li, H., Murga, M., Blanco, R., Ortega, S., Fernandez-Capetillo, O., Serrano, M., and Blasco, M. A. (2009) A p53-mediated DNA damage response limits reprogramming to ensure iPS cell genomic integrity. *Nature* **460,** 1149–1153 CrossRef Medline

38. Kawamura, T., Suzuki, J., Wang, Y. V., Menendez, S., Morera, L. B., Raya, A., Wahl, G. M., and Izpisúa Belmonte, J. C. (2009) Linking the p53 tumour suppressor pathway to somatic cell reprogramming. *Nature* **460,** 1140–1144 CrossRef Medline

39. Hong, H., Takahashi, K., Ichisaka, T., Aoi, T., Kanagawa, O., Nakagawa, M., Okita, K., and Yamanaka, S. (2009) Suppression of induced pluripotent stem cell generation by the p53–p21 pathway. *Nature* **460,** 1132–1135 CrossRef Medline

40. Utikal, J., Polo, J. M., Stadtfeld, M., Maherali, N., Kulalert, W., Walsh, R. M., Khalil, A., Rheinwald, J. G., and Hochedlinger, K. (2009) Immortalization eliminates a roadblock during cellular reprogramming into iPS cells. *Nature* **460,** 1145–1148 CrossRef Medline

41. Yoshida, Y., Takahashi, K., Okita, K., Ichisaka, T., and Yamanaka, S. (2009) Hypoxia enhances the generation of induced pluripotent stem cells. *Cell Stem Cell* **5,** 237–241 CrossRef Medline

SASBMB

J. Biol. Chem. (2019) 294(14) 5420–5429 **5427**

22

42. Mathieu, J., Zhang, Z., Nelson, A., Lamba, D. A., Reh, T. A., Ware, C., and Ruohola-Baker, H. (2013) Hypoxia induces re-entry of committed cells into pluripotency. *Stem Cells* **31,** 1737–1748 CrossRef Medline

43. Bae, D., Mondragon-Teran, P., Hernandez, D., Ruban, L., Mason, C., Bhattacharya, S. S., and Veraitch, F. S. (2012) Hypoxia enhances the generation of retinal progenitor cells from human induced pluripotent and embryonic stem cells. *Stem Cells Dev.* **21,** 1344–1355 CrossRef Medline

44. Pimton, P., Lecht, S., Stabler, C. T., Johannes, G., Schulman, E. S., and Lelkes, P. I. (2015) Hypoxia enhances differentiation of mouse embryonic stem cells into definitive endoderm and distal lung cells. *Stem Cells Dev.* **24,** 663–676 CrossRef Medline

45. Xie, Y., Zhang, J., Lin, Y., Gaeta, X., Meng, X., Wisidagama, D. R., Cinkornpumin, J., Koehler, C. M., Malone, C. S., Teitell, M. A., and Lowry, W. E. (2014) Defining the role of oxygen tension in human neural progenitor fate. *Stem Cell Rep.* **3,** 743–757 CrossRef

46. Yasui, T., Uezono, N., Nakashima, H., Noguchi, H., Matsuda, T., Noda-Andoh, T., Okano, H., and Nakashima, K. (2017) Hypoxia epigenetically confers astrocytic differentiation potential on human pluripotent cell-derived neural precursor cells. *Stem Cell Rep.* **8,** 1743–1756 CrossRef

47. Pei, Y., Yue, L., Zhang, W., Wang, Y., Wen, B., Zhong, L., Xiang, J., Li, J., Zhang, S., Wang, H., Mu, H., Wei, Q., and Han, J. (2015) Improvement in Mouse iPSC induction by Rab32 reveals the importance of lipid metabolism during reprogramming. *Sci. Rep.* **5,** 16539 CrossRef Medline

48. Son, M. J., Jeong, B. R., Kwon, Y., and Cho, Y. S. (2013) Interference with the mitochondrial bioenergetics fuels reprogramming to pluripotency via facilitation of the glycolytic transition. *Int. J. Biochem. Cell Biol.* **45,** 2512–2518 CrossRef Medline

49. Saretzki, G., Walter, T., Atkinson, S., Passos, J. F., Bareth, B., Keith, W. N., Stewart, R., Hoare, S., Stojkovic, M., Armstrong, L., von Zglinicki, T., and Lako, M. (2008) Downregulation of multiple stress defense mechanisms during differentiation of human embryonic stem cells. *Stem Cells* **26,** 455–464 CrossRef Medline

50. Schmelter, M., Ateghang, B., Helmig, S., Wartenberg, M., and Sauer, H. (2006) Embryonic stem cells utilize reactive oxygen species as transducers of mechanical strain-induced cardiovascular differentiation. *FASEB J.* **20,** 1182–1184 CrossRef Medline

51. Kasahara, A., Cipolat, S., Chen, Y., Dorn, G. W., 2nd., and Scorrano, L. (2013) Mitochondrial fusion directs cardiomyocyte differentiation via calcineurin and Notch signaling. *Science* **342,** 734–737 CrossRef Medline

52. Moussaieff, A., Rouleau, M., Kitsberg, D., Cohen, M., Levy, G., Barasch, D., Nemirovski, A., Shen-Orr, S., Laevsky, I., Amit, M., Bomze, D., Elena-Herrmann, B., Scherf, T., Nissim-Rafinia, M., Kempa, S., *et al.* (2015) Glycolysis-mediated changes in acetyl-CoA and histone acetylation control the early differentiation of embryonic stem cells. *Cell Metab.* **21,** 392–402 CrossRef Medline

53. Cliff, T. S., Wu, T., Boward, B. R., Yin, A., Yin, H., Glushka, J. N., Prestegaard, J. H., and Dalton, S. (2017) MYC Controls human pluripotent stem cell fate decisions through regulation of metabolic flux. *Cell Stem Cell* **21,** 502–516.e9 CrossRef Medline

54. Teslaa, T., and Teitell, M. A. (2014) Pluripotent stem cell energy metabolism: an update. *EMBO J.* **34,** 138–153 CrossRef Medline

55. Yang, X., and Qian, K. (2017) Protein *O*-GlcNAcylation: emerging mechanisms and functions. *Nat. Rev. Mol. Cell Biol.* **18,** 452–465 CrossRef Medline

56. Speakman, C. M., Domke, T. C., Wongpaiboonwattana, W., Sanders, K., Mudaliar, M., van Aalten, D. M., Barton, G. J., and Stavridis, M. P. (2014) Elevated *O*-GlcNAc levels activate epigenetically repressed genes and delay mouse ESC differentiation without affecting naive to primed cell transition. *Stem Cells* **32,** 2605–2615 CrossRef Medline

57. Jang, H., Kim, T. W., Yoon, S., Choi, S. Y., Kang, T. W., Kim, S. Y., Kwon, Y. W., Cho, E. J., and Youn, H. D. (2012) *O*-GlcNAc regulates pluripotency and reprogramming by directly acting on core components of the pluripotency network. *Cell Stem Cell* **11,** 62–74 CrossRef Medline

58. Vella, P., Scelfo, A., Jammula, S., Chiacchiera, F., Williams, K., Cuomo, A., Roberto, A., Christensen, J., Bonaldi, T., Helin, K., and Pasini, D. (2013) Tet proteins connect the *O*-linked *N*-acetylglucosamine transferase Ogt to chromatin in embryonic stem cells. *Mol. Cell* **49,** 645–656 CrossRef Medline

59. Hardivillé, S., and Hart, G. W. (2016) Nutrient regulation of gene expression by *O*-GlcNAcylation of chromatin. *Curr. Opin. Chem. Biol.* **33,** 88–94 CrossRef Medline

60. Shi, F. T., Kim, H., Lu, W., He, Q., Liu, D., Goodell, M. A., Wan, M., and Songyang, Z. (2013) Ten-eleven translocation 1 (Tet1) is regulated by *O*-linked *N*-acetylglucosamine transferase (Ogt) for target gene repression in mouse embryonic stem cells. *J. Biol. Chem.* **288,** 20776–20784 CrossRef Medline

61. Constable, S., Lim, J. M., Vaidyanathan, K., and Wells, L. (2017) *O*-GlcNAc transferase regulates transcriptional activity of human Oct4. *Glycobiology* **27,** 927–937 CrossRef Medline

62. van den Berg, D. L., Snoek, T., Mullin, N. P., Yates, A., Bezstarosti, K., Demmers, J., Chambers, I., and Poot, R. A. (2010) An Oct4-centered protein interaction network in embryonic stem cells. *Cell Stem Cell* **6,** 369–381 CrossRef Medline

63. Andres, L. M., Blong, I. W., Evans, A. C., Rumachik, N. G., Yamaguchi, T., Pham, N. D., Thompson, P., Kohler, J. J., and Bertozzi, C. R. (2017) Chemical modulation of protein *O*-GlcNAcylation via OGT inhibition promotes human neural cell differentiation. *ACS Chem. Biol.* **12,** 2030–2039 CrossRef Medline

64. Kizuka, Y., Kitazume, S., Okahara, K., Villagra, A., Sotomayor, E. M., and Taniguchi, N. (2014) Epigenetic regulation of a brain-specific glycosyltransferase *N*-acetylglucosaminyltransferase-IX (GnT-IX) by specific chromatin modifiers. *J. Biol. Chem.* **289,** 11253–11261 CrossRef Medline

65. Hayakawa, K., Hirosawa, M., Tabei, Y., Arai, D., Tanaka, S., Murakami, N., Yagi, S., and Shiota, K. (2013) Epigenetic switching by the metabolism-sensing factors in the generation of orexin neurons from mouse embryonic stem cells. *J. Biol. Chem.* **288,** 17099–17110 CrossRef Medline

66. Boyer, L. A., Lee, T. I., Cole, M. F., Johnstone, S. E., Levine, S. S., Zucker, J. P., Guenther, M. G., Kumar, R. M., Murray, H. L., Jenner, R. G., Gifford, D. K., Melton, D. A., Jaenisch, R., and Young, R. A. (2005) Core transcriptional regulatory circuitry in human embryonic stem cells. *Cell* **122,** 947–956 CrossRef Medline

67. Lee, T. I., Jenner, R. G., Boyer, L. A., Guenther, M. G., Levine, S. S., Kumar, R. M., Chevalier, B., Johnstone, S. E., Cole, M. F., Isono, K., Koseki, H., Fuchikami, T., Abe, K., Murray, H. L., Zucker, J. P., *et al.* (2006) Control of developmental regulators by Polycomb in human embryonic stem cells. *Cell* **125,** 301–313 CrossRef Medline

68. Shafi, R., Iyer, S. P., Ellies, L. G., O'Donnell, N., Marek, K. W., Chui, D., Hart, G. W., and Marth, J. D. (2000) The *O*-GlcNAc transferase gene resides on the X chromosome and is essential for embryonic stem cell viability and mouse ontogeny. *Proc. Natl. Acad. Sci. U.S.A.* **97,** 5735–5739 CrossRef Medline

69. Yang, Y. R., Song, M., Lee, H., Jeon, Y., Choi, E. J., Jang, H. J., Moon, H. Y., Byun, H. Y., Kim, E. K., Kim, D. H., Lee, M. N., Koh, A., Ghim, J., Choi, J. H., Lee-Kwon, W., *et al.* (2012) *O*-GlcNAcase is essential for embryonic development and maintenance of genomic stability. *Aging Cell* **11,** 439–448 CrossRef Medline

70. Olivier-Van Stichelen, S., Wang, P., Comly, M., Love, D. C., and Hanover, J. A. (2017) Nutrient-driven *O*-linked *N*-acetylglucosamine (*O*-GlcNAc) cycling impacts neurodevelopmental timing and metabolism. *J. Biol. Chem.* **292,** 6076–6085 CrossRef Medline

71. Kim, G., Cao, L., Reece, E. A., and Zhao, Z. (2017) Impact of protein *O*-GlcNAcylation on neural tube malformation in diabetic embryopathy. *Sci. Rep.* **7,** 11107 CrossRef Medline

72. Carey, B. W., Finley, L. W., Cross, J. R., Allis, C. D., and Thompson, C. B. (2015) Intracellular α-ketoglutarate maintains the pluripotency of embryonic stem cells. *Nature* **518,** 413–416 CrossRef Medline

73. TeSlaa, T., Chaikovsky, A. C., Lipchina, I., Escobar, S. L., Hochedlinger, K., Huang, J., Graeber, T. G., Braas, D., and Teitell, M. A. (2016) α-Ketoglutarate accelerates the initial differentiation of primed human pluripotent stem cells. *Cell Metab.* **24,** 485–493 CrossRef Medline

74. Maury, J. J., El Farran, C. A., Ng, D., Loh, Y. H., Bi, X., Bardor, M., and Choo, A. B. (2015) RING1B *O*-GlcNAcylation regulates gene targeting of polycomb repressive complex 1 in human embryonic stem cells. *Stem Cell Res.* **15,** 182–189 CrossRef Medline

75. Shyh-Chang, N., Locasale, J. W., Lyssiotis, C. A., Zheng, Y., Teo, R. Y., Ratanasirintrawoot, S., Zhang, J., Onder, T., Unternaehrer, J. J., Zhu, H.,

23

Asara, J. M., Daley, G. Q., and Cantley, L. C. (2013) Influence of threonine metabolism on *S*-adenosylmethionine and histone methylation. *Science* **339,** 222–226 CrossRef Medline

76. Shiraki, N., Shiraki, Y., Tsuyama, T., Obata, F., Miura, M., Nagae, G., Aburatani, H., Kume, K., Endo, F., and Kume, S. (2014) Methionine metabolism regulates maintenance and differentiation of human pluripotent stem cells. *Cell Metab.* **19,** 780–794 CrossRef Medline

77. Hore, T. A., von Meyenn, F., Ravichandran, M., Bachman, M., Ficz, G., Oxley, D., Santos, F., Balasubramanian, S., Jurkowski, T. P., and Reik, W. (2016) Retinol and ascorbate drive erasure of epigenetic memory and enhance reprogramming to naive pluripotency by complementary mechanisms. *Proc. Natl. Acad. Sci. U.S.A.* **113,** 12202–12207 CrossRef Medline

78. Esteban, M. A., Wang, T., Qin, B., Yang, J., Qin, D., Cai, J., Li, W., Weng, Z., Chen, J., Ni, S., Chen, K., Li, Y., Liu, X., Xu, J., Zhang, S., *et al.* (2010) Vitamin C enhances the generation of mouse and human induced pluripotent stem cells. *Cell Stem Cell* **6,** 71–79 CrossRef Medline

79. Chen, J., Guo, L., Zhang, L., Wu, H., Yang, J., Liu, H., Wang, X., Hu, X., Gu, T., Zhou, Z., Liu, J., Liu, J., Wu, H., Mao, S. Q., Mo, K., *et al.* (2013) Vitamin C modulates TET1 function during somatic cell reprogramming. *Nat. Genet.* **45,** 1504–1509 CrossRef Medline

80. Calvanese, V., Lara, E., Suárez-Alvarez, B., Abu Dawud, R., Vázquez-Chantada, M., Martínez-Chantar, M. L., Embade, N., López-Nieva, P., Horrillo, A., Hmadcha, A., Soria, B., Piazzolla, D., Herranz, D., Serrano, M., Mato, J. M., *et al.* (2010) Sirtuin 1 regulation of developmental genes during differentiation of stem cells. *Proc. Natl. Acad. Sci. U.S.A.* **107,** 13736–13741 CrossRef Medline

81. Pawlowski, M., Ortmann, D., Bertero, A., Tavares, J. M., Pedersen, R. A., Vallier, L., and Kotter, M. R. (2017) Inducible and deterministic forward programming of human pluripotent stem cells into neurons, skeletal myocytes, and oligodendrocytes. *Stem Cell Rep.* **8,** 803–812 CrossRef

82. Tesar, P. J., Chenoweth, J. G., Brook, F. A., Davies, T. J., Evans, E. P., Mack, D. L., Gardner, R. L., and McKay, R. D. (2007) New cell lines from mouse epiblast share defining features with human embryonic stem cells. *Nature* **448,** 196–199 CrossRef Medline

83. Thomson, J. A., Itskovitz-Eldor, J., Shapiro, S. S., Waknitz, M. A., Swiergiel, J. J., and Marshall, V. S. (1998) Embryonic stem cell lines derived from human blastocysts. *Science* **282,** 1145–1147 Medline

84. Evans, M. J., and Kaufman, M. H. (1981) Establishment in culture of pluripotential cells from mouse embryos. *Nature* **292,** 154–156 CrossRef Medline

85. Gafni, O., Weinberger, L., Mansour, A. A., Manor, Y. S., Chomsky, E., Ben-Yosef, D., Kalma, Y., Viukov, S., Maza, I., Zviran, A., Rais, Y., Shipony, Z., Mukamel, Z., Krupalnik, V., Zerbib, M., *et al.* (2013) Derivation of novel human ground state naive pluripotent stem cells. *Nature* **504,** 282–286 CrossRef Medline

86. Zhou, W., Choi, M., Margineantu, D., Margaretha, L., Hesson, J., Cavanaugh, C., Blau, C. A., Horwitz, M. S., Hockenbery, D., Ware, C., and Ruohola-Baker, H. (2012) HIF1α induced switch from bivalent to exclusively glycolytic metabolism during ESC-to-EpiSC/hESC transition. *EMBO J.* **31,** 2103–2116 CrossRef Medline

87. Sone, M., Morone, N., Nakamura, T., Tanaka, A., Okita, K., Woltjen, K., Nakagawa, M., Heuser, J. E., Yamada, Y., Yamanaka, S., and Yamamoto, T. (2017) Hybrid cellular metabolism coordinated by Zic3 and Esrrb syner-

gistically enhances induction of naive pluripotency. *Cell Metab.* **25,** 1103–1117.e6 CrossRef Medline

88. Gu, W., Gaeta, X., Sahakyan, A., Chan, A. B., Hong, C. S., Kim, R., Braas, D., Plath, K., Lowry, W. E., and Christofk, H. R. (2016) Glycolytic metabolism plays a functional role in regulating human pluripotent stem cell state. *Cell Stem Cell* **19,** 476–490 CrossRef Medline

89. Ware, C. B., Nelson, A. M., Mecham, B., Hesson, J., Zhou, W., Jonlin, E. C., Jimenez-Caliani, A. J., Deng, X., Cavanaugh, C., Cook, S., Tesar, P. J., Okada, J., Margaretha, L., Sperber, H., Choi, M., *et al.* (2014) Derivation of naive human embryonic stem cells. *Proc. Natl. Acad. Sci. U.S.A.* **111,** 4484–4489 CrossRef Medline

90. Hanna, J., Cheng, A. W., Saha, K., Kim, J., Lengner, C. J., Soldner, F., Cassady, J. P., Muffat, J., Carey, B. W., and Jaenisch, R. (2010) Human embryonic stem cells with biological and epigenetic characteristics similar to those of mouse ESCs. *Proc. Natl. Acad. Sci. U.S.A.* **107,** 9222–9227 CrossRef Medline

91. Bernstein, B. E., Mikkelsen, T. S., Xie, X., Kamal, M., Huebert, D. J., Cuff, J., Fry, B., Meissner, A., Wernig, M., Plath, K., Jaenisch, R., Wagschal, A., Feil, R., Schreiber, S. L., and Lander, E. S. (2006) A bivalent chromatin structure marks key developmental genes in embryonic stem cells. *Cell* **125,** 315–326 CrossRef Medline

92. Takashima, Y., Guo, G., Loos, R., Nichols, J., Ficz, G., Krueger, F., Oxley, D., Santos, F., Clarke, J., Mansfield, W., Reik, W., Bertone, P., and Smith, A. (2015) Resetting transcription factor control circuitry toward ground-state pluripotency in human. *Cell* **162,** 452–453 CrossRef Medline

93. Leitch, H. G., McEwen, K. R., Turp, A., Encheva, V., Carroll, T., Grabole, N., Mansfield, W., Nashun, B., Knezovich, J. G., Smith, A., Surani, M. A., and Hajkova, P. (2013) Naive pluripotency is associated with global DNA hypomethylation. *Nat. Struct. Mol. Biol.* **20,** 311–316 CrossRef Medline

94. Hanover, J. A., Krause, M. W., and Love, D. C. (2012) Linking metabolism to epigenetics through *O*-GlcNAcylation. *Nat. Rev. Mol. Cell Biol.* **13,** 312–321 CrossRef Medline

95. Miura, T., and Nishihara, S. (2016) *O*-GlcNAc is required for the survival of primed pluripotent stem cells and their reversion to the naïve state. *Biochem. Biophys. Res. Commun.* **480,** 655–661 CrossRef Medline

96. D'Aniello, C., Habibi, E., Cermola, F., Paris, D., Russo, F., Fiorenzano, A., Di Napoli, G., Melck, D. J., Cobellis, G., Angelini, C., Fico, A., Blelloch, R., Motta, A., Stunnenberg, H. G., De Cesare, D., *et al.* (2017) Vitamin C and L-proline antagonistic effects capture alternative states in the pluripotency continuum. *Stem Cell Rep.* **8,** 1–10 CrossRef

97. Shen, Y., Matsuno, Y., Fouse, S. D., Rao, N., Root, S., Xu, R., Pellegrini, M., Riggs, A. D., and Fan, G. (2008) X-inactivation in female human embryonic stem cells is in a nonrandom pattern and prone to epigenetic alterations. *Proc. Natl. Acad. Sci. U.S.A.* **105,** 4709–4714 CrossRef Medline

98. Sperber, H., Mathieu, J., Wang, Y., Ferreccio, A., Hesson, J., Xu, Z., Fischer, K. A., Devi, A., Detraux, D., Gu, H., Battle, S. L., Showalter, M., Valensisi, C., Bielas, J. H., Ericson, N. G., *et al.* (2015) The metabolome regulates the epigenetic landscape during naïve to primed human embryonic stem cell transition. *Nat. Cell Biol.* **17,** 1523–1535 CrossRef Medline

99. Hore, T. A., von Meyenn, F., Ravichandran, M., Bachman, M., Ficz, G., Oxley, D., Santos, F., Balasubramanian, S., Jurkowski, T. P., and Reik, W. (2016) Retinol and ascorbate drive erasure of epigenetic memory and enhance reprogramming to naïve pluripotency by complementary mechanisms. *Proc. Natl. Acad. Sci. U.S.A.* **113,** 12202–12207 CrossRef Medline

24

CHAPTER 3:

Metabolism in Pluripotent Stem Cells and Early Mammalian Development

and

Alpha-ketoglutarate: A 'Magic' Metabolite in Early Germ Cell Development

Metabolism in Pluripotent Stem Cells and Early Mammalian Development

Jin Zhang,[1,*] Jing Zhao,[1] Perrine Dahan,[2] Vivian Lu,[3] Cheng Zhang,[4] Hu Li,[4] and Michael A. Teitell[2,5,6,7,8,9,*]
[1]The First Affiliated Hospital and Center for Stem Cell and Regenerative Medicine, Department of Basic Medical Sciences, School of Medicine, Institute of Hematology, Zhejiang University, Hangzhou, Zhejiang 310058, China
[2]Department of Pathology and Laboratory Medicine
[3]Department of Molecular and Medical Pharmacology
David Geffen School of Medicine, University of California, Los Angeles, Los Angeles, CA 90095, USA
[4]Center for Individualized Medicine, Department of Molecular Pharmacology & Experimental Therapeutics, Mayo Clinic, Rochester, MN 55905, USA
[5]California NanoSystems Institute
[6]Department of Bioengineering
[7]Molecular Biology Institute
[8]Jonsson Comprehensive Cancer Center, David Geffen School of Medicine
[9]Eli and Edythe Broad Center of Regenerative Medicine and Stem Cell Research
University of California, Los Angeles, Los Angeles, CA 90095, USA
*Correspondence: zhgene@zju.edu.cn (J.Z.), mteitell@mednet.ucla.edu (M.A.T.)
https://doi.org/10.1016/j.cmet.2018.01.008

Emerging and seminal studies have shown that cell metabolism influences gene expression by modifying the epigenome, which can regulate stem cell pluripotency, differentiation, and somatic cell reprogramming. Core pluripotency factors and developmental regulators reciprocally control the expression of key metabolism genes and their encoded pathways. Recent technological advances enabling sensitive detection methods during early mammalian development revealed the state-specific and context-dependent coordination of signal transduction, histone modifications, and gene expression in developing, resting, and malnourished embryos. Here, we discuss metabolism as a potential driver of earliest cell fate through its influence on the epigenome and gene expression in embryos and their *in vitro* surrogate pluripotent stem cells.

Introduction

In its broadest sense, cellular metabolism is a dynamic orchestration of interconnected signaling networks involving the coordination of nutrient utilization to generate energy (ATP) and biomass as well as energy consumption and biomass removal and recycling. The importance of cell metabolism is straightforward in certain contexts, such as building biomass for cell proliferation, compared with less obvious contexts, such as during cell-state transitions driven by epigenetic remodeling and specific gene activation or suppression. There is rapidly accumulating evidence for extensive, interdependent interactions between metabolism and epigenetics in cancerous transformation (Kinnaird et al., 2016), immune system activation and silencing (Raghuraman et al., 2016), and now stem cell maintenance and differentiation (Ryall et al., 2015). A robust example of concurrent changes in epigenome remodeling and cell proliferation occurs during early mammalian embryo development. Blastomeres formed by cleavage divisions do not grow and show minimal gene expression, which suddenly transitions to re-setting of the chromatin structure, massive genome transcription, protein translation, and increased cell proliferation following zygotic genome activation (ZGA) (Jukam et al., 2017). After ZGA, additional changes in epigenetic and gene expression programs occur during pre- and post-implantation embryonic development.

Pluripotent stem cells (PSCs) model cells from pre- and post-implantation embryos and grow indefinitely in culture. They have garnered tremendous attention because of multiple potential applications. Biochemical, molecular, and functional features of PSCs, including metabolism, are being intensively studied. Similarities and distinctions between PSC metabolism and metabolic features from early-stage embryos reported more than 40 years ago are being revisited today with newer, small sample techniques (Leese, 2012). This re-examination has practical consequences as investigators attempt to identify optimal *ex vivo* conditions for generating mature and functional cell types from PSC differentiation protocols.

In contrast to 40 years ago, today there are several types of cultured mammalian PSCs with differing developmental potential that resemble cells at different stages of early embryo development. "Naive"-state PSCs functionally resemble the pre-implantation blastocyst inner cell mass with differentiation potential for all three germ layers and primordial germ cells. "Primed"-state PSCs (Tesar et al., 2007; Brons et al., 2007) resemble post-implantation epiblast cells that have a low capacity to contribute to embryonic chimeras and a low competence for germline differentiation (Weinberger et al., 2016). "Extended" PSCs can form both embryonic and extraembryonic tissues, reminiscent of early blastomeres (Yang et al., 2017). A key challenge for studying early embryos are small sample sizes with limited starting materials. Fortunately, technological advances are beginning to provide versatile omics tools that can analyze the molecular features of small samples directly from early embryos (Lu et al., 2016; Wu et al., 2016; Xue et al., 2013). Profiling

studies are starting to reveal that metabolic programs are regulated by stage-specific transcription factors or other types of regulators and also that, reciprocally, metabolism may promote fate regulator expression in humans and mice. This new insight helps integrate metabolic patterns with upstream regulatory circuits and uncovers potential causal roles for specific aspects of metabolism that confer downstream cell-fate determination. Beyond development, epidemiologic studies on the pathological effects of parental and fetal malnutrition are increasingly being explored using small animal models (Sharma and Rando, 2017). It is possible that understanding metabolism in early development will uncover mechanisms for diseases with embryonic origins and also linked malnutrition causes. In this Review, we evaluate, interpret, and discuss recent metabolic findings for embryos and for *in vitro* surrogate cultured PSCs. We further assess the current state of integration of metabolism into the PSC regulatory circuitry and its potential impact on cell fate with implications for malnutrition in embryo development and causal connections to adult diseases.

Metabolic Features of PSCs

Embryonic stem cells (ESCs) or induced pluripotent stem cells (iPSCs), collectively referred to as PSCs, are the most accessible cell types to study metabolic events in early mammalian development. Although valuable, PSC studies, nevertheless, may or may not represent the intrinsic metabolic features of their *in vivo* counterparts, as PSCs may acquire unique metabolic features to support infinite self-renewal in several types of culture conditions (Tang et al., 2010). A decade ago, studies began revealing unique patterns of cellular metabolism during PSC differentiation (Chung et al., 2007), during reprogramming to pluripotency (Folmes et al., 2011), and in naive-versus primed-state PSCs (Zhou et al., 2012). Combined, these studies showed a link between metabolic patterns and the loss, gain, or maintenance of PSC pluripotency.

In general, PSCs exhibit a high glycolytic flux to support high energy and biosynthetic demands during rapid proliferation (Folmes et al., 2011; Zhang et al., 2011). These metabolic features are also reacquired during nucleus reprogramming of somatic cells to iPSCs prior to the induction of pluripotency gene expression (Folmes et al., 2011; Kida et al., 2015). Robust metabolism in PSCs supports proliferation and metabolite production for epigenome modifications, as, for example, acetyl-CoA produced by glycolysis maintains histone acetylation and pluripotency (Moussaieff et al., 2015). Naive—or more primitive—and primed—or developmentally more advanced—stages of pluripotency have been defined for mouse PSCs. Naive PSCs and primed epiblast stem cells (EpiSCs) are both metabolically active, but naive PSCs respire more than primed EpiSCs (Zhou et al., 2012), which has been reviewed in detail previously (Teslaa and Teitell, 2015). This metabolic pattern could support the production of the TCA cycle intermediates for amino acid biosynthesis and the mitochondrial folate cycle for nucleotide biosynthesis. Higher oxygen consumption through respiration is consistent with a slightly lower proliferation rate for naive PSCs because nutrient carbons may be lost as CO_2 to lessen the rate of biomass accumulation required for cell replication. Differences in mitochondrial metabolism between naive and primed PSCs likely foster large epigenome differences, such as global hypomethylation in naive PSCs and hypermethylation in primed PSCs, because metabolites

serve as co-factors or substrates for epigenome-modifying enzymes, as discussed below. Clearly, there are additional effects from active mitochondria in naive PSCs that need further study and that go beyond support for growth and proliferation. Finally, recent work has also begun to examine metabolic remodeling linked to lineage-specific differentiation, which has refined the concept that differentiation from pluripotency always requires a shift from glycolytic to oxidative metabolism. Sustained high-level glycolysis without an oxidative shift through maintained expression of MYC/MYCN during ectoderm lineage differentiation contrasts with a shift to oxidative metabolism and MYC/MYCN repression for mesoderm and endoderm lineage differentiation (Cliff et al., 2017).

Metabolism in Early Mammalian Embryos

In contrast to our increasing knowledge of cell metabolism in easily expandable PSCs, our understanding of metabolism in early mammalian embryos remains rudimentary and mostly based on whole-embryo nutritional needs (Brown and Whittingham, 1991), metabolic activities (Acton et al., 2004; Houghton et al., 1996), and the abundance of certain metabolites in whole embryos (Barbehenn et al., 1978). Few studies have dissected embryonic metabolism with spatial or temporal resolution or by specific cell types, such as differences and similarities between trophectoderm and the blastocyst inner cell mass (Gopichandran and Leese, 2003; Houghton, 2006; Robinson and Benos, 1991). Cultured PSCs are likely imperfect surrogates for *in vivo* counterparts within a developing embryo because microenvironment differences may cause variation in metabolism gene expression (Tang et al., 2010), which limits our extrapolation of *in vitro* PSC results. New transcriptome profiling studies of individual cells from each stage of early embryo development and each lineage within an embryo are providing expression data for all genes, including metabolism-regulating genes. Concurrently, new epigenome profiling studies requiring just a few cells (Liu et al., 2016; Zhang et al., 2016a) are providing potential mechanistic data for metabolism gene regulation and perhaps how certain environmental insults influence the epigenome at the earliest stages in mammalian development. A missing component for profiling technologies applied to embryogenesis is the metabolome, as current metabolomics and metabolic flux studies remain challenging for small numbers of cells.

Recent transcriptome and epigenome profiling has revealed clues for changes in metabolism during certain stages of early embryo development (Figure 1). Two studies examining single-cell RNA transcriptomes of mouse and human pre-implantation embryos showed the induction of genes controlling OXPHOS during the blastocyst stage of development (Yan et al., 2013; Xue et al., 2013). These results agree with prior studies that showed blastocysts consuming high levels of oxygen, most likely through mitochondrial respiration (Houghton et al., 1996; Leese, 2012). They also align well with naive PSCs that resemble pre-implantation epiblast cells (Boroviak et al., 2015) showing active respiration (Zhou et al., 2012). Open questions include which signals, epigenome modifications, and transcription factors activate expression and translation of OXPHOS genes. Also, what are the carbon fuel sources for the TCA cycle and respiration, and in what way(s) does respiration support the blastocyst and other early stages?
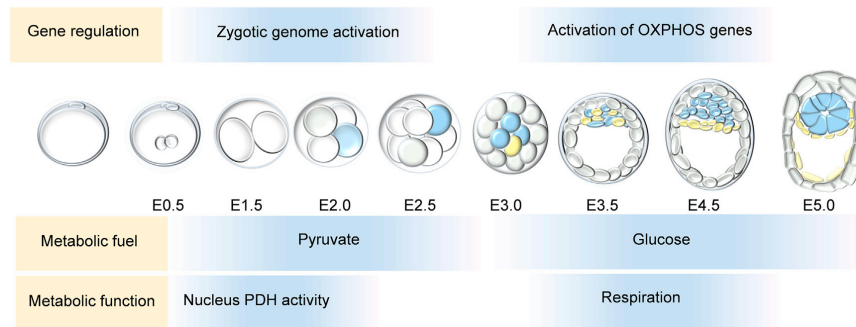
Figure 1. Dynamic Gene and Metabolic Regulation during Early Mouse Embryo Development
The nutrient pyruvate supports the one-cell-to-morula transition in mice prior to glucose becoming an essential nutrient. Enzymatically active PDH and a subset of the TCA cycle enzymes transiently localize into the nucleus at the two-cell stage in mice and between four- and eight-cell stages in human development, coincident with ZGA for each species. Mitochondrial respiration activates during the mouse blastocyst stage and inactivates after implantation, around the same time blastocyst epiblast activation of OXPHOS genes occurs as revealed by transcriptome profiling, and is consistent with high mitochondrial activity in cultured naive-versus primed-state PSCs. PDH, pyruvate dehydrogenase; ZGA, zygotic gene activation.

Transcriptome studies of mammalian diapause embryos, and embryos deficient in mTOR or MYC that resemble diapause (Bulut-Karslioglu et al., 2016; Scognamiglio et al., 2016; Boroviak et al., 2015), are providing new connections between metabolism and this physiologic dormant reproductive state. Naive ESCs deficient in both *c-Myc* and *N-Myc* enter a quiescent state with a strong reduction in protein and nucleic acid biosynthesis, similar to inhibition of MYC in blastocysts, which also induces a dormant state with reduced protein biosynthesis (Scognamiglio et al., 2016). Inhibition of mTOR in ESCs caused global transcription repression, and inhibition of mTOR in blastocysts led to paused embryo development, similar to mammalian diapause (Bulut-Karslioglu et al., 2016). Diapause embryos, with lower expression of *c-Myc* and *N-Myc* (Scognamiglio et al., 2016), maintain naive epiblast gene expression patterns and also show lowered expression of glycolytic genes and serine metabolism genes, such as *Aldoa* and *Phgdh* (Boroviak et al., 2015). Upstream inhibition of the one-carbon serine metabolism pathway might account for reductions in nucleotide biosynthesis, DNA/RNA metabolism, and lower proliferation in diapause (Locasale, 2013; Yang and Vousden, 2016). Whether diapause also induces other one-carbon metabolism changes, such as in S-adenosylmethionine (SAM) production that could alter the methylation state of the epigenome, or changes in the cellular redox state mediated by glutathione is currently unknown. An additional regulator of pluripotency, LIN28, is an intermediate in the MYC to mTOR pathway. LIN28 expression can be induced by c-MYC (Chang et al., 2009) and is co-regulated by ERK/MEK signaling as both c-MYC and LIN28A proteins are phosphorylated and stabilized by ERK (Sears et al., 2000; Tsanov et al., 2017). LIN28 also influences mTOR signaling by targeting IGF/PI3K/mTOR signaling pathway members through *let-7* in mouse embryonic fibroblasts (Zhu et al., 2011). Depletion of LIN28 in mouse ESCs also reduces one-carbon metabolism and nucleotide biosynthesis (Zhang et al., 2016b), similar to MYC-depleted ESCs or mTOR-suppressed ESCs. LIN28 suppression in mouse zygotes arrests development between two-cell and four-cell stages (Vogt et al., 2012), which is

reminiscent of MYC or mTOR deficiency-caused embryo developmental dormancy. Whether this arrested transition is due to a metabolic deficiency alone, other gene regulatory network alteration, or both causes is currently unknown.

Remarkably, a subset of TCA cycle enzymes transiently localizes in the nucleus at the two-cell embryo stage in mice and between four- and eight-cell stages in human development, coincident with ZGA for each species, and seems to be critical for ongoing development (Nagaraj et al., 2017). Pyruvate is a nutrient that is required to support the one-cell-to-morula transition in mice prior to glucose becoming an essential nutrient (Brown and Whittingham, 1991). Interestingly, the nucleus localization of several TCA enzymes during the two-cell stage of development in mice is pyruvate dependent. Lack of pyruvate in the media of cultured mouse zygotes led to a two-cell stage arrest and a reduction in citrate and α-ketoglutarate (αKG), along with reduced H3K4Ac, H3K27Ac, and H3K27me3 epigenome marks and decreased global transcription activity. These data provide evidence for a specialized nucleus metabolic program during ZGA that is required for gene activation, likely through changes in the epigenome. The relationship between this metabolic program and waves of transcriptional activity during ZGA is currently unknown (Jukam et al., 2017).

Pluripotency Circuitry and the Metabolic Network
Distinct patterns of metabolic activity associate with specific developmental stages and cell fates. This correlation suggests probable integration between the circuitry that controls pluripotency and early development and the regulation of metabolic gene expression and function (Figure 2). Accumulating evidence from PSC studies supports this suggestion. For example, to maintain or induce pluripotency, developmentally activated *c-Myc* directly *trans*-activates glycolysis genes (Folmes et al., 2013; Cao et al., 2015). Also, development factor LIN28 regulates glycolysis by repressing *let-7*, which targets the glycolysis enzyme *Pdk1* (Ma et al., 2014) and influences OXPHOS gene expression through post-translational mechanisms in mouse
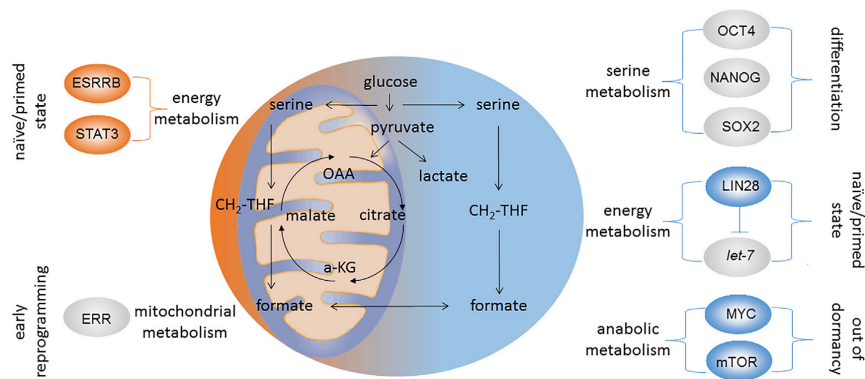
Figure 2. Glucose and One-Carbon Metabolic Pathways Regulated by Pluripotency and Early Development Factors

Naive PSC factor ESRRB activates mitochondrial OXPHOS, and STAT3 binds to the mitochondrial genome to enhance oxidative metabolism. Primed PSC factor LIN28 coordinates with *let-7* to enhance glycolysis and repress OXPHOS. Pluripotency core factors OCT4, NANOG, and SOX2 bind the serine metabolism *Psat1* gene promoter to activate transcription and influence mouse ESC differentiation. Nuclear factor ESRRB activates OXPHOS and c-MYC activates glycolysis at early stages of somatic cell reprogramming to iPSCs to pre-set the metabolism program before induction of pluripotency gene expression. MYC and mTOR are required for anabolic metabolism in mouse ESCs and embryos, with loss of mTOR and MYC generating a dormant state that resembles reproductive diapause and maintains features of naive pluripotency. In the diagram, orange-colored objects are regulators associated with naive-state metabolism. Blue-colored objects depict regulators that, upon depletion, may confer mouse ESCs' naive-like state features. Gray-colored objects indicate regulators related to metabolism in maintenance of general pluripotency, differentiation, and reprogramming.

ESCs (Zhang et al., 2016b). Pluripotency-associated *mir-290* cluster microRNAs in mouse ESCs activate glycolysis by repressing a reader for methylated CpG dinucleotides, MBD2, which represses *c-Myc* directly and glycolysis genes *Pkm2* and *Ldha* (Cao et al., 2015). The transcription factor ERR, which is a cofactor of PGC-1α that is transiently induced by somatic cell reprogramming with OSKM factors, generates a burst of OXPHOS activity at day 3 or 5 of mouse and human reprogramming, respectively (Kida et al., 2015). Finally, a serine metabolism gene, *Psat1*, is *trans*-activated by core pluripotency factors *Oct4/Sox2/Nanog* and mediates the production and effects of αKG on mouse ESC differentiation (Hwang et al., 2016). Combined, the evidence is strong and mounting that pluripotency and development factors coordinately regulate metabolic gene expression and activity in early mammalian development.

A transition between mouse PSC naive and primed states engages development factors *Stat3*, *Esrrb*, *Zic3*, and *Lin28a/b* and provides new details for how the metabolic network of these two pluripotent stages is regulated by this circuitry (Figure |Fig. 2) (Sone et al., 2017; Zhang et al., 2016b; Carbognin et al., 2016). For naive-state PSCs, *Stat3* sustains the nucleus naive gene expression profile and also interacts with the mitochondrial genome to activate genes promoting respiration (Carbognin et al., 2016). *Esrrb* induces OXPHOS through an unknown mechanism during the primed-to-naive-state transition, and it has a similar function during somatic cell reprogramming to pluripotency (Sone et al., 2017). *Esrrb* and *Zic3* synergistically enhance glycolysis during iPSC generation, and they combine to maintain pluripotency through direct binding of glycolysis promoting genes. Conversely, *Lin28a/b* represses OXPHOS to support state conversion in the opposite direction from the naive to primed state (Zhang et al., 2016b), and *Zic3* alone can repress OXPHOS and activate glycolysis to help establish the primed-state metabolic profile (Sone et al., 2017). Collectively, these reports show that key metabolic parameters are controlled by state-specific pluripotency and development factors, strongly suggesting that metabolism has an active, required role in shaping different pluripotent states.

To what Extent Can Metabolism Influence PSC and Early Embryo Fates?

Changes in metabolism could passively participate in PSC and early embryo fate determination driven by other regulatory factors, or they could help shape and even control fate outcomes (Zhang et al., 2012). Accumulating data strongly suggest an active role for metabolism in early cell-fate determination. Fate-influencing mechanisms are centered on several key metabolism-regulating signal transduction pathways, such as AMPK/mTOR (Bulut-Karslioglu et al., 2016), and intermediate metabolites, such as αKG, SAM, and acetyl-CoA (Ryall et al., 2015) (Figure 3). Changes in bioenergetics or nutrient availability resulting in a high ADP/ATP ratio inactivates the AMPK/mTOR pathway, as do mTOR inhibitors, and consequently stalls development similar to the physiologic diapause in rodent embryos (Bulut-Karslioglu et al., 2016). Additionally, AMPK/mTOR pathway activity is also required for post-implantation proliferation of embryonic and extraembryonic cells *in vivo* (Murakami et al., 2004). The TCA cycle metabolite αKG is a required co-factor for dioxygenase enzymes that include the Jumonji C (JmjC)-domain-containing histone demethylases (JHDMs) and Ten-eleven translocation (TET) DNA methylcytosine hydroxylases. αKG levels impact histone H3K9m3 and H3K27m3 marks to facilitate cell-fate outcomes between LIF/2i naive-state PSCs and a LIF/serum metastable PSC state (Carey et al., 2015) or FGF2/Activin-induced primed PSC state (Zhang et al., 2016b). αKG levels can also promote PSC differentiation through altering histone
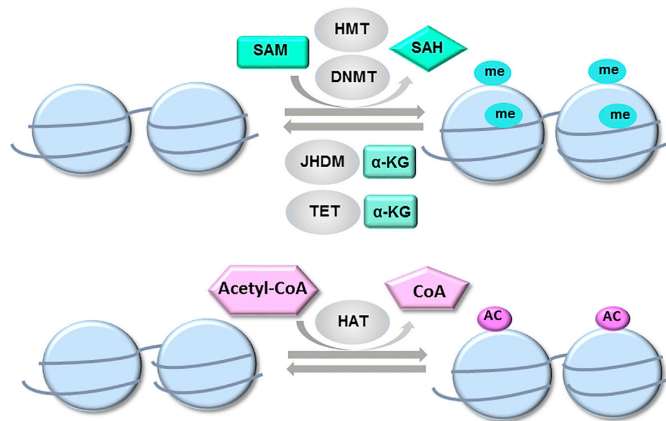
and DNA methylation levels in spontaneous mouse ESC differentiation (Hwang et al., 2016) and in directed human neuroectoderm differentiation (TeSlaa et al., 2016) even though the mechanisms of αKG production may vary in different cell contexts. Levels of the one-carbon metabolism pathway metabolite SAM influence H3K4me3 levels in mouse ESCs (Shyh-Chang et al., 2013) and in human ESCs (Shiraki et al., 2014). Acetyl-CoA produced during glycolysis affects histone acetylation and gene expression in both human and mouse ESCs, and modulation of acetyl-CoA levels either by inhibiting glycolysis enzymes or by supplementing acetate influences PSC pluripotency versus differentiation fates (Moussaieff et al., 2015). Key metabolites, including those that are produced intracellularly or those that are imported from the microenvironment or culture media, can substantially influence histone and/or DNA epigenetic marks. Nevertheless, our current understanding of how metabolic pathways influence cell fate is complicated by two unresolved challenges. One challenge is to provide evidence that the physiologic fluctuation of metabolite levels can cause significant changes of global or local chromatin modifications. Another challenge is to provide evidence that metabolism-mediated epigenetic changes can translate to specific changes in gene expression that are causal for cell-fate outcomes, which is briefly discussed below.

Interpreting the Influence of Metabolites on Epigenetics and Cell Fate
Studies to date provide relatively consistent and reinforcing data for interconnections between metabolite levels, epigenetic alterations, and fate outcomes for PSCs without resolving questions of specificity and causality. Which chromatin modifications during embryo development arise from differences in which metabolites? Which genes affected by metabolism-mediated changes in histone and/or DNA modifications are involved in cell-fate determination? Reporting correlations between metabolic rewiring, epigenetic modifications, gene expression, and cell fate is the status quo, and definitive studies showing that metabolism influences PSC fate through epigenetic alterations are still lacking. Direct evidence for causal connections and molecular mecha-

nisms requires further studies with new tools and technologies, such as site-specific epigenetic modifiers that are under development to confer causality.

A second open area is to determine how much each nutrient source contributes to a metabolite pool of interest. This is a difficult question to address because it is technically infeasible to knock out all the genes controlling a specific metabolite, leaving extracellular metabolite addition or omission as the leading way to perturb some metabolites of interest. Also, metabolite pools arise from multiple sources, making assignments of nutrient origins potentially complex. For example, in PSCs, αKG originates from the TCA cycle via isocitrate dehydrogenase, from glutaminolysis through glutaminase (TeSlaa et al., 2016), or from serine metabolism through phosphoserine aminotransferase (Hwang et al., 2016). Also, SAM can be produced from exogenous or glucose-derived serine, from threonine metabolism in mouse ESCs (Shyh-Chang et al., 2013), or from methionine metabolism in human ESCs (Shiraki et al., 2014).

Another open question is evidence *in vivo* showing that metabolite levels control biochemical reactions to modify chromatin. For example, it has not been shown within a PSC nucleus that fluctuating αKG levels impact dioxygenase or demethylase enzyme activities. This would be difficult to do currently because, unlike *in vitro* biochemical reactions, there is no way to add or reduce only αKG without perturbing other systems within a cell. Similarly, a one-carbon subunit, such as a methyl group, from any nutrient source has not yet been shown to generate a methylation mark on a histone or deoxynucleotide. Therefore, development of new tools to monitor, quantify, and even manipulate specific metabolite levels within living cells will potentially provide causative links between changes in cell metabolism, the epigenome, and cell fate.

Embryo Malnutrition and Disease
Improved understanding of metabolism during embryonic development can lay a foundation for comparative studies of abnormal development due to environmental insults such as malnutrition. Malnutrition can predispose individuals to diseases that manifest later in life but whose origins begin during early development (Barker, 1997). Studies using small animal models have revealed that poor nutrition may impact germ cells, and this information can be transmitted between generations and show up as changes in epigenetic modifications and/or the expression of

small noncoding RNAs (Chen et al., 2016; Huypens et al., 2016; Sharma et al., 2016), as recently reviewed (Sharma and Rando, 2017). It is technically more difficult to tease out maternal effects of malnutrition for studies on early embryo development because placental insufficiency or hormone deregulation can also be caused by malnutrition in a pregnant female. In addition to malnutrition models, genetics studies are also useful. There is evidence that the consequences of malnutrition in the unborn depend upon genetic polymorphisms in *IGF2BP2* and *PPAR-γ2* from the Dutch Famine Birth Cohort (van Hoek et al., 2009; de Rooij et al., 2006). Therefore, genetic manipulations of key metabolism-related genes may help to model fetal malnutrition in animals, and such models can be potentially disentangled from maternal effects. For example, conditional knockout of *Lin28a* and *Lin28b* in embryos using tamoxifen-induced excision can cause aberrations in growth and glucose metabolism in adults (Shinoda et al., 2013). Since most metabolism genes are ubiquitously expressed and required for normal adult tissue development and physiology, transient reduction of these genes during embryo development may be preferable for modeling effects of transient malnutrition in utero. For instance, with an inducible dCAS9 fused to an activating or repressive domain, it is possible to transiently change a metabolism gene in the embryo, then determine acute metabolic alterations, and later determine long-term adult phenotype abnormalities and epigenome changes after the animal grows up. Once an animal model is established, critical questions can be asked, such as how a malnutrition signal is translated to long-lasting epigenetic memories that can be manifested in adult life, or even in the next generation.

Concluding Remarks

Great advances in our understanding of metabolism in PSCs have been made, with next steps to understand upstream regulators and downstream impact that are directly hard wired into PSC fates. Additionally, there are tremendous opportunities to understand metabolism in the physiological context of early embryo development, and in the pathological context of malnutrition and the early origins of diseases.

REFERENCES

Acton, B.M., Jurisicova, A., Jurisica, I., and Casper, R.F. (2004). Alterations in mitochondrial membrane potential during preimplantation stages of mouse and human embryo development. Mol. Hum. Reprod. *10*, 23–32.

Barbehenn, E.K., Wales, R.G., and Lowry, O.H. (1978). Measurement of metabolites in single preimplantation embryos; a new means to study metabolic control in early embryos. J. Embryol. Exp. Morphol. *43*, 29–46.

Barker, D.J.P. (1997). Maternal nutrition, fetal nutrition, and disease in later life. Nutrition *13*, 807–813.

Boroviak, T., Loos, R., Lombard, P., Okahara, J., Behr, R., Sasaki, E., Nichols, J., Smith, A., and Bertone, P. (2015). Lineage-specific profiling delineates the emergence and progression of naive pluripotency in mammalian embryogenesis. Dev. Cell *35*, 366–382.

Brons, I.G.M., Smithers, L.E., Trotter, M.W.B., Rugg-Gunn, P., Sun, B., Chuva de Sousa Lopes, S.M., Howlett, S.K., Clarkson, A., Ahrlund-Richter, L., Pedersen, R.A., and Vallier, L. (2007). Derivation of pluripotent epiblast stem cells from mammalian embryos. Nature *448*, 191–195.

Brown, J.J., and Whittingham, D.G. (1991). The roles of pyruvate, lactate and glucose during preimplantation development of embryos from F1 hybrid mice in vitro. Development *112*, 99–105.

Bulut-Karslioglu, A., Biechele, S., Jin, H., Macrae, T.A., Hejna, M., Gertsenstein, M., Song, J.S., and Ramalho-Santos, M. (2016). Inhibition of mTOR induces a paused pluripotent state. Nature *540*, 119–123.

Cao, Y., Guo, W.-T., Tian, S., He, X., Wang, X.-W., Liu, X., Gu, K.-L., Ma, X., Huang, D., Hu, L., et al. (2015). miR-290/371-Mbd2-Myc circuit regulates glycolytic metabolism to promote pluripotency. EMBO J. *34*, 609–623.

Carbognin, E., Betto, R.M., Soriano, M.E., Smith, A.G., and Martello, G. (2016). Stat3 promotes mitochondrial transcription and oxidative respiration during maintenance and induction of naive pluripotency. EMBO J. *35*, 618–634.

Carey, B.W., Finley, L.W.S., Cross, J.R., Allis, C.D., and Thompson, C.B. (2015). Intracellular α-ketoglutarate maintains the pluripotency of embryonic stem cells. Nature *518*, 413–416.

Chang, T.-C., Zeitels, L.R., Hwang, H.-W., Chivukula, R.R., Wentzel, E.A., Dews, M., Jung, J., Gao, P., Dang, C.V., Beer, M.A., et al. (2009). Lin-28B transactivation is necessary for Myc-mediated let-7 repression and proliferation. Proc. Natl. Acad. Sci. USA *106*, 3384–3389.

Chen, Q., Yan, M., Cao, Z., Li, X., Zhang, Y., Shi, J., Feng, G.H., Peng, H., Zhang, X., Zhang, Y., et al. (2016). Sperm tsRNAs contribute to intergenerational inheritance of an acquired metabolic disorder. Science *351*, 397–400.

Chung, S., Dzeja, P.P., Faustino, R.S., Perez-Terzic, C., Behfar, A., and Terzic, A. (2007). Mitochondrial oxidative metabolism is required for the cardiac differentiation of stem cells. Nat. Clin. Pract. Cardiovasc. Med. *4* (Suppl 1), S60–S67.

Cliff, T.S., Wu, T., Boward, B.R., Yin, A., Yin, H., Glushka, J.N., Prestegaard, J.H., and Dalton, S. (2017). MYC controls human pluripotent stem cell fate decisions through regulation of metabolic flux. Cell Stem Cell *21*, 502–516.e9.

de Rooij, S.R., Painter, R.C., Phillips, D.I.W., Osmond, C., Tanck, M.W.T., Defesche, J.C., Bossuyt, P.M.M., Michels, R.P.J., Bleker, O.P., and Roseboom, T.J. (2006). The effects of the Pro12Ala polymorphism of the peroxisome proliferator-activated receptor-γ2 gene on glucose/insulin metabolism interact with prenatal exposure to famine. Diabetes Care *29*, 1052–1057.

Folmes, C.D., Nelson, T.J., Martinez-Fernandez, A., Arrell, D.K., Lindor, J.Z., Dzeja, P.P., Ikeda, Y., Perez-Terzic, C., and Terzic, A. (2011). Somatic oxidative bioenergetics transitions into pluripotency-dependent glycolysis to facilitate nuclear reprogramming. Cell Metab. *14*, 264–271.

Folmes, C.D.L., Martinez-Fernandez, A., Faustino, R.S., Yamada, S., Perez-Terzic, C., Nelson, T.J., and Terzic, A. (2013). Nuclear reprogramming with c-Myc potentiates glycolytic capacity of derived induced pluripotent stem cells. J. Cardiovasc. Transl. Res. *6*, 10–21.

Gopichandran, N., and Leese, H.J. (2003). Metabolic characterization of the bovine blastocyst, inner cell mass, trophectoderm and blastocoel fluid. Reproduction *126*, 299–308.

Houghton, F.D. (2006). Energy metabolism of the inner cell mass and trophectoderm of the mouse blastocyst. Differentiation *74*, 11–18.

Houghton, F.D., Thompson, J.G., Kennedy, C.J., and Leese, H.J. (1996). Oxygen consumption and energy metabolism of the early mouse embryo. Mol. Reprod. Dev. *44*, 476–485.

Huypens, P., Sass, S., Wu, M., Dyckhoff, D., Tschöp, M., Theis, F., Marschall, S., Hrabě de Angelis, M., and Beckers, J. (2016). Epigenetic germline inheritance of diet-induced obesity and insulin resistance. Nat. Genet. *48*, 497–499.

Hwang, I.Y., Kwak, S., Lee, S., Kim, H., Lee, S.E., Kim, J.H., Kim, Y.A., Jeon, Y.K., Chung, D.H., Jin, X., et al. (2016). Psat1-dependent fluctuations in α-ketoglutarate affect the timing of ESC differentiation. Cell Metab. *24*, 494–501.

Jukam, D., Shariati, S.A.M., and Skotheim, J.M. (2017). Zygotic genome activation in vertebrates. Dev. Cell *42*, 316–332.

Kida, Y.S., Kawamura, T., Wei, Z., Sogo, T., Jacinto, S., Shigeno, A., Kushige, H., Yoshihara, E., Liddle, C., Ecker, J.R., et al. (2015). ERRs mediate a

metabolic switch required for somatic cell reprogramming to pluripotency. Cell Stem Cell *16*, 547–555.

Kinnaird, A., Zhao, S., Wellen, K.E., and Michelakis, E.D. (2016). Metabolic control of epigenetics in cancer. Nat. Rev. Cancer *16*, 694–707.

Leese, H.J. (2012). Metabolism of the preimplantation embryo: 40 years on. Reproduction *143*, 417–427.

Liu, X., Wang, C., Liu, W., Li, J., Li, C., Kou, X., Chen, J., Zhao, Y., Gao, H., Wang, H., et al. (2016). Distinct features of H3K4me3 and H3K27me3 chromatin domains in pre-implantation embryos. Nature *537*, 558–562.

Locasale, J.W. (2013). Serine, glycine and one-carbon units: cancer metabolism in full circle. Nat. Rev. Cancer *13*, 572–583.

Lu, F., Liu, Y., Inoue, A., Suzuki, T., Zhao, K., and Zhang, Y. (2016). Establishing chromatin regulatory landscape during mouse preimplantation development. Cell *165*, 1375–1388.

Ma, X., Li, C., Sun, L., Huang, D., Li, T., He, X., Wu, G., Yang, Z., Zhong, X., Song, L., et al. (2014). Lin28/let-7 axis regulates aerobic glycolysis and cancer progression via PDK1. Nat. Commun. *5*, 5212.

Moussaieff, A., Rouleau, M., Kitsberg, D., Cohen, M., Levy, G., Barasch, D., Nemirovski, A., Shen-Orr, S., Laevsky, I., Amit, M., et al. (2015). Glycolysis-mediated changes in acetyl-CoA and histone acetylation control the early differentiation of embryonic stem cells. Cell Metab. *21*, 392–402.

Murakami, M., Ichisaka, T., Maeda, M., Oshiro, N., Hara, K., Edenhofer, F., Kiyama, H., Yonezawa, K., and Yamanaka, S. (2004). mTOR is essential for growth and proliferation in early mouse embryos and embryonic stem cells. Mol. Cell. Biol. *24*, 6710–6718.

Nagaraj, R., Sharpley, M.S., Chi, F., Braas, D., Zhou, Y., Kim, R., Clark, A.T., and Banerjee, U. (2017). Nuclear localization of mitochondrial TCA cycle enzymes as a critical step in mammalian zygotic genome activation. Cell *168*, 210–223.e11.

Raghuraman, S., Donkin, I., Versteyhe, S., Barrès, R., and Simar, D. (2016). The emerging role of epigenetics in inflammation and immunometabolism. Trends Endocrinol. Metab. *27*, 782–795.

Robinson, D.H., and Benos, D.J. (1991). Glucose metabolism in the trophectoderm and inner cell mass of the rabbit embryo. J. Reprod. Fertil. *91*, 493–499.

Ryall, J.G., Cliff, T., Dalton, S., and Sartorelli, V. (2015). Metabolic reprogramming of stem cell epigenetics. Cell Stem Cell *17*, 651–662.

Scognamiglio, R., Cabezas-Wallscheid, N., Thier, M.C., Altamura, S., Reyes, A., Prendergast, A.M., Baumgärtner, D., Carnevalli, L.S., Atzberger, A., Haas, S., et al. (2016). Myc depletion induces a pluripotent dormant state mimicking diapause. Cell *164*, 668–680.

Sears, R., Nuckolls, F., Haura, E., Taya, Y., Tamai, K., and Nevins, J.R. (2000). Multiple Ras-dependent phosphorylation pathways regulate Myc protein stability. Genes Dev. *14*, 2501–2514.

Sharma, U., and Rando, O.J. (2017). Metabolic inputs into the epigenome. Cell Metab. *25*, 544–558.

Sharma, U., Conine, C.C., Shea, J.M., Boskovic, A., Derr, A.G., Bing, X.Y., Belleannee, C., Kucukural, A., Serra, R.W., Sun, F., et al. (2016). Biogenesis and function of tRNA fragments during sperm maturation and fertilization in mammals. Science *351*, 391–396.

Shinoda, G., Shyh-Chang, N., Soysa, T.Y., Zhu, H., Seligson, M.T., Shah, S.P., Abo-Sido, N., Yabuuchi, A., Hagan, J.P., Gregory, R.I., et al. (2013). Fetal deficiency of lin28 programs life-long aberrations in growth and glucose metabolism. Stem Cells *31*, 1563–1573.

Shiraki, N., Shiraki, Y., Tsuyama, T., Obata, F., Miura, M., Nagae, G., Aburatani, H., Kume, K., Endo, F., and Kume, S. (2014). Methionine metabolism regulates maintenance and differentiation of human pluripotent stem cells. Cell Metab. *19*, 780–794.

Shyh-Chang, N., Locasale, J.W., Lyssiotis, C.A., Zheng, Y., Teo, R.Y., Ratanasirintrawoot, S., Zhang, J., Onder, T., Unternaehrer, J.J., Zhu, H., et al. (2013). Influence of threonine metabolism on S-adenosylmethionine and histone methylation. Science *339*, 222–226.

Sone, M., Morone, N., Nakamura, T., Tanaka, A., Okita, K., Woltjen, K., Nakagawa, M., Heuser, J.E., Yamada, Y., Yamanaka, S., and Yamamoto, T. (2017).

Hybrid cellular metabolism coordinated by Zic3 and Esrrb synergistically enhances induction of naive pluripotency. Cell Metab. *25*, 1103–1117.e6.

Tang, F., Barbacioru, C., Bao, S., Lee, C., Nordman, E., Wang, X., Lao, K., and Surani, M.A. (2010). Tracing the derivation of embryonic stem cells from the inner cell mass by single-cell RNA-seq analysis. Cell Stem Cell *6*, 468–478.

Tesar, P.J., Chenoweth, J.G., Brook, F.A., Davies, T.J., Evans, E.P., Mack, D.L., Gardner, R.L., and McKay, R.D. (2007). New cell lines from mouse epiblast share defining features with human embryonic stem cells. Nature *448*, 196–199.

Teslaa, T., and Teitell, M.A. (2015). Pluripotent stem cell energy metabolism: an update. EMBO J. *34*, 138–153.

TeSlaa, T., Chaikovsky, A.C., Lipchina, I., Escobar, S.L., Hochedlinger, K., Huang, J., Graeber, T.G., Braas, D., and Teitell, M.A. (2016). α-Ketoglutarate accelerates the initial differentiation of primed human pluripotent stem cells. Cell Metab. *24*, 485–493.

Tsanov, K.M., Pearson, D.S., Wu, Z., Han, A., Triboulet, R., Seligson, M.T., Powers, J.T., Osborne, J.K., Kane, S., Gygi, S.P., et al. (2017). LIN28 phosphorylation by MAPK/ERK couples signalling to the post-transcriptional control of pluripotency. Nat. Cell Biol. *19*, 60–67.

van Hoek, M., Langendonk, J.G., de Rooij, S.R., Sijbrands, E.J.G., and Roseboom, T.J. (2009). Genetic variant in the IGF2BP2 gene may interact with fetal malnutrition to affect glucose metabolism. Diabetes *58*, 1440–1444.

Vogt, E.J., Meglicki, M., Hartung, K.I., Borsuk, E., and Behr, R. (2012). Importance of the pluripotency factor LIN28 in the mammalian nucleolus during early embryonic development. Development *139*, 4514–4523.

Weinberger, L., Ayyash, M., Novershtern, N., and Hanna, J.H. (2016). Dynamic stem cell states: naive to primed pluripotency in rodents and humans. Nat. Rev. Mol. Cell Biol. *17*, 155–169.

Wu, J., Huang, B., Chen, H., Yin, Q., Liu, Y., Xiang, Y., Zhang, B., Liu, B., Wang, Q., Xia, W., et al. (2016). The landscape of accessible chromatin in mammalian preimplantation embryos. Nature *534*, 652–657.

Xue, Z., Huang, K., Cai, C., Cai, L., Jiang, C.Y., Feng, Y., Liu, Z., Zeng, Q., Cheng, L., Sun, Y.E., et al. (2013). Genetic programs in human and mouse early embryos revealed by single-cell RNA sequencing. Nature *500*, 593–597.

Yan, L., Yang, M., Guo, H., Yang, L., Wu, J., Li, R., Liu, P., Lian, Y., Zheng, X., Yan, J., et al. (2013). Single-cell RNA-seq profiling of human preimplantation embryos and embryonic stem cells. Nat. Struct. Mol. Biol. *20*, 1131–1139.

Yang, M., and Vousden, K.H. (2016). Serine and one-carbon metabolism in cancer. Nat. Rev. Cancer *16*, 650–662.

Yang, Y., Liu, B., Xu, J., Wang, J., Wu, J., Shi, C., Xu, Y., Dong, J., Wang, C., Lai, W., et al. (2017). Derivation of pluripotent stem cells with in vivo embryonic and extraembryonic potency. Cell *169*, 243–257.e25.

Zhang, J., Khvorostov, I., Hong, J.S., Oktay, Y., Vergnes, L., Nuebel, E., Wahjudi, P.N., Setoguchi, K., Wang, G., Do, A., et al. (2011). UCP2 regulates energy metabolism and differentiation potential of human pluripotent stem cells. EMBO J. *30*, 4860–4873.

Zhang, J., Nuebel, E., Daley, G.Q., Koehler, C.M., and Teitell, M.A. (2012). Metabolic regulation in pluripotent stem cells during reprogramming and self-renewal. Cell Stem Cell *11*, 589–595.

Zhang, B., Zheng, H., Huang, B., Li, W., Xiang, Y., Peng, X., Ming, J., Wu, X., Zhang, Y., Xu, Q., et al. (2016a). Allelic reprogramming of the histone modification H3K4me3 in early mammalian development. Nature *537*, 553–557.

Zhang, J., Ratanasirintrawoot, S., Chandrasekaran, S., Wu, Z., Ficarro, S.B., Yu, C., Ross, C.A., Cacchiarelli, D., Xia, Q., Seligson, M., et al. (2016b). LIN28 regulates stem cell metabolism and conversion to primed pluripotency. Cell Stem Cell *19*, 66–80.

Zhou, W., Choi, M., Margineantu, D., Margaretha, L., Hesson, J., Cavanaugh, C., Blau, C.A., Horwitz, M.S., Hockenbery, D., Ware, C., and Ruohola-Baker, H. (2012). HIF1α induced switch from bivalent to exclusively glycolytic metabolism during ESC-to-EpiSC/hESC transition. EMBO J. *31*, 2103–2116.

Zhu, H., Shyh-Chang, N., Segrè, A.V., Shinoda, G., Shah, S.P., Einhorn, W.S., Takeuchi, A., Engreitz, J.M., Hagan, J.P., Kharas, M.G., et al.; DIAGRAM Consortium; MAGIC Investigators (2011). The Lin28/let-7 axis regulates glucose metabolism. Cell *147*, 81–94.

32

Alpha-ketoglutarate: a "magic" metabolite in early germ cell development

Vivian Lu[1] & Michael A Teitell[2,3,4,5,6,7]

A causal relationship between cell metabolism and the fate of pluripotent stem cells through epigenome regulation is emerging. A recent study shows that the tricarboxylic acid cycle intermediate alpha-ketoglutarate (αKG) can both sustain naïve mouse embryonic stem cell pluripotency and promote primordial germ cell differentiation. This observation together with other studies provides intriguing possibilities for stabilizing ephemeral embryonic cell states and enhancing desired fate transitions through specific metabolite manipulations.

Primordial germ cells (PGCs) are precursors of gametes that connect one generation to the next. Modeling early mouse germ cell development *in vitro* begins with the transition of naïve mouse embryonic stem cells (mESCs) into transient, primed mouse epiblast-like cells (EpiLCs) (Fig 1). This is followed by conversion of EpiLCs into PGC-like cells (PGCLCs), which can produce sperm and oocytes. mESCs and PGCs are similar in expressing pluripotency regulators Oct4, Nanog, and Sox2, but are unique from epigenome and transcriptome changes that yield cell states with distinct developmental potentials (Hayashi *et al*, 2011). A key question under study in many lineage-specific developmental systems is what is the role for metabolism in cell fate transitions and outcomes?

Now, Tischler *et al* (2018) identify roles for alpha-ketoglutarate (αKG) in maintaining mESC pluripotency and enhancing PGCLC differentiation. Using single-cell RNA-Seq over a developmental time course referred to as a "pseudotime analysis", they show a transition from mainly oxidative (OXPHOS) to glycolytic metabolism with progression from mESCs to EpiLCs. On conversion of EPiLCs to PGCLCs, OXPHOS increases and glycolysis decreases, consistent with a prior study (Hayashi *et al*, 2017). Repressing glycolysis or elevating αKG levels favors retention of mESC self-renewal over exit from naïve pluripotency. Adding αKG boosts PGCLC production by ~50%, and added αKG can replace 2i/Lif medium to maintain mESC self-renewal or can substitute for BMP4/8 in PGCLC fate induction. Remarkably, αKG addition also extends EpiLC competency to form PGCLCs without affecting cell quality, with H3K9me2 and H3K27me3 histone marks stabilized.

Alpha-ketoglutarate is a cofactor for Jumonji C (JmjC)-domain-containing histone demethylases (JHDMs) and ten-eleven translocation (TET) DNA demethylases. Cell-permeable dimethyl-αKG (dm-αKG) used to elevate αKG also has non-epigenome activities and can stabilize hypoxia-inducible factor 1α (HIF1α) to induce a pseudo-hypoxic state with altered gene expression (Hou *et al*, 2014). αKG can also inhibit the ATP synthase and mTOR (Chin *et al*, 2014), although added αKG did not affect the ATP synthase and could substitute for dm-αKG to promote human ESC differentiation in a prior study (TeSlaa *et al*, 2016). Consistent with an epigenome effect, dm-αKG altered H3K9me3 and H3K27me3 levels to promote self-renewal of naïve mESCs in another study (Carey *et al*, 2015). Added αKG also enhanced spontaneous mESC differentiation (Hwang *et al*, 2016) and directed human neuroectoderm differentiation (TeSlaa *et al*, 2016) with altered histone and DNA methylation levels.

Using pseudotime modeling, the current RNA-Seq analysis revealed cell heterogeneity in differentiation capacity on EpiLC induction, with added αKG increasing PGC competency. Also, αKG preserved histone methylation patterns and prolonged a transient state for PGC competency. Whether succinate, a product and inhibitor of dioxygenase epigenome modifying enzyme reactions, would impair PGC competency was not examined. Also, the epigenetic state resulting from increased αKG may be physiologic or aberrant and requires further comparison studies. These results further suggest that αKG or other metabolites could prolong (or shorten) other transitory intermediate cell states. For example, cancer cells use glutaminolysis to generate αKG as an anapleurotic fuel for the TCA cycle and drug resistance may occur by induction of a transient transcriptional state via epigenome remodeling (Shaffer *et al*, 2017). Manipulating αKG levels by glutamine reduction could deplete TCA cycle intermediates and block transient drug-resistant cancer cell states.

In vivo studies of αKG and other metabolites on cell fate are largely unexplored, yielding questions about how diet and environment influence germ cell metabolite levels and outcomes. Most epigenetic marks

1   Department of Molecular and Medical Pharmacology, UCLA, Los Angeles, CA, USA
2   Department of Pathology and Laboratory Medicine, UCLA, Los Angeles, CA, USA. E-mail: mteitell@mednet.ucla.edu
3   California NanoSystems Institute, UCLA, Los Angeles, CA, USA
4   Department of Bioengineering, UCLA, Los Angeles, CA, USA
5   Molecular Biology Institute, UCLA, Los Angeles, CA, USA
6   Eli and Edythe Broad Center of Regenerative Medicine, UCLA, Los Angeles, CA, USA
7   Jonsson Comprehensive Cancer Center, UCLA, Los Angeles, CA, USA
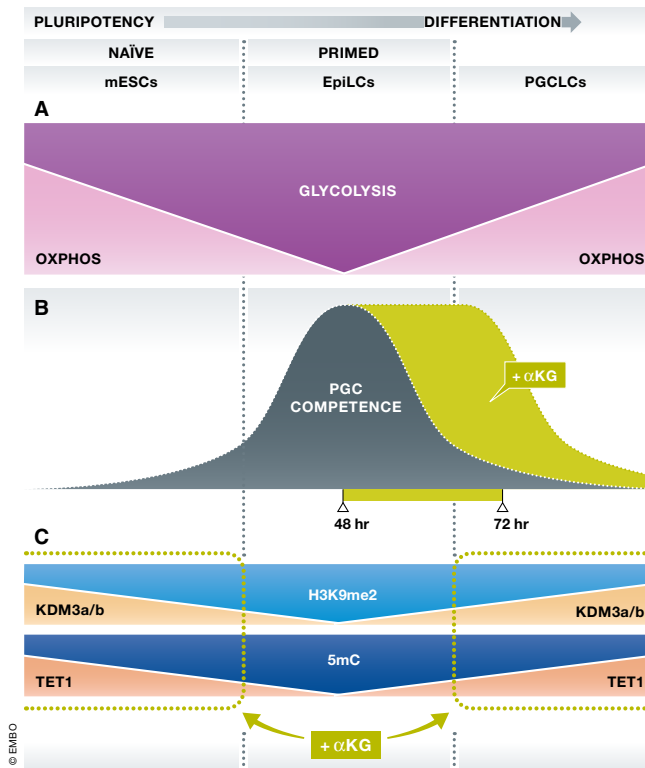
Figure 1. αKG effects on PGC competency and primordial germ cell development.
(A) A transition from naïve mESCs to primed EpiLCs coincides with reduced OXPHOS and increased glycolysis that reverses when EpiLCs convert to PGCLCs. (B,C) Addition of αKG prolongs PGC competency from 48 to 72 h, potentially by locking-in an epigenetic pattern regulated by KDM3a/b and TET1 enzyme activities. mESC, mouse embryonic stem cells; EpiLCs, epiblast-like cells; PGCLCs, primordial germ cell-like cells; PGC, primordial germ cell; αKG, alpha-ketoglutarate.

shaped by short-term environmental conditions are not inherited even with known imprinting (Heard & Martienssen, 2014). Caloric restriction, high-fat diet, and malnourishment in parents can impact the epigenome and small noncoding RNAs transmitted by gametes to offspring (Sharma & Rando, 2017). Emerging genome editing technologies may abet *in vivo* manipulations of metabolite levels at specific times within a developing embryo to start addressing the role of metabolites *in vivo*. Indeed, large knowledge gaps exist for (i) how to assess the contribution of diet to key metabolite levels in both somatic and germ cells, (ii) the responsiveness of epigenetic regulators and cofactors to specific metabolite levels, and (iii) whether metabolite-influenced epigenome modifications persist and manifest into adulthood and across generations. An impediment to early embryo studies is the paucity of starting materials, with advances in single-cell methods holding promise to bridge the gap between metabolism, epigenetics, and stem cell fates (Zhang *et al*, 2018). Advancing this emerging opportunity *in vitro* at first, Tischler *et al* (2018) deploy single-cell technologies to reveal how targeted metabolic manipulations augment (or potentially retard) dynamic cell state conversions during PCG development.

References

Carey BW, Finley LW, Cross JR, Allis CD, Thompson CB (2015) Intracellular alphaketoglutarate maintains the pluripotency of embryonic stem cells. *Nature* 518: 413−416

Chin RM, Fu X, Pai MY, Vergnes L, Hwang H, Deng G, Diep S, Lomenick B, Meli VS, Monsalve GC, Hu E, Whelan SA, Wang JX, Jung G, Solis GM, Fazlollahi F, Kaweeteerawat C, Quach A, Nili M, Krall AS *et al* (2014) The metabolite alphaketoglutarate extends lifespan by inhibiting ATP synthase and TOR. *Nature* 510: 397−401

Hayashi K, Ohta H, Kurimoto K, Aramaki S, Saitou M (2011) Reconstitution of the mouse germ cell specification pathway in culture by pluripotent stem cells. *Cell* 146: 519−532

Hayashi Y, Otsuka K, Ebina M, Igarashi K, Takehara A, Matsumoto M, Kanai A, Igarashi K, Soga T, Matsui Y (2017) Distinct requirements for energy metabolism in mouse primordial germ cells and their reprogramming to embryonic germ cells. *Proc Natl Acad Sci USA* 114: 8289−8294

Heard E, Martienssen RA (2014) Transgenerational epigenetic inheritance: myths and mechanisms. *Cell* 157: 95−109

Hou P, Kuo CY, Cheng CT, Liou JP, Ann DK, Chen Q (2014) Intermediary metabolite precursor dimethyl-2-ketoglutarate stabilizes hypoxia-inducible factor-1alpha by inhibiting prolyl-4-hydroxylase PHD2. *PLoS ONE* 9: e113865

Hwang IY, Kwak S, Lee S, Kim H, Lee SE, Kim JH, Kim YA, Jeon YK, Chung DH, Jin X, Park S, Jang H, Cho EJ, Youn HD (2016) Psat1-dependent fluctuations in alpha-ketoglutarate affect the timing of ESC differentiation. *Cell Metab* 24: 494−501

Shaffer SM, Dunagin MC, Torborg SR, Torre EA, Emert B, Krepler C, Beqiri M, Sproesser K, Brafford PA, Xiao M, Eggan E, Anastopoulos IN, Vargas-Garcia CA, Singh A, Nathanson KL, Herlyn M, Raj A (2017) Rare cell variability and drug-induced reprogramming as a mode of cancer drug resistance. *Nature* 546: 431−435

Sharma U, Rando OJ (2017) Metabolic inputs into the epigenome. *Cell Metab* 25: 544−558

TeSlaa T, Chaikovsky AC, Lipchina I, Escobar SL, Hochedlinger K, Huang J, Graeber TG, Braas D, Teitell MA (2016) alpha-ketoglutarate accelerates the initial differentiation of primed human pluripotent stem cells. *Cell Metab* 24: 485−493

Tischler J, Gruhn WH, Reid R, Allgeyer E, Buettner F, Marr C, Theis F, Simons BD, Lorenz Wernisch L, Surani MA (2018) Metabolic regulation of pluripotency and germ cell fate through alpha−ketoglutarate. *EMBO J* https://doi.org/10.15252/embj.201899518

Zhang J, Zhao J, Dahan P, Lu V, Zhang C, Li H, Teitell MA (2018) Metabolism in pluripotent stem cells and early mammalian development. *Cell Metab* 27: 332−338

CHAPTER 4:

Use of Chemically Defined, Nutrient-Balanced Media for Germ Lineage Differentiation of Primed

Human Pluripotent Stem Cells

Use of chemically defined, nutrient-balanced media for germ lineage differentiation of primed human pluripotent stem cells

Vivian Lu[1], Mary T. Doan[1], Irena J. Roy[2], Alejandro Torres Jr.[3], and Michael A. Teitell[3,4,5,6,7,8]*

[1]Department of Molecular and Medical Pharmacology, David Geffen School of Medicine, University of California at Los Angeles, Los Angeles, CA, 90095, USA

[2]Developmental and Stem Cell Biology Program, University of California at San Francisco, San Francisco, CA, 94143, USA

[3]Molecular Biology Institute, University of California at Los Angeles, Los Angeles, CA, 90095, USA

[4]Department of Pathology and Laboratory Medicine, David Geffen School of Medicine, University of California at Los Angeles, Los Angeles, CA, 90095, USA

[5]Department of Bioengineering, California NanoSystems Institute, and Broad Center for Regenerative Medicine and Stem Cell Research, University of California at Los Angeles, Los Angeles, CA, 90095, USA

[6]Department of Pediatrics, David Geffen School of Medicine, University of California at Los Angeles, Los Angeles, CA, 90095, USA

[7]Jonsson Comprehensive Cancer Center, David Geffen School of Medicine, University of California at Los Angeles, Los Angeles, CA, 90095, USA

[8]Lead Contact

*Correspondence: mteitell@mednet.ucla.edu

Highlights

- Instructions for biomarker analysis of primed and lineage differentiated hPSCs
- Guide to making nutrient-balanced media for primed hPSC differentiation
- Steps for directed differentiation of primed hPSCs into ectoderm, mesoderm, or endoderm
- Detailed proof-of-concept example with manipulation of glutamine (Gln) availability

Summary

Metabolism regulates cell fates during early mammalian cell differentiation (Carey et al., 2015; Cliff et al., 2017; Folmes et al., 2011; Moussaieff et al., 2015; TeSlaa et al., 2016; Varum et al., 2011). Here, we provide a chemically defined nutrient-balanced media formulation for directed differentiation of primed-stage human pluripotent stem cells (hPSCs) into the three primary germ lineages, ectoderm, endoderm and mesoderm. Although the transient removal and addition of specific nutrients does not

occur *in vivo* during earliest embryonic development, manipulation of nutrients *in vitro* provides a handy, easily available method for evaluating and understanding how extracellular and intracellular metabolites help to determine PSC fate.

For complete details on the use and execution of this protocol, please refer to Lu et al. (2019) and Lu et al. (2022).

Graphical abstract

STAR✦Protocols
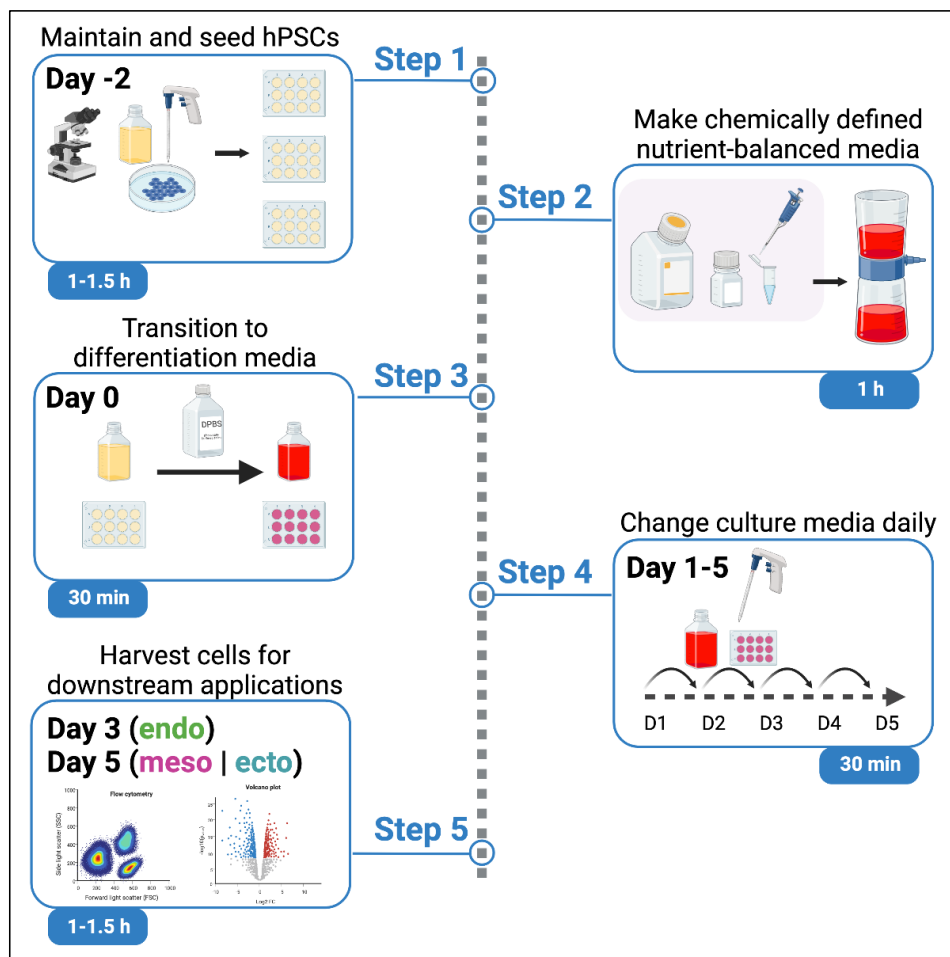
Before you begin

We have had experience and success with commercially available ready-to-use human pluripotent stem cell (hPSC) differentiation kits, although these reagents may present a cost barrier for certain hPSC projects or applications. Additionally, the formulations of these kits are often proprietary and opaque to users. In designing experiments in which eliminating confounding variables is paramount, differing nutrient and/or metabolite concentrations within and between different differentiation media formulations may bias the interpretation of results unknowingly. Here, we provide a validated (Lu et al., 2019) and accessible methodology for differentiating primed hPSCs into early germ lineage-specific cells using chemically defined, nutrient-balanced media.

This protocol provides detailed instructions for differentiating primed hPSCs into endoderm, mesoderm and ectoderm using readily available cytokines and equivalent media-supplied nutrient concentrations. We have used this protocol successfully for differentiating human embryonic stem cell (hESC) and induced pluripotent stem cell (iPSC) lines including H9 (WA09; RRID:CVCL_9773), H1 (WA01; RRD:CVCL_9771), HSF-1 (RRID:CVCL-D003), hIPS2 (RRID:CVCL_B508), and UCLA1 (RRID:CVCL_9951). We also include instructions for biomarker analysis of primed-undifferentiated and differentiated hPSCs (**Table 1**), as well as a detailed proof-of-concept example with the manipulation of extracellular glutamine (Gln) availability.

Depending on the organization where this protocol will be performed, prior approval for the use of hPSCs may be required, such as from an institutional Stem Cell Research Oversight Committee. Standard cell culture procedures and equipment are required for the maintenance and differentiation of primed hPSCs. In addition, all steps of this protocol utilize a humidified incubator at 37°C and 5% CO_2, without regulating the O_2 level, for cell culture and Matrigel® matrix gelation. It is also recommended that primed hPSCs in culture are tested bi-weekly for mycoplasma contamination, which can adversely affect mammalian cells.

Table 1. Commonly used biomarkers for primed-undifferentiated and differentiated hPSCs	
Category	**Transcription factor (full name)**
pluripotent/ undifferentiated	SOX2 (SRY-box 2)
pluripotent/ undifferentiated	NANOG (Nanog homeobox)
pluripotent/ undifferentiated	POU5F1 (POU class 5 homeobox 1)
endoderm	FOXA2 (Forkhead Box A2)
endoderm	SOX17 (SRY-box 17)
endoderm	EOMES (Eomesodermin)
endoderm	LEFTY1 (Left-right determination factor 1)
endoderm	AFP (Alpha fetoprotein)
mesoderm	MIXL1 (Mixed paired-like homeobox)
mesoderm	T (T brachyury transcription factor)
mesoderm	HAND1 (Heart and neural crest derivatives expressed 1)
mesoderm	DES (Desmin)
mesoderm	CD34 (Transmembrane phosphoglycoprotein)
mesoderm	SNAI2 (Snail family transcriptional repressor 2)
ectoderm	NCAM1 (Neural cell adhesion molecule 1)
ectoderm	PAX6 (Paired box 6)
ectoderm	OTX2 (Orthodenticle homeobox 2)
ectoderm	NES (Nestin)
ectoderm	TFAP2A (Transcription factor AP-2 alpha)
ectoderm	SOX 1 (SRY-box 1)

Coating plates with Matrigel®
hPSCs will be maintained in culture and differentiated in feeder-free conditions on tissue culture-treated polystyrene microplates coated with Corning Matrigel® basement membrane matrix. For our protocol, we describe hPSC culturing conditions using a 6-well plate format and differentiation with a 12-well plate setup.

Timing: 30 min

Note: Corning Matrigel® matrix should be handled on ice as it will start to polymerize at temperatures above 10°C. Each lot of Matrigel® matrix varies in protein concentration and dilution, which is indicated on the Certificate of Analysis from the manufacturer. For additional information on the handling and use of Matrigel® matrix, visit the Corning® Matrigel® Matrix information page (here) for detailed instructions.

In general, we coat 6- and 12-well tissue culture-treated polystyrene microplates with 1 ml/well (6-well plate) or 0.5 mL/well (12-well plate) of cell feeder-free Matrigel® basement membrane matrix diluted in ice-cold DMEM/F-12 media in a sterile hood, followed by incubation in a 5% CO_2 tissue culture incubator for gelation for at least 30 min at 37°C.

CRITICAL: Do not leave coated plates at 37°C incubation for more than 48 h. Coated plates left to incubate for extended periods of time are susceptible to evaporation and drying out. hPSCs will not adhere to dry plates.

Preparing media and stock reagents
Obtain media and reagents indicated in the **Key resources table**. Prepare mTeSR(+) and working stocks of reagents as described in **Table 2** and **Table 3**, respectively.

Thawing hPSCs for culture
Here, we provide a general procedure for thawing and reviving hPSC lines onto a 6-well tissue culture-treated polystyrene microplate for culturing stock hPSCs for further differentiation.

Timing: 30 min

1. Prepare a 6-well tissue culture-treated polystyrene microplate coated with Corning Matrigel® basement membrane matrix (as described above in **Coating plates with Matrigel®**).
2. Obtain a frozen cryotube of hPSCs stored in liquid nitrogen and gently swirl the sealed vial in a 37°C water bath until frozen liquid contents are almost completely melted.
3. In a sterile tissue culture hood, carefully transfer vial contents using a 5-mL serological pipette into a 15-mL conical tube containing 5 mL of 37°C DMEM/F-12 media. Do not pipette up and down vigorously because cell colonies will dissociate.
4. Centrifuge cells at 300 x g at room temperature for 5 min.
5. Aspirate the media off the coated 6-well tissue culture-treated polystyrene microplate.
6. Aspirate the supernatant and resuspend the cell pellet with 6 mL, 37°C mTeSR(+) by gently pipetting up and down 2-3x with a 10-mL serological pipette.

7. Pipette 1 mL/well of cell suspension into the 6-well tissue culture-treated polystyrene microplate. Make sure that hPSC colonies are evenly distributed, then incubate the microplate at 37°C in a 5% CO_2 tissue culture incubator without disturbing for 24 h.

CRITICIAL: Avoid over-pipetting the resuspension to avoid single celling colonies and inducing apoptosis. Colonies in suspension should look no smaller than ~8-10-cell clusters under the microscope.

Maintaining hPSCs

This step describes daily maintenance of hPSCs in culture.

During primed hPSC maintenance and expansion, it is vital to assess and sustain the quality of cells and colonies until the time of seeding for differentiation experiments. Visible changes in hPSC colony morphology will be noticeable and must be removed to reduce unwanted genetic aberrations or loss of pluripotency due to poor cell quality and spontaneous differentiation (Garitaonandia et al., 2015).

There are variations in the morphological appearance of hPSC colonies that a user may encounter, with the experience of the user helping to identify acceptable or unacceptable appearance variations. As an example, **Figure 1** brightfield images illustrate different morphologies of high- and low-quality primed hPSC colonies. Desirable primed hPSC features include relatively uniform appearing colonies with defined borders, rounded shapes and dense colony centers (**Figure 1A**). By contrast, undesirable primed hPSC colony features include non-uniform shapes and borders between colonies, especially with modest to large colony areas of apparent spontaneous differentiation showing increasingly 'fibroblast-like' shaped cells (**Figure 1B**). Note that culling may not be necessary when differentiation involves <5% of cells and colonies within a well, but spontaneous differentiation regions should not exceed 20% of the well when the stock culture is high quality. It is best to revive a new cell stock when there are high levels of low quality colonies.

It is recommended that a user visually inspects growing primed hPSC colonies every day to mark and remove low quality colonies or regions (**Figure 1C**). Use brightfield microscopy at low magnification (either 4x or 10x) to identify and mark unacceptable hPSC colonies using a microscope lens cell dotting marker, such as this, to stamp the bottom of each well. Remove selected regions by gently aspirating the marked colonies.

Note: Be sure to wear gloves and wipe down benchtop surfaces with 70% ethanol before beginning daily maintenance. Maintain culture sterility during visual inspection by keeping the microplate lid on at all times when working outside a sterile tissue culture hood. Do not leave the culture plate out of the incubator for more than 15 min at a time during inspection.

Timing: 30 min

1. Aspirate spent media from each well of the 6-well plate and replace daily with 2 mL 37°C mTeSR(+).
2. Repeat daily maintenance until hPSCs are ready to seed for differentiation experiments.

Figure 1
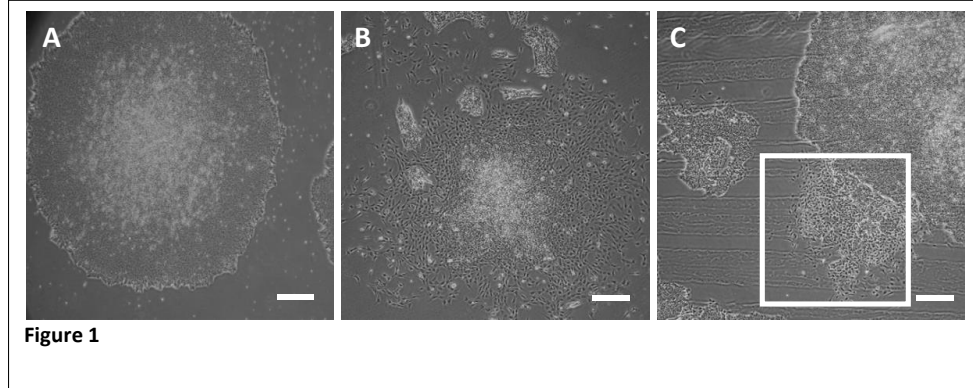
Key resources table

REAGENT or RESOURCE	SOURCE	IDENTIFIER
Antibodies		
Bacterial and virus strains		
Biological samples		
Chemicals, peptides, and recombinant proteins		
Gentle Cell Dissociation Reagent	Stemcell Technologies	Cat#07174
mTeSR Plus Kit (mTeSR(+))	Stemcell Technologies	Cat#100-0276
DMEM/F12	Gibco	Cat#11320033
ROCK Inhibitor; Y-27632	Stemcell Technologies	Cat#72304
Monothioglycerol	Millipore Sigma	Cat#M6145
BSA Fraction V, 7.5%	Gibco	Cat#15260037
2-mercaptoethanol	Thermofisher	Cat#21985-023
GlutaMAX supplement	Thermofisher	Cat#35050-061
N2 supplement	Gibco	Cat#17502048
B27 supplement	Gibco	Cat#17504044
SB43154	Stemgent	Cat#04-0010
Dorsomorphin	Stemgent	Cat#04-0024
Human recombinant insulin	Millipore Sigma	Cat#11376497001
Transferrin from human serum	Millipore Sigma	Cat#10652202001
Chemically defined lipid concentrate (CDLC)	Gibco	Cat#11905031
Human recombinant VEGF-165	Stemcell Technologies	Cat#78073.1
Human recombinant BMP-4	PeproTech	Cat#120-05ET
Human recombinant FGF2	Stemcell Technologies	Cat#78003
Human recombinant Activin A	Stemcell Technologies	Cat#78001.1
CHIR99021 (GSK3i)	Stemcell Technologies	Cat#72052
PI-103 hydrochloride	Tocris/Fisher Scientific	Cat#29-301

Stemolecule LDN-1931189	Stemgent	Cat#04-0074
Matrigel	Corning/Fisher Scientific	Cat#CB-4023A
DMEM/F12, no Gln	Gibco	Cat#21331020
DPBS, 1x, without calcium or magnesium	Corning	Cat#21031CV
Cell Culture Grade Water	Fisher Scientific	Cat# MT25055CI
Dimethyl Sulfoxide (DMSO)	Fisher Scientific	Cat# MT-25950CQC
Critical commercial assays		
MycoAlert detection kit	Lonza	Cat#LT08-418
Deposited data		
Experimental models: cell lines		
H9 (WA09); Female	UCLA BSCRC hESC core bank	RRID:CVCL_9773
Experimental models: organisms/strains		
Oligonucleotides		
Recombinant DNA		
Software and algorithms		
Other		
Sterile vacuum filtration system	Fisher Scientific	Cat#0974101
Polystyrene microplates	Falcon	Cat#087721
Hemocytometer	Fisher Scientific	Cat#02-671-5
Cell scrapers	Fisher Scientific	Cat#08-100-241
UltiMate 3000 RSLC (HPLC)	Thermo Scientific	n/a
Q Exactive (MS)	Thermo Scientific	n/a

Materials and Equipment

All cell culture and material preparation must be performed under sterile conditions. When preparing media and reagents, we suggest the use of sterile cell culture materials, such as sterile centrifuge tubes, pipette tips, serological pipettes, and solvents. Sterilization using a 0.22-micron polyethersulfone (PES) membrane filter is also an option. Aliquot and pre-warm media to 37°C before usage. Excess warmed media should be discarded and not be re-stored at 4°C and re-warmed for usage due to reduced protein efficacy of media components essential for maintaining cell viability and proliferation.

Table 2. mTeSR™ Plus (mTeSR(+)) media – commercially available kit		
Reagent	**Final concentration**	**Amount**
mTeSR™ Plus Basal Medium	n/a	400 mL
mTeSR™ Plus 5x Supplement	1x	100 mL
Total	**n/a**	**500 mL**

Store at 4°C for up to 2 weeks. Visit Stemcell Technologies™ mTeSR™ Plus information page ([here](#)) for official guidelines on storage and handling of mTeSR™ Plus kit reagents and preparation and usage of complete mTeSR™ Plus.

Table 3. Stock and working concentration of reagents			
Reagent	**Solvent**	**Stock concentration**	**Working concentration**
Y-27632	water	10 mM	10 µM
Insulin	water	10 mg/mL	0.7 µg/mL
Transferrin	n/a	30 mg/mL	15 µg/mL
Activin A	water	100 µg/mL	100 ng/mL
CHIR99021	water	10 mM	2 µM
PI-103	water	50 µM	50 nM
LDN 1931189	DMSO	250 µM	250 nM
VEGF-165	water	100 µg/mL	100 ng/mL
BMP4	5 mM HCl pH3, 0.1% BSA in DPBS	100 µg/mL	100 ng/mL
FGF2	water	20 µg/mL	20 ng/mL
N-2 supplement	n/a	100x	1%
B-27 supplement	n/a	50x	2%
SB43154	DMSO	10 mM	10 µM
Dorsomorphin	DMSO	2 mM	0.2 µM

Store reagents as stated on the Certificate of Analysis from the manufacturer.

Note: We store working aliquots at -20°C, except for transferrin, which we store at 4°C. We recommend making working aliquots of each reagent solution to avoid multiple freeze thaw cycles. Working aliquot amounts are based on the user's experimental necessity.

Step-by-step method details

The above section describes best practices for maintaining and expanding healthy primed hPSC colonies using visual inspection and culling, as needed, until the time of seeding for differentiation experiments. The following step-by-step method details the directed differentiation of primed hPSCs into each of the three primary germ lineages using chemically defined nutrient-balanced media formulations (**Figure 2**).

CRITICAL: No antibiotics are present or used in hPSC culture medium. All steps must be performed under sterile conditions. Take extra caution in all steps by using sterile reagents and filtration. If any cloudiness or opaqueness appear in culture media, or when colonies are dying in suspension, throw the stock away and start with new cells, as contamination is likely to have occurred.
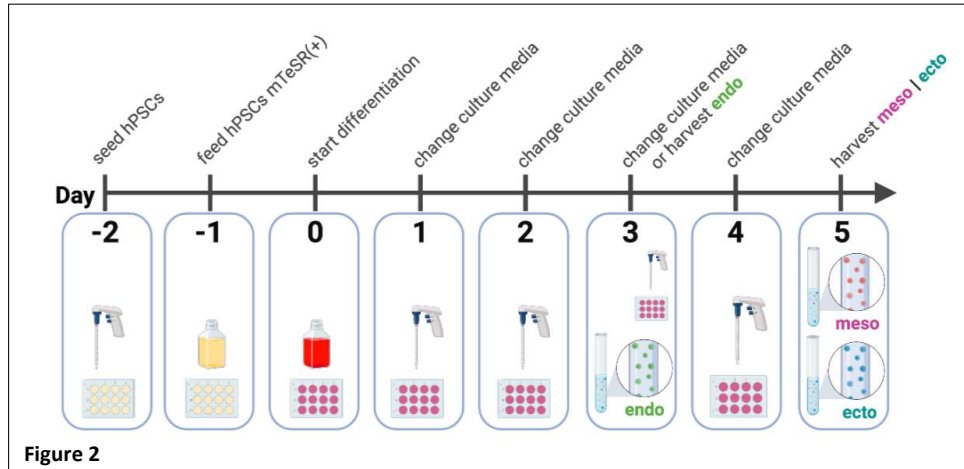
Figure 2

hPSC plating for differentiation

Timing: 1-1.5 h, two days prior to differentiation

This section covers harvesting and single cell seeding of primed hPSCs for directed differentiation experiments. We encourage users to test cells for mycoplasma contamination using standard kits of choice, such as the Lonza MycoAlert Kit, prior to starting the differentiation procedure. Additionally, take care to visually inspect the spent culture media for any cloudiness or opaqueness, as this may indicate bacterial or fungal contamination. Users should routinely check stock hPSC cells for the presence of pluripotency and absence of differentiation biomarkers using flow cytometry or RT-qPCR to ensure starting cell populations are of high quality (**Table 1**). Growth and expansion of hPSC colonies to 70-80% confluency, which yields ~2.0-3.0 x 10^6 cells in the 6-well microplate format, is optimal for harvest and seeding of growing colonies at the start of the differentiation procedure. The protocol below provides detailed procedures for harvesting hPSCs from a 6-well tissue culture-treated polystyrene microplate and seeding into 12-well plates. These steps can be adapted to other plating formats by adjusting the numbers of cells or colonies and media volumes accordingly.

1. Prepare 12-well tissue culture-treated polystyrene microplates coated with Corning Matrigel® basement membrane matrix (as described in **Before you begin**).
2. Identify and remove regions of differentiation using aspiration (as described in **Figure 1C**) in the stock 6-well hPSC culture plate before harvesting.
3. Remove the media from the 6-well hPSC culture plate by needle aspiration.
4. Wash hPSCs gently to not disrupt colonies with 1 mL 1x Dulbecco's phosphate-buffered saline (DPBS) without calcium or magnesium. Aspirate to remove the 1x DPBS.
5. Add 1 mL/well of Gentle Cell Dissociation Reagent to hPSC colonies at 37°C in a 5% CO_2 tissue culture incubator for 10 min.
6. Add 1 mL/well of 37°C DMEM/F-12 media to dilute out Gentle Cell Dissociation Reagent.

7. Using a cell scraper, gently scrape colonies and cells off the bottom of the 6-well culture plate and ensure they are dissociated into single cells by pipetting against the surface of each well with a P1000 3x before collecting the combined contents of the plate into a 50 mL conical tube.
8. Count the number of hPSCs harvested for use with a hemocytometer.

Optional: Automated cell counters are acceptable, but we recommend validating automated counting machines using a hemocytometer.

9. Centrifuge the harvested hPSCs at 450 x g for 5 m. Aspirate media gently to avoid disrupting the cell pellet and resuspend the hPSCs in 1 mL of 37°C mTeSR(+) containing 10 µM Rho-associated protein kinase (ROCK) inhibitor, Y-27632.

CRITICAL: It is critical to add ROCK inhibitor, Y-27632, into the media because it prevents apoptosis induced by single cell dissociation of hPSC colonies. Otherwise, the survival of hPSCs post-seeding will be markedly reduced (Kurosawa, 2012).

10. Calculate the volume required to resuspend primed hPSCs in mTeSR(+) media with 10 µM Y-27632 at 6.5×10^4 cells/cm^2 final concentration.
11. Place 1 mL/well of hPSCs in mTeSR(+) media with 10 µM Y-27632 into Matrigel®-coated 12-well tissue culture-treated polystyrene microplates. Make sure that hPSCs are evenly distributed, and then incubate the seeded microplate at 37°C in a 5% CO_2 tissue culture incubator for 24 h.
12. 24 h post-plating (**Figure 3A**), gently wash the primed hPSCs with 1 mL 1x DPBS without calcium or magnesium. Aspirate the 1x DPBS gently, then add 1 mL/well of 37°C mTeSR(+) media (without ROCK inhibitor) and return the microplate to the 37°C, 5% CO_2 tissue culture incubator.
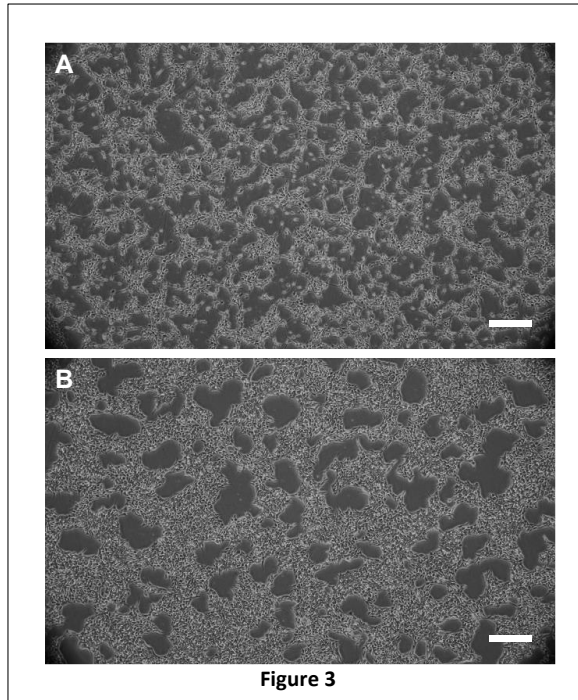
Figure 3

13. Allow the primed hPSCs to grow in mTeSR(+) media for 24 h before beginning the directed differentiation procedure.

CRITICAL: In the event that the primed hPSCs do not appear ~70-80-% confluent in their seeded wells (**Figure 3B**) on Day 0 (**Figure 2**), allow the hPSCs to continue growing in replaced, fresh 1 mL mTeSR(+) media for an additional 24 h prior to initiating the directed differentiation procedure.

Making chemically defined, nutrient-balanced media for tri-lineage differentiation
Timing: 1 h

This section details the preparation of media for chemically defined, nutrient-balanced directed differentiation of primed hPSCs into ectoderm, mesoderm, and endoderm lineages. Of note, the protocol endpoint for endoderm is three days (72 h) post-start of differentiation, whereas the endpoint for mesoderm and ectoderm differentiation is five days (120 h) post-start of differentiation

(**Figure 2**). Additionally, be sure to exclude insulin, transferrin, and chemically defined lipid concentrate from the base media for ectoderm differentiated cells because B-27 and N2 supplements already contain these factors. The Base Media Preparation Tables provided below note this difference. These cytokine combinations have been optimized and adapted from previous studies (Chambers et al., 2009; Loh et al., 2014; Loh et al., 2016). Here, we also include formulation instructions for Gln-free medium as an example; however, this protocol for chemically defined, nutrient-balanced media is non-limiting, meaning that it can be adjusted for any nutrient deprivation study.

14. Make mesoderm/endoderm or ectoderm base media according to the following tables for lineage differentiation of choice (**Tables 4-5**).
    a. A range of experimental manipulations can be made by modifying DMEM/F12 nutrient composition. Below, we provide an example for Gln-free base media (**Tables 6-7**). In this instance, DMEM/F12 no Gln is used and GlutaMAX was excluded.

Note: We recommend first sterile filtering base media and then adding sterile cytokines to generate differentiation media because lineage-inducing cytokines could stick to the filter membrane, affecting their final concentrations, and causing undesirable reduction or variability in hPSC differentiation within or between experiments.

Optional: A substitute for GlutaMAX is L-Gln. However, L-Gln is not stable at 4°C and is therefore not recommended.

Table 4. Preparation of Base Media – mesoderm or endoderm (ME or EN) differentiation		
Reagent	**Final concentration**	**Amount**
DMEM/F12	n/a	96.5 mL
1-thioglycerol	450 µM	3.9 µL
BSA	1 mg/mL	1.33 mL
2-mercaptoethanol	0.11 µM	182 µL
GlutaMAX	1%	1 mL
insulin	0.7 µg/mL	7 µL
transferrin	15 µg/mL	50 µL
chemically defined lipid concentrate	1 mL/100 mL	1 mL
Total	**n/a**	**100 mL**

Table 5. Preparation of Base Media – ectoderm (EC) differentiation		
Reagent	**Final concentration**	**Amount**
DMEM/F12	n/a	97.5 mL
1-thioglycerol	450 µM	3.9 µL
BSA	1 mg/mL	1.33 mL
2-mercaptoethanol	0.11 µM	182 µL
GlutaMAX	1%	1 mL
Total	**n/a**	**100 mL**

Table 6. Preparation of *Gln-free* Base Media – mesoderm or endoderm (ME or EN) differentiation		
Reagent	**Final concentration**	**Amount**
DMEM/F12, no Gln	n/a	97.5 mL
1-thioglycerol	450 µM	3.9 µL
BSA	1 mg/mL	1.33 mL
2-mercaptoethanol	0.11 µM	182 µL
insulin	0.7 µg/mL	7 µL
transferrin	15 µg/mL	50 µL
chemically defined lipid concentrate	1 mL/100 mL	1 mL
Total	**n/a**	**100 mL**

Table 7. Preparation of *Gln-free* Base Media – Ectoderm (EC) differentiation		
Reagent	**Final concentration**	**Amount**
DMEM/F12, no Gln	n/a	98.5 mL
1-thioglycerol	450 µM	3.9 µL
BSA	1 mg/mL	1.33 mL
2-mercaptoethanol	0.11 µM	182 µL
Total	**n/a**	**100 mL**

15. Sterilize each final media preparation using a 0.22-micron polyethersulfone (PES) membrane filter.

Pause point: At this step, base media preparations can be stored at 4°C for use within two weeks.

CRITICAL: Sterile, non-expired cytokines that have not undergone multiple freeze-thaw cycles should be added immediately prior to the start of each experiment to ensure efficacy.

16. At the start of differentiation (D0) (**Figure 2**), add sterile lineage-inducing cytokines to each respective base media for each desired indication (**Tables 8-12**).
    a. Below, we provide tables to guide the addition of cytokines to the different types of base media for lineage-specific differentiations. Dilute stock cytokine solutions using sterile techniques and store according to the manufacturers' instructions.

CRITICAL: Prepare aliquots of stock cytokine solutions to extend storage life and avoid repeated freeze-thaw cycles that can reduce potency.

Note: Be careful because each day of differentiation may require the addition of different cytokine combinations to enhance the success of this protocol. See specific schedules in the tables, below.

Table 8. Endoderm differentiation cytokines for Day 0			
Reagent	Stock concentration	Final concentration	Per 1 mL EN media
Activin A	100 µg/mL	100 ng/mL	1 µL
CHIR99021	10 mM	2 µM	0.2 µL
PI-103	50 µM	50 nM	1 µL

Table 9. Endoderm differentiation cytokines for Days 1-3			
Reagent	Stock concentration	Final concentration	Per 1 mL EN media
Activin A	100 µg/mL	100 ng/mL	1 µL
LDN 1931189	250 µM	250 nM	1 µL

Table 10. Mesoderm differentiation cytokines for Day 0			
Reagent	Stock concentration	Final concentration	Per 1 mL ME media
VEGF-165	100 µg/mL	100 ng/mL	1 µL
BMP4	100 µg/mL	100 ng/mL	1 µL
FGF2	20 µg/mL	20 ng/mL	1 µL
Activin A	100 µg/mL	100 ng/mL	1 µL

Table 11. Mesoderm differentiation cytokines for Days 1-5			
Reagent	Stock concentration	Final concentration	Per 1 mL ME media
VEGF-165	100 µg/mL	100 ng/mL	1 µL
BMP4	100 µg/mL	100 ng/mL	1 µL
FGF2	20 µg/mL	20 ng/mL	1 µL

Table 12. Ectoderm differentiation cytokines for Days 0-5			
Reagent	Stock concentration	Final concentration	Per 1 mL EC media
N-2 supplement	n/a	1%	10 µL
B-27 supplement	n/a	2%	20 µL
SB43154	10 mM	10 µM	1 µL
Dorsomorphin	2 mM	0.2 µM	0.1 µL

Directed differentiation of hPSCs to primary germ lineages

Timing: 30 min – 1 h per day

This section provides instructions for the execution of hPSC directed differentiation into each of the three germ lineages, starting with the transition of mTeSR(+) hPSC maintenance cultures to lineage-specific differentiation media.

17. Remove spent mTeSR(+) maintenance media from wells and wash the hPSC colonies gently with room temperature 1x DPBS w/o calcium & magnesium.

18. Add 1 mL/well (~263 uL/cm^2) of 37°C appropriate differentiation media and then incubate cells at 37°C in a 5% CO_2 incubator for 24 h.
19. Every 24 h, repeat gentle washing and media changes according to the cytokine schedule above (**Tables 6-10**) until hPSCs have committed to a directed lineage (**Table 1, Figures 2, 4**).
20. Harvest cells according to planned downstream applications and analyses.
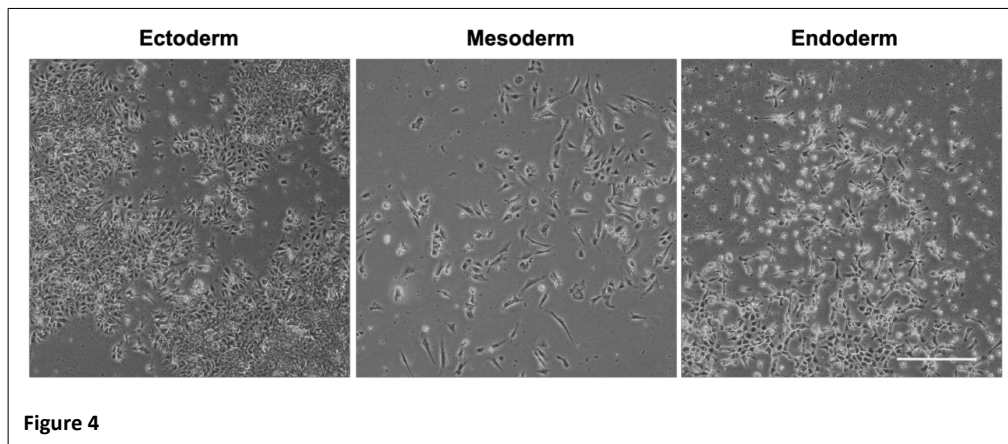
Figure 4

Expected outcomes

There is growing, multidisciplinary appreciation for the role of nutrients in governing developmental cell fate decisions (Lu et al., 2021). An increased understanding for how specific nutrients that are present in certain niches *in vivo*, and our ability to alter these nutrients in hPSC culture media, provides a valuable experimental tool to yield new insights into the regulation of early cell fate transitions, potentially within a developing human embryo. This protocol provides an accessible and customizable way to uncover the influence of nutrients in *in vitro* culture, with the following comments providing details of the expected outcomes of implementing this protocol. To confirm equivalent amounts of nutrients in each lineage differentiation media, we used ultra high-performance liquid chromatography mass spectrometry (UHPLC-MS) to quantify carbon sources and amino acids present in freshly prepared, unspent media. Results indicate that unspent media for induction of each lineage consisted of equivalent levels of metabolites (**Figure 5**). This is the expected outcome when directed differentiation media is prepared properly since the base media composition and cytokine cocktails net out to the same concentration of nutrients. Successful, directed hPSC differentiation into each specific germ lineage was also verified using RNA-Seq transcriptome profiling and lineage-specifying biomarker protein expression by flow cytometry and immunoblot analyses (**Table 1**) (Lu et al., 2019; Lu et al., 2022).

Proof-of-Concept Example:
Using our chemically defined, nutrient-balanced differentiation media, our group recently showed that there is an essential need for Gln during germ lineage differentiation, with each lineage having its own unique Gln dependency (Lu et al., 2019). Specifically, we uncovered that initial ectoderm is

independent of extracellular Gln (Lu et al., 2022). Directed tri-lineage differentiation with and without Gln in the media revealed varying reliance for this nutrient in the formation and viability of hPSCs undergoing cell fate transitions (**Figure 6**). For the full execution and proof-of-concept for this protocol that examined Gln availability during hPSC differentiation, please refer to Lu et al., 2022.
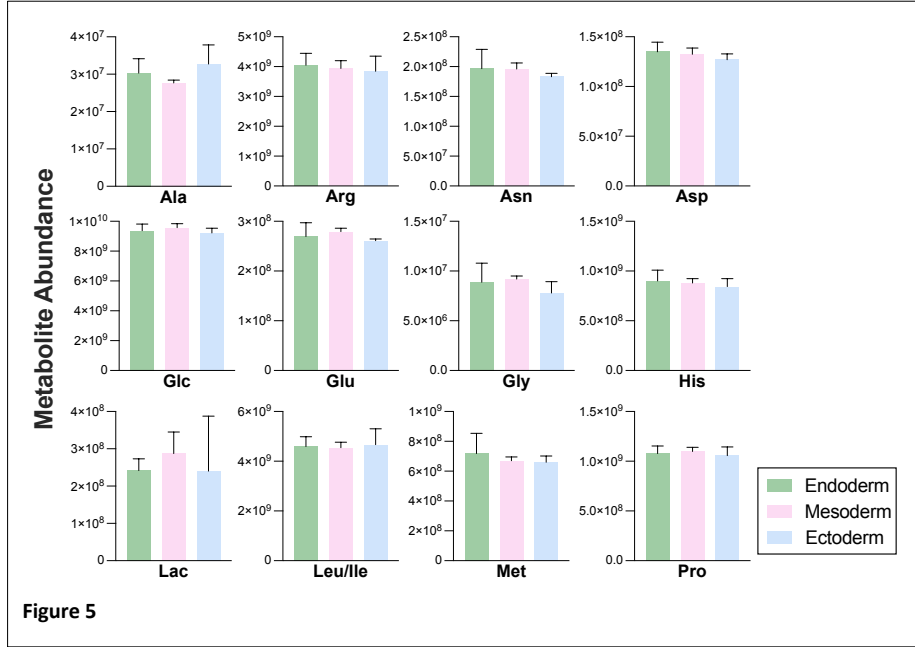
Figure 5
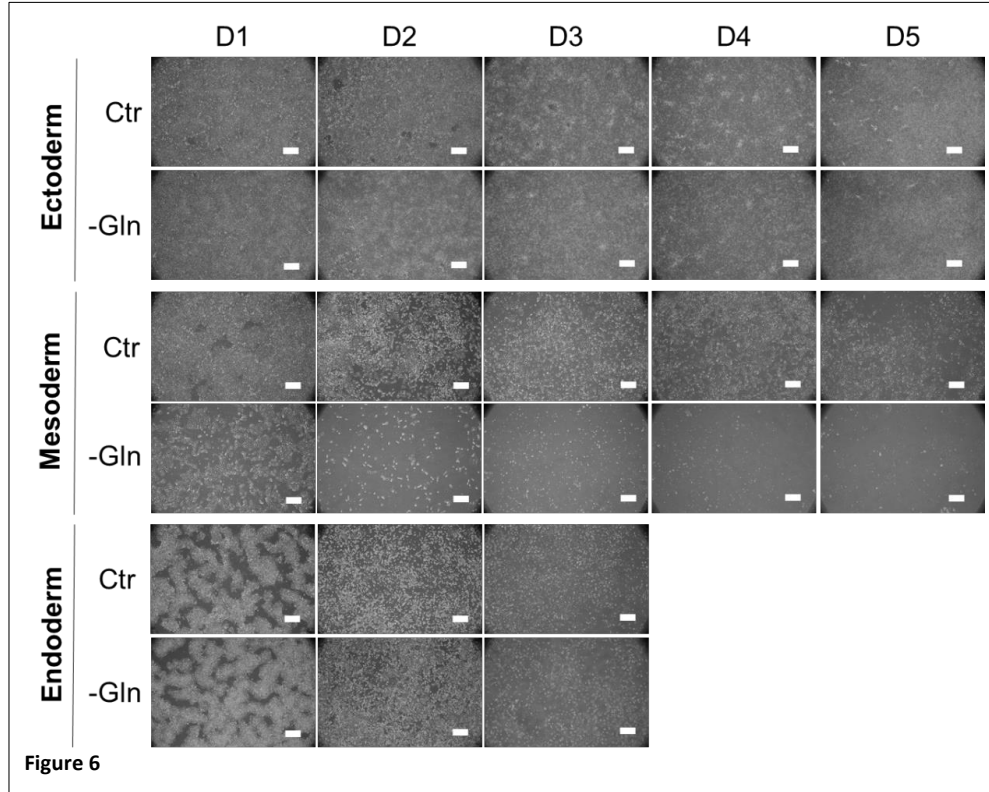
Figure 6

Limitations

Using this protocol, chemically defined, nutrient-equivalent lineage directed differentiation of primed hPSCs is limited to feeder-free systems that use Matrigel® matrix, gelatin, or other solid substrates. Studies comparing feeder-free and feeder-dependent systems reported differences in hPSC metabolic characteristics and differentiation potential (Gu et al., 2016; Zhang et al., 2016), which guided our initial decision to optimize this protocol in feeder-free hPSC culture. Other factors that limit the translational impact of this protocol include: (1) shifting nutrient concentrations that exclude one nutrient or another almost certainly do not occur *in vivo* during development and (2) nutrient concentration levels used in this *in vitro* culture system may be supra-physiologic and likely do not resemble *in vivo* levels.

Troubleshooting

Problem 1:
Stock or seeded hPSCs exhibit a high amount of cell death and/or release from culture plate surface as flakes or whole colonies.

Potential solution:
This could be from several issues related to the sterility of the cell culture. Note that this protocol does not utilize antibiotics, so extra precaution is required. In addition, it is advisable to routinely examine the stock hPSC culture for mycoplasma infection by testing spent media removed from plate wells with 70-80% confluent hPSC growth, followed by mycoplasma testing using commercially available kits, such as the Lonza MycoAlert Kit. Additionally, visual checks for clarity or cloudiness of spent media could suggest or exclude bacterial, fungal or yeast contamination as a potential source for this problem. Another reason for high death could be exclusion of ROCK inhibitor to single cell suspensions during the hPSC seeding step, which will induce apoptosis due to single cell dissociation.

Problem 2:
Stock, seeded, or differentiating cells are flaking off into suspension during media changes and/or during DPBS washes.

Potential solution:
Primed hPSC colonies are sensitive to physical dislodging from a plate surface. When performing daily culture media changes, gently pipette the media to the side of the well to avoid direct interaction of the media stream with the colonies. Additionally, when aspirating media from wells, take care not to directly touch the bottom of the well with the aspirator tip, as doing so may disrupt the Matrigel® coating and/or aspirate off colonies.

Problem 3:
Cells are not differentiating properly, as verified by morphological or biomarker assessments.

Potential solution:
A problem could be the potency of small molecules or cytokines used to induce differentiation. Ensure that cytokines are not used beyond their expiration date after aliquoting and fresh dilution before each addition to base media. For example, failed mesoderm differentiation could be from multiple freeze-thaw cycles, or old and expired, low potency BMP4.

Problem 4:
There is high variability of differentiation efficiencies between biological replicates.

Potential solution:
It is typical for different hPSC lines to vary in functional differentiation capacities (Cahan and Daley, 2013). However, when an experimentalist is experiencing high differentiation variability between replicate studies of the same hPSC line, several issues may be at fault. First, ensure primed hPSC

seeding is consistent and confluence at the start of differentiation (Day 0) is ~70-80% in each plate well. When the starting hPSC confluence is too low, differentiating cells may experience high cell death rates. When the starting hPSC confluence is too high, differentiation may be impaired because amount of available cytokine of interest is insufficient. Second, it is crucial to ensure all cytokines, reagents, and base media components are presumably active (non-expired, not continuously freeze-thawed, correct storage conditions, non-contaminated). In our experience, it may be helpful to contact technical support to inquire whether other users are having similar issues with a particular lot. Third, check the genomic integrity and stability of the hPSC stock cells to ensure the starting cells are high quality. Karyotypic abnormalities can be detected using qPCR analysis with products such as this hPSC Genetic Analysis Kit.

Resource availability

Lead contact
Further information and requests for resources and reagents should be directed to and will be fulfilled by the lead contact, Michael A. Teitell (mteitell@mednet.ucla.edu).

Materials availability
This study did not generate new unique reagents.

Data and code availability
This protocol did not generate new datasets or code.

Author contributions
V.L., M.T.D., and M.A.T. conceptualized and wrote the manuscript. I.J.R. and A.T. assisted in developing the protocol.

Declaration of interests
The authors declare no competing interests.

STAR Protocols

CellPress

References

Cahan, P., and Daley, G.Q. (2013). Origins and implications of pluripotent stem cell variability and heterogeneity. Nat Rev Mol Cell Biol *14*, 357-368.

Carey, B.W., Finley, L.W., Cross, J.R., Allis, C.D., and Thompson, C.B. (2015). Intracellular alpha-ketoglutarate maintains the pluripotency of embryonic stem cells. Nature *518*, 413-416.

Chambers, S.M., Fasano, C.A., Papapetrou, E.P., Tomishima, M., Sadelain, M., and Studer, L. (2009). Highly efficient neural conversion of human ES and iPS cells by dual inhibition of SMAD signaling. Nat Biotechnol *27*, 275-280.

Cliff, T.S., Wu, T., Boward, B.R., Yin, A., Yin, H., Glushka, J.N., Prestegaard, J.H., and Dalton, S. (2017). MYC Controls Human Pluripotent Stem Cell Fate Decisions through Regulation of Metabolic Flux. Cell Stem Cell *21*, 502-516 e509.

Folmes, C.D., Nelson, T.J., Martinez-Fernandez, A., Arrell, D.K., Lindor, J.Z., Dzeja, P.P., Ikeda, Y., Perez-Terzic, C., and Terzic, A. (2011). Somatic oxidative bioenergetics transitions into pluripotency-dependent glycolysis to facilitate nuclear reprogramming. Cell Metab *14*, 264-271.

Garitaonandia, I., Amir, H., Boscolo, F.S., Wambua, G.K., Schultheisz, H.L., Sabatini, K., Morey, R., Waltz, S., Wang, Y.C., Tran, H.*, et al.* (2015). Increased risk of genetic and epigenetic instability in human embryonic stem cells associated with specific culture conditions. PLoS One *10*, e0118307.

Gu, W., Gaeta, X., Sahakyan, A., Chan, A.B., Hong, C.S., Kim, R., Braas, D., Plath, K., Lowry, W.E., and Christofk, H.R. (2016). Glycolytic Metabolism Plays a Functional Role in Regulating Human Pluripotent Stem Cell State. Cell Stem Cell *19*, 476-490.

Kurosawa, H. (2012). Application of Rho-associated protein kinase (ROCK) inhibitor to human pluripotent stem cells. J Biosci Bioeng *114*, 577-581.

Loh, K.M., Ang, L.T., Zhang, J., Kumar, V., Ang, J., Auyeong, J.Q., Lee, K.L., Choo, S.H., Lim, C.Y., Nichane, M.*, et al.* (2014). Efficient endoderm induction from human pluripotent stem cells by logically directing signals controlling lineage bifurcations. Cell Stem Cell *14*, 237-252.

Loh, K.M., Chen, A., Koh, P.W., Deng, T.Z., Sinha, R., Tsai, J.M., Barkal, A.A., Shen, K.Y., Jain, R., Morganti, R.M.*, et al.* (2016). Mapping the Pairwise Choices Leading from Pluripotency to Human Bone, Heart, and Other Mesoderm Cell Types. Cell *166*, 451-467.

Lu, V., Dahan, P., Ahsan, F.M., Patananan, A.N., Roy, I.J., Torres, A., Jr., Nguyen, R.M.T., Huang, D., Braas, D., and Teitell, M.A. (2019). Mitochondrial metabolism and glutamine are essential for mesoderm differentiation of human pluripotent stem cells. Cell Res *29*, 596-598.

Lu, V., Roy, I.J., and Teitell, M.A. (2021). Nutrients in the fate of pluripotent stem cells. Cell Metab.

Lu, V., Roy, I.J., Torres, A., Jr., Joly, J.H., Ahsan, F.M., Graham, N.A., and Teitell, M.A. (2022). Glutamine-dependent signaling controls pluripotent stem cell fate. Dev Cell.

Moussaieff, A., Rouleau, M., Kitsberg, D., Cohen, M., Levy, G., Barasch, D., Nemirovski, A., Shen-Orr, S., Laevsky, I., Amit, M*., et al.* (2015). Glycolysis-mediated changes in acetyl-CoA and histone acetylation control the early differentiation of embryonic stem cells. Cell Metab *21*, 392-402.

TeSlaa, T., Chaikovsky, A.C., Lipchina, I., Escobar, S.L., Hochedlinger, K., Huang, J., Graeber, T.G., Braas, D., and Teitell, M.A. (2016). alpha-Ketoglutarate Accelerates the Initial Differentiation of Primed Human Pluripotent Stem Cells. Cell Metab *24*, 485-493.

Varum, S., Rodrigues, A.S., Moura, M.B., Momcilovic, O., Easley, C.A.t., Ramalho-Santos, J., Van Houten, B., and Schatten, G. (2011). Energy metabolism in human pluripotent stem cells and their differentiated counterparts. PLoS One *6*, e20914.

Zhang, H., Badur, M.G., Divakaruni, A.S., Parker, S.J., Jager, C., Hiller, K., Murphy, A.N., and Metallo, C.M. (2016). Distinct Metabolic States Can Support Self-Renewal and Lipogenesis in Human Pluripotent Stem Cells under Different Culture Conditions. Cell Rep *16*, 1536-1547.

Figure legends

Figure 1: Assessing the quality of primed hPSCs by visual inspection. Representative brightfield images of (**A**) high and (**B**) poor quality hPSC morphologies. (**C**) An example of an area of differentiation (boxed in white) near a healthy hPSC colony that should be removed during routine maintenance. Scale bar: 400 μM.

Figure 2: Workflow timeline schematic. Illustration of a primed hPSC-derived differentiation timeline for each germ lineage. Primed hPSCs should be seeded two days (48 h) prior to the start of differentiation. Culture media must be changed every day (24 h). The differentiation endpoint for endoderm is three days (72 h) post-start of differentiation, whereas the endpoint for mesoderm and ectoderm differentiation is five days (120 h) post-start of differentiation. The method of differentiated cell harvesting depends on downstream applications.

Figure 3. Primed hPSCs post-plating for differentiation. Representative brightfield images of hPSCs post-seeding (Day -1 and 0). hPSCs (**A**) 24 h and (**B**) 48 h post-seeding grown in mTeSR(+) medium. Scale bar: 400 μM.

Figure 4. Morphologies of primed hPSCs differentiate into specific embryonic germ lineages. Representative brightfield images of directed germ lineage differentiation. Expected morphologies of differentiated hPSCs at the end of this protocol: ectoderm and mesoderm after five days and endoderm after three days. Scale bar: 400 μM.

Figure 5. Quantification of metabolite abundances in tri-lineage differentiation media show equivalent nutrient formulations. Metabolites were extracted from endoderm, mesoderm, and ectoderm differentiation media, without addition of cells, and processed using UHPLC-MS. Nutrient abundances for each lineage-inducing media were quantified. Alanine (Ala), Arginine (Arg),

Asparagine (Asn), Aspartic acid (Asp), Glucose (Glc), Glutamic acid (Glu), Glycine (Gly), Histidine (His), Lactate (Lac), Leucine/Isoleucine (Leu/Ile), Methionine (Met), Proline (Pro).

Figure 6. Stages of hPSC differentiation to directed germ lineages with and without Gln deprivation.
Representative brightfield images of day-by-day (D) stages of hPSC differentiation grown in Gln-supplemented (Ctr) or Gln-free (-Gln) conditions to each specific lineage. Scale bar: 400 µM.

CHAPTER 5:

Nutrients and the Fate of Pluripotent Stem Cells

Perspective

Nutrients in the fate of pluripotent stem cells

Vivian Lu,[1,8] Irena J. Roy,[2,8] and Michael A. Teitell[3,4,5,6,7,*]

[1]Department of Molecular and Medical Pharmacology, David Geffen School of Medicine, University of California, Los Angeles, Los Angeles, CA 90095, USA
[2]Developmental and Stem Cell Biology, School of Medicine, University of California, San Francisco, San Francisco, CA 94143, USA
[3]Department of Pathology and Laboratory Medicine, David Geffen School of Medicine, University of California, Los Angeles, Los Angeles, CA 90095, USA
[4]Department of Pediatrics, David Geffen School of Medicine, University of California, Los Angeles, Los Angeles, CA 90095, USA
[5]Molecular Biology Institute, University of California, Los Angeles, Los Angeles, CA 90095, USA
[6]Department of Bioengineering, University of California, Los Angeles, Los Angeles, CA 90095, USA
[7]Jonsson Comprehensive Cancer Center, California NanoSystems Institute, and Broad Center for Regenerative Medicine and Stem Cell Research, University of California, Los Angeles, Los Angeles, CA 90095, USA
[8]These authors contributed equally
*Correspondence: mteitell@mednet.ucla.edu
https://doi.org/10.1016/j.cmet.2021.09.013

SUMMARY

Pluripotent stem cells model certain features of early mammalian development *ex vivo*. Medium-supplied nutrients can influence self-renewal, lineage specification, and earliest differentiation of pluripotent stem cells. However, which specific nutrients support these distinct outcomes, and their mechanisms of action, remain under active investigation. Here, we evaluate the available data on nutrients and their metabolic conversion that influence pluripotent stem cell fates. We also discuss key questions open for investigation in this rapidly expanding area of increasing fundamental and practical importance.

INTRODUCTION

Pluripotent stem cells (PSCs) self-renew or, with specific cues, can differentiate into the three primary germ lineages *in vitro*. A defining feature of pluripotency is remarkable plasticity in cell identity, leading to potential applications in tissue engineering, regenerative medicine, and studies of early embryonic development (Smith, 2017; Tsogtbaatar et al., 2020). In considering the fate of PSCs, we define pluripotent/self-renewing stem cells as cells that express core pluripotency transcription factors including OCT4, NANOG, SOX2, and others, and differentiation as the silencing of core pluripotency transcription factors coupled with the gain of lineage-specifying biomarkers (Yeo and Ng, 2013). Functionally, two principal hallmarks that define PSCs are blastocyst chimerism and teratoma formation, which test *in vivo* ability to re-enter development in a host embryo and spontaneous generation of the three germ layers, respectively (De Los Angeles et al., 2015). Of particular interest here are studies suggesting that supplied nutrients, with or without intracellular processing, have active, guiding roles in PSC identity and cell fate transitions (Intlekofer and Finley, 2019; Shyh-Chang and Ng, 2017; Tsogtbaatar et al., 2020). For example, the metabolic flux of nutrients through glycolysis, the tricarboxylic acid (TCA) cycle, and one-carbon metabolism generates intermediate metabolites used in reactions to modify the PSC epigenome, chromatin structure, and gene expression (Carey et al., 2015; Moussaieff et al., 2015; Shiraki et al., 2014; Shyh-Chang et al., 2013b; TeSlaa et al., 2016).

In addition to studies linking PSC-produced intermediate metabolites with epigenome modifications, many interesting questions remain regarding the role of nutrients, including sugars,

amino acids, lipids, and others, in the control of PSC fate. For example, recent results suggest that nutrients can also influence PSC fate through mechanisms that do not include metabolic flux through anabolic or catabolic pathways (Chi et al., 2020; Cornacchia et al., 2019; Na et al., 2020; Song et al., 2019; Vardhana et al., 2019; Zhu et al., 2020). One potential interpretation of these studies is that specific nutrients signal conditions in the microenvironment prior to, or concomitant with, triggers that control PSC fate. In this perspective, we examine the contributions of nutrients in PSC fate through both metabolic conversion and nutrient-triggered signaling.

NUTRIENTS AND PSCs IN CONTEXT

Studies of mammalian pre-implantation embryos grown in chemically defined media showed that certain nutrients alone, without added growth factors, could induce cell identity transitions (Summers and Biggers, 2003). This result suggested that the presence of specific niche nutrients could initiate PSC fate and not just support a pre-established PSC fate. Additional studies also showed that specific nutrients reinforced pre-established pluripotency/self-renewal and differentiation fates by influencing fate-specifying transcription programs, enzyme-mediated chromatin changes, and/or nutrient-sensitive signaling (Baksh and Finley, 2021). Together, these studies suggest that the same nutrient(s) can either initiate or support PSC fates, with differential effects that depend on context, such as the state of pluripotency, differentiation cues, culture media conditions, and timed nutrient addition or deprivation (Table 1).

Specific nutrient deprivation or addition does not occur naturally *in vivo*, but *in vitro* nutrient changes provide a valuable

experimental tool. For example, the timed withdrawal of glutamine from PSC culture medium shows differential effects on PSC fate. Short-term glutamine withdrawal eliminated cells with a high dependence on glutamine for TCA cycle anaplerosis, enriching for surviving mouse embryonic stem cells (mESCs) and human PSCs (hPSCs) with increased expression of pluripotent transcription factors OCT4 and SOX2 (Vardhana et al., 2019). Other studies conversely showed that high levels of glutamine metabolism prevented the degradation of OCT4 and preserved hPSC self-renewal (Marsboom et al., 2016). Long-term glutamine deprivation also caused more oxidative PSCs to die from a reduction in TCA cycle activity and oxidative phosphorylation (OXPHOS) (Tohyama et al., 2016). In this context, glutamine withdrawal provided a strategy to eliminate PSCs and enrich for hPSC-derived cardiomyocytes (Tohyama et al., 2016) or enhance the angiogenic capacity of endothelial cells (Marsboom et al., 2016). These combined, nuanced results suggest that short-term glutamine withdrawal followed by repletion eliminates more oxidative PSCs (Folmes et al., 2011; Moussaieff et al., 2015; Varum et al., 2011) and yields more homogeneous PSCs with higher expression of pluripotency transcription factors. Thus, manipulating the timing of glutamine exposure in PSC culture can control whether PSCs or non-pluripotent cells enrich.

Investigators subdivide PSCs into a continuum of states that resemble different gestational stages of blastocyst development, with each state showing specific nutrient requirements and activities (Hackett and Surani, 2014; Smith, 2017). A hypothesized, and recently captured, intermediate "formative" pluripotent state has expanded the dynamic nature of pluripotency (Hoogland and Marks, 2021; Kinoshita et al., 2021; Wang et al., 2021b; Yu et al., 2021). Thus far, only one study investigated the metabolism of formative state PSCs, which upregulate glycolysis and downregulate mitochondrial respiration enzymes (Yu et al., 2021). Reports have also consistently shown that naive PSCs display bivalent glycolytic and mitochondrial respiration compared to primed PSCs, which are exclusively glycolytic (Hackett and Surani, 2014; Hoogland and Marks, 2021). In usual culture conditions, hPSCs resemble more developmentally advanced, or "primed," PSCs, corresponding to post-implantation epiblast, whereas mESCs resemble less advanced, or "naive," PSCs, corresponding to pre-implantation epiblast (Hackett and Surani, 2014). Interestingly, differentiation potential varies with glutamine withdrawal for naive compared to primed PSCs. Maintenance of naive mESCs requires 2i (MEK and GSK3β inhibitors) plus leukemia inhibitory factor (LIF) media supplementation, which promotes independence from added glutamine (Carey et al., 2015). By contrast, mESCs grown in LIF-containing medium without 2i supplementation are more advanced, with glutamine deprivation causing increased spontaneous differentiation, mainly into trophectoderm (TE) and mesoderm, and decreased pluripotency transcription factor expression (Carey et al., 2015; Ryu et al., 2015). In primed hPSCs, spontaneous differentiation upon glutamine deprivation inhibits mesoderm and promotes ectoderm lineage development, suggesting a lineage-specific requirement for glutamine (Lu et al., 2019). Together, these reports suggest a context-specific glutamine requirement with different PSC differentiation outcomes based on PSC status. Further studies should reveal whether the species of origin, mouse or human, also contributes to differences

in differentiation potential for naive or primed PSCs with glutamine withdrawal.

Glucose, another key nutrient for mammalian cells, also appears to control PSC outcomes. *Ex vivo* culture with pyruvate, lactate, and glucose as nutrients, without added growth factors or cytokines, initiates pre-implantation mouse embryos through 5 days of development, suggesting embryo self-sufficiency in cell specification with specific nutrients only (Biggers et al., 1997; Nagaraj et al., 2017; Summers and Biggers, 2003). In early mouse embryogenesis, at the compacted 8-cell morula stage, glycolysis is dispensable although glucose is essential (Chi et al., 2020). During the transition from morula to TE and the blastocyst inner cell mass, which is the first fate specification, glucose-dependent signaling directs the formation of extra-embryonic TE, but not the ICM (Chi et al., 2020). These *ex vivo* mouse studies showed glucose import support of pentose phosphate pathway (PPP) nucleotide production and hexosamine biosynthesis pathway (HBP) signaling that activated the TE-specifying transcription factor, CDX2. Culture in glucose-deficient medium showed decreased expression of TE biomarkers with unaffected ICM-specifying OCT4 and NANOG expression (Chi et al., 2020). Thus, earliest cell fate specification shows developmental cues controlled, at least partly, by nutrient availability and nutrient-sensitive signaling.

Mammalian zygotic genome activation (ZGA) triggers increased gene transcription, with metabolism shifting from maternal to embryonic control. During this period, glycolytic flux increases as protein synthesis and metabolic shuttles activate (Gardner, 1998; Gardner and Harvey, 2015; Leese and Barton, 1984; Schulz and Harrison, 2019; Zhang et al., 2018a). These changes add flexibility in nutrient dependence because the developing embryo increases enzymes capable of interconverting nutrients (Sharpley et al., 2021). Later stage development, modeled *in vitro* by PSC-derived tri-lineage germ layer differentiation, loses a requirement for glucose (Chi et al., 2020; Cliff et al., 2017). Initial ectoderm differentiation shifts to glycolysis-dependent, rather than glucose-dependent, metabolism. Inhibition of ectoderm differentiation by blocking upstream steps in glycolysis can be overcome by added galactose or fructose, which enter glycolysis downstream of hexokinase at glucose-6-phosphate or fructose-1-phosphate steps, respectively (Cliff et al., 2017). Glucose oxidation is also not required to sustain pluripotency, as a culture surface embedded with non-degradable glucose enriched for mESCs with elevated pluripotent and low differentiation biomarker expression (Mashayekhan et al., 2008).

Studies indicate that additional nutrients, such as ascorbic acid and amino acids proline and methionine, also regulate pluripotency. Reprogramming of mouse and human somatic cells into induced PSCs (iPSCs) accelerates with the addition of ascorbic acid by reducing p53 levels to impede cellular senescence (Esteban et al., 2010), by reducing H3K36me3/2 levels through Jhdm1a1/b demethylases (Wang et al., 2011), and by increasing STAT2 phosphorylation, which increases binding to and activation of the *Nanog* promoter (Wu et al., 2014). In human iPSC colonies, ascorbic acid actively promotes pluripotency and inhibits spontaneous differentiation through enhancement of histone demethylase JARID1 expression (Eid and Abdel-Rehim, 2016). A vast body of work, described elsewhere, provides the unique and varied roles of ascorbic acid in stem cell

Table 1. Examples of a nutrient eliciting distinct PSC fates

Nutrient	Cell state	Possible outcomes	Context	Reference
Glutamine	pluripotency (less committed)	(−) cell death	withdrawal in hPSCs (long-term)	Tohyama et al., 2016
		(−) increased self-renewal	withdrawal in mESCs and hSPCs (short-term, followed by repletion)	Vardhana et al., 2019
		(−) maintained pluripotency marker expression	naive mESC state with 2i	Carey et al., 2015
		(−) decreased pluripotency marker expression	naive mESC state without 2i	Carey et al., 2015; Ryu et al., 2015
	differentiation (more committed)	(−) increased trophectoderm and mesoderm lineage expression	naive mESC state without 2i	Ryu et al., 2015
		(−) inhibited mesoderm expression and promoted ectoderm expression	hPSC spontaneous differentiation (embryoid bodies)	Lu et al., 2019
Glucose	pluripotency	(−) inhibited formation of the extra-embryonic TE, but not embryonic ICM	pre-implantation mouse morula	Chi et al., 2020
	differentiation	(−) inhibition of glucose oxidation (2-DG, 3-BrPA, DCA) inhibited ectoderm, but not mesoderm and endoderm, differentiation; defect can be rescued with glucose-6-phosphate and fructose-1-phosphate, so ectoderm exhibits glycolysis, not glucose, requirement	hPSC spontaneous differentiation	Cliff et al., 2017
		(+) culturing mESCs in high glucose concentration promotes generation of cardiomyocytes	mESC lineage-directed differentiation	Crespo et al., 2010
		(+) culturing mESCs in high glucose concentration inhibits generation of neural lineage cells	mESC lineage-directed differentiation	Chen et al., 2018; Yang et al., 2016
Ascorbic acid	pluripotency	(+) accelerated reprogramming of somatic cells into iPSCs	mouse and human somatic cells	Esteban et al., 2010; Wang et al., 2011; Wu et al., 2014
		(+) promoted pluripotency	human iPSC colonies	Eid and Abdel-Rehim, 2016
	differentiation	(+) inhibited spontaneous differentiation	human iPSC colonies	Eid and Abdel-Rehim, 2016
		(+) promoted cardiac differentiation, but only occurs when supplemented during early window of differentiation	cardiac cell differentiation	Sato et al., 2006; Takahashi et al., 2003; Cao et al., 2012

62

Table 1. Continued

Nutrient	Cell state	Possible outcomes	Context	Reference
Proline	pluripotency	(−) blocking proline transport into cell maintained mESC pluripotency	mESC cultured in maintenance media (+LIF)	Tan et al., 2011
	differentiation	(+) promoted mESC adoption of primitive endoderm-like morphology and gene expression	mESC cultured in maintenance media (+LIF)	Washington et al., 2010
		(−) blocking proline transport into cell impaired spontaneous differentiation	hPSC spontaneous differentiation (embryoid bodies)	Tan et al., 2011
		(+) promoted the differentiation of naive mESCs into more committed epiblast-like stem cells (EpiSCs)	mESC to EpiSC differentiation	Casalino et al., 2011
Methionine	pluripotency	(−) transient cell-cycle arrest	withdrawal in hPSCs (short-term)	Shiraki et al., 2014
		(−) cell death	withdrawal in hPSCs (long-term)	Shiraki et al., 2014
		(−) triggered loss of pluripotency	withdrawal in hPSCs (short-term), parallel findings with threonine deprivation in mESCs (short-term)	Shiraki et al., 2014
	differentiation	(−) promoted differentiation into the three germ lineages	withdrawal in hPSCs (short-term), parallel findings with threonine deprivation in mESCs (short-term)	Shiraki et al., 2014
Lipids	pluripotency	(+) mRNA expression of *OCT4* is unaffected	hPSCs cultured in E8 minimal media + AlbuMAX (short-term)	Zhang et al., 2016
		(+) stimulated self-renewal and pluripotency retention	hPSC cultured in differentiation media + AlbuMAX (long-term)	Garcia-Gonzalo and Izpisúa Belmonte, 2008
		(+) favored dedifferentiation/pluripotent state	porcine iPSC reprogramming + AlbuMAX	Zhang et al., 2018b
		fatty acid synthesis promoted dedifferentiation/pluripotent state by regulating acetyl-CoA and mitochondrial fission	mouse and human iPSC reprogramming	Vazquez-Martin et al., 2013; Wang et al., 2017
		(−) induced reprogramming from primed to "naive-to-primed" intermediate PSC state through endogenous ERK inhibition	hPSC cultured in minimal (E8) pluripotency maintenance media	Cornacchia et al., 2019
		FASN inhibition eliminated pluripotent cells and prevented differentiation	hPSC cultured in maintenance media	Tanosaki et al., 2020
	differentiation	(−) germ layer differentiation bias; increased ectoderm but reduced mesoderm/endoderm propensities	hPSC lineage-directed differentiation	Cornacchia et al., 2019
		FASN inhibition did not affect committed cell types: hPSC-derived cardiomyocytes (mesoderm), hepatocytes (endoderm), and neurons (ectoderm)	hPSC lineage-directed differentiation	Tanosaki et al., 2020

(Continued on next page)

Table 1. Continued

Nutrient	Cell state	Possible outcomes	Context	Reference
Pyruvate	pluripotency	blocking pyruvate entrance into mitochondria favored pluripotency; increased pyruvate flux opposed pluripotency	mESC and hPSC pluripotency maintenance and iPSC reprogramming	Rodrigues et al., 2015; Zhang et al., 2017a, Vozza et al., 2014; Zhang et al., 2011
	differentiation	(+) high concentrations of exogenous pyruvate enhanced mesoderm and endoderm lineage differentiation	hPSC lineage-directed differentiation	Song et al., 2019
		pyruvate consumption decreased during ectoderm lineage neural progenitor differentiation	hPSC lineage-directed differentiation	Lees et al., 2018

(−) withdrawal, (+) supplementation.

differentiation (D'Aniello et al., 2017). For example, under cardiac differentiation cues, ascorbic acid promotes cardiac differentiation (Sato et al., 2006; Takahashi et al., 2003) by increasing the proliferation of cardiac progenitor cells through increased collagen synthesis, but only when supplemented to the culture medium during an early time window of differentiation (Cao et al., 2012). While it is clear that ascorbic acid plays a significant role in promoting pluripotency or differentiation depending on different contextual cues, it will be interesting to see whether there are additional ascorbic acid context dependencies—for example, during naive or primed PSC stages.

Added proline promotes mESC adoption of a primitive ectoderm-like morphology and elevates the expression of genes associated with primitive ectoderm even in culture medium designed to sustain mESCs (Washington et al., 2010). Proline import is through the amino acid transporter SNAT2. Inhibition of SNAT2 with competitive substrates blocks proline transport, maintains mESC pluripotency, and impairs spontaneous embryoid body (EB) tri-lineage differentiation (Tan et al., 2011). Concordantly, the level of SNAT2 increases in mESCs prior to primitive ectoderm development (Tan et al., 2016), suggesting a role for proline in pluripotency exit. Proline supplementation also promotes the differentiation of naive mESCs into more mature epiblast-like stem cells (EpiSCs) (Casalino et al., 2011). This proline-dependent induction of mESCs into EpiSCs also shows features of the blastocyst to epiblast transition during mouse embryo implantation (Casalino et al., 2011). Implantation involves the degradation of a proline-rich extracellular matrix, raising the possibility that this process makes proline available to support an epiblast transition (McEwan et al., 2009).

Like proline, methionine has a role in pluripotency and differentiation. In hPSCs, SAM-supported histone methylation relies on methionine and not threonine metabolism because TDH is a nonfunctional pseudogene. (Shiraki et al., 2014). Short-term methionine deprivation in hPSCs decreases both intracellular S-methyl-5′-thioadenosine (MTA), a methionine precursor, and SAM (Shiraki et al., 2014), which is generated from methionine (Figure 1). This short-term manipulation causes transient cell-cycle arrest, whereas long-term methionine deprivation results in cell death. Supplementation with either MTA or SAM during long-term methionine deprivation rescues hPSC proliferation (Shiraki et al., 2014), indicating that methionine-derived metabolites are essential for sustained hPSC self-renewal. Short-term methionine deprivation can also trigger loss of pluripotency and differentiation of hPSCs into the three germ lineages. These changes are similar to mESCs with threonine deprivation and associate with a rapid decrease in global DNA methylation and H3K4me3 (Shiraki et al., 2014). How proline and methionine impact pluripotency status at different developmental stages would be an interesting subject of future investigation.

Together, these studies suggest that the availability of certain nutrients, such as glutamine, glucose, ascorbic acid, proline, and methionine, can elicit differing, and at times opposing, PSC fate outcomes (Table 1). An open question is whether certain nutrients provide sufficient instructive signals to control specific developmental stages or transitions. For example, can a specific nutrient(s) substitute for certain signaling cytokines, growth factors, hormones, or reprogramming factors to achieve

64

Figure 1. Nutrient sensing pathways impact pluripotent stem cell fate

Nutrient-specific sensing occurs via the hexosamine biosynthesis pathway (HBP, gray), mTORC1 (blue), and AMPK (yellow). HBP integrates carbohydrates (glucose), amino acids (glutamine), lipids (acetyl-CoA), and nucleotides (UTP), culminating in the generation of UDP-GlcNAC, a substrate for O-GlcNAcylation reactions by OGA/OGT. Signaling by mTORC1 and AMPK is regulated by concentrations of glucose and amino acids at multiple sensors, with activities localized to the lysosomal membrane. These specific nutrients fuel enzyme-based alterations in the epigenome, gene transcription, translation, and PTMs to shape PSC fate (Table 2). Glucose-6-phosphate, G6P; fructose-6-phosphate, F6P; glutamine-fructose-6-phosphate transaminase, GFAT; fructose 1,6-bisphosphate, FBP; endoplasmic reticulum, ER; O-GlcNAc transferase, OGT; O-GlcNAcase, OGA; dihydroxyacetone phosphate, DHAP.

or sustain pluripotency, or to promote lineage-specific differentiation?

INTRACELLULAR NUTRIENT ROUTING INFLUENCES PSC IDENTITY

Controlled oxidation and intracellular routing of nutrients by specific enzyme activities and transporters can induce or maintain pluripotency (Fathi et al., 2014; Konze et al., 2017; Shyh-Chang et al., 2013a), suggesting that nutrient handling pathway configurations regulate PSC fate. Lipid metabolism, such as fatty acid (FA) oxidation, is essential for early mouse and human embryonic development (Dunning et al., 2010, 2014; Oey et al., 2005). Indeed, lipid signaling has been implicated in pluripotency, with lysophosphatidic acid (LPA) supplementation promoting conversion from the primed to naive state transcription factor program in mouse PSCs (Kime et al., 2016). However, *in vitro* studies of PSC fate by addition of lipid-rich bovine serum albumin, or AlbuMAX, yielded differential results. One study showed that added AlbuMAX decreased FA biosynthesis and NADPH regeneration without affecting *OCT4* expression in hPSCs (Zhang et al., 2016). Separately, AlbuMAX addition stimulated hPSC self-renewal (Garcia-Gonzalo and Izpisúa Belmonte, 2008) and porcine iPSC reprogramming by activating protein kinase A signaling (Zhang et al., 2018b). A potential explanation for these differential results could relate to differences in lipid exposure time, which occurs for other nutrients, such as glutamine (discussed above), as well. In studies reporting hPSCs without changes in *OCT4* expression, cell assays followed short-term AlbuMAX addition (Zhang et al., 2016). Another study also found that an AlbuMAX effect on hPSC colony shape was reversed following short-term addition and withdrawal (Cornacchia

et al., 2019), indicating short-term AlbuMAX supplementation has minimal effect on hPSC identity. In contrast, in studies reporting hPSCs with increased self-renewal, cells were adapted to AlbuMAX addition for >5 passages in culture, followed by spontaneous differentiation for 26 days (Garcia-Gonzalo and Izpisúa Belmonte, 2008). Additional studies could clarify the effect(s) of lipid supplementation on PSC fate by systematically testing different lipid compositions and exposure times on PSCs in different states.

Using lipid deprivation as a tool, mouse and human PSC studies showed that *de novo* FA biosynthesis promotes PSC self-renewal and somatic cell reprogramming to pluripotency, and inhibits spontaneous PSC differentiation. *De novo* FA biosynthesis, triggered by exogenous lipid deprivation with added glucose as the major substrate, increased the utilization of acetyl-CoA for protein acetylation and enhanced mitochondrial fission (Vazquez-Martin et al., 2013; Wang et al., 2017; Zhong et al., 2019). Lipid deprivation induced primed hPSCs to a less advanced "naive-to-primed" intermediate PSC stage of development, even with growth factors that promote the primed stage (Cornacchia et al., 2019). This finding suggests that lipid availability outweighed growth factor signaling at this PSC stage. PSCs express *de novo* FA biosynthesis enzymes acetyl-CoA carboxylase 1 (ACC1) and fatty acid synthase (FASN), which converts glucose-derived acetyl-CoA to FAs, which could siphon substrates for membrane production during self-renewal. Indeed, hPSCs contain more FASN compared to differentiated cells, and inhibition of FASN caused mitochondria-triggered apoptosis, loss of OCT4, and failure to form teratomas, a measure of pluripotency, in mice (Tanosaki et al., 2020). We posit that PSCs potentially elevate glucose-supplied FA biosynthesis as a mechanism to increase glycolytic flux and route carbons

Table 2. Nutrient-sensitive signal transduction pathways consist of (1) substrate (nutrient), (2) sensor, (3) transducer, and (4) effector

Nutrient-sensing pathway	Substrates	Sensors	Transducers	Effectors
HBP	glucose, glutamine, glucosamine	GFAT (OGA and OGT: unclear)	OGA, OGT	O-GlcNAcylation of core pluripotency transcription factors
mTOR	methionine, leucine, arginine, glutamine, asparagine, glucose, SAM, α-KG	Rag GTPases, Arf1 GTPases, V-ATPase, SAMTOR, GATOR, Sestrins, SLC38A9	mTOR complex	4E-BP, S6K
AMPK	glucose	V-ATPase, AMPK	AMPK	ULK1, acetyl-CoA carboxylase 1, SREBP1c

away from OXPHOS consumption in mitochondria, increasing substrates available for acetylation and/or cell replication (Moussaieff et al., 2015). It is unknown whether enforced expression and activation of ACC1 and FASN is sufficient to promote PSC self-renewal. Together, these findings relating lipid availability to PSC fate suggest the absence of lipids triggers elevated glucose routing through FA biosynthesis, which supports pluripotency.

Intracellular pyruvate routing can occur to (1) produce lactate via lactate dehydrogenase (LDH) with NAD+ generated to sustain glycolytic flux, (2) produce acetyl-CoA via pyruvate dehydrogenase (PDH) for TCA cycle oxidation, (3) produce oxaloacetate via pyruvate carboxylase (PCB) to replenish TCA cycle intermediates, and (4) localize to the nucleus to regulate the epigenome (Figure 1) (Sutendra et al., 2014). PDH inhibition, which blocks pyruvate entrance into the TCA cycle, supports mouse iPSC reprogramming and viability, whereas increased pyruvate flux into the mitochondria decreases pluripotency biomarker expression, reduces PSC self-renewal, and lowers PSC viability (Rodrigues et al., 2015; Zhang et al., 2017a). Upon differentiation, *PDH* gene expression rapidly decreases, but PDH protein levels stay the same. By contrast, ATP-citrate lyase (*ACYL*) and acetyl-CoA synthetase (*ACCS2*), which provide pyruvate-derived acetyl-CoA for histone acetylation reactions that support pluripotency, rapidly decrease upon differentiation (Moussaieff et al., 2015). This fate-dependent pattern of metabolism enzyme expression suggests that, upon pluripotency exit, the hierarchy of pyruvate routing shifts toward mitochondrial TCA cycle oxidation to support PSC differentiation.

Several studies show that the activation of metabolic enzymes and expression of transporters precede changes in gene expression and PSC identity, potentially as a mechanism to prepare for cell identity transitions (Folmes et al., 2011; Moussaieff et al., 2015; Zhang et al., 2011). As an example, another regulator of pyruvate fate is uncoupling protein 2 (UCP2), a uniporter that exports TCA cycle four-carbon metabolites from the mitochondria to the cytosol, making them unavailable for OXPHOS (Vozza et al., 2014; Zhang et al., 2011). UCP2 repression promotes mitochondrial oxidation of pyruvate and precedes exit from pluripotency with PSC differentiation (Zhang et al., 2011). During differentiation, intracellular pyruvate routing changes from pluripotency to lineage-specific patterns. Accordingly, media supplementation with pyruvate at high concentrations enhances induced mesoderm and endoderm lineage differentiation (Song et al., 2019), whereas pyruvate consumption decreases during ectoderm lineage differentiation of neural progenitor cells (Lees

et al., 2018). These data suggest interesting questions regarding the mechanism(s) PSCs primed for directed differentiation use to sense pyruvate concentration, and whether a threshold influences lineage choice. Additionally, the mechanism(s) underlying rapid transcription, translation, localization, turnover, and/or activation of nutrient routing proteins in PSCs preceding a fate transition remains unknown.

The fate of pyruvate and its role in PSC outcome is critical during mouse ZGA. Transient nuclear localization of exogenous pyruvate, PDH, PCB, and select TCA cycle enzymes enables chromatin-localized synthesis of metabolites used in epigenome remodeling during ZGA (Nagaraj et al., 2017). How large enzyme complexes that typically reside within the mitochondrial matrix instead transiently localize within the nucleus of cleavage-division stage mouse embryos requires further study. Nevertheless, the conversion of exogenous pyruvate into both acetyl-CoA (via PDH) and oxaloacetate (via PCB) occurs within the nucleus, thereby providing a "two-for-one" reactant for sustained production of alpha-ketoglutarate (α-KG). Since α-KG is a co-factor for dioxygenases, such as Jumonji-C histone demethylases and ten-eleven translocation (TET) DNA demethylases, and acetyl-CoA is required for histone acetylation reactions, the local generation of α-KG and acetyl-CoA in the nucleus prioritizes essential epigenome modifications during early genome activation to initiate mouse development.

NUTRIENTS AND PSC FATE

mTOR in pluripotency

Mammalian target of rapamycin (mTOR) complex 1 (mTORC1) is a serine/threonine protein kinase whose activation in response to specific nutrient levels phosphorylates downstream substrates that regulate cell growth, proliferation, and survival (Saxton and Sabatini, 2017). An amino acid-mediated interaction between the Rag family of guanosine triphosphatases (GTPases) and mTORC1 causes mTORC1 re-localization from the cytosol to the lysosomal membrane (Kim et al., 2008; Sancak et al., 2008). Specific amino acid-responsive upstream regulators of mTORC1, including lysosomal vacuolar H(+)-adenosine triphosphatase (v-ATPase), SAM sensors, leucine sensor Sestrin2, arginine sensor CASTOR1, SLC38A9, and SAMTOR (Chantranupong et al., 2016; Gu et al., 2017; Wang et al., 2015; Wolfson et al., 2016; Ye et al., 2015), signal to the Rag GTPases to activate or inactivate mTORC1 (Figure 1; Table 2).

Similar to amino acids arginine, leucine, and glutamine, glucose can also directly activate mTORC1. In glucose

deprivation studies, mouse embryonic fibroblasts (MEFs) showed a decrease in mTORC1 kinase activation (Kalender et al., 2010). Mechanistically, glucose controls mTORC1 activity by influencing the binding of the v-ATPase to the Ragulator, a complex of five LAMTOR proteins that associates with the Rag GTPases (Figure 1) in order to activate mTORC1 (Efeyan et al., 2013). Additional recent studies showed intracellular glucose detection by mTORC1 occurs through a glucose-derived metabolite, dihydroxyacetone (DHAP). In glucose-starved conditions with decreased mTOR activity, the synthesis of DHAP restored mTOR activity (Orozco et al., 2020). In sum, mTORC1 activation occurs by several distinct amino acid and glucose signaling mechanisms, which aligns with its central role as a nutrient sensor and actuator of cell growth, proliferation, and survival (Figure 1; Table 2).

In conditions of nutrient abundance, mTORC1 binds ULK1 to inhibit autophagy, and conversely, nutrient starvation dissociates mTORC1 from ULK1, triggering autophagosomes to form (Rabinowitz and White, 2010). In hPSCs, nutrient starvation inhibited mTORC1 activation, increased autophagosome formation, and decreased levels of OCT4, SOX2, and NANOG transcription factors (Cho et al., 2014; Zhou et al., 2009). Autophagy inhibition in starvation conditions caused pluripotency transcription factors to accumulate, suggesting a role for nutrients in controlling pluripotency by regulating autophagy (Cho et al., 2014). Immunofluorescence microscopy and immunogold-stained electron microscopy during nutrient starvation confirmed pluripotency transcription factor interactions with autophagosomes (Cho et al., 2014), suggesting altogether that loss of pluripotency from nutrient starvation occurs through an mTORC1-autophagy response.

Amino acid deprivation is the most studied trigger for mTORC1 inhibition and subsequent induction of autophagy (Saxton and Sabatini, 2017). Amino acids such as glutamine, methionine, and threonine have demonstrated roles in pluripotency maintenance (Carey et al., 2015; Shiraki et al., 2014; Shyh-Chang et al., 2013b; Vardhana et al., 2019) and may promote pluripotency by signaling nutrient abundance to activate mTORC1. For example, threonine is a positive regulator of mESC self-renewal (Han et al., 2013; Shyh-Chang et al., 2013b; Wang et al., 2009). Culture medium deficient in threonine, but not in any other amino acid, caused a decrease in alkaline-phosphatase-positive mESC colonies (Wang et al., 2009). Threonine dehydrogenase (TDH), the rate-limiting enzyme in threonine catabolism, supports somatic cell reprogramming into mouse iPSCs because TDH knockdown decreased reprogramming efficiency (Han et al., 2013). Threonine supports pluripotency by maintaining histone methylation levels (Shyh-Chang et al., 2013b; Wang et al., 2009) and by regulating mTORC1 activity (Ryu and Han, 2011). mESCs incubated with threonine increased expression of pluripotency proteins OCT4, NANOG, and SOX2 (Ryu and Han, 2011). Inhibition of mTORC1 signaling activity with rapamycin abolished this effect, further suggesting a role for nutrient-activated mTORC1 in regulating pluripotency (Ryu and Han, 2011). It is possible that threonine promotes mESC self-renewal by keeping mTORC1 activity below the level that triggers autophagy and degradation of pluripotency transcription factors. Future studies could identify whether other nutrients, such as glucose, or specific amino acids, such as proline,

also sustain pluripotency through mTORC1 inhibition of autophagy. Of course, mTOR effects on transcription, translation, and metabolism could also influence pluripotency. For example, nutrient starvation could inhibit mTORC1 activity and reduce translation of pluripotency-related transcripts.

It is important to note that contradicting studies indicate that an autophagy response can promote instead of inhibit pluripotency. For example, FOXO1, a master regulator of core autophagy genes, maintains high autophagic flux to maintain mESC pluripotency, likely by generating substrates that support rapid cell proliferation (Liu et al., 2017). Similarly, PINK1/OPTN-mediated mitophagy is important for clearing depolarized mitochondria in order to maintain mitochondrial homeostasis that appears critical for pluripotency (Wang et al., 2021a). A possible explanation for these contradictory results is that a precise balance of autophagic activities—neither complete activation nor complete inhibition—is required to maintain pluripotency.

mTOR complex activity is also implicated in a process that suspends, or reversibly halts, development, called diapause (Bulut-Karslioglu et al., 2016; Hussein et al., 2020). Preimplantation mammalian embryos can survive ex vivo for up to 2 days, but deprivation of glucose, arginine, and leucine can induce diapause (Gwatkin, 1966; Naeslund, 1979). The Bulut-Karslioglu group hypothesized that inhibiting growth pathways could replicate this nutrient-starved diapause state. Their work identified mTOR as a regulator of developmental timing and pluripotency, determining that mTOR inhibition could induce a diapause state that significantly prolonged pluripotency. Specifically, nutrient starvation activates the serine-threonine liver kinase B1 (LKB1)-AMPK signal transduction pathway, which inhibits mTORC2 to cause diapause (Hussein et al., 2020). While these studies suggest that nutrient-regulated mTORC2 is a primary player in controlling diapause and prolonging pluripotency, mTORC2 has been documented to additionally regulate mTORC1 activity (Szwed et al., 2021), making it possible that mTORC1 may also play a role in this phenomenon.

A role for nutrients in mTORC1 regulation of pluripotency exit and subsequent differentiation is less clear. Inhibition of mTORC1 during germ lineage non-directed embryoid body formation increased mesoderm and endoderm differentiation and decreased ectoderm differentiation (Jung et al., 2016; Zhou et al., 2009). Chemical screens with additional mTORC1 inhibitors confirmed this result (Nazareth et al., 2016). Furthermore, mouse embryos containing a loss-of-function mutation in *mTOR* showed malformations in the ectoderm-derived telencephalon with subsequent loss of viability (Hentges et al., 2001). Similarly, a loss-of-function mutation in *TSC2*, an inhibitor of mTOR, also caused embryonic lethality due to overgrowth of ectoderm-derived neuroepithelium (Rennebeck et al., 1998). These studies combined highlight a role for mTORC1 activity in promoting ectoderm differentiation. Because mTORC1 responds to many different nutrients, it will be interesting to determine whether a particular nutrient can promote lineage differentiation through mTORC1 activated signaling, or whether a combination of nutrients will be necessary for this effect.

AMPK in pluripotency
AMP-activated protein kinase (AMPK) is a well-characterized energy sensor that responds to levels of AMP, ADP, and

ATP, molecules whose ratios indicate cell energy charge and nutrient status. AMPK activity in low-energy charge states (high ratios of AMP/ATP) opposes mTOR activity by limiting energy expenditure, thereby slowing or halting cell growth and proliferation. For many years, it was thought that ATP production from glucose oxidation was the only mechanism by which AMPK sensed glucose availability (Salt et al., 1998). However, a second glucose-sensing mechanism for AMPK was identified recently. With glucose starvation, an AXIN/LKB1 complex near the lysosome accesses the v-ATPase-Regulator complex (Figure 1) to form an AXIN-based, AMPK-activating complex (Zhang et al., 2013). Interaction of these lysosomal components during simultaneous glucose stress causes dissociation and inactivation of mTOR from the lysosome (Zhang et al., 2013). This non-canonical mechanism could also activate autophagy, although this remains unknown. Opposing this activity, fructose 1,6-bisphosphate (FBP), a glycolytic intermediate sensed by aldolase, triggers dissociation of the AXIN/LKB1 complex from the v-ATPase-Ragulator complex, suppressing AMPK activation (Zhang et al., 2017b). In sum, AMPK is an energy charge and nutrient sensor that effects metabolic change through glucose-sensing mechanisms (Figure 1; Table 2).

Emerging evidence suggests that nutrient regulation of AMPK may impact pluripotency. In response to glucose starvation, activated AMPK phosphorylates ULK1 at S317 and S777 (Kim et al., 2011) and simultaneously inhibits mTOR, halting mTOR phosphorylation of ULK1 at S757 (Kim et al., 2011). Phosphorylation of ULK1 at S317 and S777, without phosphorylation at S757, supports autophagy, whereas impaired phosphorylation at these sites blocks autophagy (Kim et al., 2011). A recent study showed that AMPK-dependent phosphorylation of ULK1 is required to maintain mESC pluripotency (Gong et al., 2018). ULK1 knockout mESC lines showed decreased colony formation and pluripotent gene expression, with rescue by re-addition of wild-type ULK1 or mutant S757 ULK1 (Gong et al., 2018). By contrast, ULK1 knockout mESC lines containing expression constructs producing both mutant S317 and S777 ULK1 are unable to restore pluripotency (Gong et al., 2018), indicating an AMPK-specific role in mESC self-renewal (Gong et al., 2018). Compounds such as resveratrol, which increases mESC pluripotent gene expression through activation of the AMPK/ULK1 pathway, support a role for AMPK in PSC maintenance (Suvorova et al., 2019). However, whether glucose through AMPK regulates pluripotency, and if so, whether the mechanism is by AMPK phosphorylation of ULK1 remains unknown.

AMPK may also regulate mESC differentiation through Tfeb, a master transcriptional regulator of lysosomal genes (Young et al., 2016). A genetic gain- and loss-of-function study determined that AMPK-regulated Tfeb is required for endoderm differentiation, with Tfeb overexpression in AMPK knockout mESCs restoring lysosomal function and efficient endoderm differentiation (Young et al., 2016). Recent evidence also supports a role for nutrient-regulated AMPK in controlling differentiation from PSCs, as pyruvate activates AMPK in a dose-dependent manner, which in turn promotes mesoderm development, with AMPK inhibition conversely impairing mesoderm differentiation (Song et al., 2019).

Glycosylation in pluripotency

The hexosamine biosynthesis pathway (HBP) is a nexus of nutrient-responsive signaling that integrates substrates from carbohydrate (glucose), nucleotide (uridine triphosphate; UTP), amino acid (glutamine), and FA (acetyl-CoA) metabolism. The terminal step of the HBP is the production of an acetylated aminosugar nucleotide, uridine diphosphate N-acetylglucosamine (UDP-GlcNAc), which is the substrate for cycling of O-linked N-acetylglucosamine (O-GlcNAc) post-translational modifications (PTMs) at serine and threonine residues of nuclear and cytoplasmic proteins (Bond and Hanover, 2015) (Figure 1; Table 2). O-GlcNAc addition, by O-GlcNAc transferase (OGT), and its removal by O-GlcNAcase (OGA) significantly alter the posttranslational properties and functions of target proteins known to regulate the epigenome (Shi et al., 2013; Vella et al., 2013; Zhu et al., 2020), transcription, proliferation, apoptosis, and proteasome degradation (Love and Hanover, 2005).

The dynamic cycling of O-GlcNAc PTMs regulates PSC maintenance and embryonic development, with knockout of either OGT or OGA causing embryonic lethality in mice (O'Donnell et al., 2004; Shafi et al., 2000; Yang et al., 2012). Pluripotency transcription factors OCT4 and SOX2 contain O-GlcNAcylation motifs that are rapidly removed upon differentiation, and point mutations that block OCT4 and SOX2 Ser/Thr residues normally targeted for O-GlcNAcylation cause a decrease in pluripotency and reprogramming efficiency (Constable et al., 2017; Jang et al., 2012; Myers et al., 2016; Webster et al., 2009). Recently, another pluripotency transcription factor, ESRRB, was identified as an additional O-GlcNAc target. O-GlcNAcylation stabilized ESRRB levels and promoted interactions with OCT4 and NANOG (Hao et al., 2019). Additional evidence that O-GlcNAcylation is essential for pluripotency maintenance comes from OGT and OGA perturbation studies. Pharmacological or genetic inhibition of OGA during the induction of neuron or cardiomyocyte differentiation caused excessive O-GlcNAcylation of proteins with accompanying suppression of lineage-specific biomarkers and aberrant retention of pluripotency biomarkers (Kim et al., 2009; Maury et al., 2013; Olivier-Van Stichelen et al., 2017; Speakman et al., 2014). Conversely, OGT inhibition resulted in decreased protein O-GlcNAcylation and accelerated PSC differentiation into neuroectoderm lineage cells (Andres et al., 2017).

Recent evidence suggests that nutrient regulation of O-GlcNAcylation may have a role in controlling pluripotency. MEFs reprogrammed in low-glucose culture medium showed reduced cellular O-GlcNAc levels and generated fewer mouse iPSC colonies compared to MEF reprogramming in high glucose (Jang et al., 2012). Furthermore, during the formation of TE and ICM in early mouse embryos, levels of HBP intermediates glucosamine and UDP-GlcNAc were highly sensitive to glucose deprivation (Chi et al., 2020). Glucose-regulated HBP glycosylation was essential for nuclear localization of YAP1 to activate TE-specifying transcription factors, but not for ICM specification (Chi et al., 2020). Combined, these findings indicate that nutrients and their HBP converted products, such as UDP-GlcNAc, are required for nutrient-sensitive O-GlcNAcylation of pluripotency master regulator proteins.

An additional layer of complexity exists for O-GlcNAcylation in regulating PSC fate because a linear relationship between the levels of nutrients and O-GlcNAcylation may not exist. Several

studies reported that glucose (Marshall et al., 2004; Swamy et al., 2016; Taylor et al., 2008, 2009), glutamine (Hamiel et al., 2009; Liu et al., 2007; Swamy et al., 2016), and amino acids (Chaveroux et al., 2016; Zhu et al., 2020) do not show a dose-dependent connection with protein O-GlcNAc levels. This suggests that nutrient regulation of O-GlcNAcylation may be PSC context-dependent, a recurring theme for nutrients controlling PSC fate. For example, whether specific nutrient availability increases or decreases O-GlcNAcylation levels of pluripotency transcription factors may depend on differentiation cues or PSC state, rather than overall HBP flux.

FUTURE PERSPECTIVES AND CONCLUSIONS

Studies over the past two decades have convinced most investigators of the active, rather than consequential, role of metabolism in controlling PSC fate, but many questions remain. These include the role for nutrients in PSC fate commitment, before or during cell identity transitions. For example, does specific nutrient availability initiate or merely reinforce a PSC fate "decision"? What roles do exogenous nutrients versus cell-intrinsic nutrient requirements have in instructing or reinforcing PSC fate? Because of evidence for both instructive and supportive roles, it is likely that nutrient availability plays a synergistic and potentially cyclic role in enabling PSC fates through metabolic conversion and/or nutrient-sensitive signaling. Progress in technology, with detection and sensitivity advances in mass spectrometry for single-cell metabolomics, could uncover which nutrients are consumed, produced, and secreted by different niche cell types *in vivo* and during PSC identity transitions *in vitro* (Duncan et al., 2019).

A practical area for future study is determining threshold concentrations that trigger a nutrient signal that affects PSC fate. Results from such studies could have implications for how maternal diet and/or diabetes affects development. As an example, an exceedingly high concentration of glucose is detrimental to PSC-derived neural lineage generation due to oxidative and endoplasmic reticulum stress, but also promotes PSC-derived cardiomyocyte generation (Chen et al., 2018; Crespo et al., 2010; Yang et al., 2016). In addition, a high concentration of pyruvate promotes mesoderm, but not ectoderm, differentiation through AMPK-activated signaling (Song et al., 2019). PSC culture methods can affect the amount of imported glucose (Gu et al., 2016), raising questions on how nutrient concentrations in culture medium can affect pluripotency/self-renewal and differentiation biases through altered metabolic flux and/or signaling. A potential approach to understanding biologically significant nutrient concentrations is to replicate the *in vivo* growth environment of the developing embryo, similar to an approach with human plasma-like medium used for growing tissue culture cells (Cantor et al., 2017).

Reports on nutrient-sensitive signaling in pluripotency are increasing as interest is growing, yet studies uniting nutrient availability, nutrient-sensitive signaling, and PSC fate outcome remain limited. The emergence of additional data connecting nutrient availability and signaling in PSC outcomes promises to inform on how maternal diet/malnutrition, metabolic disorders, and/or the embryonic microenvironment affects mammalian development.

REFERENCES

Andres, L.M., Blong, I.W., Evans, A.C., Rumachik, N.G., Yamaguchi, T., Pham, N.D., Thompson, P., Kohler, J.J., and Bertozzi, C.R. (2017). Chemical modulation of protein O-GlcNAcylation via OGT inhibition promotes human neural cell differentiation. ACS Chem. Biol. *12*, 2030–2039.

Baksh, S.C., and Finley, L.W.S. (2021). Metabolic coordination of cell fate by α-ketoglutarate-dependent dioxygenases. Trends Cell Biol. *31*, 24–36.

Biggers, J.D., Summers, M.C., and McGinnis, L.K. (1997). Polyvinyl alcohol and amino acids as substitutes for bovine serum albumin in culture media for mouse preimplantation embryos. Hum. Reprod. Update *3*, 125–135.

Bond, M.R., and Hanover, J.A. (2015). A little sugar goes a long way: the cell biology of O-GlcNAc. J. Cell Biol. *208*, 869–880.

Bulut-Karslioglu, A., Biechele, S., Jin, H., Macrae, T.A., Hejna, M., Gertsenstein, M., Song, J.S., and Ramalho-Santos, M. (2016). Inhibition of mTOR induces a paused pluripotent state. Nature *540*, 119–123.

Cantor, J.R., Abu-Remaileh, M., Kanarek, N., Freinkman, E., Gao, X., Louissaint, A., Jr., Lewis, C.A., and Sabatini, D.M. (2017). Physiologic medium rewires cellular metabolism and reveals uric acid as an endogenous inhibitor of UMP synthase. Cell *169*, 258–272.e17.

Cao, N., Liu, Z., Chen, Z., Wang, J., Chen, T., Zhao, X., Ma, Y., Qin, L., Kang, J., Wei, B., et al. (2012). Ascorbic acid enhances the cardiac differentiation of induced pluripotent stem cells through promoting the proliferation of cardiac progenitor cells. Cell Res. *22*, 219–236.

Carey, B.W., Finley, L.W., Cross, J.R., Allis, C.D., and Thompson, C.B. (2015). Intracellular α-ketoglutarate maintains the pluripotency of embryonic stem cells. Nature *518*, 413–416.

Casalino, L., Comes, S., Lambazzi, G., De Stefano, B., Filosa, S., De Falco, S., De Cesare, D., Minchiotti, G., and Patriarca, E.J. (2011). Control of embryonic stem cell metastability by L-proline catabolism. J. Mol. Cell Biol. *3*, 108–122.

Chantranupong, L., Scaria, S.M., Saxton, R.A., Gygi, M.P., Shen, K., Wyant, G.A., Wang, T., Harper, J.W., Gygi, S.P., and Sabatini, D.M. (2016). The CASTOR proteins are arginine sensors for the mTORC1 pathway. Cell *165*, 153–164.

Chaveroux, C., Sarcinelli, C., Barbet, V., Belfeki, S., Barthelaix, A., Ferraro-Peyret, C., Lebecque, S., Renno, T., Bruhat, A., Fafournoux, P., and Manié, S.N. (2016). Nutrient shortage triggers the hexosamine biosynthetic pathway via the GCN2-ATF4 signalling pathway. Sci. Rep. *6*, 27278.

Chen, X., Shen, W.B., Yang, P., Dong, D., Sun, W., and Yang, P. (2018). High glucose inhibits neural stem cell differentiation through oxidative stress and endoplasmic reticulum stress. Stem Cells Dev. *27*, 745–755.

Chi, F., Sharpley, M.S., Nagaraj, R., Roy, S.S., and Banerjee, U. (2020). Glycolysis-independent glucose metabolism distinguishes TE from ICM fate during mammalian embryogenesis. Dev. Cell *53*, 9–26.e4.

Cho, Y.H., Han, K.M., Kim, D., Lee, J., Lee, S.H., Choi, K.W., Kim, J., and Han, Y.M. (2014). Autophagy regulates homeostasis of pluripotency-associated proteins in hESCs. Stem Cells 32, 424–435.

Cliff, T.S., Wu, T., Boward, B.R., Yin, A., Yin, H., Glushka, J.N., Prestegaard, J.H., and Dalton, S. (2017). MYC controls human pluripotent stem cell fate decisions through regulation of metabolic flux. Cell Stem Cell 21, 502–516.e9.

Constable, S., Lim, J.M., Vaidyanathan, K., and Wells, L. (2017). O-GlcNAc transferase regulates transcriptional activity of human Oct4. Glycobiology 27, 927–937.

Cornacchia, D., Zhang, C., Zimmer, B., Chung, S.Y., Fan, Y., Soliman, M.A., Tchieu, J., Chambers, S.M., Shah, H., Paull, D., et al. (2019). Lipid deprivation induces a stable, naive-to-primed intermediate state of pluripotency in human PSCs. Cell Stem Cell 25, 120–136.e10.

Crespo, F.L., Sobrado, V.R., Gomez, L., Cervera, A.M., and McCreath, K.J. (2010). Mitochondrial reactive oxygen species mediate cardiomyocyte formation from embryonic stem cells in high glucose. Stem Cells 28, 1132–1142.

D'Aniello, C., Cermola, F., Patriarca, E.J., and Minchiotti, G. (2017). Vitamin C in stem cell biology: impact on extracellular matrix homeostasis and epigenetics. Stem Cells Int. 2017, 8936156.

De Los Angeles, A., Ferrari, F., Xi, R., Fujiwara, Y., Benvenisty, N., Deng, H., Hochedlinger, K., Jaenisch, R., Lee, S., Leitch, H.G., et al. (2015). Hallmarks of pluripotency. Nature 525, 469–478.

Duncan, K.D., Fyrestam, J., and Lanekoff, I. (2019). Advances in mass spectrometry based single-cell metabolomics. Analyst (Lond.) 144, 782–793.

Dunning, K.R., Cashman, K., Russell, D.L., Thompson, J.G., Norman, R.J., and Robker, R.L. (2010). Beta-oxidation is essential for mouse oocyte developmental competence and early embryo development. Biol. Reprod. 83, 909–918.

Dunning, K.R., Russell, D.L., and Robker, R.L. (2014). Lipids and oocyte developmental competence: the role of fatty acids and β-oxidation. Reproduction 148, R15–R27.

Efeyan, A., Zoncu, R., Chang, S., Gumper, I., Snitkin, H., Wolfson, R.L., Kirak, O., Sabatini, D.D., and Sabatini, D.M. (2013). Regulation of mTORC1 by the Rag GTPases is necessary for neonatal autophagy and survival. Nature 493, 679–683.

Eid, W., and Abdel-Rehim, W. (2016). Vitamin C promotes pluripotency of human induced pluripotent stem cells via the histone demethylase JARID1A. Biol. Chem. 397, 1205–1213.

Esteban, M.A., Wang, T., Qin, B., Yang, J., Qin, D., Cai, J., Li, W., Weng, Z., Chen, J., Ni, S., et al. (2010). Vitamin C enhances the generation of mouse and human induced pluripotent stem cells. Cell Stem Cell 6, 71–79.

Fathi, A., Hatami, M., Vakilian, H., Han, C.L., Chen, Y.J., Baharvand, H., and Salekdeh, G.H. (2014). Quantitative proteomics analysis highlights the role of redox hemostasis and energy metabolism in human embryonic stem cell differentiation to neural cells. J. Proteomics 101, 1–16.

Folmes, C.D., Nelson, T.J., Martinez-Fernandez, A., Arrell, D.K., Lindor, J.Z., Dzeja, P.P., Ikeda, Y., Perez-Terzic, C., and Terzic, A. (2011). Somatic oxidative bioenergetics transitions into pluripotency-dependent glycolysis to facilitate nuclear reprogramming. Cell Metab. 14, 264–271.

Garcia-Gonzalo, F.R., and Izpisúa Belmonte, J.C. (2008). Albumin-associated lipids regulate human embryonic stem cell self-renewal. PLoS ONE 3, e1384.

Gardner, D.K. (1998). Changes in requirements and utilization of nutrients during mammalian preimplantation embryo development and their significance in embryo culture. Theriogenology 49, 83–102.

Gardner, D.K., and Harvey, A.J. (2015). Blastocyst metabolism. Reprod. Fertil. Dev. 27, 638–654.

Gong, J., Gu, H., Zhao, L., Wang, L., Liu, P., Wang, F., Xu, H., and Zhao, T. (2018). Phosphorylation of ULK1 by AMPK is essential for mouse embryonic stem cell self-renewal and pluripotency. Cell Death Dis. 9, 38.

Gu, W., Gaeta, X., Sahakyan, A., Chan, A.B., Hong, C.S., Kim, R., Braas, D., Plath, K., Lowry, W.E., and Christofk, H.R. (2016). Glycolytic metabolism plays a functional role in regulating human pluripotent stem cell state. Cell Stem Cell 19, 476–490.

Gu, X., Orozco, J.M., Saxton, R.A., Condon, K.J., Liu, G.Y., Krawczyk, P.A., Scaria, S.M., Harper, J.W., Gygi, S.P., and Sabatini, D.M. (2017). SAMTOR is an S-adenosylmethionine sensor for the mTORC1 pathway. Science 358, 813–818.

Gwatkin, R.B.L. (1966). Amino acid requirements for attachment and outgrowth of the mouse blastocystin vitro. J. Cell. Physiol. 68, 335–343.

Hackett, J.A., and Surani, M.A. (2014). Regulatory principles of pluripotency: from the ground state up. Cell Stem Cell 15, 416–430.

Hamiel, C.R., Pinto, S., Hau, A., and Wischmeyer, P.E. (2009). Glutamine enhances heat shock protein 70 expression via increased hexosamine biosynthetic pathway activity. Am. J. Physiol. Cell Physiol. 297, C1509–C1519.

Han, C., Gu, H., Wang, J., Lu, W., Mei, Y., and Wu, M. (2013). Regulation of L-threonine dehydrogenase in somatic cell reprogramming. Stem Cells 31, 953–965.

Hao, Y., Fan, X., Shi, Y., Zhang, C., Sun, D.E., Qin, K., Qin, W., Zhou, W., and Chen, X. (2019). Next-generation unnatural monosaccharides reveal that ESRRB O-GlcNAcylation regulates pluripotency of mouse embryonic stem cells. Nat. Commun. 10, 4065.

Hentges, K.E., Sirry, B., Gingeras, A.C., Sarbassov, D., Sonenberg, N., Sabatini, D., and Peterson, A.S. (2001). FRAP/mTOR is required for proliferation and patterning during embryonic development in the mouse. Proc. Natl. Acad. Sci. USA 98, 13796–13801.

Hoogland, S.H.A., and Marks, H. (2021). Developments in pluripotency: a new formative state. Cell Res. 31, 493–494.

Hussein, A.M., Wang, Y., Mathieu, J., Margaretha, L., Song, C., Jones, D.C., Cavanaugh, C., Miklas, J.W., Mahen, E., Showalter, M.R., et al. (2020). Metabolic control over mTOR-dependent diapause-like state. Dev. Cell 52, 236–250.e7.

Intlekofer, A.M., and Finley, L.W.S. (2019). Metabolic signatures of cancer cells and stem cells. Nat. Metab. 1, 177–188.

Jang, H., Kim, T.W., Yoon, S., Choi, S.Y., Kang, T.W., Kim, S.Y., Kwon, Y.W., Cho, E.J., and Youn, H.D. (2012). O-GlcNAc regulates pluripotency and reprogramming by directly acting on core components of the pluripotency network. Cell Stem Cell 11, 62–74.

Jung, J.H., Kang, K.W., Kim, J., Hong, S.C., Park, Y., and Kim, B.S. (2016). CXCR2 inhibition in human pluripotent stem cells induces predominant differentiation to mesoderm and endoderm through repression of mTOR, β-Catenin, and hTERT activities. Stem Cells Dev. 25, 1006–1019.

Kalender, A., Selvaraj, A., Kim, S.Y., Gulati, P., Brûlé, S., Viollet, B., Kemp, B.E., Bardeesy, N., Dennis, P., Schlager, J.J., et al. (2010). Metformin, independent of AMPK, inhibits mTORC1 in a rag GTPase-dependent manner. Cell Metab. 11, 390–401.

Kim, E., Goraksha-Hicks, P., Li, L., Neufeld, T.P., and Guan, K.-L. (2008). Regulation of TORC1 by Rag GTPases in nutrient response. Nat. Cell Biol. 10, 935–945.

Kim, H.S., Park, S.Y., Choi, Y.R., Kang, J.G., Joo, H.J., Moon, W.K., and Cho, J.W. (2009). Excessive O-GlcNAcylation of proteins suppresses spontaneous cardiogenesis in ES cells. FEBS Lett. 583, 2474–2478.

Kim, J., Kundu, M., Viollet, B., and Guan, K.-L. (2011). AMPK and mTOR regulate autophagy through direct phosphorylation of Ulk1. Nat. Cell Biol. 13, 132–141.

Kime, C., Sakaki-Yumoto, M., Goodrich, L., Hayashi, Y., Sami, S., Derynck, R., Asahi, M., Panning, B., Yamanaka, S., and Tomoda, K. (2016). Autotaxin-mediated lipid signaling intersects with LIF and BMP signaling to promote the naive pluripotency transcription factor program. Proc. Natl. Acad. Sci. USA 113, 12478–12483.

Kinoshita, M., Barber, M., Mansfield, W., Cui, Y., Spindlow, D., Stirparo, G.G., Dietmann, S., Nichols, J., and Smith, A. (2021). Capture of mouse and human stem cells with features of formative pluripotency. Cell Stem Cell 28, 453–471.e8.

Konze, S.A., Werneburg, S., Oberbeck, A., Olmer, R., Kempf, H., Jara-Avaca, M., Pich, A., Zweigerdt, R., and Buettner, F.F. (2017). Proteomic analysis of human pluripotent stem cell cardiomyogenesis revealed altered expression of metabolic enzymes and PDLIM5 isoforms. J. Proteome Res. 16, 1133–1149.

Lees, J.G., Gardner, D.K., and Harvey, A.J. (2018). Mitochondrial and glycolytic remodeling during nascent neural differentiation of human pluripotent stem cells. Development *145*, dev168997.

Leese, H.J., and Barton, A.M. (1984). Pyruvate and glucose uptake by mouse ova and preimplantation embryos. J. Reprod. Fertil. *72*, 9–13.

Liu, J., Marchase, R.B., and Chatham, J.C. (2007). Glutamine-induced protection of isolated rat heart from ischemia/reperfusion injury is mediated via the hexosamine biosynthesis pathway and increased protein O-GlcNAc levels. J. Mol. Cell. Cardiol. *42*, 177–185.

Liu, P., Liu, K., Gu, H., Wang, W., Gong, J., Zhu, Y., Zhao, Q., Cao, J., Han, C., Gao, F., et al. (2017). High autophagic flux guards ESC identity through coordinating autophagy machinery gene program by FOXO1. Cell Death Differ. *24*, 1672–1680.

Love, D.C., and Hanover, J.A. (2005). The hexosamine signaling pathway: deciphering the "O-GlcNAc code". Sci. STKE *2005*, re13.

Lu, V., Dahan, P., Ahsan, F.M., Patananan, A.N., Roy, I.J., Torres, A., Jr., Nguyen, R.M.T., Huang, D., Braas, D., and Teitell, M.A. (2019). Mitochondrial metabolism and glutamine are essential for mesoderm differentiation of human pluripotent stem cells. Cell Res. *29*, 596–598.

Marsboom, G., Zhang, G.F., Pohl-Avila, N., Zhang, Y., Yuan, Y., Kang, H., Hao, B., Brunengraber, H., Malik, A.B., and Rehman, J. (2016). Glutamine metabolism regulates the pluripotency transcription factor OCT4. Cell Rep. *16*, 323–332.

Marshall, S., Nadeau, O., and Yamasaki, K. (2004). Dynamic actions of glucose and glucosamine on hexosamine biosynthesis in isolated adipocytes: differential effects on glucosamine 6-phosphate, UDP-N-acetylglucosamine, and ATP levels. J. Biol. Chem. *279*, 35313–35319.

Mashayekhan, S., Kim, M.H., Miyazaki, S., Tashiro, F., Kino-oka, M., Taya, M., and Miyazaki, J. (2008). Enrichment of undifferentiated mouse embryonic stem cells on a culture surface with a glucose-displaying dendrimer. Biomaterials *29*, 4236–4243.

Maury, J.J., Chan, K.K., Zheng, L., Bardor, M., and Choo, A.B. (2013). Excess of O-linked N-acetylglucosamine modifies human pluripotent stem cell differentiation. Stem Cell Res. (Amst.) *11*, 926–937.

McEwan, M., Lins, R.J., Munro, S.K., Vincent, Z.L., Ponnampalam, A.P., and Mitchell, M.D. (2009). Cytokine regulation during the formation of the fetal-maternal interface: focus on cell-cell adhesion and remodelling of the extracellular matrix. Cytokine Growth Factor Rev. *20*, 241–249.

Moussaieff, A., Rouleau, M., Kitsberg, D., Cohen, M., Levy, G., Barasch, D., Nemirovski, A., Shen-Orr, S., Laevsky, I., Amit, M., et al. (2015). Glycolysis-mediated changes in acetyl-CoA and histone acetylation control the early differentiation of embryonic stem cells. Cell Metab. *21*, 392–402.

Myers, S.A., Peddada, S., Chatterjee, N., Friedrich, T., Tomoda, K., Krings, G., Thomas, S., Maynard, J., Broeker, M., Thomson, M., et al. (2016). SOX2 O-GlcNAcylation alters its protein-protein interactions and genomic occupancy to modulate gene expression in pluripotent cells. eLife *5*, e10647.

Na, H.J., Akan, I., Abramowitz, L.K., and Hanover, J.A. (2020). Nutrient-driven O-GlcNAcylation controls DNA damage repair signaling and stem/progenitor cell homeostasis. Cell Rep. *31*, 107632.

Naeslund, G. (1979). The effect of glucose-, arginine- and leucine-deprivation on mouse blastocyst outgrowth in vitro. Ups. J. Med. Sci. *84*, 9–20.

Nagaraj, R., Sharpley, M.S., Chi, F., Braas, D., Zhou, Y., Kim, R., Clark, A.T., and Banerjee, U. (2017). Nuclear localization of mitochondrial TCA cycle enzymes as a critical step in mammalian zygotic genome activation. Cell *168*, 210–223.e11.

Nazareth, E.J.P., Rahman, N., Yin, T., and Zandstra, P.W. (2016). A multi-lineage screen reveals mTORC1 inhibition enhances human pluripotent stem cell mesendoderm and blood progenitor production. Stem Cell Reports *6*, 679–691.

O'Donnell, N., Zachara, N.E., Hart, G.W., and Marth, J.D. (2004). Ogt-dependent X-chromosome-linked protein glycosylation is a requisite modification in somatic cell function and embryo viability. Mol. Cell. Biol. *24*, 1680–1690.

Oey, N.A., den Boer, M.E., Wijburg, F.A., Vekemans, M., Augé, J., Steiner, C., Wanders, R.J., Waterham, H.R., Ruiter, J.P., and Attié-Bitach, T. (2005). Long-chain fatty acid oxidation during early human development. Pediatr. Res. *57*, 755–759.

Olivier-Van Stichelen, S., Wang, P., Comly, M., Love, D.C., and Hanover, J.A. (2017). Nutrient-driven O-linked N-acetylglucosamine (O-GlcNAc) cycling impacts neurodevelopmental timing and metabolism. J. Biol. Chem. *292*, 6076–6085.

Orozco, J.M., Krawczyk, P.A., Scaria, S.M., Cangelosi, A.L., Chan, S.H., Kunchok, T., Lewis, C.A., and Sabatini, D.M. (2020). Dihydroxyacetone phosphate signals glucose availability to mTORC1. Nat. Metab. *2*, 893–901.

Rabinowitz, J.D., and White, E. (2010). Autophagy and metabolism. Science *330*, 1344–1348.

Rennebeck, G., Kleymenova, E.V., Anderson, R., Yeung, R.S., Artzt, K., and Walker, C.L. (1998). Loss of function of the tuberous sclerosis 2 tumor suppressor gene results in embryonic lethality characterized by disrupted neuroepithelial growth and development. Proc. Natl. Acad. Sci. USA *95*, 15629–15634.

Rodrigues, A.S., Correia, M., Gomes, A., Pereira, S.L., Perestrelo, T., Sousa, M.I., and Ramalho-Santos, J. (2015). Dichloroacetate, the pyruvate dehydrogenase complex and the modulation of mESC pluripotency. PLoS ONE *10*, e0131663.

Ryu, J.M., and Han, H.J. (2011). L-threonine regulates G1/S phase transition of mouse embryonic stem cells via PI3K/Akt, MAPKs, and mTORC pathways. J. Biol. Chem. *286*, 23667–23678.

Ryu, J.M., Lee, S.H., Seong, J.K., and Han, H.J. (2015). Glutamine contributes to maintenance of mouse embryonic stem cell self-renewal through PKC-dependent downregulation of HDAC1 and DNMT1/3a. Cell Cycle *14*, 3292–3305.

Salt, I.P., Johnson, G., Ashcroft, S.J.H., and Hardie, D.G. (1998). AMP-activated protein kinase is activated by low glucose in cell lines derived from pancreatic β cells, and may regulate insulin release. Biochem. J. *335*, 533–539.

Sancak, Y., Peterson, T.R., Shaul, Y.D., Lindquist, R.A., Thoreen, C.C., Bar-Peled, L., and Sabatini, D.M. (2008). The Rag GTPases bind raptor and mediate amino acid signaling to mTORC1. Science *320*, 1496–1501.

Sato, H., Takahashi, M., Ise, H., Yamada, A., Hirose, S., Tagawa, Y., Morimoto, H., Izawa, A., and Ikeda, U. (2006). Collagen synthesis is required for ascorbic acid-enhanced differentiation of mouse embryonic stem cells into cardiomyocytes. Biochem. Biophys. Res. Commun. *342*, 107–112.

Saxton, R.A., and Sabatini, D.M. (2017). mTOR signaling in growth, metabolism, and disease. Cell *168*, 960–976.

Schulz, K.N., and Harrison, M.M. (2019). Mechanisms regulating zygotic genome activation. Nat. Rev. Genet. *20*, 221–234.

Shafi, R., Iyer, S.P., Ellies, L.G., O'Donnell, N., Marek, K.W., Chui, D., Hart, G.W., and Marth, J.D. (2000). The O-GlcNAc transferase gene resides on the X chromosome and is essential for embryonic stem cell viability and mouse ontogeny. Proc. Natl. Acad. Sci. USA *97*, 5735–5739.

Sharpley, M.S., Chi, F., Hoeve, J.T., and Banerjee, U. (2021). Metabolic plasticity drives development during mammalian embryogenesis. Dev. Cell *56*, 2329–2347.e6.

Shi, F.T., Kim, H., Lu, W., He, Q., Liu, D., Goodell, M.A., Wan, M., and Songyang, Z. (2013). Ten-eleven translocation 1 (Tet1) is regulated by O-linked N-acetylglucosamine transferase (Ogt) for target gene repression in mouse embryonic stem cells. J. Biol. Chem. *288*, 20776–20784.

Shiraki, N., Shiraki, Y., Tsuyama, T., Obata, F., Miura, M., Nagae, G., Aburatani, H., Kume, K., Endo, F., and Kume, S. (2014). Methionine metabolism regulates maintenance and differentiation of human pluripotent stem cells. Cell Metab. *19*, 780–794.

Shyh-Chang, N., and Ng, H.H. (2017). The metabolic programming of stem cells. Genes Dev. *31*, 336–346.

Shyh-Chang, N., Daley, G.Q., and Cantley, L.C. (2013a). Stem cell metabolism in tissue development and aging. Development *140*, 2535–2547.

Shyh-Chang, N., Locasale, J.W., Lyssiotis, C.A., Zheng, Y., Teo, R.Y., Ratana-sirintrawoot, S., Zhang, J., Onder, T., Unternaehrer, J.J., Zhu, H., et al. (2013b). Influence of threonine metabolism on S-adenosylmethionine and histone methylation. Science *339*, 222–226.

71

Smith, A. (2017). Formative pluripotency: the executive phase in a developmental continuum. Development *144*, 365–373.

Song, C., Xu, F., Ren, Z., Zhang, Y., Meng, Y., Yang, Y., Lingadahalli, S., Cheung, E., Li, G., Liu, W., et al. (2019). Elevated exogenous pyruvate potentiates mesodermal differentiation through metabolic modulation and AMPK/mTOR pathway in human embryonic stem cells. Stem Cell Reports *13*, 338–351.

Speakman, C.M., Domke, T.C., Wongpaiboonwattana, W., Sanders, K., Mudaliar, M., van Aalten, D.M., Barton, G.J., and Stavridis, M.P. (2014). Elevated O-GlcNAc levels activate epigenetically repressed genes and delay mouse ESC differentiation without affecting naïve to primed cell transition. Stem Cells *32*, 2605–2615.

Summers, M.C., and Biggers, J.D. (2003). Chemically defined media and the culture of mammalian preimplantation embryos: historical perspective and current issues. Hum. Reprod. Update *9*, 557–582.

Sutendra, G., Kinnaird, A., Dromparis, P., Paulin, R., Stenson, T.H., Haromy, A., Hashimoto, K., Zhang, N., Flaim, E., and Michelakis, E.D. (2014). A nuclear pyruvate dehydrogenase complex is important for the generation of acetyl-CoA and histone acetylation. Cell *158*, 84–97.

Suvorova, I.I., Knyazeva, A.R., Petukhov, A.V., Aksenov, N.D., and Pospelov, V.A. (2019). Resveratrol enhances pluripotency of mouse embryonic stem cells by activating AMPK/Ulk1 pathway. Cell Death Discov. *5*, 61.

Swamy, M., Pathak, S., Grzes, K.M., Damerow, S., Sinclair, L.V., van Aalten, D.M., and Cantrell, D.A. (2016). Glucose and glutamine fuel protein O-GlcNAcylation to control T cell self-renewal and malignancy. Nat. Immunol. *17*, 712–720.

Szwed, A., Kim, E., and Jacinto, E. (2021). Regulation and metabolic functions of mTORC1 and mTORC2. Physiol. Rev. *101*, 1371–1426.

Takahashi, T., Lord, B., Schulze, P.C., Fryer, R.M., Sarang, S.S., Gullans, S.R., and Lee, R.T. (2003). Ascorbic acid enhances differentiation of embryonic stem cells into cardiac myocytes. Circulation *107*, 1912–1916.

Tan, B.S.N., Lonic, A., Morris, M.B., Rathjen, P.D., and Rathjen, J. (2011). The amino acid transporter SNAT2 mediates L-proline-induced differentiation of ES cells. Am. J. Physiol. Cell Physiol. *300*, C1270–C1279.

Tan, B.S.N., Rathjen, P.D., Harvey, A.J., Gardner, D.K., and Rathjen, J. (2016). Regulation of amino acid transporters in pluripotent cell populations in the embryo and in culture; novel roles for sodium-coupled neutral amino acid transporters. Mech. Dev. *141*, 32–39.

Tanosaki, S., Tohyama, S., Fujita, J., Someya, S., Hishiki, T., Matsuura, T., Nakanishi, H., Ohto-Nakanishi, T., Akiyama, T., Morita, Y., et al. (2020). Fatty acid synthesis is indispensable for survival of human pluripotent stem cells. iScience *23*, 101535.

Taylor, R.P., Parker, G.J., Hazel, M.W., Soesanto, Y., Fuller, W., Yazzie, M.J., and McClain, D.A. (2008). Glucose deprivation stimulates O-GlcNAc modification of proteins through up-regulation of O-linked N-acetylglucosaminyltransferase. J. Biol. Chem. *283*, 6050–6057.

Taylor, R.P., Geisler, T.S., Chambers, J.H., and McClain, D.A. (2009). Up-regulation of O-GlcNAc transferase with glucose deprivation in HepG2 cells is mediated by decreased hexosamine pathway flux. J. Biol. Chem. *284*, 3425–3432.

TeSlaa, T., Chaikovsky, A.C., Lipchina, I., Escobar, S.L., Hochedlinger, K., Huang, J., Graeber, T.G., Braas, D., and Teitell, M.A. (2016). α-ketoglutarate accelerates the initial differentiation of primed human pluripotent stem cells. Cell Metab. *24*, 485–493.

Tohyama, S., Fujita, J., Hishiki, T., Matsuura, T., Hattori, F., Ohno, R., Kanazawa, H., Seki, T., Nakajima, K., Kishino, Y., et al. (2016). Glutamine oxidation is indispensable for survival of human pluripotent stem cells. Cell Metab. *23*, 663–674.

Tsogtbaatar, E., Landin, C., Minter-Dykhouse, K., and Folmes, C.D.L. (2020). Energy metabolism regulates stem cell pluripotency. Front. Cell Dev. Biol. *8*, 87.

Vardhana, S.A., Arnold, P.K., Rosen, B.P., Chen, Y., Carey, B.W., Huangfu, D., Carmona Fontaine, C., Thompson, C.B., and Finley, L.W.S. (2019). Glutamine independence is a selectable feature of pluripotent stem cells. Nat. Metab. *1*, 676–687.

Varum, S., Rodrigues, A.S., Moura, M.B., Momcilovic, O., Easley, C.A., 4th, Ramalho-Santos, J., Van Houten, B., and Schatten, G. (2011). Energy metabolism in human pluripotent stem cells and their differentiated counterparts. PLoS ONE *6*, e20914.

Vazquez-Martin, A., Corominas-Faja, B., Cufi, S., Vellon, L., Oliveras-Ferraros, C., Menendez, O.J., Joven, J., Lupu, R., and Menendez, J.A. (2013). The mitochondrial H(+)-ATP synthase and the lipogenic switch: new core components of metabolic reprogramming in induced pluripotent stem (iPS) cells. Cell Cycle *12*, 207–218.

Vella, P., Scelfo, A., Jammula, S., Chiacchiera, F., Williams, K., Cuomo, A., Roberto, A., Christensen, J., Bonaldi, T., Helin, K., and Pasini, D. (2013). Tet proteins connect the O-linked N-acetylglucosamine transferase Ogt to chromatin in embryonic stem cells. Mol. Cell *49*, 645–656.

Vozza, A., Parisi, G., De Leonardis, F., Lasorsa, F.M., Castegna, A., Amorese, D., Marmo, R., Calcagnile, V.M., Palmieri, L., Ricquier, D., et al. (2014). UCP2 transports C4 metabolites out of mitochondria, regulating glucose and glutamine oxidation. Proc. Natl. Acad. Sci. USA *111*, 960–965.

Wang, J., Alexander, P., Wu, L., Hammer, R., Cleaver, O., and McKnight, S.L. (2009). Dependence of mouse embryonic stem cells on threonine catabolism. Science *325*, 435–439.

Wang, T., Chen, K., Zeng, X., Yang, J., Wu, Y., Shi, X., Qin, B., Zeng, L., Esteban, M.A., Pan, G., and Pei, D. (2011). The histone demethylases Jhdm1a/1b enhance somatic cell reprogramming in a vitamin-C-dependent manner. Cell Stem Cell *9*, 575–587.

Wang, S., Tsun, Z.Y., Wolfson, R.L., Shen, K., Wyant, G.A., Plovanich, M.E., Yuan, E.D., Jones, T.D., Chantranupong, L., Comb, W., et al. (2015). Metabolism. Lysosomal amino acid transporter SLC38A9 signals arginine sufficiency to mTORC1. Science *347*, 188–194.

Wang, L., Zhang, T., Wang, L., Cai, Y., Zhong, X., He, X., Hu, L., Tian, S., Wu, M., Hui, L., et al. (2017). Fatty acid synthesis is critical for stem cell pluripotency via promoting mitochondrial fission. EMBO J. *36*, 1330–1347.

Wang, C., Liu, K., Cao, J., Wang, L., Zhao, Q., Li, Z., Zhang, H., Chen, Q., and Zhao, T. (2021a). PINK1-mediated mitophagy maintains pluripotency through optineurin. Cell Prolif. *54*, e13034.

Wang, X., Xiang, Y., Yu, Y., Wang, R., Zhang, Y., Xu, Q., Sun, H., Zhao, Z.A., Jiang, X., Wang, X., et al. (2021b). Formative pluripotent stem cells show features of epiblast cells poised for gastrulation. Cell Res. *31*, 526–541.

Washington, J.M., Rathjen, J., Felquer, F., Lonic, A., Bettess, M.D., Hamra, N., Semendric, L., Tan, B.S.N., Lake, J.-A., Keough, R.A., et al. (2010). L-Proline induces differentiation of ES cells: a novel role for an amino acid in the regulation of pluripotent cells in culture. Am. J. Physiol. Cell Physiol. *298*, C982–C992.

Webster, D.M., Teo, C.F., Sun, Y., Wloga, D., Gay, S., Klonowski, K.D., Wells, L., and Dougan, S.T. (2009). O-GlcNAc modifications regulate cell survival and epiboly during zebrafish development. BMC Dev. Biol. *9*, 28.

Wolfson, R.L., Chantranupong, L., Saxton, R.A., Shen, K., Scaria, S.M., Cantor, J.R., and Sabatini, D.M. (2016). Sestrin2 is a leucine sensor for the mTORC1 pathway. Science *351*, 43–48.

Wu, H., Wu, Y., Ai, Z., Yang, L., Gao, Y., Du, J., Guo, Z., and Zhang, Y. (2014). Vitamin C enhances Nanog expression via activation of the JAK/STAT signaling pathway. Stem Cells *32*, 166–176.

Yang, Y.R., Song, M., Lee, H., Jeon, Y., Choi, E.J., Jang, H.J., Moon, H.Y., Byun, H.Y., Kim, E.K., Kim, D.H., et al. (2012). O-GlcNAcase is essential for embryonic development and maintenance of genomic stability. Aging Cell *11*, 439–448.

Yang, P., Shen, W.B., Reece, E.A., Chen, X., and Yang, P. (2016). High glucose suppresses embryonic stem cell differentiation into neural lineage cells. Biochem. Biophys. Res. Commun. *472*, 306–312.

Ye, J., Palm, W., Peng, M., King, B., Lindsten, T., Li, M.O., Koumenis, C., and Thompson, C.B. (2015). GCN2 sustains mTORC1 suppression upon amino acid deprivation by inducing Sestrin2. Genes Dev. *29*, 2331–2336.

Yeo, J.C., and Ng, H.H. (2013). The transcriptional regulation of pluripotency. Cell Res. *23*, 20–32.

Young, N.P., Kamireddy, A., Van Nostrand, J.L., Eichner, L.J., Shokhirev, M.N., Dayn, Y., and Shaw, R.J. (2016). AMPK governs lineage specification through Tfeb-dependent regulation of lysosomes. Genes Dev. *30*, 535–552.

Yu, L., Wei, Y., Sun, H.X., Mahdi, A.K., Pinzon Arteaga, C.A., Sakurai, M., Schmitz, D.A., Zheng, C., Ballard, E.D., Li, J., et al. (2021). Derivation of intermediate pluripotent stem cells amenable to primordial germ cell specification. Cell Stem Cell *28*, 550–567.e12.

Zhang, J., Khvorostov, I., Hong, J.S., Oktay, Y., Vergnes, L., Nuebel, E., Wahjudi, P.N., Setoguchi, K., Wang, G., Do, A., et al. (2011). UCP2 regulates energy metabolism and differentiation potential of human pluripotent stem cells. EMBO J. *30*, 4860–4873.

Zhang, Y.-L., Guo, H., Zhang, C.-S., Lin, S.-Y., Yin, Z., Peng, Y., Luo, H., Shi, Y., Lian, G., Zhang, C., et al. (2013). AMP as a low-energy charge signal autonomously initiates assembly of AXIN-AMPK-LKB1 complex for AMPK activation. Cell Metab. *18*, 546–555.

Zhang, H., Badur, M.G., Divakaruni, A.S., Parker, S.J., Jäger, C., Hiller, K., Murphy, A.N., and Metallo, C.M. (2016). Distinct metabolic states can support self-renewal and lipogenesis in human pluripotent stem cells under different culture conditions. Cell Rep. *16*, 1536–1547.

Zhang, C., Skamagki, M., Liu, Z., Ananthanarayanan, A., Zhao, R., Li, H., and Kim, K. (2017a). Biological significance of the suppression of oxidative phosphorylation in induced pluripotent stem cells. Cell Rep. *21*, 2058–2065.

Zhang, C.-S., Hawley, S.A., Zong, Y., Li, M., Wang, Z., Gray, A., Ma, T., Cui, J., Feng, J.-W., Zhu, M., et al. (2017b). Fructose-1,6-bisphosphate and aldolase mediate glucose sensing by AMPK. Nature *548*, 112–116.

Zhang, J., Zhao, J., Dahan, P., Lu, V., Zhang, C., Li, H., and Teitell, M.A. (2018a). Metabolism in pluripotent stem cells and early mammalian development. Cell Metab. *27*, 332–338.

Zhang, W., Wang, H., Zhang, S., Zhong, L., Wang, Y., Pei, Y., Han, J., and Cao, S. (2018b). Lipid supplement in the cultural condition facilitates the porcine iPSC derivation through cAMP/PKA/CREB signal pathway. Int. J. Mol. Sci. *19*, 509.

Zhong, X., Cui, P., Cai, Y., Wang, L., He, X., Long, P., Lu, K., Yan, R., Zhang, Y., Pan, X., et al. (2019). Mitochondrial dynamics is critical for the full pluripotency and embryonic developmental potential of pluripotent stem cells. Cell Metab. *29*, 979–992.e4.

Zhou, J., Su, P., Wang, L., Chen, J., Zimmermann, M., Genbacev, O., Afonja, O., Horne, M.C., Tanaka, T., Duan, E., et al. (2009). mTOR supports long-term self-renewal and suppresses mesoderm and endoderm activities of human embryonic stem cells. Proc. Natl. Acad. Sci. USA *106*, 7840–7845.

Zhu, Q., Cheng, X., Cheng, Y., Chen, J., Xu, H., Gao, Y., Duan, X., Ji, J., Li, X., and Yi, W. (2020). O-GlcNAcylation regulates the methionine cycle to promote pluripotency of stem cells. Proc. Natl. Acad. Sci. USA *117*, 7755–7763.

CHAPTER 6:

Mitochondrial Metabolism and Glutamine are Essential for Mesoderm Differentiation

LETTER TO THE EDITOR

Mitochondrial metabolism and glutamine are essential for mesoderm differentiation of human pluripotent stem cells

Dear Editor,

Human pluripotent stem cells (hPSCs) generate energy mainly by aerobic glycolysis, with glutamine oxidation in the tricarboxylic acid (TCA) cycle providing additional ATP required for survival.[1–3] During the exit from pluripotency and initial differentiation into multiple germ lineage precursors, energy production shifts from mainly aerobic glycolysis to mitochondrial oxidative phosphorylation (OXPHOS).[1] Until recently, consensus in the field was that as PSCs exit pluripotency, a metabolic switch from aerobic glycolysis to OXPHOS is required. However, a more detailed examination of nascent ectoderm (EC) metabolism showed unexpected maintenance of a high, MYC-dependent glycolytic flux, resembling sustained hPSC metabolism, in contrast to mesoderm (ME) and endoderm (EN),[4] generating questions for the role(s) of mitochondrial metabolism in early hPSC tri-lineage differentiation. To examine this issue, we differentiated hPSCs into early EN, ME, and EC lineages using a non-limiting, nutrient-balanced culture media that differed only by established lineage-driving cytokines,[5,6] so that intrinsic metabolic preferences were not derived from a variance in nutrient composition (Supplementary information, Data S1). Principal component analysis (PCA) of these early lineages using RNA-Seq was equivalent to a previous study using nutrient-balanced and chemically defined growth media.[4] Furthermore, transcriptomic and protein biomarker expression matched established profiles for hPSCs and hPSC-derived EN, ME, and EC (Supplementary information, Fig. S1a–c, Table S1),[7] confirming the validity of our model system.

To quantify the impact of mitochondrial OXPHOS on lineage potentiation, mitochondrial stress tests showed that ME has the highest basal and maximal oxygen consumption rate (OCR), greatest spare respiratory capacity, and largest approximate respiration-to-glycolysis ratio (OCR/ECAR) compared to hPSCs, EN, and EC (Fig. 1a, Supplementary information, Fig. S1d, e). To compare nutrient preferences, we used media footprint analysis, which showed decreased glucose (Glc) consumption, decreased lactate production, increased glutamine (Gln) consumption, and increased glutamate production in ME compared to EC (Fig. 1b). Live cell interferometry quantification of normalized biomass accumulation (growth) rate revealed that ME and EC cell clusters were statistically equivalent and higher than EN (Fig. 1c). Taken together, the data reveal a striking metabolic plasticity in that ME and EC differ dramatically in nutrient source and pathways for energy and metabolite production, yet yield the same growth rate during early lineage specification.

Prior studies show that cell biomass accumulation during proliferation depends mainly on the consumption of non-Gln amino acids.[8] Since our data reveal that ME and EC have equivalent growth rates, we examined biomass accumulation-independent roles for Glc and Gln, such as facilitating cell fate specifications in these two lineages. Initially, we determined whether Glc or Gln is most crucial for each lineage. Early EN, ME, and EC lineages did not robustly convert $^{13}C_6$-glucose into TCA cycle metabolites, suggesting that Glc is not a major carbon source for the germ lineages (Fig. 1d, Supplementary information, Fig. S2a). In contrast to Glc, Gln is a major fuel source for all three cell lineages, with >70% of $^{13}C_5$-glutamine metabolized to glutamate and subsequent TCA cycle metabolites (Fig. 1e, Supplementary information, Table S2). Specifically, the mass isotopologue distribution (MID) of $^{13}C_5$-glutamine shows increased $m + 5$ αKG and $m + 4$ succinate, fumarate, malate, and citrate levels in ME, indicating that ME preferentially uses Gln compared to EC (Fig. 1f). Increased $m + 5$ citrate due to reductive carboxylation[9] was detected in EC compared to ME, suggesting that Gln may be preferentially shunted toward lipid biosynthesis and/or gluconeogenesis through citrate rather than into other TCA cycle intermediates in EC (Fig. 1f).[10] Overall, the data show that Gln is a major contributor to the TCA cycle in all three lineages, yet displays increased incorporation into first turn TCA cycle metabolites in ME compared to EC.

Since ME exhibits increased preference for Gln contribution into the TCA cycle, we next asked whether Gln deprivation would result in a bias in lineage potentiation in non-directed embryoid body (EB) differentiation, which has been previously demonstrated to recapitulate features of early embryogenesis.[11] As expected, Gln withdrawal from EB culture media at the start of non-directed differentiation resulted in significantly reduced levels of TCA cycle metabolites, with the exception of citrate at 48 h (Fig. 1g). Concurrent 1 mM dichloroacetate (DCA) treatment with Gln withdrawal to inhibit pyruvate dehydrogenase kinase and increase the flux of Glc supplied pyruvate into the TCA cycle[12] surprisingly did not replenish TCA cycle metabolite levels (Fig. 1g). This finding is consistent with a prior study reporting that hPSCs are highly dependent on both Glc and Gln oxidation, and that pyruvate addition cannot rescue Glc and Gln depleted conditions.[2] A mitochondrial stress test on EC and ME differentiated cells with Gln removed from the culture media revealed a decrease in maximal OCR and OCR/ECAR ratio in ME compared to EC, consistent with increased reliance on Gln in ME for respiration (Supplementary information, Fig. S2b, c). Additionally, differentiation under Gln deprivation did not affect EB formation, morphology, or viability (Supplementary information, Fig. S2d).[13] Interestingly, in EBs differentiated under Gln deprivation, immunoblot analysis revealed a decrease in the SLUG protein level, while qRT-PCR analysis showed significantly decreased HAND1 expression, indicating that Gln is essential for ME production (Fig. 1h, Supplementary information, Fig. S2e). Additionally, phase contrast microscopy of ME lineage directed differentiation

Figure 1. a–h
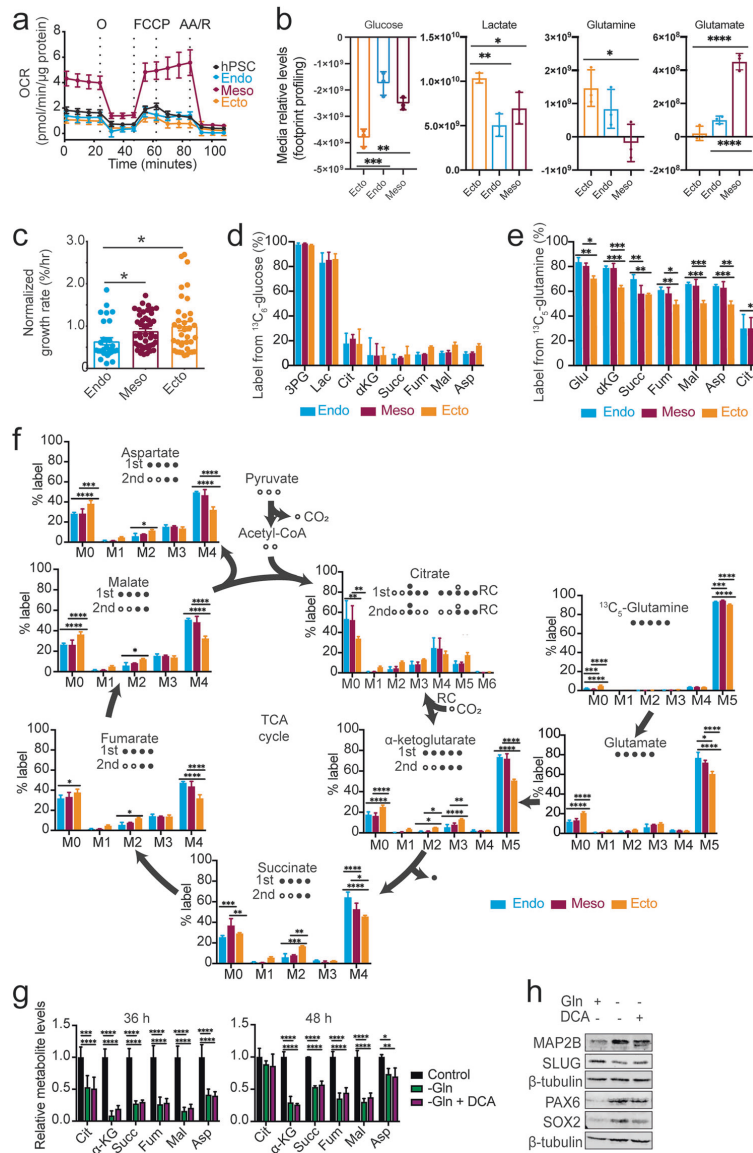
revealed widespread cell death under Gln deprivation, suggesting that Gln is indispensable for ME formation (Supplementary information, Fig. S2f). In contrast, Gln withdrawal led to an increase in EC specifying biomarker proteins PAX6 and MAP2B during 21 days of EB differentiation (Fig. 1h, Supplementary information, Fig. S2e). Increased EC production may be linked to a compensation for Gln deprivation by recovery of glycolytic metabolites (Fig. 1g, h, Supplementary information, Fig. S2g).

Together, this EB differentiation profile suggests that Gln withdrawal skews potentiation of ME negatively and EC positively.

This report provides a deeper understanding of distinct metabolic shifts in early germ lineages by showing that mitochondrial respiration and Gln oxidation is essential for ME differentiation. Further studies are needed to elucidate the functional roles of metabolic reprogramming in early germ lineages, with possibilities including transcriptional program

Fig. 1 Human pluripotent stem cell-derived mesoderm differentiation requires glutaminolysis and distinct mitochondrial metabolism. **a** Oxygen consumption rate (OCR) measured by mitochondrial stress test of H9 hPSC and H9-derived endoderm (EN), mesoderm (ME), and ectoderm (EC) lineages at 5 days of directed differentiation. Data are normalized by microgram of protein content per well. Injections of 1 μM oligomycin, 0.33 μM FCCP, 0.5 μM FCCP, and 1 μM each Antimycin A/Rotenone were performed. Data represent $n = 6$ technical replicates of 1 biological experiment with additional $n \geq 2$ biological experiments provided in Supplementary information, Fig. S1e. **b** Media footprint analysis (relative metabolite consumption and production into media) of nutrient-balanced EN, ME, and EC samples, quantifying levels of (i) glucose consumption, (ii) lactate production, (iii) glutamine consumption, and (iv) glutamate production at 5 days of directed differentiation. Positive values indicate increased production of cellular metabolites into spent media, whereas negative values indicate cellular consumption of media metabolites. Data are normalized to initial unspent fresh media levels as measured by UHPLC–MS, and represent $n = 3$ independent experiments. Media of differentiated H9 hESCs were changed 24 h prior to spent media metabolite extraction. **c** Normalized single colony biomass accumulation and growth rates (%/hour) of nutrient-balanced H9-derived EN/ME/EC samples measured over 24 h. Data represent $n = 29$ EN, $n = 45$ ME, and $n = 37$ EC colonies. **d, e** Fractional contribution of $^{13}C_6$-labeled metabolites from [U-$^{13}C_6$] glucose (**d**) or $^{13}C_5$-labeled metabolites from [U-$^{13}C_5$] glutamine (**e**) after 18 h quantified by UHPLC-MS. **f** Mass isotopomer distribution (MID) of TCA cycle-associated metabolites from [U-$^{13}C_5$] glutamine. The carbon labeling of TCA cycle-associated metabolites from [U-$^{13}C_5$] glutamine is schematically illustrated in black for the first (1st) and second (2nd) turn or α-ketoglutarate (α-KG) reductive carboxylation (RC) into citrate. Media of differentiated H9 hESCs were changed 18 h prior to intracellular metabolite extraction. **g** Relative levels of TCA cycle metabolites in H9 hPSCs under 36 h and 48 h spontaneous differentiation in the presence or the absence of Gln in the culture media co-treated or untreated with 1 mM DCA, quantified by UHPLC-MS. **h** Immunoblot of ME (SLUG) and EC (PAX6, SOX2 and MAP2) markers in H9-derived EB at 21 days of differentiation in the presence or the absence of Gln in the culture media co-treated or untreated with 1 mM DCA. *$P \leq 0.05$, **$P \leq 0.01$, ***$P \leq 0.001$, ****$P \leq 0.0001$. p values are determined using unpaired Student's t-test (**c**–**e**) or two-way ANOVA with multiple comparisons Bonferroni correction (**b**, **f**, **g**). Data represent mean ± SD (**a**, **b**, **d**–**g**) or mean ± SEM (**c**) of independent experiments indicated above

changes regulated by metabolite-sensitive epigenetic modifiers[14] or carbon source-specific dependencies.

AUTHOR CONTRIBUTIONS

Conceptualization: P.D., V.L. M.A.T.; Methodology: P.D., V.L., M.A.T.; Software: F.M.A., D.H., D.B.; Formal Analysis: P.D., V.L., F.M.A., A.N.P., I.J.R., D.H., D.B., R.M.T.N.; Investigation: P.D., V.L., F.M.A., I.J.R., A.T.,Jr., R.M.T.N.; Resources: F.M.A., D.B., M.A.T.; Data Curation: V.L., F.M.A., A.N.P., I.J.R., D.B.; Writing-Original Draft: V.L., F.M.A., A.N.P., I.J.R., M.A.T.; Writing—Review & Editing: V.L., F.M.A., A.N.P., I.J.R., M.A.T.; Validation: V.L., F.M.A., A.N.P., I.J.R., M.A.T.; Visualization: V.L., F.M.A., A.N.P., I.J.R.; Supervision: P.D., M.A.T.; Project Administration: P.D., M.A.T.; Funding Acquisition: A.N.P., M.A.T.

ADDITIONAL INFORMATION

Supplementary information accompanies this paper at https://doi.org/10.1038/s41422-019-0191-2.

Competing interests: The authors declare no competing interests.

Vivian Lu[1], Perrine Dahan[2], Fasih M. Ahsan[2], Alexander N. Patananan[2], Irena J. Roy[2], Alejandro Torres Jr.[3], Robert M. T. Nguyen[2], Dian Huang[4], Daniel Braas[1] and Michael A. Teitell[2,4,5]
[1]Department of Molecular and Medical Pharmacology, David Geffen School of Medicine, University of California, Los Angeles, Los Angeles, CA 90095, USA; [2]Department of Pathology and Laboratory Medicine, David Geffen School of Medicine, University of California, Los Angeles, Los Angeles, CA 90095, USA; [3]Department of Chemistry and Biochemistry, University of California, Los Angeles, CA 90095, USA; [4]Department of Bioengineering, University of California, Los Angeles, CA 90095, USA and [5]Jonsson Comprehensive Cancer Center, Molecular Biology Interdepartmental Program, California NanoSystems Institute, Department of Pediatrics, and Broad Center for Regenerative Medicine and Stem Cell Research, University of California, Los Angeles, CA 90095, USA
These authors contributed equally: Vivian Lu, Perrine Dahan
Correspondence: Michael A. Teitell (mteitell@mednet.ucla.edu)

REFERENCES
1. Zhang, J. et al. *EMBO J.* **30**, 4860–4873 (2011).
2. Tohyama, S. et al. *Cell Metab.* **23**, 663–674 (2016).
3. Marsboom, G. et al. *Cell Rep.* **16**, 323–332 (2016).
4. Cliff, T. S. et al. *Cell Stem Cell* **21**, 502–516 (2017).
5. Gifford, C. A. et al. *Cell* **153**, 1149–1163 (2013).
6. Loh, K. M. et al. *Cell Stem Cell* **14**, 237–252 (2014).
7. Xie, W. et al. *Cell* **153**, 1134–1148 (2013).
8. Hosios, A. M. et al. *Dev. Cell* **36**, 540–549 (2016).
9. Fendt, S. M. et al. *Nat. Commun.* **4**, 2236 (2013).
10. Brady, R. O., Mamoon, A. M. & Stadtman, E. R. *J. Biol. Chem.* **222**, 795–802 (1956).
11. Kurosawa, H. *J. Biosci. Bioeng.* **103**, 389–398 (2007).
12. Crabb, D. W., Yount, E. A. & Harris, R. A. *Metabolism* **30**, 1024–1039 (1981).
13. Zitka, O. et al. *Oncol. Lett.* **4**, 1247–1253 (2012).
14. TeSlaa, T. et al. *Cell Metab.* **24**, 485–493 (2016).

Supplementary information, Data S1

EXPERIMENTAL MODEL AND SUBJECT DETAILS

Cell Culture

All work with human embryonic stem cells (hESCs) has been approved under the UCLA

Institutional Biosafety Committee (IBC) and UCLA Embryonic Stem Cell Research Oversight

(ESCRO) Committee under Protocol # 2007-003-12. H9 (WA09 – Female; RRID:CVCL_9773),

H1 (WA01 – Male; RRD:CVCL_9771), HSF-1 (Male; RRID:CVCL-D003), hiPS2 (Male; RRID:

CVCL_B508) and UCLA-1 (Female; RRID:CVCL_9951) primed human pluripotent stem cells

(hPSCs) were provided low-passage and contamination tested through the UCLA BSCRC

hESC Core Bank (Jerome Zack, UCLA). Following receipt, hPSCs were shifted to feeder-free

Matrigel (Corning) in mTeSR1 medium (Stemcell Technologies) and passaged using Gentle

Cell Dissociation Reagent (Stemcell Technologies).

Trilineage Directed-Differentiation Protocol

6-wells plates were coated with 1:10 Matrigel (Corning) and incubated for 30 minutes prior to

seeding. 80-90% confluent hPSCs were incubated in Gentle Cell Dissociation Reagent

(Stemcell Technologies) for 8 minutes at 37°C, dissociated to single cells using a 40µm cell

strainer, and harvested in plain media (DMEM/F12; Gibco) for counting. Cells were centrifuged

at 450xg for 5 minutes.

Ectoderm Differentiation

1.2×10^6 cells were seeded in each well of a 6 well plate in mTeSR1 media (Stemcell

Technologies) with 10 µM ROCK inhibitor (Y-27632; Stemcell Technologies). Media was

changed to differentiation media 24 hours after seeding. hPSCs were differentiated over a 5-day

period by culturing in a 50% DMEM/F12 and 50% IMDM-based medium (Gibco) supplemented

with 450 µM monothioglycerol (Millipore Sigma), 1 mg/ml BSA (Gibco), 0.11 µM 2-

mercaptoethanol (Gibco), 1% Glutamax (Gibco), 1% N2 supplement (Thermofisher), 2% B27

supplement (Thermofisher), 10 µM SB43154 (Stemgent), and 0.2 µM Dorsomorphin

(Stemgent).

Mesoderm Differentiation

1.8×10^6 cells were seeded in each well of a 6 well plate in mTeSR1 media with 10 µM ROCK

inhibitor (Y-27632; Stemcell Technologies). hPSCs were differentiated over a 5-day period by

culturing in a 50% DMEM/F12 and 50% IMDM-based medium (Gibco) supplemented with 450

µM monothioglycerol (Millipore Sigma), 1 mg/ml BSA (Gibco), 0.11 µM 2-mercaptoethanol

(Gibco), 1% Glutamax (Gibco), 0.7 µg/mL insulin (Millipore Sigma), 15 µg/mL transferrin

(Millipore Sigma), 1 mL/100mL chemically-defined lipid concentrate (Gibco), 100 ng/mL VEGF-

165 (Stemcell Technologies), 100 ng/mL BMP4 (Peprotech), and 20 ng/mL FGF2 (Peprotech).

Medium for the first 24 hours of differentiation was supplemented with 100 ng/mL Activin A

(Stemcell Technologies).

Endoderm Differentiation

1.8×10^6 cells were seeded in each well of a 6 well plate in mTeSR1 media with 10 µM ROCK

inhibitor (Y-27632; Stemcell Technologies). hPSCs were differentiated over a 3-day period by

culturing in a 50% DMEM/F12 and 50% IMDM-based medium (Gibco) supplemented with 450

µM monothioglycerol (Millipore Sigma), 1 mg/ml BSA (Gibco), 0.11 µM 2-mercaptoethanol

(Gibco), and 1% Glutamax (Gibco). Medium for the first 24 hours was supplemented with 100

ng/mL Activin A (Stemcell Technologies), 2 µM CHIR99021 (Cayman Chemicals), and 50 nM

PI-103 (Fisher Scientific). Medium after the first 24 hours was supplemented with 100 ng/mL

Activin A (Stemcell Technologies), and 250 nM LDN 1931189 (Stemgent).

Embryoid Body Differentiation

3.5 x 10^6 cells per well were seeded in AggreWell EB Formation Media (Stemcell Technologies) with 10 µM ROCK inhibitor (Y-27632; Stemcell Technologies) into 6-well AggreWell 400 plates (Stemcell Technologies) for consistent size and shape. Within 24 hours, embryoid bodies were harvested through a cell strainer and transferred to 6-well Ultra-Low Attachment plates (Corning Costar) and grown in DMEM/F12 (Gibco) supplemented with 20% KnockOut Serum Replacement (Gibco), 1% Glutamax (Gibco), 1% Penicillin/Streptomycin (Corning), 1% Non-Essential Amino Acids (Corning), and 0.1 mM 2-mercaptoethanol (Gibco). Media was changed every day throughout 21 days of differentiation. For DCA treated condition, media was supplemented with 1mM dichloroacetate (DCA; Millipore Sigma). For glutamine deprivation condition, DMEM/F12 without glutamine (Gibco) was used and Glutamax (Gibco) was excluded from media preparation.

METHOD DETAILS

Nutrient Balanced Media Formulation

For all differentiation protocols indicated, a chemically defined, nutrient balanced base media (CDM2) was prepared using 50% DMEM-F12 and 50% IMDM media (Gibco). Media was supplemented with 1mg/mL BSA (Gibco), 1% chemically defined lipid concentrate CDLC (Gibco), 450 µM monothioglycerol (Millipore Sigma), 0.7 µg/mL insulin (Millipore Sigma), 15 µg/mL Transferrin (Millipore Sigma), 1% Glutamax (Gibco), and 0.18% 2-mercaptoethanol (Gibco). CDM2 base media was then filter sterilized through a 0.22 µM filter (Millipore Sigma) prior to use.

Extracellular Flux Analysis

HPSC, ME, EN, and EC cells were plated on a XF96 (Agilent) 96-well plate at 10^5-10^6 cells/well seeding density. The following day, respective media was replaced one hour prior to assay with nutrient balanced XF media (Agilent) supplemented with 1mM sodium pyruvate (Corning), 17.5

mM glucose, and 2mM glutamine (without glutamine in glutamine deprivation assays). Oxygen consumption rate (pmol/min) and extracellular acidification rate (mpH/min) were assessed using a Seahorse XF96 Extracellular Flux Analyzer mitochondrial stress test (Agilent) using the following drug concentrations: 1 µM oligomycin, 0.5 µM/0.33 µM FCCP, and 1 µM each of Rotenone/Antimycin A. Measurements are normalized to protein concentration measured by BCA (Pierce).

Media Footprint Analysis

Following a minimum of 24 hours of nutrient balanced media culturing, 20µL of media was removed per sample and added to 300 µL of 80% HPLC-grade methanol (Fisher Scientific). Samples were then vortexed, centrifuged, washed, evaporated, and processed as indicated in the *Metabolite Extraction and UHPLC-MS Processing* methods section below. Measurements are normalized to protein concentration measured by BCA (Pierce), followed by normalization to fresh unspent media for each of the trilineage formulations as an internal blank control.

Biomass Accumulation

Biomass accumulation and growth rate measurements were obtained using quantitative phase microscopy (OPM) using a live cell interferometer (LCI), as described previously [2]. The LCI system consists of a Zeiss Axio Observer Z1 inverted microscope and an on-stage incubation chamber (Zeiss) with temperature, CO2 and humidity modulations (Zeiss). QPM images were captured by a SID4BIO (Phasics) quadriwave lateral shearing interferometry (QWSLI) camera. All cells were imaged using a 20x 0.4NA objective and a 660nm collimated LED (Thorlabs) light source. 2-4 hours prior to imaging, 25,000-30,000 hPSC and hPSC-derived D5 ME, EN, and EC cells were seeded into ibidi polymer-treated µ-slide 4 well plates (ibidi GmbH). Immediately prior to imaging, media is carefully changed to remove cells in suspension and sealed with anti-

evaporation oil (ibidi USA). During imaging, the sample plate is moved by the motorized stage, collecting 15 images/well on each stop at the rate of 10min/row of four wells. Following data acquisition, phase images are automatically processed in a custom pipeline that includes background flattening, cell detection, colony segmentation, and biomass calculation. Normalized growth rate plots are generated by subtracting the biomass of each colony by its initial biomass at every captured time point.

Flow Cytometry

Cells were harvested using Gentle Cell Dissociation Reagent (Stemcell Technologies) and resuspended in plain DMEM (Corning). Samples were fixed using the Cytofix/Cytoperm Kit (BD Biosciences) and processed on a LSRII or LSRFortessa flow cytometer (BD Biosciences). Samples were analyzed using FlowJo software (FlowJo, Inc). Antibodies and isotype controls used and their dilutions are indicated below.

RNA Extraction

All cells were grown to 70-80% confluence and purified using the RNeasy Mini Kit (Qiagen) and RNase-free DNase (Qiagen) following the manufacturer's protocols. All samples showed a A260/280 ratio > 1.99 (Nanodrop; Thermo Scientific). For RNA-Sequencing, prior to library preparation, quality control of the RNA was performed using the Advanced Analytical Technologies Fragment Analyzer (Advanced Analytical, Inc.) and analyzed using PROSize 2.0.0.51 software. RNA Quality Numbers (RQNs) were computed per sample between 8.1 and 10, indicating intact total RNA per sample prior to library preparation.

RNA-Sequencing Library Preparation

Strand-specific ribosomal RNA (rRNA) depleted RNA-Seq libraries were prepared from 1 µg of total RNA using the KAPA Stranded RNA-Seq Kit with Ribo-Erase (Kapa Biosystems, Roche). Briefly, rRNA was depleted from total RNA samples, the remaining RNA was heat fragmented, and strand-specific cDNA was synthesized using a first strand random priming and second strand dUTP incorporation approach. Fragments were then A-tailed, adapters were ligated, and libraries were amplified using high-fidelity PCR. All libraries were prepared in technical duplicates per sample (n = 30 samples, 60 libraries total), and resulting raw sequencing reads merged for downstream alignment and analysis. Libraries were paired-end sequenced at 2x150 bp on an Illumina NovaSeq 6000.

Immunoblotting

Immunoblotting was performed as previously described [3]. All images were captured using an Odyssey Fc with IRDye-conjugated secondary antibodies (LiCor). Antibodies used and their respective dilutions are listed below.

Metabolite Extraction and UHPLC-MS Processing

Intracellular metabolites were extracted with cold 80% methanol and analyzed using ultra-high performance liquid chromatography-mass spectrometry (UHPLC-MS) as previously described [4]. Media of differentiated H9 hESCs were changed 18h prior to metabolite extraction. For experiments with glucose and glutamine tracing, unlabeled glucose and glutamine were replaced with [U-^{13}C] glucose and [U-^{13}C] glutamine isotopologues (Cambridge Isotope Laboratories), respectively, in a DMEM/F12 only base medium. After, cells were rinsed with cold D-PBS and 150mM ammonium acetate (pH 7.3) and then collected in cold 80% MeOH in water. To the cell suspensions, 10nmol D/L-norvaline were added and vortexed three times on ice, followed by centrifugation (12,130g, 4°C). The supernatant was transferred into a glass vial and

a second extraction was repeated with 150 μL of cold 80% MeOH. Metabolites were dried using an EZ-2 evaporator (Genevac) and resuspended in 70% acetonitrile.

For the mass spectrometry-based analysis of the sample, 5 ul was injected onto a Luna NH2 (150mm 2 mm, Phenomenex) column. The samples were analyzed with an UltiMate 3000RSLC (Thermo Scientific) coupled to a Q Exactive mass spectrometer (Thermo Scientific). The Q Exactive was run with polarity switching (+3.50 kV/-3.50 kV) in full scan mode with an m/z range of 65 -975. Separation was achieved using A) 5mM NH4AcO (pH 9.9) and B) ACN. The gradient started with 15% A) going to 90% A) over 18 min, followed by an isocratic step for 9 min and reversal to the initial 15% A) for 7 min.

QUANTIFICATION AND STATISTICAL ANALYSIS

QPM Image Analysis

All images were processed with custom MATLAB (MathWorks) scripts. Cells were identified and segmented using a local adaptive threshold based on Otsu's method [2] and tracked using particle tracking code [5]. QPM biomass data was summed over the projected area of each cell to obtain total cell biomass at each collection time point. Biomass accumulation rates were calculated by fitting a first-order polynomial to each biomass versus time plot using MATLAB Polyfit (MathWorks). Individual cell growth tracks were quality filtered using an upper cutoff of ±5% uncertainty (s.d. of residuals) in the calculated growth rate, as determined by linear fitting the biomass versus time data.

Metabolomics Data Analysis

Metabolites were quantified with TraceFinder 3.3 using accurate mass measurements (3 ppm) and retention times.

Data was corrected for naturally occurring ^{13}C in isotopologue distribution measurements [6]. Data analysis was calculated using the formula statistical language R. Fractional contributions were measured using the formula described previously, where mi denotes the intensity of the isotopologue, and n marks the number of carbons in the metabolite [7].

RNA-Sequencing Analysis

Fibroblasts, iPSCs, and MSCs were each sequenced in biological triplicates and technical duplicates (n = 60 total samples) to account for variation in extraction and culturing. Raw sequencing reads were converted into fastq files and filtered for low quality reads and Illumina sequencing adapter contamination using bcl2fastq (Illumina). Reads were then quasi-mapped and quantified to the *Homo sapiens* GENCODE 28 (GRCh38.p12, Ensembl 92, April 2018) transcriptome using the alignment-free transcript level quantifier Salmon v0.9.1 [8-10]. A quasi-mapping index was prepared using parameters *"salmon index -k 31 –type quasi"*, and comprehensive transcript level estimates were calculated using parameters *"salmon quant -l A – seqBias –gcBias --discardOrphansQuasi"*. Transcript level counts were collapsed to gene level (HGNC) counts, transcripts per million abundances (TPM) and estimated lengths using R Bioconductor package tximport v1.6.0 [11].

Differential Gene Expression Analysis

The resulting sample gene count matrix was size factor normalized and analyzed for pairwise differential gene expression using R Bioconductor package DESeq2 v1.18.1. Expression changes were estimated using an empirical Bayes procedure to generate moderated fold change values with design "~ Batch + Sample", modeling batch effect variation due to day of RNA extraction [12,13]. Significance testing was performed using the Wald test, and resulting *P* values were adjusted for multiple testing using the Benjamini-Hochberg procedure [14]. DEGs

were filtered using an adjusted false discovery rate (FDR) q value < 0.05 and an absolute $\log_2$ transformed fold-change > 1.

<u>Gene Expression PCA</u>

Variance stabilized transform (VST) values in the gene count matrix were calculated and plotted for PCA using R Bioconductor packages DESeq2, FactoMineR, and factoextra [12,13]. Whole transcriptome PCA was performed with comparison to existing RNA-sequencing data of nutrient balanced trilineage differentiations previously provided in GEO: GSE101655 [1]. RNA-sequencing samples were batch effect normalized across library preparation differences between this study and previously published reports [1] using limma v3.34.9 [15]. PCA of nucleus-encoded mitochondrial protein and mtDNA transcripts were extracted using localization evidence derived from MitoMiner v4.0, subsetting VST matrices using genes listed in MitoCarta 2.0 [16,17]. Scatterplots and MA plots of gene expression fold-changes between fibroblasts, iPSCs, and MSCs were performed, and Pearson/Spearman correlation coefficients calculated, using R package ggpubr v0.1.6 (https://cran.r-project.org/web/packages/ggpubr/index.html). Genes of interest were extracted and averaged clonal heatmaps were prepared using R Bioconductor packages pheatmap v1.0.8 and gplots v3.0.1 [18,19]. Venn diagram intersections of DEG lists were generated using Venny 2.1.0 (http://bioinfogp.cnb.csic.es/tools/venny/index.html)

Statistical Testing

Statistical testing for all data except for RNA-sequencing was performed using Prism 7 and 8 (Graphpad). All RNA-sequencing statistical analysis are described in the Quantification and Statistical Analysis sections. Unpaired Student's t testing was performed for all extracellular flux, media footprint, and interferometry analysis. 2-way ANOVA with multiple comparisons Bonferroni adjustment was used for all metabolomics-based mass isotopomer and fractional

contribution distribution data. Unless otherwise indicated, all data represent the mean ± the

standard deviation of n = 3 independent biological experiments.

DATA AND SOFTWARE AVAILIABILITY

RNA-Sequencing processed and raw files are deposited to the NCBI Gene Expression Omnibus

(GEO) under accession GSE127270. Code used to process RNA-Sequencing data is provided

under Atlassian Bitbucket at https://bitbucket.org/ahsanfasih/OxPhosMesoderm/src/master.

Metabolomics and RNA-Seq processed data are provided in MS Excel format (Data Tables S1

and S2). All other data requests should be directed to and will be fulfilled by the Lead Contact,

Michael A. Teitell (MTeitell@mednet.ucla.edu).

Key Resources Table

REAGENT or RESOURCE	SOURCE	IDENTIFIER
Antibodies		
Mouse anti-β-tubulin; 1/1000	Millipore Sigma	Cat#T4026; RRID:AB_477577
Rabbit anti-PAX6; 1/500	Cell Signaling Technology	Cat#60433S
Rabbit anti-SOX2; 1/1000	Cell Signaling Technology	Cat#4900; RRID:AB_10560516
Rabbit anti-OCT4; 1/1000	Cell Signaling Technology	Cat#2840S; RRID:AB_2167691
Rabbit anti-MAP2; 1/500	Cell Signaling Technology	Cat#4542; RRID:AB_10693782
Rabbit anti-SNAIL; 1/500	Cell Signaling Technology	Cat#9585; RRID:AB_2239535
PerCPCy5.5 Mouse anti-Human PAX6	BD Biosciences	Cat#562388; RRID:AB_11153319
Alexa Fluor 488 Mouse anti-MAP2B	BD Biosciences	Cat#560399; RRID:AB_1645358

Alexa Fluor 488 Mouse anti-OCT3/4	BD Biosciences	Cat#561628; RRID:AB_10895977
Alexa Fluor 700 Mouse anti-Human CD34	BD Biosciences	Cat#561440; RRID:AB_10715443
V450 Mouse anti-SOX2	BD Biosciences	Cat#561610; RRID:AB_10715443
Alexa Fluor 488 Mouse IgG1 κ Isotype Control	BD Biosciences	Cat#557782; RRID:AB_396870
Alexa Fluor 700 Mouse IgG1, κ Isotype Control	BD Biosciences	Cat#557882; RRID:AB_396920
V450 Mouse IgG1, κ Isotype Control	BD Biosciences	Cat#560373; RRID:AB_1645606
PerCP-Cy5.5 Mouse IgG2a, κ Isotype Control	BD Biosciences	Cat#558020; RRID:AB_396989
PerCP-Cy5.5 Mouse IgG1 κ Isotype Control	BD Biosciences	Cat#550795; RRID:AB_393885
Alexa Fluor 647 Rat IgG2a, κ Isotype Control	BD Biosciences	Cat#557857; RRID:AB_396900
IRDye 680RD Donkey anti-Rabbit IgG (H + L)	LI-COR Biosciences	Cat#926-68073; RRID:AB_10954442
IRDye® 800CW Goat anti-Mouse IgG (H + L)	LI-COR Biosciences	Cat#925-32210; RRID:AB_2687825
IRDye® 800CW Goat anti-Rabbit IgG (H + L), 0.5 mg	LI-COR Biosciences	Cat#926-32211; RRID:AB_621843
IRDye 800CW Donkey anti-Goat IgG (H+L)	LI-COR Biosciences	Cat#926-32214; RRID:AB_621846
IRDye 680RD Donkey anti-Mouse IgG (H+L)	LI-COR Biosciences	Cat#926-68072; RRID:AB_10953628
IRDye 680RD Goat Anti-Mouse 0.5 mg	LI-COR Biosciences	Cat#926-68070; RRID:AB_10956588
Chemicals, Peptides, and Recombinant Proteins		
Gentle Cell Dissociation Reagent	Stemcell Technologies	Cat#07174

mTeSR1	Stemcell Technologies	Cat#85850
DMEM/F12	Thermofisher	Cat#11320-082
IMDM	Gibco	Cat#12440053
ROCK Inhibitor; Y-27632	Stemcell Technologies	Cat#72304
Monothioglycerol	Millipore Sigma	Cat#M6145
BSA Fraction V, 7.5%	Gibco	Cat#15260037
2-mercaptoethanol	Thermofisher	Cat#21985-023
GlutaMAX Supplement	Thermofisher	Cat#35050-061
N2 Supplement	Thermofisher	Cat#A1370701
B27 Supplement	Thermofisher	Cat#17504044
SB43154	Stemgent	Cat#04-0010-10
Dorsomorphin	Stemgent	Cat#04-0024
Human Recombinant Insulin	Millipore Sigma	Cat#11376497001
Transferrin from human serum	Millipore Sigma	Cat#10652202001
Chemically Defined Lipid Concentrate (CDLC)	Gibco	Cat#11905031
Human Recombinant VEGF-165	Stemcell Technologies	Cat#78073.1
Human Recombinant BMP-4	PeproTech	Cat#120-05ET
Human Recombinant FGF2	Stemcell Technologies	Cat#78003
Human Recombinant Activin A	Stemcell Technologies	Cat#78001.1
CHIR99021 (GSK3i)	Cayman Chemicals	Cat#13122
PI-103 Hydrochloride	Tocris/Fisher Scientific	Cat#29-301
Stemolecule LDN-1931189	Stemgent	Cat#04-0074
KnockOut Serum Replacement	Thermofisher	Cat#10828-028

Penicillin/Streptomycin Solution, 100X	VWR	Cat#45000-652
MEM Non-Essential Amino Acids	Gibco	Cat#11140-050
Sodium dichloroacetate (DCA), 98%	Millipore Sigma	Cat#347795
Agilent XF Base Media, without phenol red	Agilent Technologies	Cat#103335-100
Anti-evaporation Silicone Oil	ibidi USA	Cat#50051
AggreWell EB Formation Medium	Stemcell Technologies	Cat#05221
AggreWell Rinsing Solution	Stemcell Technologies	Cat#07010
Matrigel	Corning/Fisher Scientific	Cat#CB-4023A
RNAse-Free DNase Set	Qiagen	Cat#79254
DMEM/F12, no glutamine	Thermofisher	Cat#21331020
D-GLUCOSE (U-13C6, 99%)	Cambridge Isotope Laboratories	Cat#CLM-1396-1
L-GLUTAMINE (13C5, 99%)	Cambridge Isotope Laboratories	Cat#CLM-1822-H-0.1
Critical Commercial Assays		
RNeasy Mini Kit	Qiagen	Cat#74106
Seahorse XF Cell Mito Stress Test Kit	Agilent Technologies	Cat#103015-100
KAPA Stranded RNA-Seq with RiboErase	KAPA Biosystems	Cat#KK8484
BCA Protein Assay Kit	Pierce/Thermofisher	Cat#23225
Deposited Data		
RNA-Sequencing Data for Nutrient Balanced hPSC and Trilineage Differentiation to EN/EC/ME	This Paper	GEO: GSE127270

RNA-Sequencing Data for hPSC Trilineage Differentiation Comparisons	Stephen Dalton Lab [1]	GEO: GSE101655
Experimental Models: Cell Lines		
H9 (WA09); Female	UCLA BSCRC hESC Core Bank	RRID:CVCL_9773
H1 (WA01); Male	UCLA BSCRC hESC Core Bank	RRID:CVCL_9771
HSF-1; Male	UCLA BSCRC hESC Core Bank	RRID:CVCL_D003
hiPS2; Male	UCLA BSCRC hESC Core Bank	RRID:CVCL_B508
UCLA-1; Female	UCLA BSCRC hESC Core Bank	RRID:CVCL_9951
Software and Algorithms		
Seahorse Wave Desktop Software	Agilent Technologies	https://www.agilent.com/en/products/cell-analysis/cell-analysis-software/data-analysis/wave-desktop-2-6
ImageJ	NIH	https://imagej.nih.gov/ij/
Salmon v0.9.1	[10]	https://combine-lab.github.io/salmon/
Tximport v1.6.0	[11]	http://bioconductor.org/packages/release/bioc/html/tximport.html
DESeq2 v1.18.1	[13]	https://bioconductor.org/packages/release/bioc/html/DESeq2.html
Pheatmap v1.0.8	[19]	https://github.com/raivokolde/pheatmap
Gplots v3.0.1	[18]	https://cran.r-project.org/web/packages/gplots/index.html
Prism 7 and 8	Graphpad	https://www.graphpad.com/scientific-software/prism/
TraceFinder v3.3	Thermofisher	https://www.thermofisher.com/order/catalog/product/OPTON-30491
Matlab Scripts for Live Cell Interferometry	Mathworks; [2,5]	N/A
Limma v3.34.9	[15]	https://bioconductor.org/packages/release/bioc/html/limma.html
R v3.4.4	The R Project for Statistical Computing	https://www.r-project.org
Bioconductor v3.6	[12]	https://www.bioconductor.org

Supplementary References

1   Cliff, T. S. *et al.* MYC Controls Human Pluripotent Stem Cell Fate Decisions through Regulation of Metabolic Flux. *Cell Stem Cell* **21**, 502-516 e509, doi:10.1016/j.stem.2017.08.018 (2017).

2   Zangle, T. A., Chun, J., Zhang, J., Reed, J. & Teitell, M. A. Quantification of biomass and cell motion in human pluripotent stem cell colonies. *Biophys J* **105**, 593-601, doi:10.1016/j.bpj.2013.06.041 (2013).

3   TeSlaa, T. *et al.* alpha-Ketoglutarate Accelerates the Initial Differentiation of Primed Human Pluripotent Stem Cells. *Cell Metab* **24**, 485-493, doi:10.1016/j.cmet.2016.07.002 (2016).

4   Thai, M. *et al.* Adenovirus E4ORF1-induced MYC activation promotes host cell anabolic glucose metabolism and virus replication. *Cell Metab* **19**, 694-701, doi:10.1016/j.cmet.2014.03.009 (2014).

5   Zangle, T. A., Burnes, D., Mathis, C., Witte, O. N. & Teitell, M. A. Quantifying biomass changes of single CD8+ T cells during antigen specific cytotoxicity. *PLoS One* **8**, e68916, doi:10.1371/journal.pone.0068916 (2013).

6   Moseley, H. N. Correcting for the effects of natural abundance in stable isotope resolved metabolomics experiments involving ultra-high resolution mass spectrometry. *BMC Bioinformatics* **11**, 139, doi:10.1186/1471-2105-11-139 (2010).

7   Fendt, S. M. *et al.* Reductive glutamine metabolism is a function of the alpha-ketoglutarate to citrate ratio in cells. *Nat Commun* **4**, 2236, doi:10.1038/ncomms3236 (2013).

8   Harrow, J. *et al.* GENCODE: the reference human genome annotation for The ENCODE Project. *Genome Res* **22**, 1760-1774, doi:10.1101/gr.135350.111 (2012).

9   Mudge, J. M. & Harrow, J. Creating reference gene annotation for the mouse C57BL6/J genome assembly. *Mamm Genome* **26**, 366-378, doi:10.1007/s00335-015-9583-x (2015).

10   Patro, R., Duggal, G., Love, M. I., Irizarry, R. A. & Kingsford, C. Salmon provides fast and bias-aware quantification of transcript expression. *Nat Methods* **14**, 417-419, doi:10.1038/nmeth.4197 (2017).

11   Soneson, C., Love, M. I. & Robinson, M. D. Differential analyses for RNA-seq: transcript-level estimates improve gene-level inferences. *F1000Res* **4**, 1521, doi:10.12688/f1000research.7563.2 (2015).

12   Huber, W. *et al.* Orchestrating high-throughput genomic analysis with Bioconductor. *Nat Methods* **12**, 115-121, doi:10.1038/nmeth.3252 (2015).

13   Love, M. I., Huber, W. & Anders, S. Moderated estimation of fold change and dispersion for RNA-seq data with DESeq2. *Genome Biol* **15**, 550, doi:10.1186/s13059-014-0550-8 (2014).

14   Benjamini, Y. & Hochberg, Y. Controlling the False Discovery Rate - a Practical and Powerful Approach to Multiple Testing. *J Roy Stat Soc B Met* **57**, 289-300 (1995).

15   Ritchie, M. E. *et al.* limma powers differential expression analyses for RNA-sequencing and microarray studies. *Nucleic Acids Res* **43**, e47, doi:10.1093/nar/gkv007 (2015).

16   Calvo, S. E., Clauser, K. R. & Mootha, V. K. MitoCarta2.0: an updated inventory of mammalian mitochondrial proteins. *Nucleic Acids Res* **44**, D1251-1257, doi:10.1093/nar/gkv1003 (2016).

17   Smith, A. C. & Robinson, A. J. MitoMiner v3.1, an update on the mitochondrial proteomics database. *Nucleic Acids Res* **44**, D1258-1261, doi:10.1093/nar/gkv1001 (2016).

18   Gregory Warnes, B. B., Lodewijk Bonebakker, Robert Gentleman, Wolfgang Huber, Andy Liaw, Thomas Lumley, Martin Maechler, Arni Magnusson, Steffen Moeller, Marc Schwartz, Bill Venables. *gplots: Various R Programming Tools for Plotting Data*, <https://cran.r-project.org/web/packages/gplots/index.html> (2016).

19   Kolde, R. *Package 'pheatmap' - Pretty Heatmaps*, <https://cran.r-project.org/web/packages/pheatmap/index.html> (2015).
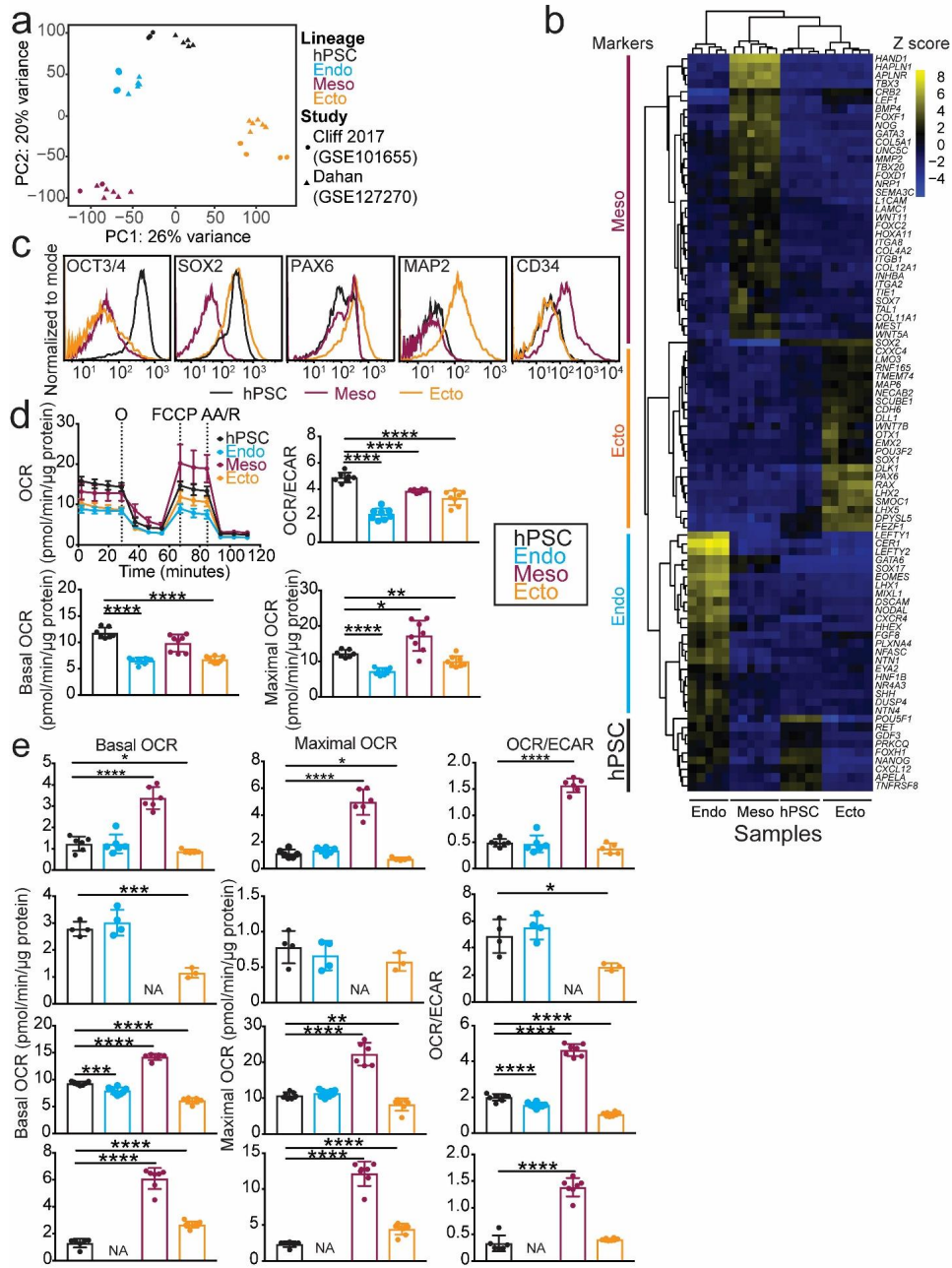
Supplementary information, Fig. S1 Molecular and transcriptomic characterization of germ layers generated with nutrient-balanced media. a Principal components analysis (PCA) plot of transcriptomic variance between H9 and H9-derived lineage-directed differentiations from this study (n = 5, GSE127270) and a previously established nutrient-balanced strategy[1] (n = 2, GSE101655). **b** Heatmap of hPSC and lineage-restricted marker gene expression. Heatmap values are plotted as the *variance stabilized transform* (VST) subtracted by the gene row average mean between samples (Z score). Values shown are unaveraged replicates (n = 5 each lineage). **c** Representative flow cytometry traces for expression of pluripotency (OCT4, SOX2), EC (SOX2, PAX6, MAP2) and ME (CD34) markers under EC and ME directed differentiation. **d** Representative OCR trace and quantification of basal OCR, maximal OCR, and maximal OCR/ECAR ratio determined by mitochondrial stress test of UCLA1 hPSCs at 5 days of lineage-directed differentiation. Data are normalized by μg of protein content per well. **e** Quantification and additional biological replicates provided of mitochondrial stress tests for H9 hPSC and H9-derived progenitors. Each row represents one independent biological experiment. Data represent n = 3 ME, n = 3 EN, n = 4 EC. Related to Fig. 1a. *$p \leq 0.05$, ** $p \leq 0.01$, *** $p \leq 0.001$, **** $p \leq 0.0001$. *p* values are determined using (e) unpaired Student's t-test. Data represent mean ± SD of independent experiments indicated above.

Supplementary References

1   Cliff, T. S. *et al.* MYC Controls Human Pluripotent Stem Cell Fate Decisions through Regulation of Metabolic Flux. *Cell Stem Cell* **21**, 502-516 e509, doi:10.1016/j.stem.2017.08.018 (2017).
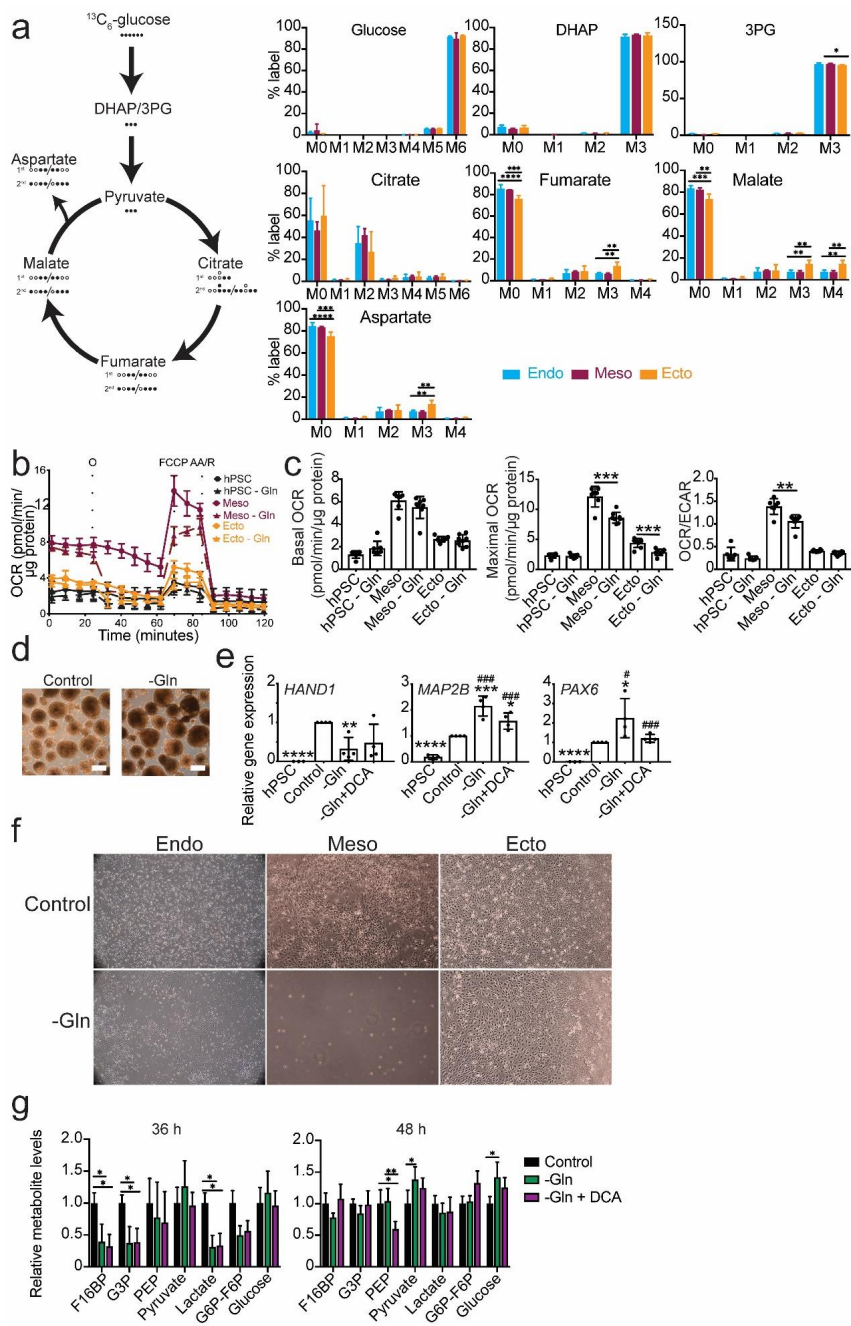
Supplementary information, Fig. S2 Impact of glutamine removal on metabolism and cell fate. a Schematic and mass isotopomer distribution (MID) percent labeled of select glycolysis, citrate, and significant TCA metabolites (fumarate, malate, aspartate) from [U-$^{13}C_6$] glucose labeling. Media of differentiated H9 hESCs were changed 18h prior to intracellular metabolite extraction. **b-c** Representative OCR trace and quantification of basal OCR, maximal OCR, and maximal OCR/ECAR ratio determined by mitochondrial stress test of H9 hPSCs and H9-derived EC and ME in presence or absence (-Gln) of glutamine in XF media. **d** Morphology of H9-derived EB at 21 day differentiation in presence or absence of glutamine in culture media. Scale indicates 100 µm. **e** Relative transcriptional expression of transcription factors ME (HAND1) and EC (MAP2B, PAX6) in H9-derived EB at 21 day differentiation in presence (Control) or absence of glutamine (-Gln) and co-treated or untreated with 1mM DCA in the culture media. *$p ≤ 0.05$, ** $p ≤ 0.01$, *** $p ≤ 0.001$, **** $p ≤ 0.0001$ when compared to EB control, $^#$ $p ≤ 0.05$, $^{##}$ $p ≤ 0.01$, $^{###}$ $p ≤ 0.001$, $^{####}$ $p ≤ 0.0001$ when compared to hPSC control. Relative expression quantification is normalized to Control (set to 1). **f** Phase contrast microscopy images of cytokine-induced directed differentiation of EC, ME, and EN in the presence (Ctr) or absence (-Gln) of glutamine. Images taken are at 40X magnification. Data represent n = 3 independent experiments. **g** Relative levels of glycolytic metabolites in H9 hPSCs under 36h and 48h spontaneous differentiation in presence or absence of Gln and co-treated or untreated with 1mM DCA in the culture media, quantified by UHPLC-MS.*$p ≤ 0.05$, ** $p ≤ 0.01$, *** $p ≤ 0.001$, **** $p ≤ 0.0001$. p values are determined using (**b-e**) unpaired Student's t-test or (g) two-way ANOVA with multiple comparisons Bonferroni correction. Data represent mean ± SD of n = 3 independent experiments.
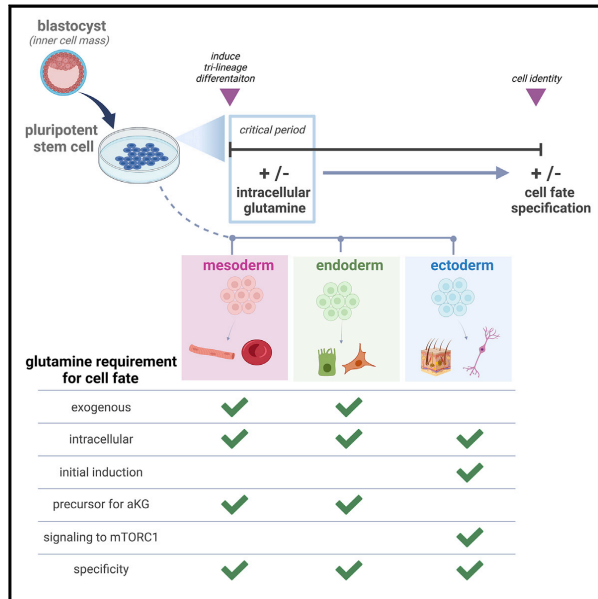
CHAPTER 7:

Glutamine-Dependent Signaling Controls Pluripotent Stem Cell Fate

Developmental Cell

Glutamine-dependent signaling controls pluripotent stem cell fate

Graphical abstract

Highlights

- All three lineages make *de novo* Gln, but only ectoderm can survive in Gln-free media

- Intracellular Gln is more crucial than cytokines for enabling ectoderm specification

- Exogenous Gln is the preferred precursor for α-KG in mesoderm and endoderm

- Transcriptome of a human embryo shows unique Gln enzyme-encoding expression patterns

Authors

Vivian Lu, Irena J. Roy,
Alejandro Torres, Jr., James H. Joly,
Fasih M. Ahsan, Nicholas A. Graham,
Michael A. Teitell

Correspondence

mteitell@mednet.ucla.edu

In brief

Lu et al. report that cell-type-specific Gln requirements distinguish the three embryonic germ lineages upon pluripotency exit. They further reveal that Gln acts as a signaling molecule to activate mTORC1 and enable downstream ectoderm, but not mesoderm or endoderm, differentiation.

CellPress

Article

Glutamine-dependent signaling controls pluripotent stem cell fate

Vivian Lu,[1] Irena J. Roy,[2] Alejandro Torres, Jr.,[3] James H. Joly,[4,10] Fasih M. Ahsan,[5] Nicholas A. Graham,[4,6,7] and Michael A. Teitell[2,3,8,9,11,*]

[1]Department of Molecular and Medical Pharmacology, David Geffen School of Medicine, University of California at Los Angeles, Los Angeles, CA, USA
[2]Department of Pathology and Laboratory Medicine, David Geffen School of Medicine, University of California at Los Angeles, Los Angeles, CA, USA
[3]Molecular Biology Institute, University of California at Los Angeles, Los Angeles, CA, USA
[4]Mork Family Department of Chemical Engineering and Materials Science, Los Angeles, CA 90089, USA
[5]Program in Biological and Biomedical Sciences, Harvard Medical School, Boston, MA, USA
[6]Norris Comprehensive Cancer Center, University of Southern California, Los Angeles, CA 90089, USA
[7]Leonard Davis School of Gerontology, University of Southern California, Los Angeles, CA 90089, USA
[8]Department of Bioengineering, Department of Pediatrics, California NanoSystems Institute, and Broad Center for Regenerative Medicine and Stem Cell Research, University of California at Los Angeles, Los Angeles, CA, USA
[9]Jonsson Comprehensive Cancer Center, David Geffen School of Medicine, University of California at Los Angeles, Los Angeles, CA, USA
[10]Present address: Nautilus Biotechnology, San Carlos, CA, USA
[11]Lead contact
*Correspondence: mteitell@mednet.ucla.edu
https://doi.org/10.1016/j.devcel.2022.02.003

SUMMARY

Human pluripotent stem cells (hPSCs) can self-renew indefinitely or can be induced to differentiate. We previously showed that exogenous glutamine (Gln) withdrawal biased hPSC differentiation toward ectoderm and away from mesoderm. We revealed that, although all three germ lineages are capable of *de novo* Gln synthesis, only ectoderm generates sufficient Gln to sustain cell viability and differentiation, and this finding clarifies lineage fate restrictions under Gln withdrawal. Furthermore, we found that Gln acts as a signaling molecule for ectoderm that supersedes lineage-specifying cytokine induction. In contrast, Gln in mesoderm and endoderm is the preferred precursor of α-ketoglutarate without a direct signaling role. Our work raises a question about whether the nutrient environment functions directly in cell differentiation during development. Interestingly, transcriptome analysis of a gastrulation-stage human embryo shows that unique Gln enzyme-encoding gene expression patterns may also distinguish germ lineages *in vivo*. Together, our study suggests that intracellular Gln may help coordinate differentiation of the three germ layers.

INTRODUCTION

Human pluripotent stem cells (hPSCs) self-renew indefinitely or can be induced to differentiate into the three embryonic lineages: mesoderm, definitive endoderm (endoderm), and ectoderm (Takahashi et al., 2007; Thomson et al., 1998). Multiple studies show that specific nutrients can supply specific metabolic pathways to generate enzyme cofactors or substrates that enable or amplify PSC self-renewal or differentiation signals (Carey et al., 2015; Chantranupong et al., 2015; Moussaieff et al., 2015; Reid et al., 2017; Shiraki et al., 2014; TeSlaa et al., 2016; Vozza et al., 2014; Wellen et al., 2010). We recently reported that mesoderm, endoderm, and ectoderm all consume Gln supplied in cell culture media; yet, exogenous Gln deprivation suppressed mesoderm and endoderm lineages and promoted the ectoderm lineage upon spontaneous non-directed-differentiation without affecting cell growth or proliferation. This result indicated that the lack of environmental Gln skewed cell fate specification (Lu et al., 2019), with a mechanism for Gln control of stem cell plasticity and lineage differentiation potential unknown.

Multiple case studies have shown the importance of Gln availability in fetal development. For example, inborn glutamine synthetase (GS) enzyme deficiency resulted in severe abnormalities in ectoderm-derived brain development and infant death in two unrelated newborns (Häberle et al., 2005, 2006). Although the role of Gln as a metabolic precursor and anaplerotic fuel is well known, whether Gln itself has a direct role in stem cell fate determination remains unknown. A recent study reported that nonmetabolized glucose controlled lineage specification of totipotent stem cells in cleavage stage mouse embryos. Glucose as a nutrient, independent of glycolysis, initiated signaling and transcription to induce trophectoderm, which formed the extraembryonic structures of the placenta but not the embryonic inner cell mass (Chi et al., 2020). Accordingly, our finding that Gln
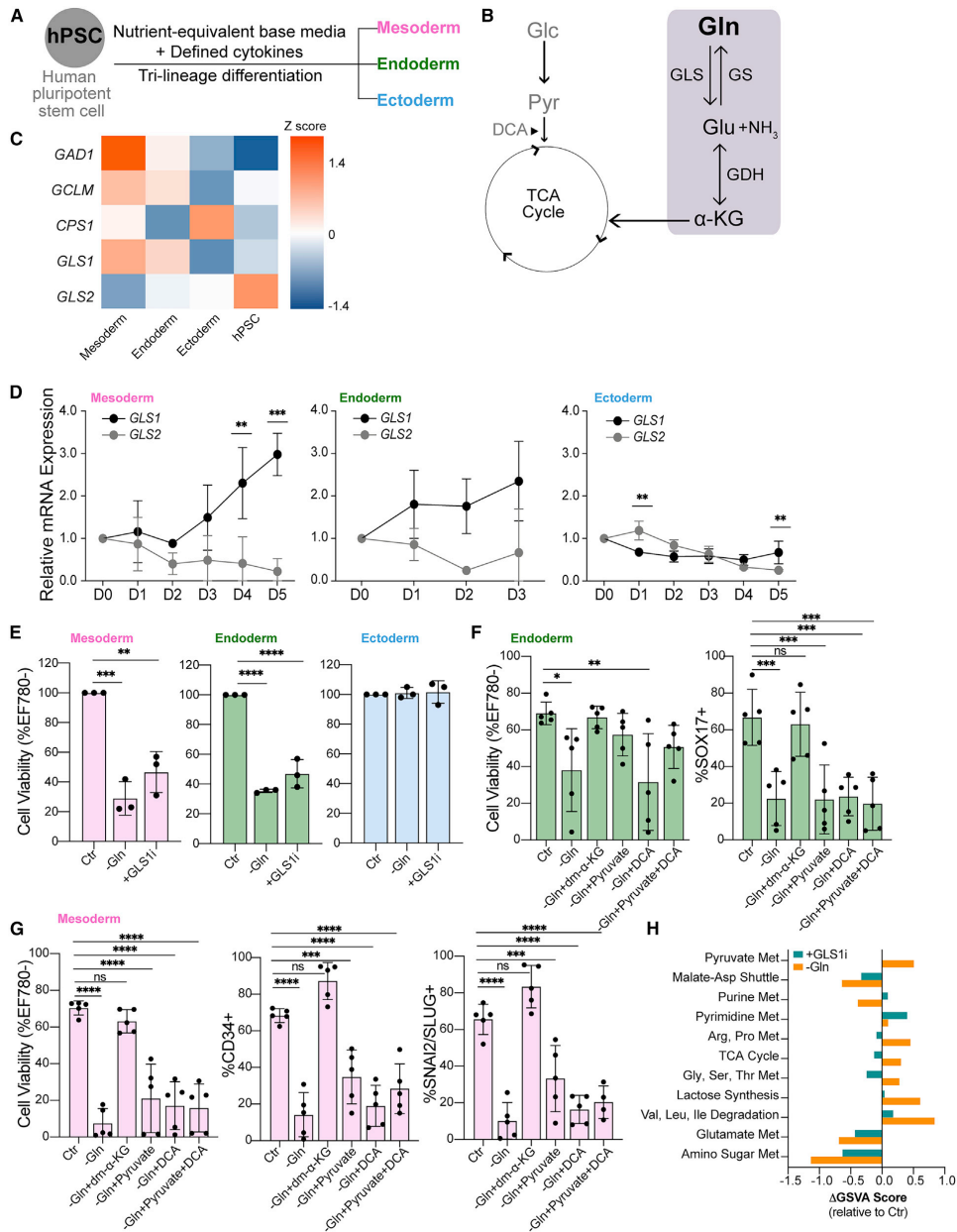
Figure 1. The germ lineages have distinct dependencies on exogenous Gln and catabolism

(A) hPSC differentiation into three embryonic germ lineages mesoderm, endoderm, and ectoderm in nutrient-equivalent culture media.

(B) Schematic of Glc and Gln entry into the TCA cycle. Gln catabolism and anabolism pathways highlighted in gray box. Dichloroacetate (DCA) increases pyruvate flux into the TCA cycle.

(legend continued on next page)

withdrawal induced one cell lineage over others led to a more general question of whether nutrients, without conversion to their metabolic derivatives, can regulate embryonic cell fates.

Here, we report that Gln functions as a signaling molecule that enables the acquisition of ectoderm fate. The requirement for a Gln signal in ectoderm induction supersedes differentiation cues from lineage-inducing cytokines present in the media environment. In contrast, Gln has no direct signaling role and is mainly converted to α-KG to drive mesoderm and endoderm specification. Gln also cannot be substituted by another nutrient, carbon source, or amino acid in tri-lineage differentiation, reinforcing its specificity in germ layer development. Additionally, we uncover that gene expression signatures of Gln utilization are differentially regulated in each germ lineage *in vivo*. Transcriptome signature analysis of a rare gastrulation-stage human embryo resembles enzyme-encoding gene expression patterns found in our *in vitro* studies, generating the hypothesis that distinct Gln utilization may characterize germ lineages *in vivo*. Thus, our study suggests that nutrient signaling, particularly Gln signaling, may coordinate and facilitate germ layer fate determination.

RESULTS

Germ lineages have different Gln dependencies
We investigated Gln processing in hPSCs and the three embryonic germ lineages. hPSCs were directed to differentiate into mesoderm, endoderm, and ectoderm cells using nutrient-equivalent base media and lineage-inducing cytokines (Figure 1A). We previously confirmed that this differentiation method generates homogeneous, lineage-specific cell populations by RNA-seq and transcription factor biomarker expression analyses (Lu et al., 2019) and also cross-referenced transcript profiles with an independent study to verify the reproducibility of this chemically defined differentiation system (Cliff et al., 2017).

To begin, we examined how each lineage handles Gln from the culture media. Two genes, *GLS* (herein, *GLS1*) and *GLS2*, encode the first enzyme in Gln metabolism, glutaminase (GLS), and its isoenzymes, GLS1 (low K_m) and GLS2 (high K_m) (Figure 1B). GLS amidohydrolase activity converts Gln into ammonia and glutamate (Glu), which can be processed into α-KG for tricarboxylic acid (TCA) cycle anaplerosis or other uses (Katt et al., 2017). We used RNA-seq to identify differential expression of glutaminolysis-related and Gln metabolism genes between hPSCs and lineage-induced progeny cells (Figure 1C). hPSC differentiation repressed *GLS2* expression in all lineages, whereas

induction of *GLS1* occurred in mesoderm and endoderm compared with slight repression in ectoderm during differentiation (Figures 1C and 1D). This lineage-specific isoenzyme switching suggests that increased *GLS1* expression in mesoderm and endoderm could favor exogenous Gln processing, whereas ectoderm may depend less upon Gln from the external environment, consistent with our prior results (Lu et al., 2019).

To study whether ectoderm depends on external Gln, hPSCs were induced to differentiate in Gln-supplemented culture media (Ctr), Gln-free media (−Gln, except for trace/negligible amounts in Matrigel), or Gln-supplemented culture media with added GLS1 inhibitor, CB-839 (+GLS1i). Mesoderm perished in Gln-free and glutaminolysis-inhibited conditions (Figures 1E, S1A, and S1B), and endoderm had a similar but less drastic response to Gln perturbations (Figures 1E and S1A). In contrast, ectoderm viability was unaffected by Gln-free and glutaminolysis-inhibited conditions (Figures 1E, S1A, and S1B). Our prior ^{13}C-isotopologue tracing studies showed that Gln supplied the TCA cycle, with significant Gln-derived carbons and negligible glucose-derived carbons incorporated into α-KG in all three germ lineages (Lu et al., 2019). To clarify whether mesoderm and endoderm cell death is from a dependence on Gln fueling the TCA cycle, the culture media was supplemented with cell-permeable dimethyl α-KG (dm-α-KG) or pyruvate. Addition of dm-α-KG or pyruvate, but not dichloroacetate (DCA; Figure 1B) alone, to Gln-free media fully rescued endoderm viability (Figures 1F and S1C). To quantify differentiation efficacy, differentiated cells were gated by lineage-defining transcription factor positive versus negative populations, which were set by hPSC expression levels. Only dm-α-KG addition to Gln-free conditions resulted in the recovery of endoderm differentiation, as measured by the population of SOX17$^+$ cells, whereas added pyruvate restored viability but not endoderm differentiation (Figure 1F). Similarly, only dm-α-KG, but not pyruvate, supplementation in Gln-free media completely restored both viability and biomarker validated mesoderm differentiation, as measured by populations of CD34$^+$ and SNAI2/SLUG$^+$ cells (Figures 1G and S1C). These data indicate that the Gln carbon backbone, retained through glutaminolysis conversion to Glu and then to α-KG, is necessary for mesoderm and endoderm viability and differentiation. This substrate preference indicates that endoderm and mesoderm, but not ectoderm, favor α-KG derivation from Gln specifically because glucose/pyruvate-derived carbons cannot substitute for Gln-derived carbons, at least as an alternative TCA-cycle fuel or for other metabolic processes.

(C) Heatmap of differentially expressed glutaminolysis enzyme transcripts. Values represent the *Z* score of variance stabilizing transformation (VST) normalized RNA-seq counts across each gene listed (n = 6). Genes shown are significantly altered between pairwise combinations of hPSC, mesoderm, endoderm, and ectoderm (p < 0.05).

(D) qRT-PCR analysis of *GLS1* and *GLS2* isoenzymes in mesoderm, endoderm, and ectoderm throughout differentiation.

(E) Cell viability of D5 mesoderm, D3 endoderm, and D5 ectoderm cells grown in Gln-free (−Gln) or Gln-supplemented with added 1 μM CB-839 glutaminase inhibitor (+GLS1i) culture media relative to Gln-supplemented (Ctr).

(F and G) Cell viability and differentiation quantifications of H9-derived (F) endoderm (SOX17$^+$) and (G) mesoderm (CD34$^+$, SNAI2/SLUG$^+$) cells in Gln-free and metabolic rescue conditions.

(H) Metabolite set variation analysis of ectoderm cells in Gln-free (−Gln) or added CB-389 (+GLS1i) conditions. Scores represent pathway enrichment difference between the given treatment to baseline vehicle (Ctr) (n = 3). Pathways displayed are significantly enriched either with −Gln or +GLSi treatment relative to Ctr (p < 0.05).

Data represent mean ± SD of n ≥ 3 biological replicates. *p ≤ 0.05; **p ≤ 0.01; ***p ≤ 0.001; ****p ≤ 0.0001. The p values were determined by (C) Wald test with Benjamini-Hochberg FDR correction, (D) two-way ANOVA, (E–G) one-way ANOVA with correction for multiple comparisons, or (H) moderated t-statistics determined using empirical Bayes linear modeling.

To study the observed exogenous Gln independence of ecto-derm viability, we examined steady-state metabolite patterns in Gln-free and glutaminolysis-inhibited conditions using ultra-high performance liquid chromatography-mass spectrometry (UHPLC-MS) and quantified a panel of 153 central carbon me-tabolites. Metabolite set variation analysis (MSVA) showed that TCA cycle, amino acid, and pyruvate metabolic pathway activ-ities were elevated in Gln-free compared with Gln-supplemented media (Figures 1H and S1D), possibly through re-routing of glucose-derived carbons to maintain TCA metabolite levels. In contrast, glutaminolysis inhibition did not show significant meta-bolic pathway changes compared with no treatment (Figures 1H and S1E), except for increased purine and pyrimidine meta-bolism. This suggests that Gln blocked from GLS1 enzymatic conversion to Glu is shunted toward enhanced nucleotide biosynthesis, possibly supporting proliferation (Figures 1H and S1E). Notably, the Gln-free and glutaminolysis-inhibited metab-olomes are distinct; a Gln-free environment results in decreased nucleotide biosynthesis and increased TCA cycle metabolites compared with GLS1 inhibition (Figures 1H and S1F). Together, these findings indicate that exogenous Gln withdrawal results in widespread metabolic rewiring and that Gln oxidation in the TCA cycle is not required for ectoderm viability.

Sufficient Gln synthesis distinguishes ectoderm from mesoderm and endoderm

Compensatory metabolic adaptations and sustained ectoderm viability in Gln-free media strongly suggest that ectoderm ob-tains Gln by *de novo* synthesis from GS conversion of Glu and ammonia to Gln (Figure 1B) (Bott et al., 2015; Fu et al., 2019; Is-saq et al., 2019; Kung et al., 2011; Stadtman, 2004; Tardito et al., 2015). Consistent with this assessment, GS enzyme is highly ex-pressed in Gln-free, but not in Gln-supplemented, media during ectoderm differentiation (Figures 2A and S2A). Equivalent line-age-specifying PAX6, and suppression of pluripotent OCT4 and NANOG, transcription factor expression also indicated that downstream ectoderm differentiation was unaffected by Gln-free conditions (Figures 2A and S2A). Prior to widespread cell death, mesoderm and endoderm cells also upregulate GS in response to exogenous Gln withdrawal, which is an unex-pected finding because of the dependence of mesoderm and endoderm cells on exogenous Gln for survival (Figure S2B). However, heavy isotopologue tracing showed low levels of $^{13}C_5$-Gln derived from $^{13}C_5$-glutamic acid at steady state in mesoderm and endoderm cells in Gln-free media (Figures 2B and S2C). Additionally, there is minimal derivation of $^{13}C_5$-α-KG from $^{13}C_5$-glutamic acid in mesoderm and endoderm cells, indicating that even though these lineage cell types are capable of *de novo* Gln synthesis, insufficient levels of Gln and/or α-KG are generated, resulting in cell death upon exogenous Gln with-drawal (Figures 1F, 1G, 2B, and S2C). Combined, the data sug-gest that ectoderm uniquely responds to exogenous Gln with-drawal by synthesizing sufficient endogenous Gln, in contrast to an insufficient Gln synthesis adaptation that occurs during mesoderm and endoderm differentiation.

Requirement of intracellular Gln for all germ lineages
We next asked whether ectoderm required Gln at all. Cells were differentiated in the presence of 6-Diazo-5-*oxo*-L-norleucine

(DON), a Gln mimetic that alkylates Gln utilizing enzymes, result-ing in >95% death of mesoderm, endoderm, and ectoderm cells (Figures 2C and 2D). Pharmacological inhibition of GS with L-Methionine sulfoximine (MSO) in Gln-free media also compro-mised mesoderm, endoderm, and ectoderm cell viability (Fig-ures 2C and 2D). This hinted that Gln, and/or the by-products of Gln metabolism, are still required for ectoderm, similar to mesoderm and endoderm. The small percentage (<2%) of resid-ual viable cells at the end of differentiation grown with either Gln mimetic (Ctr+DON) or Gln-starvation (−G+M) showed signifi-cantly decreased populations of respective lineage-specifying transcription factors SNAI2/SLUG (mesoderm), SOX17 (endo-derm), and PAX6 (ectoderm) (Figures 2D and S2D). This indi-cates that intracellular Gln supports germ lineage cell survival and differentiation potential. Mesoderm and endoderm require exogenous Gln as metabolic fuel for glutaminolysis-derived α-KG (Figures 1F and 1G), whereas ectoderm synthesizes Gln for role(s) other than glutaminolysis and its reaction products (Figures 1E, 2A, 2B, S2A, and S2C).

We performed steady-state metabolite profiling by UHPLC-MS following acute Gln-starvation (−G+M) to identify altered Gln-derived metabolites in ectoderm at the initiation of the dif-ferentiation process. Aside from Gln, the largest decrease in metabolites occurred for α-KG, hexosamine biosynthesis pathway (HBP) intermediates, purine nucleosides, and gluta-thione redox status (GSH/GSSG) (Figure 2E). Metabolite rescue was attempted by supplementing Gln-starved ectoderm with cell-permeable forms of these Gln-derived metabolites (Fig-ure 2F) (Qie et al., 2019). Verification of uptake and conversion to related metabolites was confirmed for all supplementations, with the exception of GSH, which did not significantly alter intracellular GSH and GSSG levels (Figure S2E). The addition of HBP metabolite glucosamine-6-phosphate (GlcN6P) yielded the largest rescue of ectoderm cell viability with a single agent at ∼57% (Figures 2F and S2F), and the combination of GlcN6P and nucleosides resulted in the highest ectoderm cell survival at ∼69% compared with control conditions (Figures 2G and S2F), although full rescue was not achieved with any metabolite or binary combination (Figures 2F, 2G, and S2F). Despite partial viability rescue with GlcN6P supplementation, pluripotency is not completely repressed by D5 of differentiation in live-gated Gln-starved (−G+M) ectoderm cells under this metabolite rescue condition, as measured by a residual OCT4+ cell popu-lation (Figure 2G). Furthermore, supplementation with com-bined GlcN6P and nucleosides showed significantly decreased populations of PAX6+MAP2B+ and PAX6+SOX1+ ectoderm cells compared with Gln-supplemented (Ctr) and Gln-free (−Gln) conditions by D5 of differentiation (Figures 2G and S2F). Together, the data show that replenishment of HBP and nucleosides partially restored Gln-starved ectoderm cell viability, but did not restore differentiation, suggesting that Gln has a role in ectoderm generation in addition to a role as a precursor for metabolites.

Initial Gln absence impairs ectoderm differentiation
Impaired ectoderm differentiation could be a consequence of reduced cell viability due to chronic Gln-starvation. Alternatively, Gln absence could directly impact the ectoderm specification program(s). To examine these possibilities, we measured
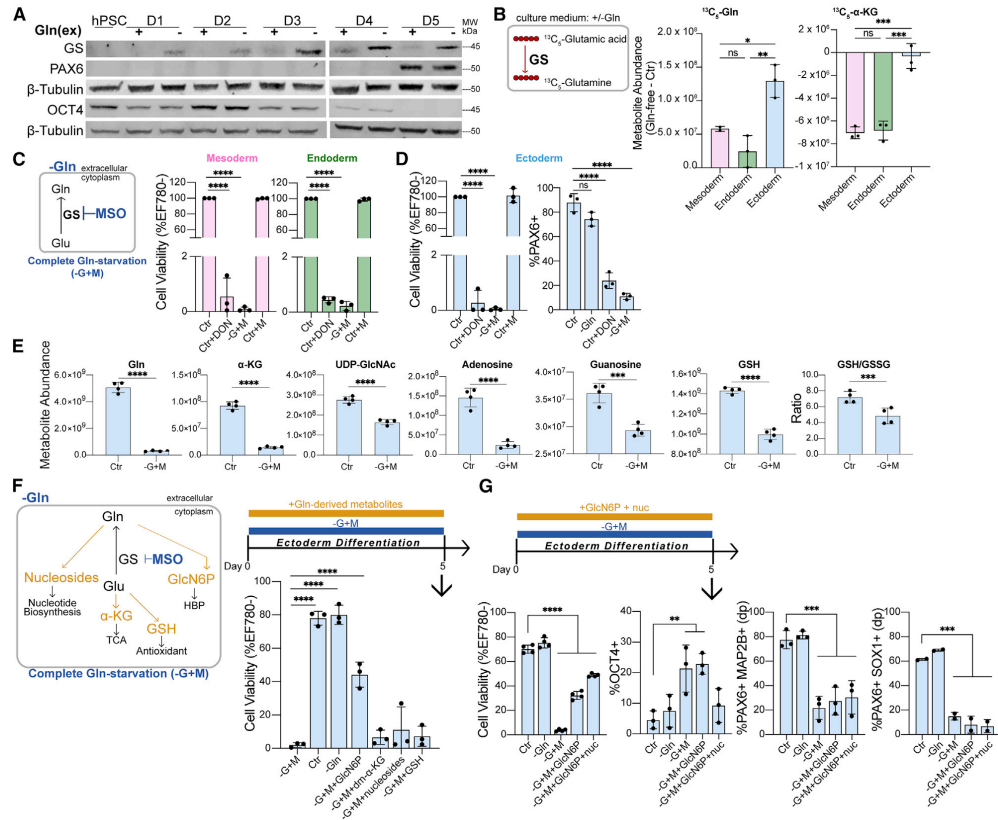
Figure 2. Sufficient Gln synthesis distinguish ectoderm from other germ lineages

(A) Immunoblot of GS, PAX6, and OCT4 expression during H9-derived ectoderm differentiation in Gln-free conditions.

(B) Difference in $^{13}C_5$-Gln and $^{13}C_5$-α-KG amounts derived from $^{13}C_5$-glutamic acid in Gln-free (−Gln) relative to supplemented (Ctr) conditions.

(C and D) (Left) Complete Gln-starvation (−G+M) is attained by culturing cells in Gln-free media and inhibiting *de novo* Gln synthesis with 1 mM MSO. (Right) Cell viability of (C) mesoderm, endoderm, and (D) differentiation of ectoderm cells grown in Gln-free (−Gln) conditions with 50 μM DON or 1 mM MSO relative to Gln-supplemented (Ctr) media.

(E) Metabolite abundance quantified by UHPLC-MS in differentiated ectoderm cells treated in Gln-supplemented (Ctr) or 1 h Gln-starvation (−G+M) conditions.

(F) (Top) Schematic of Gln-starvation (−G+M) supplemented with individual cell-permeable Gln-derived metabolites. (Bottom) Cell viability of H9-derived D5 ectoderm cells differentiated in Gln-starvation and supplemented with GlcN6P, dm-α-KG, nucleosides, or GSH.

(G) Cell viability and percentage of ectoderm (PAX6+MAP2B+ double positive (dp), PAX6+SOX1+ (n = 2)), and pluripotent (OCT4+) biomarkers in H9-derived D5 ectoderm cells grown in Gln-starvation with added GlcN6P or both GlcN6P and nucleosides.

Data represent mean ± SD of n ≥ 3 biological replicates unless indicated otherwise. *p ≤ 0.05; **p ≤ 0.01; ***p ≤ 0.001; ****p ≤ 0.0001. The p values were determined by (B–D, F, and G) one-way ANOVA, or (E) unpaired two-tailed Student's t test with correction for multiple comparisons.

differentiation status while cell viability and cell-cycle progression were progressively altered as Gln-starvation time increased (Figures 3A and S3A). We quantified ectoderm differentiation status after 24 h of Gln-starvation (−G+M), a time point with equivalent viable ectoderm cells relative to control conditions (Figure 3A). Flow cytometry of live-gated cells showed decreased ectoderm (PAX6+MAP2B+, PAX6+SOX1+) cells, and qRT-PCR showed decreased expression of *MAP2B*, *PAX6*, and *OTX2* transcripts in Gln-starvation compared with Gln-sup-

plemented and Gln-free conditions (Figures 3A and S3B). This differentiation impairment increased with starvation time, and pluripotency biomarkers (OCT4+NANOG+, OCT4+TRA1-81+) were suppressed with differentiation regardless of Gln availability (Figure 3A). Combined, these findings showed that reduced ectoderm differentiation and cell-cycle drop out occurred within 24 h of Gln-starvation.

To assess the temporal requirement for Gln in implementing ectoderm fate, we replenished Gln after pulsed Gln-starvation
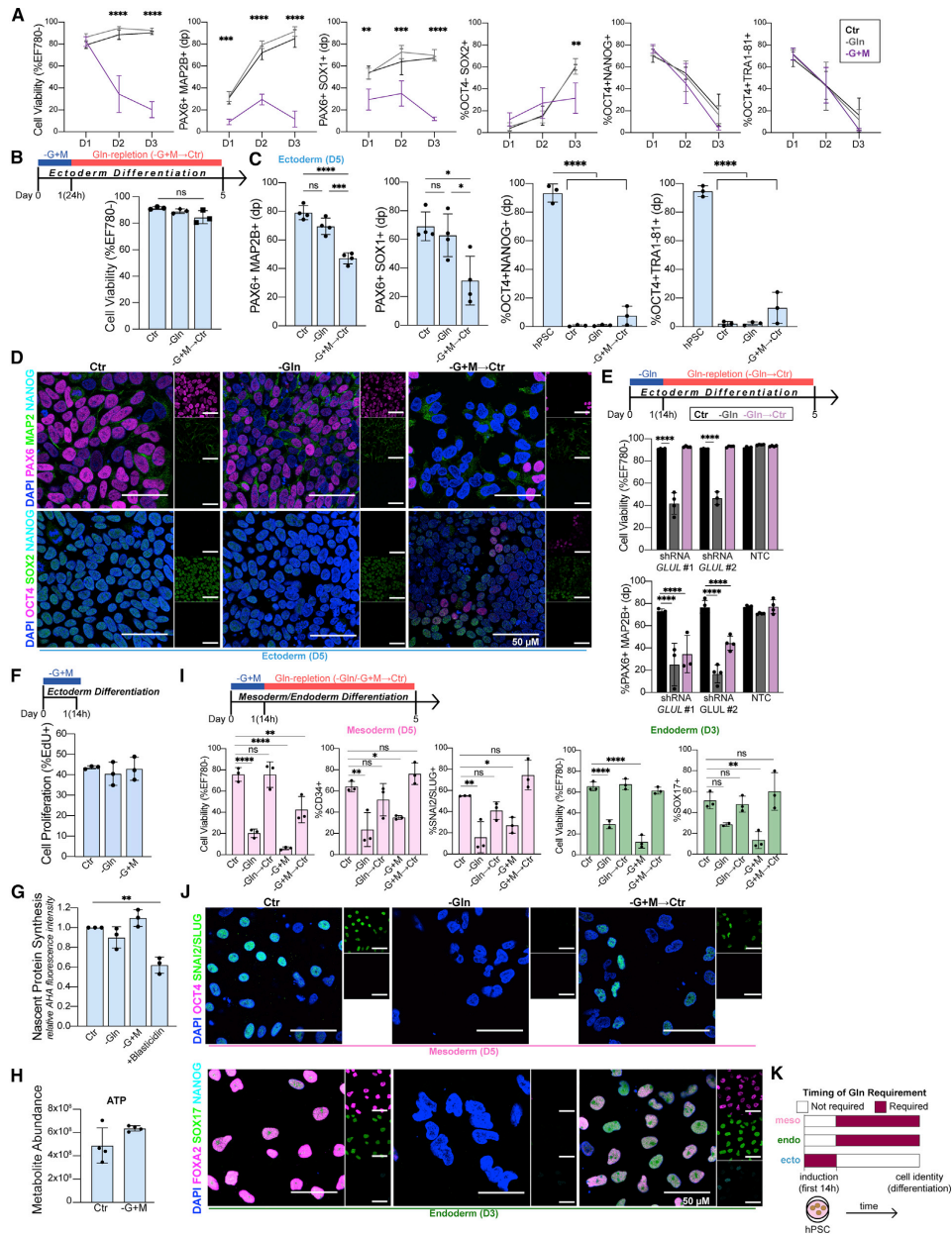
Figure 3. Gln is required at the initiation of ectoderm but not mesoderm and endoderm

(A) Cell viability and percentage of ectoderm (PAX6+MAP2B+, PAX6+SOX1+, and OCT4−SOX2+) and pluripotent (OCT4+NANOG+, OCT4+TRA1-81+) biomarkers in H9-derived ectoderm cells grown continuously in Gln-starvation for D1 (24 h), D2 (48 h), and D3 (72 h).

(legend continued on next page)

105

while retaining inducing cytokines throughout this differentiation condition (Gln-repletion) (Figure 3B). After 24 h of initial Gln-starvation, Gln-repletion (−G+M→Ctr) completely rescued the viability and cell cycle of ectoderm cells by D5 (Figures 3B and S3C). However, ectoderm differentiation was not rescued at D5 following Gln-repletion, as indicated by significantly decreased ectoderm-specifying biomarkers (PAX6, MAP2B, SOX1, and SOX2) quantified by flow cytometry and immunofluorescence imaging (Figures 3C, 3D, and S3D). Pluripotency exit occurred regardless of initial Gln availability during initial ectoderm differentiation as indicated by suppressed pluripotency biomarkers (OCT4, NANOG, TRA1-81, and SOX2) relative to hPSC progenitors, although Gln-repletion resulted in slight residual pluripotency biomarker expression compared with Gln-supplemented and Gln-free conditions (Figures 3C, 3D, and S3E). Additionally, impaired ectoderm differentiation does not compensate with alternative lineage-specific biomarker (SOX17, endoderm; CD34, mesoderm) expression, confirming the specific failure for an ectoderm fate (Figure S3E). To exclude off-target effects of MSO treatment in Gln-starved conditions, H9 hPSCs containing short hairpin RNA (shRNA) knockdown of *GLUL*, encoding for GS, were differentiated for 5 days in Gln-free media and equally led to ectoderm cell death (Figures 3E, S3F, and S3G). We found that a shorter, initial Gln-starvation period of 14 h followed by Gln-repletion (−Gln→Ctr) was sufficient to impair ectoderm differentiation, as quantified by a decreased population of PAX6+MAP2B+ cells (Figure 3E). Additionally, supplementation with Gln-derived metabolites during the initial 14 h Gln-starvation period (−G+M+GlcN-6P+nuc→Ctr) equally resulted in impaired ectoderm differentiation (Figure S3H). Impaired ectoderm differentiation was independent of cell proliferation, nascent protein synthesis, and ATP levels, which were all unaffected immediately after 14 h of Gln-starvation and at later time points after Gln-repletion (Figures 3F–3H, S3I, and S3J). These results suggest that Gln is required within the first 14 h of directed ectoderm differentiation to activate the ectoderm program, a fate that could not be rescued by Gln restoration following this window of time.

To study the ectoderm specificity of this temporal Gln requirement in the larger context of germ layer differentiation, meso-

derm and endoderm were grown in initial 14 h Gln-free (−Gln) and Gln-starvation (−G+M) media conditions followed by Gln-repletion (→Ctr). Strikingly, initial Gln absence did not affect subsequent mesoderm nor endoderm specification (Figures 3I and 3J). This demonstrates that a temporal Gln requirement is specific to ectoderm differentiation and highlights distinct signatures of Gln dependency for each respective germ lineage cell fate (Figure 3K).

Ectoderm differentiation requires Gln-dependent mTORC1 signaling

Because addition of Gln-derived metabolites and delayed Gln add-back failed to restore ectoderm fate specification, we considered an alternative possibility that Gln could signal to activate a nutrient-sensing pathway, similar to glucose signaling in trophectoderm (Chi et al., 2020). Recent work showed that Gln is a substrate that activates the mammalian target of rapamycin complex 1 (mTORC1). mTORC1 activation by Gln occurs through Rag GTPase-dependent activation by Gln exchange for exogenous leucine and arginine, or by Rag GTPase-independent activation directly from a Gln interaction with Arf1 GTPase (Jewell et al., 2015; Meng et al., 2018; Saxton and Sabatini, 2017). We observed that phosphorylation of the canonical mTORC1 substrate, ribosomal protein S6 kinase 1 (S6K1-Thr389), in 24 h Gln-starved ectoderm is significantly reduced, indicating mTORC1 inhibition (Figures 4A and S4A). Pulsed addition of mTORC1 inhibitor rapamycin during initial 14 h of tri-lineage differentiation replicated initial Gln-starvation (−G+M→Ctr), with impaired ectoderm and unaffected mesoderm and endoderm differentiation (Figures 3C–3E, 3I–3K, 4B, S3D, and S3E). This result suggests that initial mTORC1 activation, like intracellular Gln presence, is critical for and specific to ectoderm differentiation.

To investigate whether Gln-dependent mTORC1 activation is essential for ectoderm differentiation, we transduced two separate hPSC lines, H9 and UCLA1, with a constitutively active mTORC1 expression vector, *Raptor-Rheb15*, and a control, wild-type (WT) *Raptor* (Sancak et al., 2010). Construct expression was verified by puromycin selection and DYKDDDDK (FLAG) tag detection (Figure S4B), and hPSCs

(B) (Top) Schematic of pulsed Gln-starvation experiments. Ectoderm cells were Gln-starved for the first 24 h of differentiation then switched to Gln-supplemented media (Gln-repletion, −G+M→Ctr) until D5. (Bottom) Cell viability of H9-derived D5 ectoderm cells after initial 24 h Gln-starvation.

(C) Percentage of ectoderm (PAX6+MAP2B+, PAX6+SOX1+) and pluripotent (OCT4+NANOG+, OCT4+TRA1-81+) biomarkers in H9-derived D5 ectoderm cells after initial 24 h Gln-starvation (−G+M→Ctr).

(D) Representative immunofluorescence images of ectoderm and pluripotent biomarkers in H9-derived D5 ectoderm cells grown in Gln-supplemented (Ctr), Gln-free (−Gln), or Gln-repletion after initial 24 h Gln-starvation (−G+M→Ctr). (Top) PAX6 (magenta, ectoderm); MAP2B (green, ectoderm); NANOG (cyan, pluripotent). (Bottom) OCT4 (magenta, pluripotent); SOX2 (green, ectoderm/pluripotent); NANOG (cyan, pluripotent). Scale bar, 50 µm.

(E) H9-derived ectoderm expressing shRNA targeting *GLUL* (shRNA *GLUL* #1; shRNA *GLUL* #2) or a non-targeting control (NTC). Cell viability and percentage of PAX6+MAP2B+ D5 ectoderm cells in Gln-supplemented (Ctr), Gln-free (−Gln), or Gln-repletion after initial 14 h Gln-free treatment (−Gln→Ctr).

(F) Percentage of proliferating H9-derived ectoderm cells (EdU+ staining) immediately after 14 h Gln-free or Gln-starvation treatment.

(G) Nascent protein synthesis in H9-derived ectoderm cells immediately after 14 h Gln-free, Gln-starvation, or blasticidin treatment relative to Ctr.

(H) ATP levels, quantified by UHPLC-MS, in ectoderm cells after Gln-starvation.

(I) Cell viability and percentage of H9-derived D5 mesoderm (CD34+, SNAI2/SLUG+) and D3 endoderm (SOX17+) cells after initial 14 h Gln-free (−Gln→Ctr) or Gln-starvation (−G+M→Ctr) treatment.

(J) Representative immunofluorescence images of pluripotent and lineage-specific biomarkers in H9-derived (top) D5 mesoderm and (bottom) D3 endoderm cells grown in Gln-supplemented (Ctr), Gln-free (−Gln), or Gln-repletion follow initial 14 h Gln-starvation (−G+M→Ctr). (Top) OCT4 (magenta, pluripotent); SNAI2/SLUG (green, mesoderm). (Bottom) FOXA2 (magenta, endoderm); SOX17 (green, endoderm); NANOG (cyan, pluripotent). Scale bar, 50 µm.

(K) Timing of Gln requirement for downstream lineage cell identity.

Data represent mean ± SD of n ≥ 3 biological replicates. *p ≤ 0.05; **p ≤ 0.01; ***p ≤ 0.001; ****p ≤ 0.0001. The p values were determined by (A–C, F, G, and I) one-way ANOVA, (E) two-way ANOVA with correction for multiple comparisons or (H) unpaired two-tailed Student's t test.
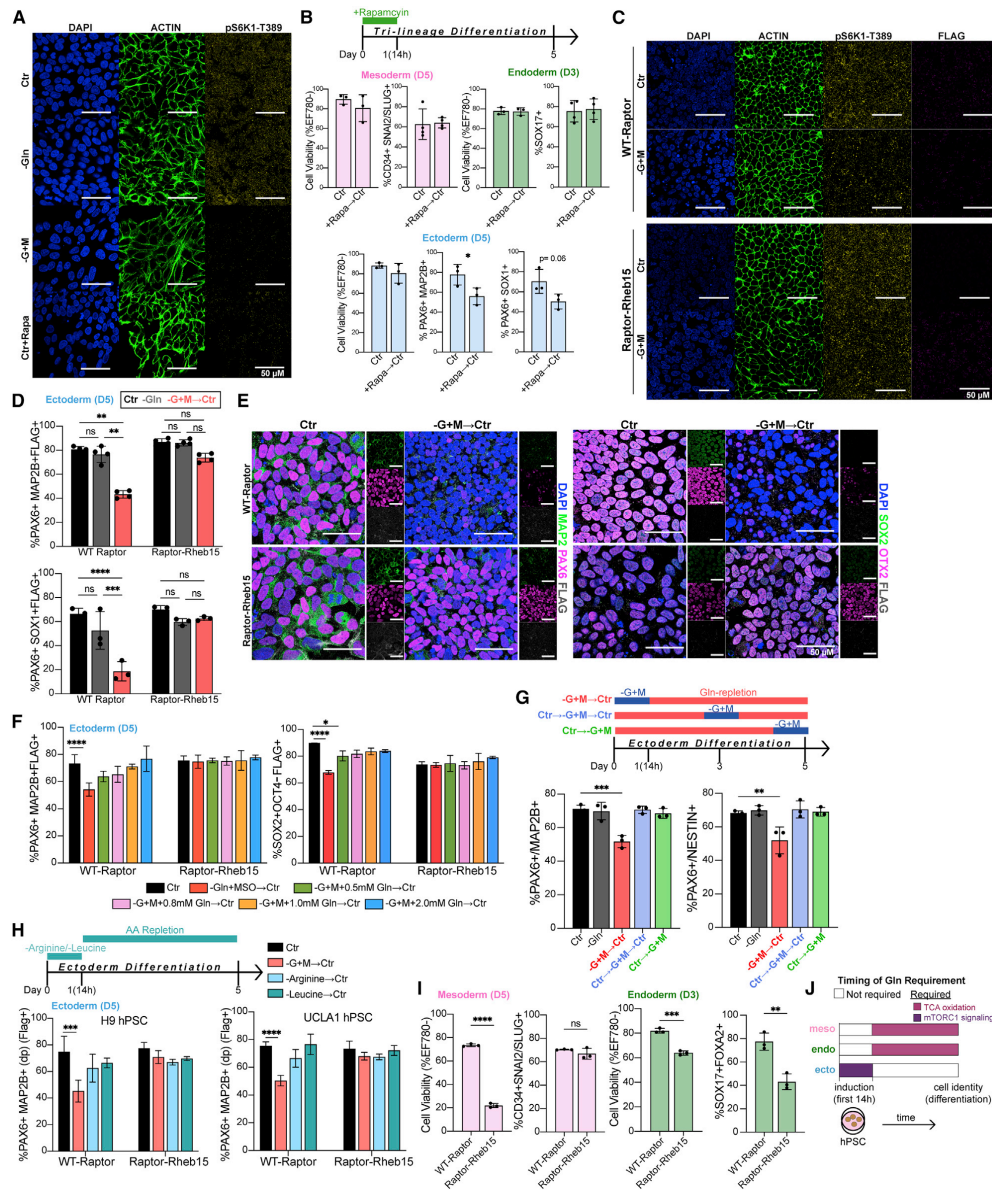
Figure 4. Ectoderm differentiation requires initial Gln-dependent mTORC1 signaling

(A) Representative immunofluorescence images of mTORC activation in H9-derived ectoderm cells grown for 24 h in Gln-supplemented (Ctr), Gln-free (−Gln), Gln-starvation (−G+M), or 200 nM rapamycin treatment (Ctr+Rapa). DAPI (blue, nucleus); ACTIN (green, cytoskeleton); pS6K1-Thr389 (yellow, mTORC1 activation). Scale bar, 50 μm.

(B) Percentage of H9-derived D5 mesoderm (CD34⁺SNAI2/SLUG⁺), D3 endoderm (SOX17⁺FOXA2⁺), and D5 ectoderm (PAX6⁺MAP2B⁺, PAX6⁺SOX1⁺) cells after initial 14 h 200 nM rapamycin treatment.

107

were directed toward ectoderm differentiation with an initial 14 h Gln-starvation. As anticipated, mTORC1 activation was sustained in Raptor-Rheb15 but not in WT-Raptor transduced hPSCs differentiated into ectoderm with Gln-starvation (Figures 4C and S4C). After an initial 14 h Gln-starvation, Gln-repletion (−G+M→Ctr) completely rescued the viability and cell cycle of ectoderm cells at D5 (Figures S4D and S4E). Gln-repletion in WT-Raptor ectoderm cells resulted in significantly reduced lineage-specifying biomarkers (PAX6, MAP2B, SOX1, SOX2, and OTX2) at D5, whereas Raptor-Rheb15 ectoderm cells grown under the same experimental conditions showed minimal, non-significant changes in ectoderm specification compared with Gln-supplemented and Gln-free conditions at D5 (Figures 4D, 4E, and S4F). These results indicated that, in addition to nascent protein synthesis being unaffected within an acute 14 h Gln-starvation period (Figures 3G and S3J), the lack of Gln incorporation into polypeptides was not the cause of impaired ectoderm differentiation because successful ectoderm specification occurred in Raptor-Rheb15 hPSCs following transient Gln absence.

To evaluate the concentration of Gln that impacts differentiation, we performed Gln add-back titrations. Reports suggest that the primary source of Gln in the embryo and fetus is derived from placental conversion of Glu to Gln, with maternal and fetal Gln concentrations ranging between 0.8 and 1.0 mM (Cruzat et al., 2018; Holm et al., 2017; McIntyre et al., 2020; Neu, 2001). This concentration range is consistent with the amount of Gln required to restore differentiation in transient 14 h Gln-starved ectoderm cells at D5, with full recovery of PAX6+MAP2B+ and SOX2+OCT4− cells starting at 0.8 mM Gln (Figures 4F, S4G, and S4H).

We tested whether only the first hours of ectoderm specification depended on intracellular Gln by performing Gln-starvation studies in the intermediate and late stages of differentiation. Results indicate that only early transient (−G+M→Ctr), but not intermediate (Ctr→−G+M→Ctr) nor late stage (Ctr→−G+M), Gln absence impaired ectoderm differentiation (Figures 4G and S4I). This suggests that Gln-dependent mTORC1 activation is

an early requirement for downstream functional ectoderm specification.

We next asked whether the initial absence of other mTORC1 sensed amino acids impacted ectoderm differentiation. Since leucine (Leu) and/or arginine (Arg) signaling to activate mTORC1 is well characterized (Wolfson and Sabatini, 2017), H9 and UCLA1 hPSCs were differentiated in Leu- or Arg-free media for the first 14 h, followed by repletion until D5. We observed that from these mTORC1 sensed amino acids, only the initial absence of Gln, and not Leu nor Arg, impaired initial mTORC1 activation and downstream ectoderm differentiation, indicating specificity for the Gln requirement (Figures 4H, S4J, and S4K).

Finally, we confirmed that constitutively active mTORC1 is not compatible with mesoderm nor endoderm directed differentiation, as indicated by significantly decreased levels of cell viability in Raptor-Rheb15 compared with WT-Raptor-transduced cells. At the differentiation endpoint, the remaining ∼20% live Raptor-Rheb15 mesoderm cells did not exhibit significantly decreased lineage nor pluripotency biomarker expression, whereas the ∼60% live endoderm cells showed decreased lineage and pluripotency biomarker expression (Figures 4I and S4L). This result supports a working model in which early mTORC1 activity is critical for ectoderm differentiation but is detrimental to mesoderm and endoderm differentiation (Figures 4A, S4A, and S4M), highlighting distinct requirements for germ lineage cell fates. The data showed that a Gln signal activates mTORC1 within the initial hours of differentiation induction to produce ectoderm (Figure 4J). Gln itself, but not the by-products of Gln metabolism, were required for ectoderm differentiation.

Transcriptome signatures suggest unique, lineage-specific Gln utilization *in vivo*

Our experimental model of Gln withdrawal and add-back is a useful tool to identify nutrient specificities *in vitro*, similar to gain and loss of function genetic studies, and provides predictions for potential differences in Gln dependency for each

---

(C) Representative immunofluorescence images of mTORC activation in H9-derived WT-Raptor or Raptor-Rheb15 ectoderm cells grown for 12 h in Gln-supplemented (Ctr) or Gln-starvation (−G+M). DAPI (blue, nucleus); ACTIN (green, cytoskeleton); pS6K1-Thr389 (yellow, mTORC1 activation); FLAG tag (magenta; transduced cell line reporter). Scale bar, 50 μm.

(D) Percentage of H9-derived D5 WT-Raptor or Raptor-Rheb15 ectoderm (PAX6+MAP2B+FLAG+, PAX6+SOX1+FLAG+) cells after initial 14 h Gln-starvation (−G+M→Ctr).

(E) Representative immunofluorescence images of ectoderm biomarkers in H9-derived D5 (Top) WT-Raptor or (Bottom) Raptor-Rheb15 ectoderm cells grown in Gln-supplemented (Ctr) or Gln-repletion follow initial 14 h Gln-starvation (−G+M→Ctr). (Left) MAP2B (green, ectoderm;) PAX6 (magenta, ectoderm); FLAG (gray, transduced cell line reporter). (Bottom) SOX2 (green, ectoderm/pluripotent); OTX2 (magenta, ectoderm), FLAG (gray, transduced cell line reporter). Scale bar, 50 μm.

(F) Percentage of ectoderm (PAX6+MAP2B+FLAG+, SOX2+OCT4−FLAG+) biomarkers in H9-derived D5 WT-Raptor or Raptor-Rheb15 ectoderm cells after initial 14 h Gln-starvation with increasing concentrations of exogenous Gln supplementation.

(G) Percentage of H9-derived D5 ectoderm (PAX6+MAP2B+, PAX6+NESTIN+) cells after initial (−G+M→Ctr), intermediate (Ctr→−G+M→Ctr), or late (Ctr→−G+M) 14 h Gln-starvation.

(H) Arginine (Arg) or leucine (Leu) were removed from culture media for 14 h then switched to Arg/Leu-supplemented conditions (AA repletion) until D5. Percentage of (Left) H9 or (Right) UCLA1-derived D5 WT-Raptor or Raptor-Rheb15 ectoderm (PAX6+MAP2B+FLAG+) cells after initial 14 h Gln-starvation, Arg deprivation, or Leu deprivation.

(I) Cell viability and percentage of H9-derived WT-Raptor or Raptor-Rheb15 D5 mesoderm (CD34+SNAI2/SLUG+FLAG+) and D3 endoderm (SOX17+FOXA2+FLAG+) cells.

(J) Timing of Gln requirement for downstream lineage cell identity. Gln is required as a metabolite precursor in mesoderm and endoderm cells and as a mTORC1 signaling activator in ectoderm cells, related to Figure 3K.

Data represent mean ± SD of n ≥ 3 biological replicates. *p ≤ 0.05; **p ≤ 0.01; ***p ≤ 0.001; ****p ≤ 0.0001. The p values were determined by (B and I) unpaired two-tailed Student's t test, (D, F, and H) two-way ANOVA, or (G) one-way ANOVA with correction for multiple comparisons.

108
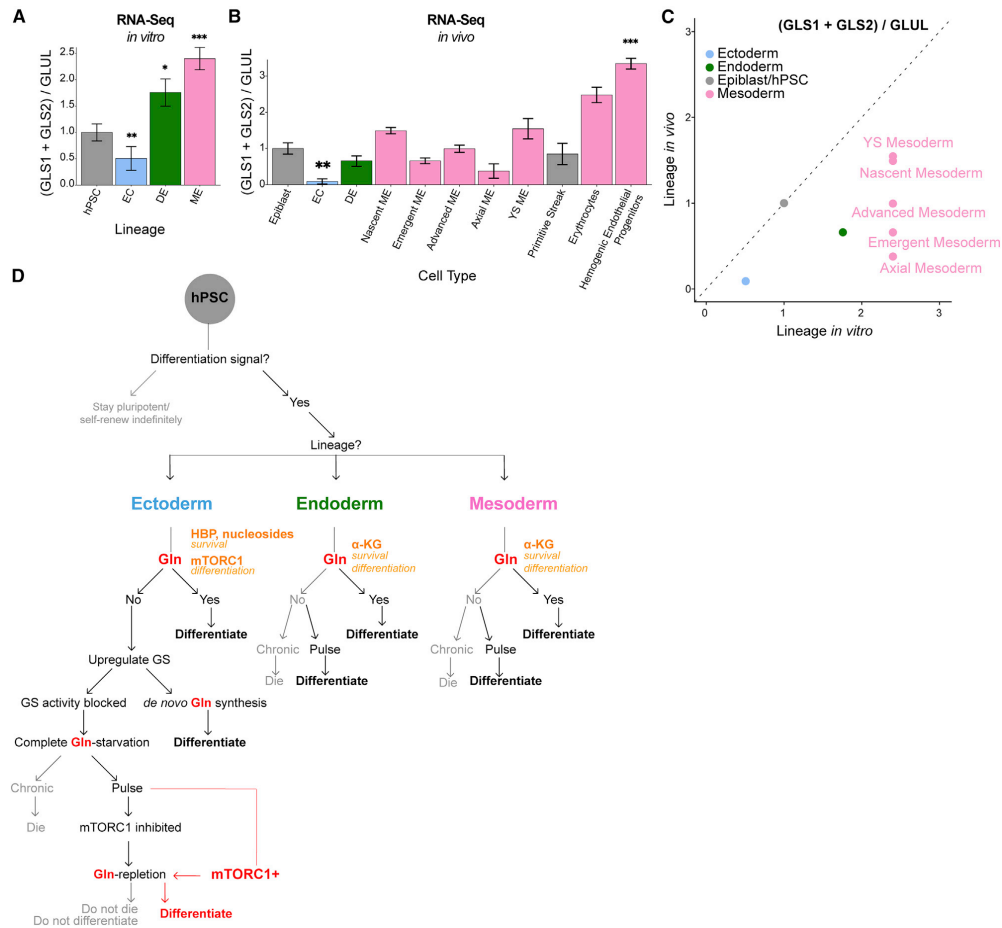
Figure 5. Distinct transcript patterns of Gln utilization characterize germ lineages *in vivo*

(A) Ectoderm but not endoderm and mesoderm cells exhibit increased Gln synthesis (*GLUL* transcripts) relative to Gln consumption (*GLS1* + *GLS2* transcripts) *in vitro*. The average *GLS1* and *GLS2* expression was divided by *GLUL* expression for each lineage and values were normalized to hPSC control.

(B) Ectoderm cells exhibit increased Gln synthesis (*GLUL* transcripts) relative to Gln consumption (*GLS* + *GLS2* transcripts) *in vivo*. Single-cell RNA-seq Data from Tyser et al. (2021) were used to calculate the same ratio as in (A). The values were normalized to the average Epiblast ratio. Lineages were taken from Tyser et al. (2021).

(C) Ectoderm cells exhibit similar trends in Gln synthesis and Gln consumption in both *in vitro* and *in vivo* contexts. Results from (A) and (B) are shown with a reference line drawn at y = x.

(D) Working model of germ lineage cell fate dependent on Gln.

Data represent mean ± SD. *p ≤ 0.05; **p ≤ 0.01; ***p ≤ 0.001. The p values were determined by (A and B) unpaired two-tailed Student's t test.

germ layer *in vivo*. Although hPSC differentiation is a reproducible method for studying human gastrulation (Taniguchi et al., 2019), cross-referencing hPSC results to available *in vivo* data would add further support for lineage-specific Gln utilization. To generate hypotheses for potential translation of these hPSC study results, we compared hPSC findings with human embryo development at approximately the same post-implan-

tation stage (Mascetti and Pedersen, 2016; Taniguchi et al., 2019). To do this, we queried the single-cell RNA-seq transcriptome of a gastrulating human embryo ~16–19 days post fertilization (Tyser et al., 2021). Since hPSC-derived mesoderm and endoderm depend on exogenous Gln, and ectoderm can synthesize sufficient Gln *de novo*, we used these distinguishing features as a proxy for Gln utilization

patterns. We calculated the ratio of Gln degradation (averaged [*GLS1* + *GLS2*] transcripts) to endogenous Gln synthesis (*GLUL* transcripts) to correlate the tendencies for Gln auxotrophy versus prototrophy in each lineage. In both *in vitro* (Figure 5A) and queried *in vivo* (Figure 5B) transcriptome datasets, we found that Gln degradation transcripts were much lower than Gln synthesis transcripts in ectoderm, but not in mesoderm- nor endoderm-related lineages, as quantified by the (averaged [*GLS1* + *GLS2*])/*GLUL* ratio. A comparison of our *in vitro* hPSC-derived germ lineage model with the *in vivo* human gastrula sample showed similar clustering of Gln degradation to synthesis ratios in corresponding lineages. Thus, relative lineage-specific Gln consumption and synthesis transcript patterns identified in the *in vitro* model and *in vivo* sample may be maintained in the human embryo (Figure 5C) and present an enticing hypothesis for future studies.

DISCUSSION

Our current understanding of how metabolism permits cell-state transitions between pluripotency and differentiation is fragmented and limited. A particular knowledge gap is that previous studies focused largely on the metabolic roles of Gln and its by-products in maintaining pluripotency (Carey et al., 2015; Marsboom et al., 2016; Tohyama et al., 2016; Vardhana et al., 2019) or regulating multipotent cell lineages (Johnson et al., 2018; Oburoglu et al., 2014; Yu et al., 2019). Here, we report that Gln itself is a required signaling molecule in ectoderm differentiation. We demonstrate that Gln synthesis and consumption is differentially regulated between lineages *in vitro*, and possibly *in vivo*, and that Gln has an irreversible temporal requirement in ectoderm, but not mesoderm nor endoderm, lineage differentiation (Figure 5D).

In vivo evidence for the developmental significance of Gln and mTORC1 has recently been reported in which dysregulated Gln-Glu cycling and mTORC1 signaling contributed to placental dysfunction and fetal growth restriction (McIntyre et al., 2020). Additionally, prior studies showed that mTORC1 inhibition favors PSC differentiation to mesoderm and endoderm lineages; yet, a mechanism has never been reported (Jung et al., 2016; Nazareth et al., 2016; Zhou et al., 2009). Our results show that a Gln activating signal for mTORC1 enables ectoderm, whereas this nutrient-signaling activation is detrimental for mesoderm and endoderm fates, as an attempt to direct differentiation of constitutively active mTORC1 Raptor-Rheb15 hPSCs into mesoderm and endoderm lineages led to widespread cell death. Gln is essential for mTORC1 activation within the first hours of ectoderm induction, because a transient absence of Gln in this initial period, but not in later time periods, caused slight residual pluripotency biomarker retention and diminished ectoderm-specifying biomarker expression. In contrast to this strict ectoderm time requirement for Gln, mesoderm and endoderm cells achieve full differentiation even with an initial Gln absence (Figures 4J, 5D, S5A–S5E, and S6A).

Gln is a non-essential amino acid not previously implicated in germ lineage differentiation, but here we reveal it is conditionally essential and depends upon cell fate context. A divergence in Gln essentiality depending on germ lineage

was unexpected since all three lineages initiate from a common pluripotent progenitor cell. We speculate on the possibility of a Gln-specific symbiotic relationship among the three germ lineages during early *in vivo* development. Specifically, ectoderm may generate *de novo* Gln to support nearby mesoderm and endoderm cells dependent on exogenous Gln, which could influence tissue patterning. This hypothesis is supported by our previous media footprint profiling data showing high secretion of Gln in ectoderm and high consumption of Gln in mesoderm (Lu et al., 2019). Patterns of Gln metabolism during blastocyst development may be one of multiple input signals for embryos experiencing nutrient gradients and discontinuities. This tempting possibility is also suggested, but not yet proven, by human embryo transcriptome data showing the Gln synthesis to consumption expression signature is higher in ectoderm compared with mesoderm and endoderm lineages, which is at least consistent with our *in vitro* model system (Figures 5A–5C). Thus, our data begin building a framework for how temporal and/or spatial fluctuations in Gln could potentially impact normal development.

In conclusion, our findings uncover a new testable model in which a nutrient acts as a signaling molecule that could differentially coordinate the development of the three embryonic germ lineages. Our study provides several testable hypotheses for nutrient-specific signaling cues as contributors to organizational structure and fidelity in early mammalian development. These include targeting key Gln gatekeeping enzymes in in *vivo* development models, and future investigations of additional nutrient specificities implicated in cell fate decisions. These findings could also provide more logical manipulations of the metabolite environment and pathway fluxes *in vitro* to produce higher quality hPSC derivatives for disease modeling, tissue engineering, and eventual therapeutic usage.

Limitations

Here, we report that specific Gln requirements define the three embryonic germ lineages upon *in vitro* pluripotency exit. We further uncover that Gln acts as a signaling molecule to activate mTORC1 and enable downstream ectoderm differentiation. However, two main limitations temper our study conclusions. First, to the best of our knowledge, transient Gln removal does not occur during *in vivo* development. Thus, this experimental perturbation does not reflect endogenous regulation, but was a useful tool to identify nutrient specificities of different cell types. Second, we present correlative evidence linking *GLS1*, *GLS2*, and *GLUL* RNA expressions to potential functional *in vivo* tri-lineage Gln dependency. This is a study limitation since transcript levels do not necessarily equate to protein abundance/activity. We note that this comparison of relative gene expression made between embryo tissue and hPSC-derived cells may inspire future work regarding *in vivo* tissue-specific regulation of Gln metabolism.

STAR★METHODS

Detailed methods are provided in the online version of this paper and include the following:

Developmental Cell
Article

SUPPLEMENTAL INFORMATION

Supplemental information can be found online at https://doi.org/10.1016/j.devcel.2022.02.003.

AUTHOR CONTRIBUTIONS

Conceptualization, V.L. and M.A.T.; design, V.L., I.J.R., and M.A.T.; methodology, V.L., I.J.R., A.T., and M.A.T.; formal analysis, V.L., I.J.R., A.T., J.H.J., and F.M.A.; investigation, V.L., I.J.R., and A.T.; writing manuscript, V.L. and M.A.T.; visualization, V.L., A.T., J.H.J., and F.M.A.; supervision, V.L. and M.A.T.; project administration, V.L. and M.A.T.; funding acquisition, V.L. and M.A.T.

DECLARATION OF INTERESTS

The authors declare no competing interests.

REFERENCES

Aaron, J., and Chew, T.L. (2021). A guide to accurate reporting in digital image processing - can anyone reproduce your quantitative analysis? J. Cell Sci. *134*.

Benjamini, Y., and Hochberg, Y. (1995). Controlling the false discovery rate – a practical and powerful approach to multiple testing. J Roy Stat. Soc. B Met. *57*, 289–300.

Bott, A.J., Peng, I.C., Fan, Y., Faubert, B., Zhao, L., Li, J., Neidler, S., Sun, Y., Jaber, N., Krokowski, D., et al. (2015). Oncogenic Myc induces expression of glutamine synthetase through promoter demethylation. Cell Metab *22*, 1068–1077.

Calvo, S.E., Clauser, K.R., and Mootha, V.K. (2016). MitoCarta2.0: an updated inventory of mammalian mitochondrial proteins. Nucleic Acids Res *44*, D1251–D1257.

Carey, B.W., Finley, L.W., Cross, J.R., Allis, C.D., and Thompson, C.B. (2015). Intracellular alpha-ketoglutarate maintains the pluripotency of embryonic stem cells. Nature *518*, 413–416.

Chantranupong, L., Wolfson, R.L., and Sabatini, D.M. (2015). Nutrient-sensing mechanisms across evolution. Cell *161*, 67–83.

Chi, F., Sharpley, M.S., Nagaraj, R., Roy, S.S., and Banerjee, U. (2020). Glycolysis-independent glucose metabolism distinguishes TE from ICM fate during mammalian embryogenesis. Dev. Cell *53*, 9–26.e4.

Cliff, T.S., Wu, T., Boward, B.R., Yin, A., Yin, H., Glushka, J.N., Prestegaard, J.H., and Dalton, S. (2017). MYC controls human pluripotent stem cell fate decisions through regulation of metabolic flux. Cell Stem Cell *21*, 502–516.e9.

Cruzat, V., Macedo Rogero, M., Noel Keane, K., Curi, R., and Newsholme, P. (2018). Glutamine: metabolism and immune function, supplementation and clinical translation. Nutrients *10*, 1564.

Fu, S., Li, Z., Xiao, L., Hu, W., Zhang, L., Xie, B., Zhou, Q., He, J., Qiu, Y., Wen, M., et al. (2019). Glutamine synthetase promotes radiation resistance via facilitating nucleotide metabolism and subsequent DNA damage repair. Cell Rep *28*, 1136–1143.e4.

Golden, R.J., Chen, B., Li, T., Braun, J., Manjunath, H., Chen, X., Wu, J., Schmid, V., Chang, T.C., Kopp, F., et al. (2017). An Argonaute phosphorylation cycle promotes microRNA-mediated silencing. Nature *542*, 197–202.

Gregory Warnes, B.B., Bonebakker, L., Gentleman, R., Huber, W., Liaw, A., Lumley, T., Maechler, M., Magnusson, A., Moeller, S., Schwartz, M., and Venables, B. (2016). gplots: various R programming tools for plotting data (CRAN: R-Project).

Häberle, J., Görg, B., Rutsch, F., Schmidt, E., Toutain, A., Benoist, J.F., Gelot, A., Suc, A.L., Höhne, W., Schliess, F., et al. (2005). Congenital glutamine deficiency with glutamine synthetase mutations. N. Engl. J. Med. *353*, 1926–1933.

Häberle, J., Görg, B., Toutain, A., Rutsch, F., Benoist, J.F., Gelot, A., Suc, A.L., Koch, H.G., Schliess, F., and Häussinger, D. (2006). Inborn error of amino acid synthesis: human glutamine synthetase deficiency. J. Inherit. Metab. Dis. *29*, 352–358.

Hänzelmann, S., Castelo, R., and Guinney, J. (2013). GSVA: gene set variation analysis for microarray and RNA-seq data. BMC Bioinformatics *14*, 7.

Holm, M.B., Bastani, N.E., Holme, A.M., Zucknick, M., Jansson, T., Refsum, H., Mørkrid, L., Blomhoff, R., Henriksen, T., and Michelsen, T.M. (2017). Uptake and release of amino acids in the fetal-placental unit in human pregnancies. PLoS One *12*, e0185760.

Huber, W., Carey, V.J., Gentleman, R., Anders, S., Carlson, M., Carvalho, B.S., Bravo, H.C., Davis, S., Gatto, L., Girke, T., et al. (2015). Orchestrating high-throughput genomic analysis with Bioconductor. Nat. Methods *12*, 115–121.

Issaq, S.H., Mendoza, A., Fox, S.D., and Helman, L.J. (2019). Glutamine synthetase is necessary for sarcoma adaptation to glutamine deprivation and tumor growth. Oncogenesis *8*, 20.

Jewell, J.L., Kim, Y.C., Russell, R.C., Yu, F.X., Park, H.W., Plouffe, S.W., Tagliabracci, V.S., and Guan, K.L. (2015). Metabolism. Differential regulation of mTORC1 by leucine and glutamine. Science *347*, 194–198.

Johnson, M.O., Wolf, M.M., Madden, M.Z., Andrejeva, G., Sugiura, A., Contreras, D.C., Maseda, D., Liberti, M.V., Paz, K., Kishton, R.J., et al. (2018). Distinct regulation of Th17 and Th1 cell differentiation by glutaminase-dependent metabolism. Cell *175*, 1780–1795.e19.

Jung, J.H., Kang, K.W., Kim, J., Hong, S.C., Park, Y., and Kim, B.S. (2016). CXCR2 inhibition in human pluripotent stem cells induces predominant differentiation to mesoderm and endoderm through repression of mTOR, β-catenin, and hTERT activities. Stem Cells Dev *25*, 1006–1019.

Kanehisa, M., Goto, S., Sato, Y., Furumichi, M., and Tanabe, M. (2012). KEGG for integration and interpretation of large-scale molecular data sets. Nucleic Acids Res *40*, D109–D114.

Kankainen, M., Gopalacharyulu, P., Holm, L., and Oresic, M. (2011). MPEA–metabolite pathway enrichment analysis. Bioinformatics *27*, 1878–1879.

Katt, W.P., Lukey, M.J., and Cerione, R.A. (2017). A tale of two glutaminases: homologous enzymes with distinct roles in tumorigenesis. Future Med. Chem. *9*, 223–243.

Kolde, R. (2015). Package 'pheatmap' – pretty heatmaps (CRAN: R-Project).

Kung, H.N., Marks, J.R., and Chi, J.T. (2011). Glutamine synthetase is a genetic determinant of cell type-specific glutamine independence in breast epithelia. PLOS Genet *7*, e1002229.

Love, M.I., Huber, W., and Anders, S. (2014). Moderated estimation of fold change and dispersion for RNA-seq data with DESeq2. Genome Biol *15*, 550.

Lu, V., Dahan, P., Ahsan, F.M., Patananan, A.N., Roy, I.J., Torres, A., Jr., Nguyen, R.M.T., Huang, D., Braas, D., and Teitell, M.A. (2019). Mitochondrial metabolism and glutamine are essential for mesoderm differentiation of human pluripotent stem cells. Cell Res *29*, 596–598.

Marsboom, G., Zhang, G.F., Pohl-Avila, N., Zhang, Y., Yuan, Y., Kang, H., Hao, B., Brunengraber, H., Malik, A.B., and Rehman, J. (2016). Glutamine metabolism regulates the pluripotency transcription factor OCT4. Cell Rep *16*, 323–332.

Mascetti, V.L., and Pedersen, R.A. (2016). Human-mouse chimerism validates human stem cell pluripotency. Cell Stem Cell *18*, 67–72.

McIntyre, K.R., Vincent, K.M.M., Hayward, C.E., Li, X., Sibley, C.P., Desforges, M., Greenwood, S.L., and Dilworth, M.R. (2020). Human placental uptake of glutamine and glutamate is reduced in fetal growth restriction. Sci. Rep. *10*, 16197.

Meng, D., Frank, A.R., and Jewell, J.L. (2018). mTOR signaling in stem and progenitor cells. Development *145*, dev152595.

Moussaieff, A., Rouleau, M., Kitsberg, D., Cohen, M., Levy, G., Barasch, D., Nemirovski, A., Shen-Orr, S., Laevsky, I., Amit, M., et al. (2015). Glycolysis-mediated changes in acetyl-CoA and histone acetylation control the early differentiation of embryonic stem cells. Cell Metab *21*, 392–402.

Nazareth, E.J.P., Rahman, N., Yin, T., and Zandstra, P.W. (2016). A multi-lineage screen reveals mTORC1 inhibition enhances human pluripotent stem cell mesendoderm and blood progenitor production. Stem Cell Rep *6*, 679–691.

Neu, J. (2001). Glutamine in the fetus and critically ill low birth weight neonate: metabolism and mechanism of action. J. Nutr. *131*, 2585S–2589S, discussion 2590S.

Oburoglu, L., Tardito, S., Fritz, V., de Barros, S.C., Merida, P., Craveiro, M., Mamede, J., Cretenet, G., Mongellaz, C., An, X., et al. (2014). Glucose and glutamine metabolism regulate human hematopoietic stem cell lineage specification. Cell Stem Cell *15*, 169–184.

Patro, R., Duggal, G., Love, M.I., Irizarry, R.A., and Kingsford, C. (2017). Salmon provides fast and bias-aware quantification of transcript expression. Nat. Methods *14*, 417–419.

Qie, S., He, D., and Sang, N. (2019). Overview of glutamine dependency and metabolic rescue protocols. Methods Mol. Biol. *1928*, 427–439.

R Core Team (2017). R: a language and environment for statistical computing (R Foundation for Statistical Computing).

Reid, M.A., Dai, Z., and Locasale, J.W. (2017). The impact of cellular metabolism on chromatin dynamics and epigenetics. Nat. Cell Biol. *19*, 1298–1306.

Ritchie, M.E., Phipson, B., Wu, D., Hu, Y., Law, C.W., Shi, W., and Smyth, G.K. (2015). limma powers differential expression analyses for RNA-sequencing and microarray studies. Nucleic Acids Res *43*, e47.

Sancak, Y., Bar-Peled, L., Zoncu, R., Markhard, A.L., Nada, S., and Sabatini, D.M. (2010). Ragulator-Rag complex targets mTORC1 to the lysosomal surface and is necessary for its activation by amino acids. Cell *141*, 290–303.

Saxton, R.A., and Sabatini, D.M. (2017). MTOR signaling in growth, metabolism, and disease. Cell *168*, 960–976.

Schmied, C., and Jambor, H.K. (2020). Effective image visualization for publications – a workflow using open access tools and concepts. F1000Res *9*, 1373.

Shiraki, N., Shiraki, Y., Tsuyama, T., Obata, F., Miura, M., Nagae, G., Aburatani, H., Kume, K., Endo, F., and Kume, S. (2014). Methionine metabolism regulates maintenance and differentiation of human pluripotent stem cells. Cell Metab *19*, 780–794.

Soneson, C., Love, M.I., and Robinson, M.D. (2015). Differential analyses for RNA-seq: transcript-level estimates improve gene-level inferences. F1000Res *4*, 1521.

Stadtman, E.R. (2004). Regulation of glutamine synthetase activity. EcoSal Plus *1*.

Stewart, S.A., Dykxhoorn, D.M., Palliser, D., Mizuno, H., Yu, E.Y., An, D.S., Sabatini, D.M., Chen, I.S., Hahn, W.C., Sharp, P.A., et al. (2003). Lentivirus-delivered stable gene silencing by RNAi in primary cells. RNA *9*, 493–501.

Takahashi, K., Tanabe, K., Ohnuki, M., Narita, M., Ichisaka, T., Tomoda, K., and Yamanaka, S. (2007). Induction of pluripotent stem cells from adult human fibroblasts by defined factors. Cell *131*, 861–872.

Taniguchi, K., Heemskerk, I., and Gumucio, D.L. (2019). Opening the black box: stem cell-based modeling of human post-implantation development. J. Cell Biol. *218*, 410–421.

Tardito, S., Oudin, A., Ahmed, S.U., Fack, F., Keunen, O., Zheng, L., Miletic, H., Sakariassen, P.Ø., Weinstock, A., Wagner, A., et al. (2015). Glutamine synthetase activity fuels nucleotide biosynthesis and supports growth of glutamine-restricted glioblastoma. Nat. Cell Biol. *17*, 1556–1568.

TeSlaa, T., Chaikovsky, A.C., Lipchina, I., Escobar, S.L., Hochedlinger, K., Huang, J., Graeber, T.G., Braas, D., and Teitell, M.A. (2016). α-Ketoglutarate Accelerates the Initial Differentiation of Primed Human Pluripotent Stem Cells. Cell Metab *24*, 485–493.

Thomson, J.A., Itskovitz-Eldor, J., Shapiro, S.S., Waknitz, M.A., Swiergiel, J.J., Marshall, V.S., and Jones, J.M. (1998). Embryonic stem cell lines derived from human blastocysts. Science *282*, 1145–1147.

Tohyama, S., Fujita, J., Hishiki, T., Matsuura, T., Hattori, F., Ohno, R., Kanazawa, H., Seki, T., Nakajima, K., Kishino, Y., et al. (2016). Glutamine oxidation is indispensable for survival of human pluripotent stem cells. Cell Metab *23*, 663–674.

Tyser, R.C.V., Mahammadov, E., Nakanoh, S., Vallier, L., Scialdone, A., and Srinivas, S. (2021). Single-cell transcriptomic characterization of a gastrulating human embryo. Nature *600*, 285–289. https://doi.org/10.1038/s41586-021-04158-y.

Vardhana, S.A., Arnold, P.K., Rosen, B.P., Chen, Y., Carey, B.W., Huangfu, D., Carmona Fontaine, C.C., Thompson, C.B., and Finley, L.W.S. (2019). Glutamine independence is a selectable feature of pluripotent stem cells. Nat. Metab. *1*, 676–687.

Vozza, A., Parisi, G., De Leonardis, F., Lasorsa, F.M., Castegna, A., Amorese, D., Marmo, R., Calcagnile, V.M., Palmieri, L., Ricquier, D., et al. (2014). UCP2 transports C4 metabolites out of mitochondria, regulating glucose and glutamine oxidation. Proc. Natl. Acad. Sci. USA *111*, 960–965.

Waters, L.R., Ahsan, F.M., Ten Hoeve, J., Hong, J.S., Kim, D.N.H., Minasyan, A., Braas, D., Graeber, T.G., Zangle, T.A., and Teitell, M.A. (2019). Ampk regulates IgD expression but not energy stress with B cell activation. Sci. Rep. *9*, 8176.

112

Wellen, K.E., Lu, C., Mancuso, A., Lemons, J.M., Ryczko, M., Dennis, J.W., Rabinowitz, J.D., Coller, H.A., and Thompson, C.B. (2010). The hexosamine biosynthetic pathway couples growth factor-induced glutamine uptake to glucose metabolism. Genes Dev *24*, 2784–2799.

Wolfson, R.L., and Sabatini, D.M. (2017). The dawn of the age of amino acid sensors for the mTORC1 pathway. Cell Metab *26*, 301–309.

Yu, Y., Newman, H., Shen, L., Sharma, D., Hu, G., Mirando, A.J., Zhang, H., Knudsen, E., Zhang, G.F., Hilton, M.J., and Karner, C.M. (2019). Glutamine metabolism regulates proliferation and lineage allocation in skeletal stem cells. Cell Metab *29*, 966–978.e4.

Zhou, J., Su, P., Wang, L., Chen, J., Zimmermann, M., Genbacev, O., Afonja, O., Horne, M.C., Tanaka, T., Duan, E., et al. (2009). mTOR supports long-term self-renewal and suppresses mesoderm and endoderm activities of human embryonic stem cells. Proc. Natl. Acad. Sci. USA *106*, 7840–7845.

113

STAR★METHODS

KEY RESOURCES TABLE

Reagent or resource	Source	Identifier
Antibodies		
Mouse anti-Glutamine Synthetase; 1/500	BD Biosciences	Cat#610517; RRID: AB_2313837
Rabbit anti-PAX6; 1/500	Cell Signaling Technology	Cat#60433; RRID: AB_2797599
Rabbit anti-Pyruvate Dehydrogenase E1-alpha subunit (phospho S293); 1/500	Abcam	Cat#ab177461; RRID: AB_2756339
Rabbit anti-Phospho-p70 S6 Kinase (Thr389) (108D2); 1/500	Cell Signaling Technology	Cat#9234; RRID: AB_2269803
Rabbit anti-p70 S6 Kinase (49D7); 1/500	Cell Signaling Technology	Cat#2708; RRID: AB_390722
Rabbit anti-OCT-4; 1/200	Cell Signaling Technology	Cat#2750; RRID: AB_823583
Mouse anti-OCT-4 (D7O5Z); 1/200	Cell Signaling Technology	Cat#75463; RRID: AB_2799870
Goat anti-human NANOG; 5 μg/mL	R&D Systems	Cat#AF1997; RRID: AB_355097
Mouse anti-SOX2; 1/400	Cell Signaling Technology	Cat#4900; RRID: AB_10560516
Mouse anti-MAP2; 1/500	Invitrogen	Cat#MA5-12826; RRID: AB_10976831
Rabbit anti-OTX2; 4 μg/mL	Abcam	Cat#ab114138
Goat anti-Brachyury/TBXT; 15 μg/mL	R&D Systems	Cat# AF2085; RRID: AB_2200235
Rabbit anti-SLUG/SNAI2; 1/400	Cell Signaling Technology	Cat#9585; RRID: AB_2239535
Mouse anti-SOX17; 1/100	Invitrogen	Cat#MA5-24891; RRID: AB_2725395
Rabbit anti-FoxA2/HNF3β (D56D6); 1/400	Cell Signaling Technology	Cat#8186; RRID: AB_10891055
Mouse anti-β-tubulin; 1/1000	Millipore Sigma	Cat#T4026; RRID: AB_477577
Alexa Fluor 647 Rat Anti-Histone H3 (pS28)	BD Biosciences	Cat#558217; RRID: AB_397065
APC anti-DYKDDDDK Tag Antibody	Biolegend	Cat#637308; RRID: AB_2561497
PE Mouse Anti-SNAI2/Slug	BD Biosciences	Cat#564615; RRID: AB_2738866
Alexa Fluor 488 Mouse Anti-Human Sox17	BD Biosciences	Cat#562205; RRID: AB_10893402
PerCPCy5.5 Mouse anti-Human PAX6	BD Biosciences	Cat#562388; RRID: AB_11153319
Alexa Fluor 488 Mouse anti-MAP2B	BD Biosciences	Cat#560399; RRID: AB_1645358
PE Mouse anti-Human Sox1	BD Biosciences	Cat#561592; RRID: AB_10714631
Alexa Fluor 488 Mouse anti-Oct3/4	BD Biosciences	Cat#560253; RRID: AB_1645304
V450 Mouse Anti-Sox2	BD Biosciences	Cat#561610; RRID: AB_10712763
PerCP-Cy5.5 Mouse IgG2a, κ Isotype Control	BD Biosciences	Cat#558020; RRID: AB_396989
Alexa Fluor 700 Mouse IgG1, κ Isotype Control	BD Biosciences	Cat#557882; RRID: AB_396920
Alexa Fluor 488 Mouse IgG1 κ Isotype Control	BD Biosciences	Cat#557782; RRID: AB_396870
PE Mouse IgG1 k Isotype Control	BD Biosciences	Cat#554680 RRID: AB_395506
V450 Mouse IgG1, κ Isotype Control	BD Biosciences	Cat#560373; RRID: AB_1645606
Chemicals, peptides, and recombinant proteins		
Fixable Viability Dye APC-Cy7 eFluor780	Thermofisher	Cat#65-0865-14
7-AAD Staining Solution	BD Pharmingen	Cat#559925
ActinRed™ 555 ReadyProbes® Reagent Protocol (Rhodamine phalloidin)	Invitrogen	Cat#R37112
Gentle Cell Dissociation Reagent	Stemcell Technologies	Cat#07174
mTeSR1 Plus	Stemcell Technologies	Cat#05825
DMEM/F12	Gibco	Cat#11320033
ROCK Inhibitor; Y-27632	Stemcell Technologies	Cat#72304
Monothioglycerol	Millipore Sigma	Cat#M6145
BSA Fraction V, 7.5%	Gibco	Cat#15260037
2-mercaptoethanol	Thermofisher	Cat#21985-023
GlutaMAX Supplement	Thermofisher	Cat#35050-061

Continued

Reagent or resource	Source	Identifier
N2 Supplement	Gibco	Cat#17502048
B27 Supplement	Gibco	Cat#17504044
SB43154	Stemgent	Cat#04-0010
Dorsomorphin	Stemgent	Cat#04-0024
Human Recombinant Insulin	Millipore Sigma	Cat#11376497001
Transferrin from human serum	Millipore Sigma	Cat#10652202001
Chemically Defined Lipid Concentrate (CDLC)	Gibco	Cat#11905031
Human Recombinant VEGF-165	Stemcell Technologies	Cat#78073.1
Human Recombinant BMP-4	PeproTech	Cat#120-05ET
Human Recombinant FGF2	Stemcell Technologies	Cat#78003
Human Recombinant Activin A	Stemcell Technologies	Cat#78001.1
CHIR99021 (GSK3i)	Stemcell Technologies	Cat#72052
PI-103 Hydrochloride	Tocris/Fisher Scientific	Cat#29-301
Stemolecule LDN-1931189	Stemgent	Cat#04-0074
10% Fetal Bovine Serum	Omega Scientific	Cat#FB-11
MEM Non-Essential Amino Acids	Gibco	Cat#11140-050
Matrigel	Corning/Fisher Scientific	Cat#CB-4023A
RNAse-Free DNase Set	Qiagen	Cat#79254
DMEM/F12, no glutamine	Gibco	Cat#21331020
L-GLUTAMINE (AMIDE-15N, 98%)	Cambridge Isotope Laboratories	Cat#NLM-577
DPBS 1x w/o calcium & magnesium	Corning	Cat#21031CV
L-methionine sulfoximine	Millipore Sigma	Cat#91016
Dimethyl 2-oxoglutarate	Millipore Sigma	Cat#ES-008
Glucosamine 6-phosphate	Millipore Sigma	Cat#G5509
L-Glutathione reduced	Millipore Sigma	Cat#G6529
Ammonium Chloride	Millipore Sigma	Cat#A9434
6-Diazo-5-oxo-L-norleucine	Millipore Sigma	Cat#D2141
CB-839	Selleckchem	Cat#S7655
1x BD Perm/Wash Buffer	BD Biosciences	Cat#554714
SYBR Green	Roche	Cat#04887352001
1x protease inhibitor	Sigma	Cat#P8340
1x phosphatase inhibitor	Sigma	Cat#P5726
1x phosphatase inhibitor	Sigma	Cat#P0044
Odyssey Blocking Buffer TBS	Li-Cor	Cat#927-50010
DMEM with L-Glutamine and Sodium Pyruvate	Corning	Cat#MT10013CV
OptiMEM	Gibco	Cat#11058021
Fugene	Promega	Cat#E2312
Non Essential Amino Acids	Gibco	Cat#1140
Lenti-X Concentrator	Clontech	Cat#631231
Critical commercial assays		
RNeasy Mini Kit	Qiagen	Cat#74106
Fixation/Permeabilization Solution Kit	BD Biosciences	Cat#555028
iSCRIPT cDNA Synthesis Kit	Bio-Rad	Cat#1708841
MycoAlert Detection Kit	Lonza	Cat#LT08-418
BCA Protein Assay Kit	Pierce/Thermofisher	Cat#23225
Deposited data		
RNA-Sequencing Data for Nutrient Balanced hPSC and Trilineage Differentiation to EN/EC/ME	Lu et al. (2019)	GEO: GSE127270
UHPLC-MS quantification of intracellular abundance of metabolites.	This Manuscript	Table S1

115

Continued

Reagent or resource	Source	Identifier
Experimental models: Cell lines		
H9 (WA09); Female	UCLA BSCRC hESC Core Bank	RRID:CVCL_9773
UCLA-1; Female	UCLA BSCRC hESC Core Bank	RRID:CVCL_9951
HEK293FT	Life Technologies	Cat#31985
Oligonucleotides		
Primers for RT-qPCR, see method details	IDT	N/A
Recombinant DNA		
pLKO-shGLUL-1	Sigma-Aldrich	SHCLNG-NM_002065 TRCN0000343991
pLKO-shGLUL-2	Sigma-Aldrich	SHCLNG-NM_002065, TRCN0000343992
shRNA NTC (non-mammalian turboGFP)	N/A	Addgene: SH202
pCMV-VSV-G	Laboratory of Robert Weinberg (Stewart et al., 2003)	Addgene: 8454
pCMV-dR8.2 dvpr	Laboratory of Robert Weinberg (Stewart et al., 2003)	Addgene: 8455
pLJM1 FLAG Raptor Rheb 15	Laboratory of David Sabatini (Sancak et al., 2010)	Addgene: 26634
pLJM1 FLAG Raptor	Laboratory of David Sabatini (Sancak et al., 2010)	Addgene: 26633
pLJM1 Empty	Laboratory of Joshua Mendell (Golden et al., 2017)	Addgene: 91980
Software and algorithms		
Seahorse Wave Desktop Software	Agilent Technologies	https://www.agilent.com/en/products/cell-analysis/cell-analysis-software/data-analysis/wave-desktop-2-6
Leica Application Suite (LAS) X Software	Leica Microsystems	https://www.leica-microsystems.com/products/microscope-software/p/leica-las-x-ls/
ImageJ	NIH	https://imagej.nih.gov/ij/
Salmon v0.9.1	Patro et al. (2017)	https://combine-lab.github.io/salmon/
Tximport v1.6.0	Soneson et al. (2015)	http://bioconductor.org/packages/release/bioc/html/tximport.html
DESeq2 v1.18.1	Love et al. (2014)	https://bioconductor.org/packages/release/bioc/html/DESeq2.html
MitoMiner v4.0	Calvo et al. (2016)	http://mitominer.mrc-mbu.cam.ac.uk/release-4.0/begin.do
Pheatmap v1.0.8	Kolde (2015)	https://github.com/raivokolde/pheatmap
Gplots v3.0.1	Gregory Warnes (2016)	https://cran.r-project.org/web/packages/gplots/index.html
GSVA v1.26.0	Hänzelmann et al. (2013)	https://bioconductor.org/packages/release/bioc/html/GSVA.html
Prism 7 and 8	Graphpad	https://www.graphpad.com/scientific-software/prism/
TraceFinder v3.3	Thermofisher	https://www.thermofisher.com/order/catalog/product/OPTON-30491
Limma v3.34.9	Ritchie et al. (2015)	https://bioconductor.org/packages/release/bioc/html/limma.html
R v3.4.4	The R Project for Statistical Computing	https://www.r-project.org
Bioconductor v3.6	Huber et al. (2015)	https://www.bioconductor.org

RESOURCE AVAILABILITY

Lead contact
Further information and requests for reagents will be addressed by the corresponding author, Michael A. Teitell (MTeitell@mednet.ucla.edu).

Materials availability

This study did not generate new unique reagents.

Data and code availability

Raw RNA-Seq data for nutrient balanced hPSCs and tri-lineage differentiation to ectoderm, mesoderm, and endoderm were deposited in the NCBI Gene Expression Omnibus (GEO: GSE127270). All raw and processed UHPLC-MS metabolomics data from this study are in Excel spreadsheet format as Table S1. All data were analyzed with standard programs and packages, as detailed above. All R Jupyter notebooks and supplemental files used to process RNA-Seq and UHPLC-MS data are uploaded to https://github.com/fahsan/GlnFateGatekeeper. All raw images, immunoblots, and values for quantification are available from the corresponding author and lead contact on request.

EXPERIMENTAL MODEL AND SUBJECT DETAILS

Cell culture

Human embryonic stem cell (hESCs) lines H9 (WA09 – Female, RRID:CVCL_9773) and UCLA1 (Female, RRID:CVCL_9951) were grown in six-well tissue culture-treated polystyrene microplates (Falcon, 08-772-1B). Polystyrene plates were coated with feeder-free Matrigel basement membrane matrix (Corning, CB-40234A) diluted at 1:60 in DMEM/F-12 w/o glutamine (Gibco, 21331020), and incubated for 30 m at 37°C. hESCs were cultured in mTeSR Plus (Stemcell Technologies, 05825), with media changes every 48h, to 80% confluency at 5% CO_2 in a 37°C incubator. For passaging, hESCs were washed with DPBS 1x w/o calcium & magnesium (Corning, 21031CV) and removed from culture plates using Gentle Cell Dissociation Reagent (Stemcell Technologies, 07174) at 37°C for 5 m. Cells were passaged onto Matrigel-coated plates in mTeSR Plus as described above. Cells were tested for mycoplasma (Lonza, LT07-418) every two weeks.

Tri-lineage directed differentiation

Twelve-well tissue culture-treated polystyrene microplates (Falcon, 08-772-29) were coated in Matrigel basement membrane matrix. hESCs at 75%-85% confluency were removed from culture plates and dissociated into single cells using Gentle Cell Dissociation Reagent at 37°C for 10 min. Gentle Cell Dissociation Reagent was diluted in an equal volume of DMEM/F-12 (Gibco, 11320033). hESCs were scraped and centrifuged at 450 x g for 5 m, and cell number was quantified with a hemocytometer.

Cells were reseeded at 125,000 cells/cm² onto Matrigel-coated plates in mTeSR Plus with 10 μM ROCK inhibitor (Y-27632; Stemcell Technologies, 72304).

Ectoderm differentiation

To generate ectoderm, seeded cells were changed to a chemically-defined nutrient-balanced differentiation media 48 h after seeding. Cells were differentiated over a five-day period, cultured in DMEM/F12 supplemented with 450 μM 1-Thioglycerol (Millipore Sigma, M6145), 1 mg/mL BSA (Gibco, 15260037), 0.11 μM 2-mercaptoethanol (Gibco, 21985023), 1% Glutamax (Gibco, 35050061), 1% N-2 supplement (Gibco, 17502048), 2% B-27 supplement (Gibco, 17504044), 10 μM SB43154 (Stemgent, 04-0010), and 0.2 μM Dorsomorphin (Stemgent, 04-0024). Media was sterilized through a 0.22 μm filter (Denville, 1210N26), and changed every 24 h until D5 differentiation.

Mesoderm differentiation

To generate mesoderm, seeded cells were changed to a chemically-defined nutrient-balanced differentiation media 48 h after seeding. Cells were differentiated over a five-day period, cultured in DMEM/F12 supplemented with 450 μM 1-Thioglycerol, 1 mg/mL BSA, 0.11 μM 2-mercaptoethanol, 1% Glutamax, 0.7 μg/mL insulin (Millipore Sigma, 11376497001), 15 μg/mL transferrin (Millipore Sigma, 10652202001), 1 mL/100 mL chemically-defined lipid concentrate (Gibco, 11905031), 100 ng/mL VEGF-165 (Stemcell Technologies, 78073.1), 100 ng/mL BMP4 (Peprotech, 120-05ET), and 20 ng/mL FGF2 (Peprotech, 78003). During the first 24 h of differentiation, media was supplemented with 100 ng/mL Activin A (Stemcell Technologies, 78001). Media was sterilized through a 0.22 μm filter (Denville, 1210N26), and changed every 24 h until D5 differentiation.

Endoderm differentiation

To generate endoderm, seeded cells were changed to a chemically-defined nutrient-balanced differentiation media 48 h after seeding. Cells were differentiated over a three-day period, cultured in DMEM/F12 supplemented with 450 μM 1-Thioglycerol, 1 mg/mL BSA, 0.11 μM 2-mercaptoethanol, 1% Glutamax, 0.7 μg/mL insulin (Millipore Sigma, 11376497001), 15 μg/mL transferrin (Millipore Sigma, 10652202001), 1 mL/100 mL chemically-defined lipid concentrate (Gibco, 11905031). During the first 24 h of differentiation, media was supplemented with 100 ng/mL Activin A, 2 μM CHIR99021 (Stemcell Technologies, 72052), and 50 nM PI-103 (Fisher Scientific, 29-301). After 24 h of differentiation, media was supplemented with 100 ng/mL Activin A and 250 nM LDN 1931189 (Stemgent, 04-0074). Media was sterilized through a 0.22 μm filter (Denville, 1210N26), changed every 24 h until D3 differentiation.

METHOD DETAILS

Glutamine perturbations

For all glutamine-free conditions, differentiation media (as described above) was made with DMEM/F-12 w/o glutamine and in the absence of 1% Glutamax (note: trace/negligible amounts of glutamine may be present in Matrigel). To achieve glutamine-starvation conditions, glutamine-free media was supplemented with 1 mM L-methionine sulfoximine (Millipore Sigma, 91016). Metabolite rescue experiments were performed under glutamine-starvation media in the presence of 8 mM dimethyl 2-oxoglutarate (Millipore Sigma, 349631), 60 μL/mL Embryomax nucleosides (Millipore Sigma, ES-008), 10 mM D-glucosamine 6-phosphate (Millipore Sigma, G5509), 2 mM D-(+)-glucosamine hydrochloride (Sigma-Aldrich, G1514), or 1 mM L-glutathione reduced (Millipore Sigma, G6529). Gln utilization was blocked by addition of 50 μM 6-diazo-5-oxo-L-norleucine (Millipore Sigma, D2141) or 1 μM CB-839 (Selleckchem, S7655) to either Gln-supplemented or Gln-free media. Gln, Arg, or Leu starvation/deprivation timed pulse experiments were performed by culturing cells in respective deprivation conditions for an initial 14 h or 24 h, washed with PBS, and then grown in Gln, Arg, or Leu replete conditions until D5 of differentiation.

Intracellular flow cytometry

Cells were dissociated using Gentle Cell Dissociation Reagent for 10 m, diluted in sterile dPBS, and pelleted at 450 x g for 5 m. Supernatant was aspirated off, and cells were re-suspended in 250 μL of Fixation/Permeabilization solution (BD Biosciences, 554714) and incubated at 4°C for 30 m. Following fixation, cells were washed with 1x BD Perm/Wash Buffer (BD Biosciences, 554714) and pelleted at 450 x g for 5 m. Cells were re-suspended in 100 uL of 1x BD Perm/Wash Buffer. Conjugated antibodies were incubated with fixed cells for 45 m at 4°C in the dark. Samples were processed on a LSRFortessa flow cytometer (BD Biosciences) and analyzed using FlowJo software (FlowJo, Inc.). For cell viability quantifications, values were generated from EF780 Fixable Viability Dye negative (EF780-) cell populations or from Annexin A5 and 7AAD double negative (%AV- 7AAD- dn) cell populations. For cell cycle quantifications, values were determined based on 7AAD-stained DNA content and histone H3 (phospho-S28). Experiments were performed at least three independent times. The following conjugated antibodies were used: Alexa Fluor 647 Rat anti-histone H3 (pS28) (BD Biosciences, 558217), APC anti-DYKDDDDK tag (Biolegend, 637308), PE Mouse anti-SNAI2/Slug (BD Biosciences, 564615), Alexa Fluor 488 Mouse anti-human Sox17 (BD Biosciences, 562205), PerCPCy5.5 Mouse anti-human PAX6 (BD Biosciences, 562388), human Pax6 PE-conjugated antibody (R&D Systems, IC8150P-100), Alexa Fluor 488 mouse anti-MAP2B (BD Biosciences, 560399), PE Mouse anti-human Sox1 (BD Biosciences, 561592), Alexa Fluor 488 mouse anti-Oct3/4 (BD Biosciences, 560253), V450 mouse anti-Sox2 (BD Biosciences, 561610), PerCP-Cy5.5 mouse IgG2a, κ isotype control (BD Biosciences, 558020), Alexa Fluor 700 mouse IgG1, κ isotype control (BD Biosciences, 557882), Alexa Fluor 488 mouse IgG1 κ isotype control (BD Biosciences, 557782), PE mouse IgG1 k isotype control (BD Biosciences, 556680), V450 mouse IgG1, and κ isotype control (BD Biosciences, 560373). For flow cytometry quantification of phosphorylated mTORC1 substrates, the following antibodies were used: rabbit anti-phospho-p70 S6 kinase (Thr389) (108D2) (Cell Signaling, 9234) and Alexa Fluor 568 goat anti-rabbit IgG (H+L) (Invitrogen, A11036, 1/1000).

Immunofluorescence

Cells were differentiated in 35 mm μ-Dish on No. 1.5 ibitreat polymer coverslips (ibidi GmbH, 81156, 80416) coated with Matrigel (Corning, CB-40234A). Cells were fixed in 4% methanol-free formaldehyde (Thermo Scientific, 28906) for 10-15 min at RT. Cells were washed with PBS, permeabilized with 0.3% Triton X-100 in PBS for 10 min at RT, washed again with PBS, and incubated in blocking buffer (5% normal donkey serum in PBS) for 1hr at RT. Cells were incubated with primary antibodies diluted in blocking buffer overnight at 4C, washed with PBS, then incubated with secondary antibodies diluted in blocking buffer for 1hr at RT. Cells were counterstained and mounted with ibidi Mounting Medium with DAPI (ibidi GmbH, 50011, nD 1.42–1.44). The following antibodies were used: rabbit anti-OCT-4 (Cell Signaling, 610517, 1/200), mouse anti-OCT-4 (Cell Signaling, 2750, 1/200), goat anti-human NANOG (R&D Systems, AF1997, 5 μg/mL), mouse anti-SOX2 (Cell Signaling, 4900, 1/400), rabbit anti-PAX6 (Cell Signaling, 60433, 1/200), mouse anti-MAP2 (Invitrogen, MA5-12826, 1/500), rabbit anti-OTX2 (Abcam, ab114138, 4 μg/mL), goat anti-Brachyury/TBXT (R&D Systems, AF2085, 15 μg/mL), rabbit anti-SLUG/SNAI2 (Cell Signaling, 9585, 1/400), rabbit anti-SLUG/SNAI2 (Cell Signaling, 9585, 1/400), mouse anti-SOX17 (Invitrogen, MA5-24891, 1/100), rabbit anti-FoxA2/HNF3β (Cell Signaling, 8186, 1/400), mouse anti-DYKDDDDK Tag (Cell Signaling, 8146, 1/200), rabbit anti-phospho-p70 S6 kinase (Thr389) (Cell Signaling, 9234). Actin counterstain was done following ActinRed™ 555 ReadyProbes® Reagent Protocol (Rhodamine phalloidin) (Invitrogen, R37112). All secondary antibodies were from sourced from donkey host of the Alexa Flour series (Life technologies, A-31573, A-21202, A-21432, A-11055, A-31570).

Confocal microscopy image acquisition and processing

Imaging was performed on Leica TCS SP8 DLS (Digital LightSheet) confocal microscope, equipped with a Galvo X resonant scanner and sCMOS camera controlled by the Leica Application Suite (LAS) X software, using a HC PL APO CS2 63x/1.40 OIL lens and a TD 488/552/638 main beamsplitter. Pinhole size was set to 1AU with an 8,000 Hz scan speed. 2048 x 2048 8- or 16-bit images at 1.25 zoom were acquired using HyD (410nm - 527nm, 655nm - 685nm) and PMT (567nm - 607nm) detectors. All samples with the same immunolabeling and/or compared to each other were acquired with the same settings. DAPI was excited with Diode 405 nm laser line and emission collected with HyD detector (455±45nm). Alexa Flour 488 was excited with OPSL 488 nm laser line and emission

collected with HyD detector (518±13nm) or PMT (518±21nm). Alexa Flour 555 was excited with OPSL 552 nm laser line and emission collected with HyD detector (584±23nm) or PMT (569±10nm). Alexa Flour 647 was excited with Diode 638 nm laser line and emission collected with HyD detector (670±15nm).

All compared image sets had identical processing in shift phase (arithmetic mean), denoising (median filtering with radius of 2-6 pixels), and histogram normalization (brightness and contrast) using the Leica Application Suite (LAS) X software according to field standards (Aaron and Chew, 2021; Schmied and Jambor, 2020). All experiment interpretations and data analysis were done on raw image files. False color LUTs and image merges were done on the Leica Application Suite (LAS) X software.

qRT-PCR

Cells were grown to between 70% and 80% confluence and harvested as described above. RNA was isolated using the RNeasy Mini Kit (Qiagen, 74104) and RNase-free DNase (Qiagen, 79254) following the manufacturer's protocols. RNA was quantified using a Nanodrop spectrophotometer (Thermo Scientific). cDNA was synthesized with 2 μg of RNA using the iScript cDNA synthesis kit (Bio-Rad, 1708841). qRT-PCR was performed on a LightCycler480 (Roche) using SYBR green (Roche, 04887352001). Experiments were performed at least three independent times. Primers were used as follows: *RPLPO*, forward, 5'-CAGATTGGCTACCCA ACTGTT-3', reverse, 5'-GGAAGGTGTAATCCGTCTCCAC-3'; *OCT4*, forward, 5'-CAAAGCAGAAACCCTCGTGC-3', reverse, 5'-TCT CACTCGGTTCTCGATACTG-3'; *NANOG*, forward, 5'-CCCCAGCCTTTACTCTTCCTA-3', reverse, 5'-CCAGGTTGAATTGTTCCAGG TC-3'; *SOX2*, forward, 5'-TACAGCATGTCCTACTCGCAG-3', reverse, 5'-GAGGAAGAGGTAACCACAGGG-3'; *MAP2*, forward, 5'-CTCAGGACCGGCTAACAGAGG-3', reverse, 5'-CATTGGCGCTTCGGGACAA-3'; *OTX2*, forward, 5'-CAAAGTGAGACCTGCCAAAAA GA-3', reverse, 5'-TGGACAAGGGATCTGACAGTG-3'; *PAX6*, forward, 5'-TGGGCAGGTATTACGAGACTG-3', reverse, 5'-ACTCCC GCTTATACTGGGCTA-3'; *GLS1*, forward, 5'- TGGTGGCCTCAGGTGAAAAT-3', reverse, 5'-CCAAGCTAGGTAACAGACCCTGTTT-3'; *GLS2*, forward, 5'- AACGAATCCCTATCCACAAGTTCA-3', reverse, 5'- GCAGTCCAGTGGCCTTTAGTG-3'; *GLUL*, forward, 5'-AAGAGTTGCCTGAGTGGAATTTC-3', reverse, 5'- AGCTTGTTAGGGTCCTTACGG-3'.

Immunoblot

Cells were grown to between 70% and 80% confluence and harvested as described above. Cells were lysed in SDS buffer (40 mM Tris-HCl pH 6.8, 3% glycerol, 1% SDS), 1x protease inhibitor (Sigma, P8340) and 1x phosphatase inhibitor (Sigma, P5726 and Sigma, P0044). Protein concentrations were quantified using a BCA assay (Pierce). 50 μg aliquots were supplemented with 5% 2-mercaptoethanol and loaded onto gels at 90 V for 20 m followed by 120 V for 75 m. Protein was transferred to a nitrocellulose membrane at 250 mA for 2 h. Membranes were blocked with Odyssey Blocking Buffer TBS (Li-Cor, 927-50010) for 30 m and incubated in primary antibodies overnight at 4°C. Following incubation, membranes were washed in TBST for 20 m. IRDye-conjugated secondary antibodies IRDye 680RD donkey anti-rabbit IgG (H + L) (LiCor, 926-68703, 1/10,000) and IRDye® 800CW goat anti-mouse IgG (H + L) (LiCor, 925-32210, 1/10,000) were added to membranes, incubated for 1 h at RT, and washed in TBST for 20 m. All images were captured with an Odyssey Fc (Licor). Experiments were performed at least three independent times. The following antibodies were used: rabbit anti-pyruvate dehydrogenase E1-alpha subunit (phospho S293) (ab177461, 1/500), rabbit anti-pyruvate dehydrogenase E1-alpha subunit (ab168379, 1/500), mouse anti-glutamine synthetase (BD Biosciences, 610517, 1/500), rabbit anti-PAX6 (Cell Signaling, 60433, 1/500), mouse anti-β-tubulin (Millipore Sigma, T4026, 1/10,000), rabbit anti-phospho-p70 S6 kinase (Thr389) (108D2) (Cell Signaling, 9234, 1/500), rabbit anti-p70 S6 kinase (49D7) (Cell Signaling, 2708, 1/500).

Click chemistry reactions
EdU labeling

Samples were cultured for 4 h with fresh media supplemented with 5 μM EdU (Invitrogen, A10044), harvested and fixed in 100 μL 4% phosphate-buffered paraformaldehyde for 15 m at RT, permeabilized in 100 μL of saponin-based permeabilization wash for 15 m at RT, and proceeded to Click-iT reaction labeling.

L-*Azidohomoalanine (AHA) labeling*

Samples were pulsed for 15 m with DMEM/F-12 w/o L-methionine (US Biological Life Sciences, D9807-05A) differentiation media for optimized AHA labeling. Then, samples were cultured in DMEM/F-12 w/o L-methionine differentiation media with 1 mM AHA (Sigma-Aldrich, 900892; labeling condition) or 0.1 mM L-methionine (Sigma-Aldrich, M5308; control condition) for 1 h. As a negative control, nascent protein synthesis was blocked by addition of 1 μM Blasticidin S HCL (Gibco, A1113903) to AHA-supplemented media. As with EdU labeling, samples were harvested and fixed in 100 μL 4% phosphate-buffered paraformaldehyde for 15 m at RT, permeabilized in 100 μL of saponin-based permeabilization wash for 15 m at RT, and proceeded to Click-iT reaction labeling.

Click chemistry reaction

For EdU labeling, Alexa Fluor 488 azide (Invitrogen, A10266) was used. For AHA labeling, Alexa Fluor 488 Alkyne (Invitrogen, A10267) was used. Freshly prepared Click-iT reagent mix was made with saponin-based wash reagent, 100 mM copper(II) sulfate (Sigma-Aldrich, C1297), Click-iT buffer additive (Invitrogen, C10269), and 1 μM Alexa Fluor 488 azide or Alexa Fluor 488 Alkyne. Following permeabilization, samples were incubated with 500 μL reagent for 30 m at RT in the dark, then washed twice with saponin-based wash reagent. Samples were then stored in saponin-based wash reagent at 4°C in the dark for flow cytometry and/or further intracellular antibody labeling.

shRNA knockdown

pLKO.1 vectors containing shRNA targeting *GLUL* RNA transcripts were purchased from Sigma-Aldrich (Sigma, SHCLNG-NM_002065 TRCN0000343991 and SHCLNG-NM_002065, TRCN0000343992). pLK0.5 vectors containing shRNA control targeting non-mammalian turboGFP were also purchased from Addgene (Sigma, SHC 202). Vectors were packaged along with pCMV-dR8.2 dvpr (Addgene, 8455) and pCMV-VSV-G (Addgene, 8454) into HEK293FT cells. HEK293FT cells were seeded into 100 mm dishes and grown to 65% - 80% confluence in DMEM with L-Glutamine and Sodium Pyruvate (Corning, MT10013CV) supplemented with 10% Fetal Bovine Serum (Omega Scientific, FB-11), 1% Glutamax, and 1% non-essential amino acids (Gibco, 1140). HEK293FT cells were transfected with 829 μL of.020 μg/μl plasmid solution (8 μg shRNA plasmids, 8 μg pCMV-dR8.9, 2 μg pCMV-VSVG) in OptiMEM (Gibco, 11058021) and Fugene HD (Promega, E2312). Media was collected 48 h and 60 h after transfection and concentrated using Lenti-X Concentrator (Clontech, 631231). hESC lines grown until 80% confluency were transduced with 5 – 10 x 10⁵ lentiviral particles and 6 μg/mL polybrene for 8 h on D1. Transduction was repeated on D2 and D3, doubling viral concentration each successive day. Transduced cell lines were selected with 1 μg/mL puromycin on D5 – 8.

cDNA transfection

pLJM1 vectors FLAG Raptor Rheb 15, FLAG Raptor, and Empty were purchased from Addgene (26634, 26633, 91980). Vectors were a gift from the laboratories of David Sabatini and Joshua Mendell. Vectors were packaged along with pCMV-dR8.2 dvpr (Addgene, 8455) and pCMV-VSV-G (Addgene, 8454) into HEK293FT cells. HEK293FT cells were seeded into 100 mm dishes and grown to 65% - 80% confluence in DMEM with L-Glutamine and Sodium Pyruvate (Corning, MT10013CV) supplemented with 10% Fetal Bovine Serum (Omega Scientific, FB-11), 1% Glutamax, and 1% non-essential amino acids (Gibco, 1140). HEK293FT cells were transfected with 829 μL of.020 μg/μl plasmid solution (8 μg shRNA plasmids, 8 μg pCMV-dR8.9, 2 μg pCMV-VSVG) in OptiMEM (Gibco, 11058021) and Fugene HD (Promega, E2312). Media was collected 48 h and 60 h after transfection and concentrated using Lenti-X Concentrator (Clontech, 631231). hESC lines grown until 80% confluency were transduced with 5 – 10 x 10⁵ lentiviral particles and 6 μg/mL polybrene for 8h on D1. Transduction was repeated on D2 and D3, doubling viral concentration each successive day. Transduced cell lines were selected with 1 μg/mL puromycin on D5 – 8.

Media preparation for metabolite extraction and UHPLC-MS processing

For Gln-free conditions, ectoderm differentiation media (as described above) was made with DMEM/F-12 w/o glutamine and in the absence of 1% Glutamax. For glutaminolysis-inhibited conditions, ectoderm differentiation media (as described above) was made with DMEM/F-12 supplemented with 1 μM CB-839. To achieve Gln-starvation conditions, Gln depleted media was additionally supplemented with 1 mM L-methionine sulfoximine (Millipore Sigma, 91016). For Gln-replete conditions, ectoderm differentiation media was made with DMEM/F-12 w/o glutamine and.01% Glutamax. For Glu conversion to Gln isotopologue tracing, cells were labeled with 0.5mM $^{13}C_5$-Glu for 1 h under defined Gln perturbation conditions.

Metabolite extraction and UHPLC-MS processing

Ultra-high performance liquid chromatography and mass spectrometry was performed as previously described (Lu et al., 2019). To extract intracellular metabolites, cells were washed with warm PBS for less than 10 s, rinsed with ice-cold 150 mM ammonium acetate (pH 7.3), and quenched with 1 mL/well of cold 80% MeOH in water. Wells were scraped and contents transferred to Eppendorf tubes and vortexed for 10 s. 5 nmol D/L-norvaline was added to each cell suspension as an internal control, and tubes were centrifuged at 16,000 x g for 15 m at 4°C. The supernatant was transferred into glass vials and dried under a vacuum. Dried metabolites were re-suspended in 50% ACN:water and one-tenth was loaded onto a Luna 3um NH2 100A (150 × 2.0 mm) column (Phenomenex). The chromatographic separation was performed on an Ultimate 3000RSLC or a Vanquish Flex (Thermo Scientific) with mobile phases A (5 mM NH4AcO pH 9.9) and B (ACN) and a flow rate of 200 μl/min. A linear gradient from 15% A to 95% A over 18 m was followed by 9 m isocratic flow at 95% A and re-equilibration to 15% A. Metabolites were detection with a Thermo Scientific Q Exactive mass spectrometer run with polarity switching (+3.5 kV/− 3.5 kV) in full scan mode with an m/z range of 65-975. TraceFinder 4.1 (Thermo Scientific) was used to quantify the targeted metabolites by area under the curve using expected retention time and accurate mass measurements (< 5 ppm). Experiments were performed with three biological replicates.

QUANTIFICATION AND STATISTICAL ANALYSIS

Metabolomics data analysis

Metabolomics analysis was performed as previously described (Waters et al., 2019). Data analysis was performed using the statistical language R v3.6.3 and Bioconductor v3.6.1 packages(Huber et al., 2015; R Core Team, 2017). Metabolite abundance was normalized per μg of protein content per metabolite extraction, and metabolites not detected were set to zero.

Pathway-level relative amounts metabolite set variation analysis (MSVA) was performed using R Bioconductor package GSVA v1.26.0 (Hänzelmann et al., 2013). Metabolite normalized relative abundances were standardized using a log₂(normalized amounts + 1) transformation, and metabolites per sample were converted to a pathways per sample matrix using function gsva() with parameters "method = gsva, rnaseq = FALSE, abs.ranking = FALSE, min.sz = 5, max.sz = 500". GSVA pathway enrichment scores were then extracted and significance testing between conditions was calculated using R Bioconductor package limma v3.34.9, fitting a linear model to each metabolite and assessing differences in normalized abundance using an empirical Bayes moderated

F-statistic with an adjusted *P* value threshold of 0.05, using the Benjamini-Hochberg false discovery rate of 0.05 (Benjamini and Hochberg, 1995; Ritchie et al., 2015). Pathway metabolite sets were constructed using the KEGG Compound Database and derived from the existing Metabolite Pathway Enrichment Analysis (MPEA) toolbox (Kanehisa et al., 2012; Kankainen et al., 2011).

RNA-Seq analysis

RNA-Seq data analysis was performed as previously described (Lu et al., 2019). TPM values were extracted from GEO:GSE127270 for genes that were determined to be differentially expressed via statistical testing using R Bioconductor package DESeq2 v1.18.1 (Love et al., 2014). Differentially expressed genes were identified using Wald significance testing, with an adjusted P value threshold below 0.05 for one or more comparisons. A *variance stabilized transform* matrix (*VST*) was generated using DESeq2, and subset for the differentially expressed genes (DEGs) identified above. *VST* values were row scaled by subtracting the average mean per gene row between samples, and then averaged per condition. Heatmaps were generated using R Bioconductor package pheatmap v1.0.8 (Kolde, 2015).

Comparison of Gln synthesis to Gln consumption

RNA-Seq data from a previous publication (Lu et al., 2019) and single cell RNA-Seq data from Tyser et al., 2021 (Tyser et al., 2021) were used to query the ratio of Gln consumption transcripts [average(*GLS1 + GLS2*)] to Gln synthesis transcripts [*GLUL*]. For the single cell RNA-Seq data, the ratio was calculated for each individual cell and then normalized to the average Epiblast value. For bulk RNA-Seq, each replicate was normalized to the average hPSC value.

Statistical testing

Statistical testing for all data except for RNA-Seq and UHPLC-MS metabolomics was performed using Prism 7 and 8 (Graphpad). Details for statistical testing of RNA-Seq and UHPLC-MS metabolomics data are included in the section above. Unless otherwise noted, each experiment is n=3, where n represents the number of independent biological replicates. Statistical details can be found in each figure legend. Parametric data were analyzed using Student's t tests or one-/two-way ANOVA with multiple comparisons correction. Metabolite pathway enrichment values were quantified using empirical Bayes linear modelling with multiple hypothesis correction. P values $\leq$ 0.05 were considered significant for all data assayed. *P $\leq$ 0.05, **P $\leq$ 0.01, ***P $\leq$ 0.001, ****P $\leq$ 0.0001.
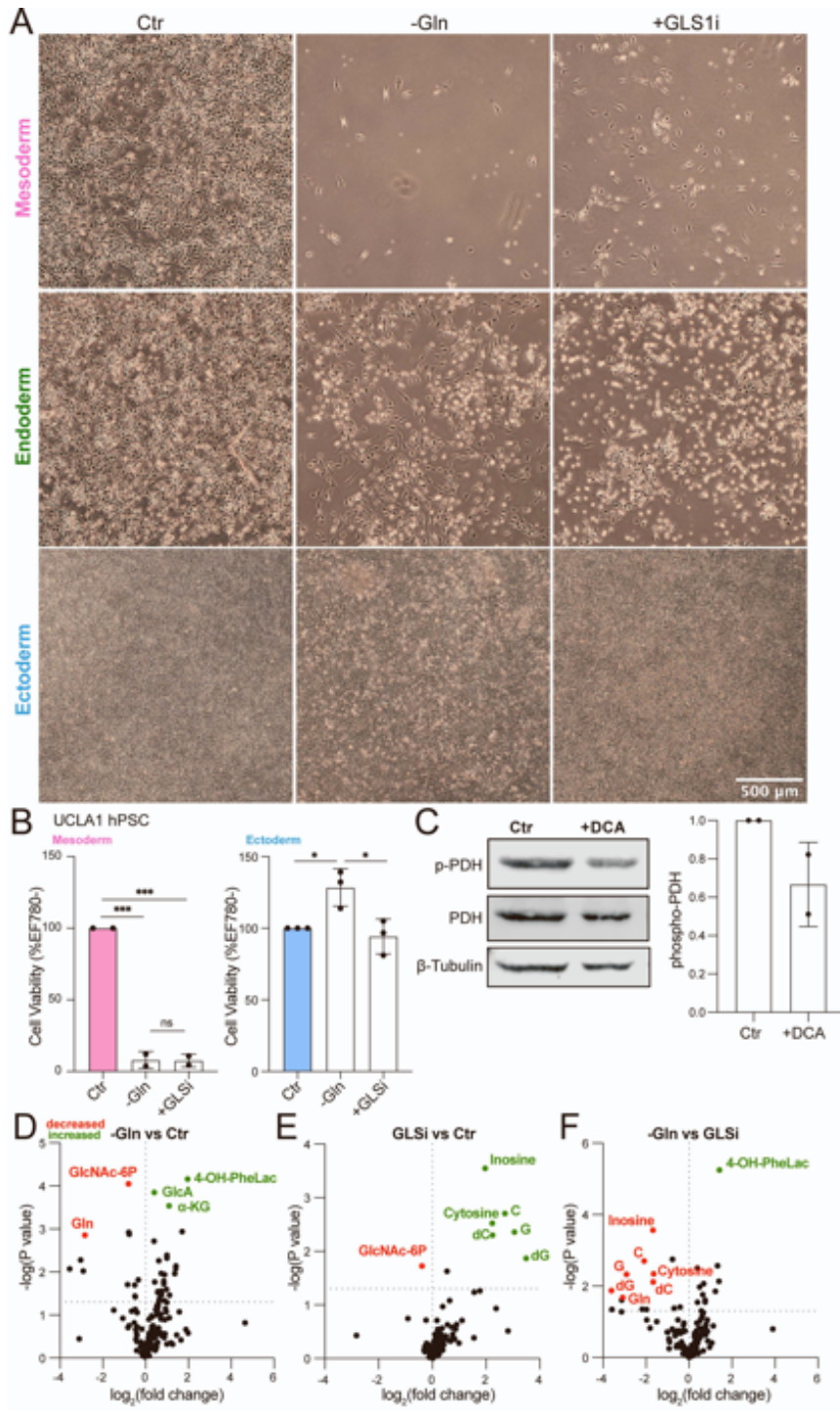
Supplemental information

Glutamine-dependent signaling controls

pluripotent stem cell fate

Vivian Lu, Irena J. Roy, Alejandro Torres Jr., James H. Joly, Fasih M. Ahsan, Nicholas A. Graham, and Michael A. Teitell

Figure S1

Supplemental Figure S1. Cell viability images and quantification under Gln deprivation
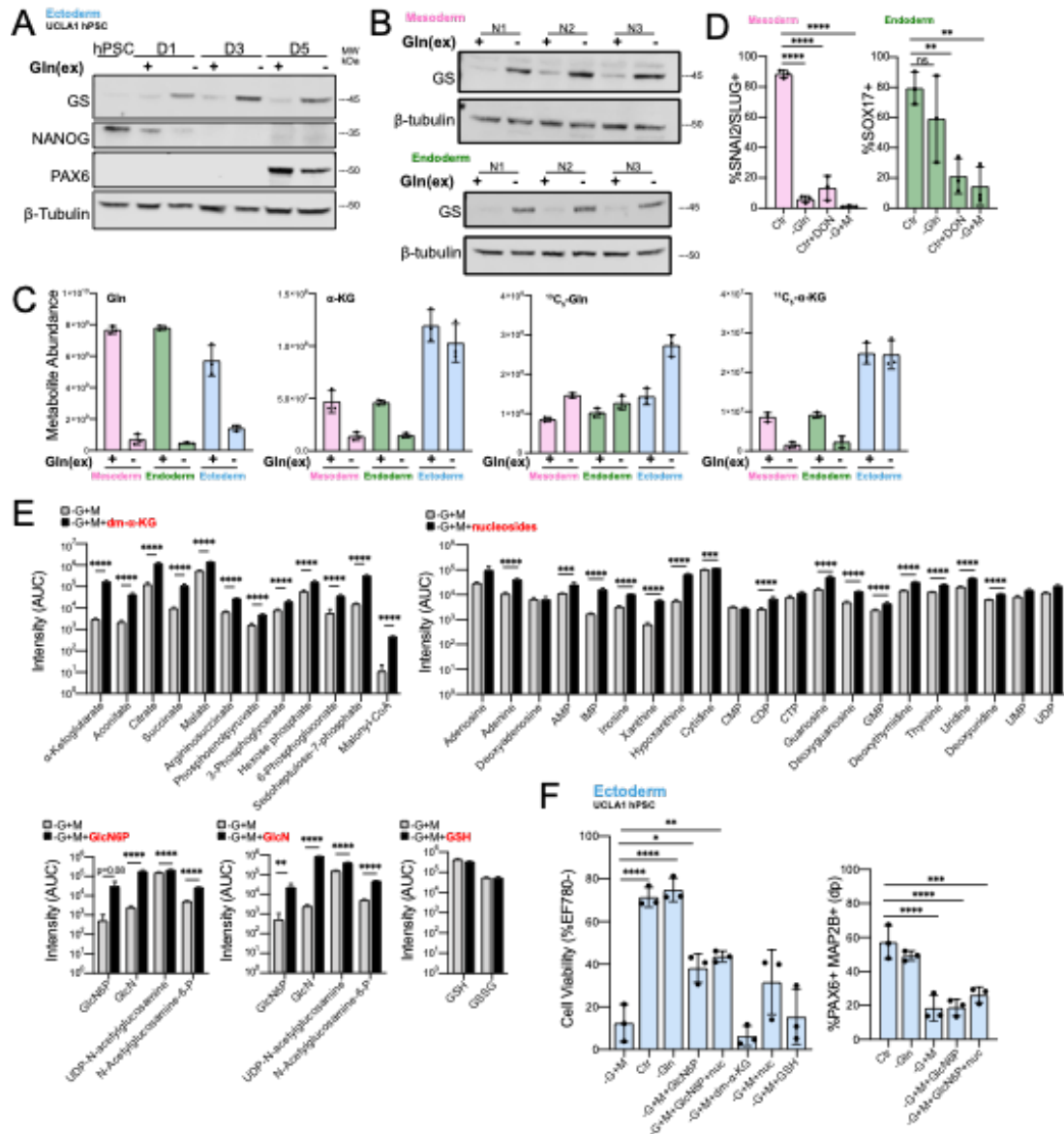*Related to Figure 1*
(A) Representative brightfield images of cell viability and confluency of D5 mesoderm, D3 endoderm, and D5 ectoderm grown in Gln-supplemented (Ctr), Gln-free (-Gln), or glutaminolysis-inhibited (+GLS1i) conditions. Scale bar indicates 500 µm.
(B) Cell viability of UCLA1-derived D5 mesoderm (n=2) and ectoderm cells relative to Ctr.
(C) Immunoblot and densitometry quantification of phosphorylated pyruvate dehydrogenase (PDH) and total PDH expression after 24h 1 mM DCA treatment (n=2).
(D-F) Volcano plots of differential metabolite abundance in (**D**) -Gln vs Ctr, (**E**) GLS1i vs Ctr, and (**F**) -Gln vs GLS1i conditions, quantified by UHPLC-MS. Differential fold change is plotted against raw p values for each metabolite comparison.

Data represent mean ± SD of n ≥ 3 biological replicates unless indicated otherwise. ∗p ≤ 0.05; ∗∗p ≤ 0.01; ∗∗∗p ≤ 0.001. The p values were determined by (**B**) one-way ANOVA with correction for multiple comparisons, or (**D-F**) using the Student's t test

Supplemental Figure S2. Tri-lineage metabolomics profiles in Gln-free media
Related to Figure 2

(A-B) Immunoblot of GS expression in (**A**) UCLA1-derived ectoderm and (**B**) H9-derived mesoderm and endoderm cells differentiated in Gln-free media.

(C) Intracellular amounts of Gln, α-KG, $^{13}C_5$-Gln, and $^{13}C_5$-α-KG derived from $^{13}C_5$-glutamic acid in D3 mesoderm, endoderm, and ectoderm cells grown in Gln-supplemented or Gln-free media.

(D) Percentage of (Left) D5 mesoderm (SNAI2/SLUG$^+$) and (Right) D3 endoderm (SOX17$^+$) cells grown in Gln-supplemented or Gln-free conditions with 50 µM DON or 1 mM MSO.

(E) Verification of intracellular uptake and conversion to related metabolites upon respective metabolite supplementations (denoted in red), quantified by UHPLC-MS. Intensity values represent area under the curve (arbitrary units).

(F) (Left) Cell viability of UCLA1-derived D5 ectoderm cells differentiated in Gln-starvation and supplemented with GlcN6P, dm-α-KG, nucleosides, or GSH. (Right) Percentage of D5 ectoderm (PAX6$^+$MAP2B$^+$) cells grown in Gln-starvation with added GlcN6P or both GlcN6P and nucleosides (nuc). Data represent mean ± SD of n = 3 biological replicates. *$p \leq 0.05$; **$p \leq 0.01$; ***$p \leq 0.001$; ****$p \leq 0.0001$. The p values were determined using (**D, F**) one-way ANOVA with correction for multiple comparisons or (**E**) Student's t test.
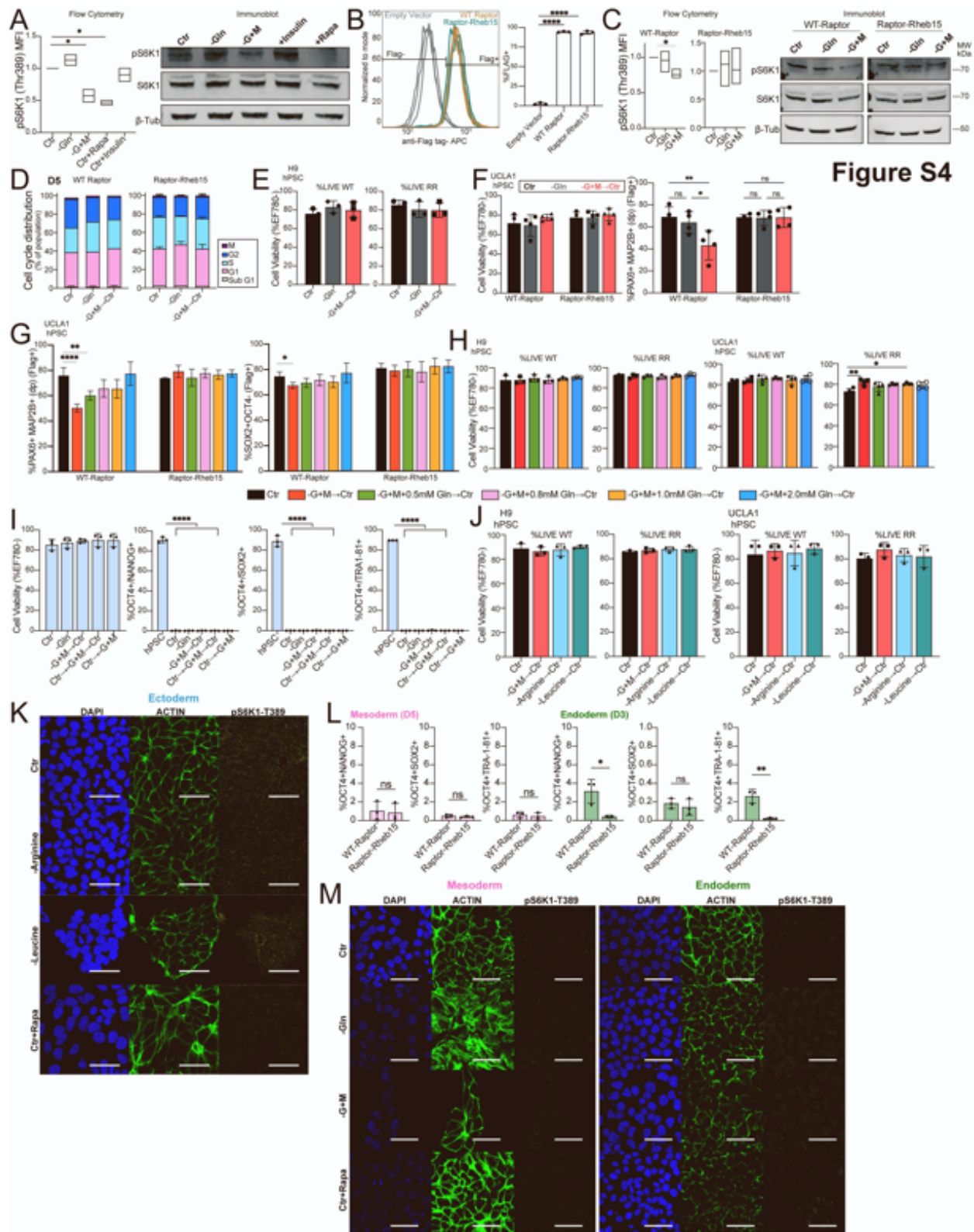
Figure S3
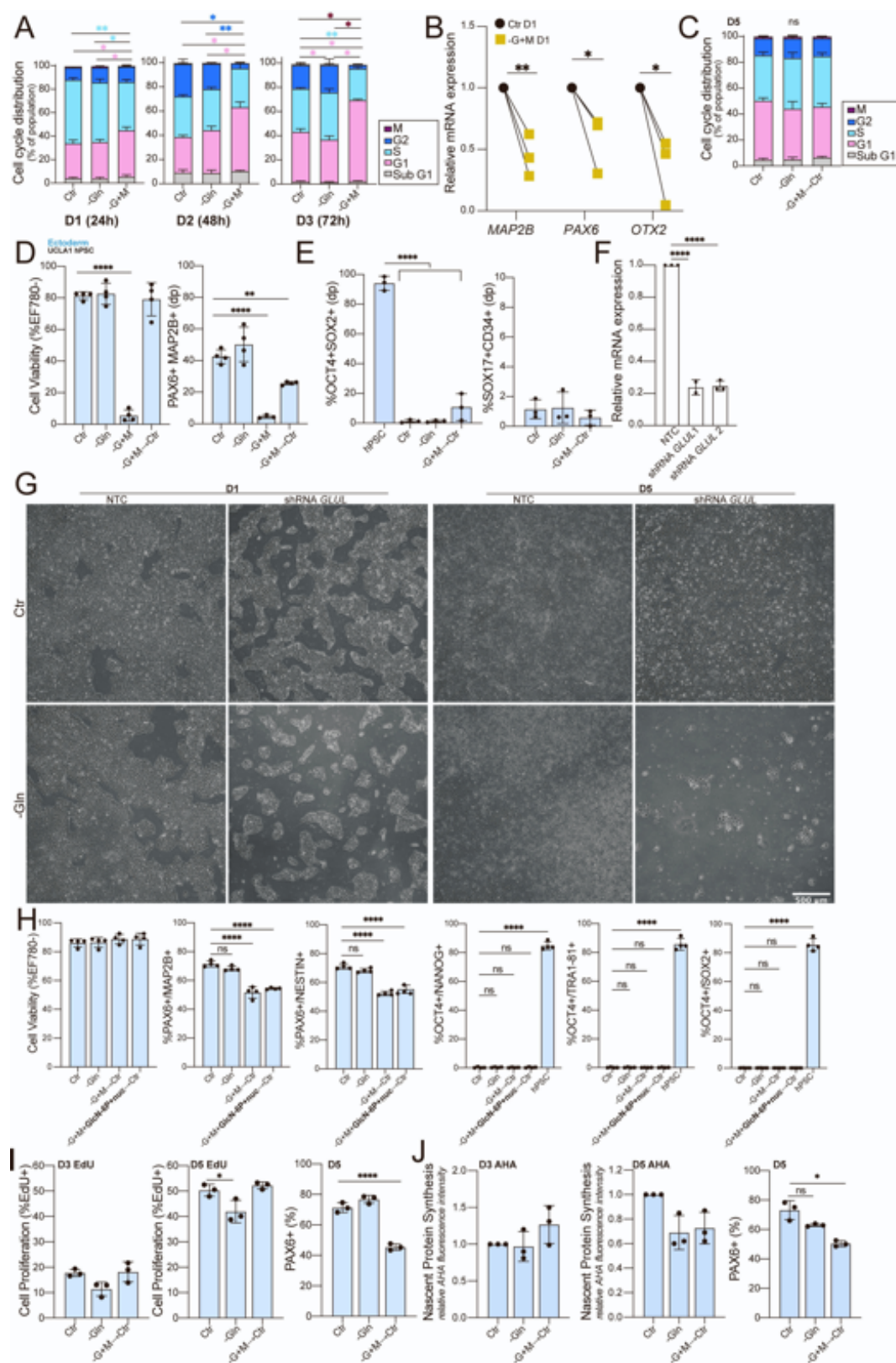
Supplemental Figure S3. Cell cycle distribution, cell proliferation, and nascent protein synthesis during Gln repletion following 14h Gln-starvation

Related to Figure 3

(A) Flow cytometry cell cycle distribution of ectoderm cells differentiated in continuous Gln-starvation for D1 (24h), D2 (48h), and D3 (72h), colored ∗p symbols represent corresponding cell cycle stage with significant difference across indicated conditions.

(B) qRT-PCR analysis of *MAP2B*, *PAX6*, and *OTX2* expression in D1 (24h) ectoderm cells grown in Gln-starvation.

(C) Flow cytometry cell cycle distribution of D5 ectoderm cells after initial 24h Gln-starvation (-G+M→Ctr).

(D) (Left) Cell viability and (Right) percentage of UCLA1-derived D5 ectoderm (PAX6+MAP2B+) cells after initial 24h Gln-starvation (G+M→Ctr).

(E) Percentage of pluripotent (OCT4+SOX2+) and endoderm/mesoderm (SOX17+CD34+) biomarkers in D5 ectoderm cells after initial 24h Gln-starvation (-G+M→Ctr).

(F) qRT-PCR analysis of *GLUL* (encoding GS) in H9 hPSCs expressing shRNA targeting *GLUL* (shRNA *GLUL*1, clone 1; shRNA *GLUL*2, clone 2) or a non-targeting control (NTC).

(G) Representative brightfield images of H9-derived ectoderm cells expressing shRNA targeting *GLUL* (shRNA *GLUL*) or a non-targeting control (NTC) grown continuously in Gln-free media at D1 (24h) and D5 (120h). Scale bar indicates 500 μm.

(H) Cell viability and percentage of ectoderm (PAX6+MAP2B+, PAX6+NESTIN+) and pluripotent (OCT4+NANOG+, OCT4+TRA1-81+, OCT4+SOX2+) biomarkers in D5 ectoderm cells after initial 14h Gln-starvation (-G+M→Ctr) or metabolite-supplemented Gln-starvation (-G+M+GlcN-6P+nuc →Ctr).

(I) Cell proliferation (EdU+ staining) in D3 and D5 ectoderm cells after initial 14h Gln-starvation.

(J) Nascent protein synthesis (relative AHA staining) in D3 and D5 ectoderm cells after initial 14h Gln-starvation.

Data represent mean ± SD of n ≥ 3 biological replicates. ∗p ≤ 0.05; ∗∗p ≤ 0.01; ∗∗∗p ≤ 0.001; ∗∗∗∗p ≤ 0.0001. The p values were determined by (**A, C**) two-way ANOVA, (**B**) Student's t test, (**D-F, H-J**) or one-way ANOVA with correction for multiple comparisons.
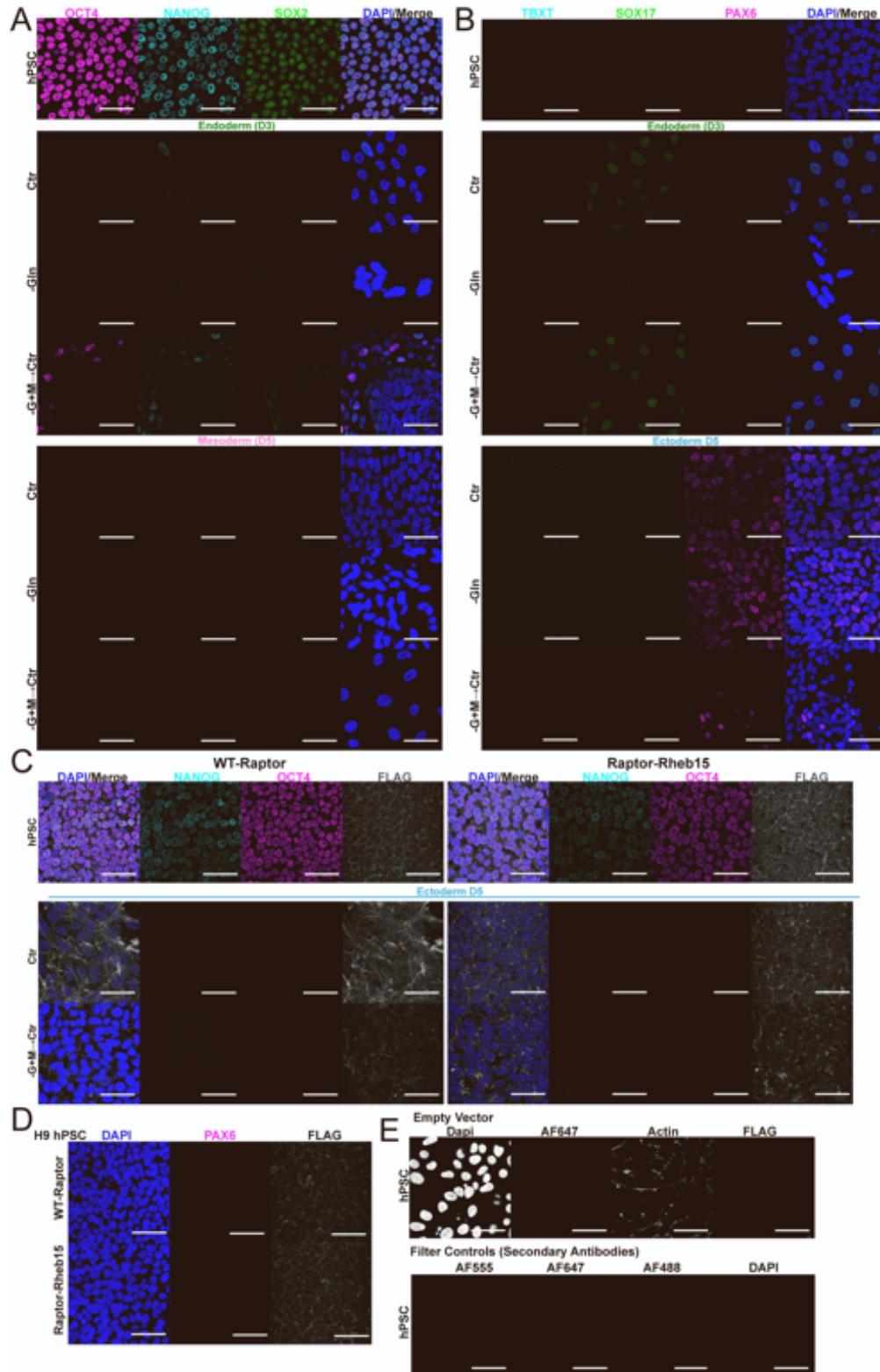
Figure S4

Supplemental Figure S4. mTORC1 inactivation under Gln-starvation
Related to Figure 4

(A) (Left) Flow cytometry quantification and (Right) representative immunoblot of mTORC activation (pS6K1-Thr389) immediately after 24h Gln-starved ectoderm differentiation.

(B) Flow cytometry traces and quantification of %FLAG$^+$ cells in H9-derived Empty Vector, WT-Raptor, and Raptor-Rheb15 hPSC lines.

(C) (Left) Flow cytometry quantification and (Right) representative immunoblot of mTORC activation (pS6K1-Thr389) immediately after 14h Gln-starved ectoderm differentiation in H9-derived WT-Raptor or Raptor-Rheb15 hPSC lines.

(D) Flow cytometry cell cycle distribution of H9-derived D5 WT-Raptor or Raptor-Rheb15 ectoderm cells after initial 14h Gln-starvation (-G+M→Ctr).

(E) Cell viability of H9-derived D5 WT-Raptor or Raptor-Rheb15 ectoderm cells after initial 14h Gln-starvation (-G+M→Ctr).

(F) (Left) Cell viability and (Right) percentage of UCLA1-derived D5 WT-Raptor or Raptor-Rheb15 ectoderm (PAX6$^+$MAP2B$^+$FLAG$^+$) cells after initial 14h Gln-starvation (-G+M→Ctr).

(G) Percentage of UCLA1-derived D5 WT-Raptor or Raptor-Rheb15 ectoderm (PAX6$^+$MAP2B$^+$FLAG$^+$, SOX2$^-$OCT4$^+$FLAG$^+$) cells after initial 14h Gln-starvation with increasing concentrations of exogenous Gln supplementation.

(H) Cell viability of (Left) H9 or (Right) UCLA1-derived D5 ectoderm cells after initial 14h Gln-starvation with increasing concentrations of exogenous Gln supplementation.

(I) (Left) Cell viability and (Right) percentage of pluripotent (OCT4$^+$NANOG$^+$, OCT4$^+$SOX2$^+$, OCT4$^+$TRA1-81$^+$) biomarkers in H9-derived D5 ectoderm cells after initial (-G+M→Ctr), intermediate (Ctr→-G+M→Ctr), or late (Ctr→-G+M) 14h Gln-starvation.

(J) Cell viability in (Left) H9 or (Right) UCLA1-derived D5 ectoderm differentiation after initial 14h Gln-starvation, Arg deprivation, or Leu deprivation in WT-Raptor or Raptor-Rheb15 hPSC lines.

(K) Representative immunofluorescence images of mTORC activation in H9-derived ectoderm cells grown for 14h in Gln-supplemented (Ctr), Arginine-free (-Arginine), Leucine-free (-Leucine), or 200 nM rapamycin treatment (Ctr+Rapa). DAPI (blue, nucleus); ACTIN (green, cytoskeleton); pS6K1-Thr389 (yellow, mTORC1 activation). Scale bar indicates 50 µm.

(L) Percentage of pluripotent (OCT4$^+$NANOG$^+$, OCT4$^+$SOX2$^+$, OCT4$^+$TRA1-81$^+$) biomarkers in H9-derived WT-Raptor or Raptor-Rheb15 D5 mesoderm and D3 endoderm cells.

(M) Representative immunofluorescence images of mTORC activation in H9-derived (Left) mesoderm and (Right) endoderm cells grown for 24h in Gln-supplemented (Ctr), Gln-free (-Gln), Gln-starvation (-G+M), or 200 nM rapamycin treatment (Ctr+Rapa). DAPI (blue, nucleus); ACTIN (green, cytoskeleton); pS6K1-Thr389 (yellow, mTORC1 activation). Scale bar indicates 50 µm.

Data represent mean ± SD or (**A, C**) min and max of n ≥ 3 biological replicates. *p ≤ 0.05; **p ≤ 0.01; ***p ≤ 0.001; ****p ≤ 0.0001. The p values were determined by (**A-C, E, H-J**) one-way ANOVA, (**D, F-G**) two-way ANOVA with correction for multiple comparisons, or (**L**) Student's t test.

Figure S5

Supplemental Figure S5. Immunofluorescence images for biological and technical controls
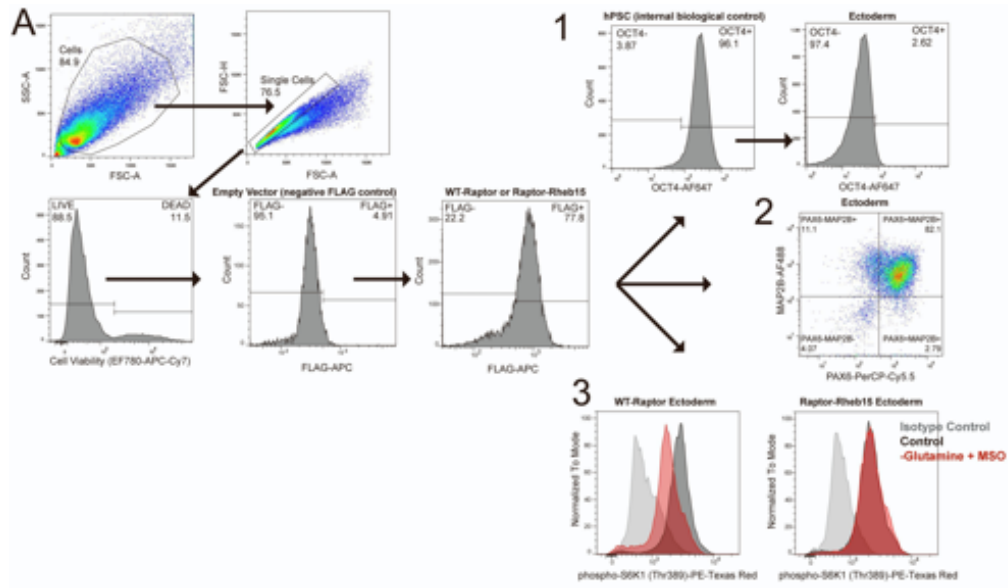*Related to Figure 3 and 4*
(A) Representative immunofluorescence images of pluripotent biomarkers in (Top) H9 hPSCs grown in mTESR, and H9-derived (Middle) D3 endoderm and (Bottom) D5 mesoderm cells grown in Gln-supplemented (Ctr), Gln-free (-Gln), or Gln-repletion follow initial 14h Gln-starvation (-G+M→Ctr). OCT4 (magenta, pluripotent); NANOG (cyan, pluripotent); SOX2 (green, pluripotent); DAPI (blue, nucleus). Scale bar indicates 50 µm.
(B) Representative immunofluorescence images of tri-lineage biomarkers in (Top) H9 hPSCs grown in mTESR, and H9-derived (Middle) D3 endoderm and (Bottom) D5 ectoderm cells grown in Gln-supplemented (Ctr), Gln-free (-Gln), or Gln-repletion follow initial 14h Gln-starvation (-G+M→Ctr). TBXT (cyan, mesoderm); SOX17 (green, endoderm); PAX6 (magenta, ectoderm); DAPI (blue, nucleus). Scale bar indicates 50 µm.
(C) Representative immunofluorescence images of pluripotent biomarkers in H9-derived D5 (Left) WT-Raptor or (Right) Raptor-Rheb15 ectoderm cells grown in Gln-supplemented (Ctr) or Gln-repletion follow initial 14h Gln-starvation (-G+M→Ctr). DAPI (blue, nucleus;) NANOG (cyan, pluripotent); OCT4 (magenta, ectoderm); FLAG (grey, transduced cell line reporter). Scale bar indicates 50 µm.
(D-E) Representative immunofluorescence images of H9 hPSC (**D**) pluripotent and (**E**) filter controls.

Figure S6

133

Supplemental Figure S6. Flow cytometry gating strategy
Related to Figure 3 and 4
(**A**) Gating strategy for flow cytometry analysis. This figure reflects gating strategy used for flow cytometry quantifications in Figures 1-4, S1-S4.

Supplemental Table 1. Spreadsheet of normalized transcript abundance values from RNA-Sequencing data and UHPLC-MS metabolomics relative abundance, pathway enrichment values, and isotopologue tracing amounts. Related to Figures 1, 2, 3 and Supplemental Figure 2.

CHAPTER 8:

CONCLUSIONS

The applications of hPSCs on human health and biological insight are almost endless, from disease modeling to regenerative medicine to corrective gene therapies. Of interest in this thesis is its inherent status as an *ex vivo* surrogate for studying early human embryo development. In particular, our current understanding of how metabolic regulation permits and/or follows PSC identity transitions across the pluripotency and differentiation continuum is fragmented. In the past decade, the pluripotent and multipotent stem cell fields gained an appreciation for metabolites as co-factors for transcriptional and epigenetic modifications that ultimately affect gene expression and cell fate determination. More recently, a study reported that non-metabolized glucose (independent of glycolysis) controls lineage specification of cleavage-stage mouse embryos by initiating signaling and transcription to enable trophectoderm, but not the embryonic inner cell mass, formation (Chi et al., 2020). Combined, this implicated metabolism as a nexus for expression pattern regulation and nutrient-sensitive signaling via integration of substrates from the extracellular and intracellular environments.

From these collective insights, two main lingering questions remain under active investigation. First, it is unclear how epigenome co-factors and substrates are regulated or recruited to specific loci to influence expression patterns during cell state transitions. Second, it is unknown whether specific nutrients and/or metabolites, and their respective mechanisms of action, support distinct cell outcomes. For instance, how does one single nutrient, such as glutamine, enhance opposite cell transition processes, such as both pluripotent biomarker expression and differentiation efficacy (Lu et al., 2021; Tohyama et al., 2016; Vardhana et al., 2019)? Our approach to studying nutrient specificity and PSC identity was first to neutralize the confounding factor of differential nutrient levels in conventional PSC tri-lineage differentiation culture media. We developed a chemically defined, nutrient-equivalent differentiation protocol to allow customizable metabolic manipulation experiments, such as determining whether all or only

certain mTORC1-sensed amino acids are required for ectoderm specification. Successful tri-lineage differentiation via expression of established biomarkers was validated with RNA-Seq, and equivalent levels of culture media metabolites were quantified with ultra-high-performance liquid chromatography mass-spectrometry (Lu et al., 2019).

As one of two major nutrients fervently studied, glutamine has taken center stage as a critical carbon and nitrogen source for cell energetics and biosynthesis. Despite the abundance of stem cell studies focused on glutamine metabolism, previous studies focused more generally on the metabolic roles of glutamine and its derivatives in maintaining pluripotency (Carey et al., 2015; Marsboom et al., 2016; Tohyama et al., 2016; Vardhana et al., 2019) or impacting multipotent functional cell differentiation (Johnson et al., 2018; Oburoglu et al., 2014; Yu et al., 2019). Here, we expand our understanding of a role for glutamine in coordinating early tri-lineage differentiation upon pluripotency exit. This insight on early upstream differentiation can enable tighter control of downstream PSC applications, such as enrichment for ectoderm-derived neural cells.

Conclusions from this thesis indicate that glutamine itself, unmetabolized and/or incorporated for use as a biosynthetic precursor, is a required signaling molecule in ectoderm differentiation. Collectively, the chapters above establish a cohesive framework in which glutamine plays a central, non-compromising role in the behavior and fate of PSCs and PSC-derived cells. Namely, we uncovered that glutamine, not glucose, is the main carbon source contributor to the TCA cycle. This was a surprising result as ectoderm was previously established as highly glycolytic, comparable to the metabolic profile of PSCs (Cliff et al., 2017), and thus presumably more reliant on glucose utilization. This finding initiated exploratory questions on the importance

of glutamine in PSC fate determination. We subsequently uncovered that extracellular glutamine deprivation blocked endoderm and mesoderm, but not ectoderm, specification, establishing a bias in glutamine dependency among the cell types. Further detailed work demonstrated that glutamine synthesis and consumption are differentially regulated among the three lineages *in vitro*, and possibly *in vivo*, and that glutamine has an irreversible temporal requirement in ectoderm, but not mesoderm or endoderm, lineage differentiation (Lu et al., 2022).

This thesis yields several testable hypotheses regarding the role of glutamine in coordinating the spatiotemporal organization of the three germ layers. Glutamine is classically known as a non-essential amino acid, but here we report it is conditionally essential depending on the cell fate context. Specifically, based on the viability profiles upon extracellular glutamine exclusion, we posit that mesoderm can be classified as a "glutamine auxotroph," endoderm as a "moderate glutamine auxotroph," and ectoderm as a "glutamine prototroph." Accordingly, we hypothesize on a possible glutamine-specific symbiotic relationship among the three germ lineages during early *in vivo* development. Ectoderm may generate endogenous glutamine from glutamate to support nearby mesoderm and endoderm cells dependent on exogenous glutamine, which could shape tissue patterning. Simultaneously, mesoderm and endoderm may provide the glutaminolysis by-product, glutamate, to enable ectoderm cells to perpetuate this glutamine-glutamate cycling. This hypothesis is supported by spent media metabolite footprint data presented in Chapter 6 showing high glutamine secretion in ectoderm and high glutamine consumption in mesoderm (Lu et al., 2019). This enticing possibility is further supported by human embryo single cell RNA-Seq data showing the glutamine synthesis to consumption signature is higher in ectoderm compared with mesoderm and endoderm lineages, which is consistent with our *in vitro* findings (Lu et al., 2022; Tyser et al., 2021). Nonetheless, some possible technical roadblocks for investigating this hypothesis could be (1) tracking the

localization, cycling, conversion, and consumption of isotopologue-labeled glutamine and glutamate between the lineage cells and (2) co-culture of all three germ lineages, which are induced by differing cytokines.

Another question for future study is related to downstream glutamine-dependent mTORC1 activation enabling ectoderm specification. What signaling mechanism(s) are required for initiation of differentiation, and how is specificity to the ectoderm transcription factor program regulated? As detailed in Chapter 7, while glutamine-specific mTORC1 signaling is required for ectoderm specification, constitutive mTORC1 activation is detrimental to endoderm and mesoderm survival and identity. Additionally, the absence of intracellular glutamine, but not other mTORC1-sensed amino acids (leucine and arginine), blocks the induction of ectoderm. These findings suggest specificity of mTORC1 requirement in both lineage cell type and substrate. A possible approach to investigating this phenomenon could be a multi-omics screen to identify downstream transcriptional and epigenetic targets underlying mTORC1 signaling at the initiation of differentiation (Yang et al., 2019). Comprehensive profiling of the phosphoproteome, epigenome, transcriptome, and proteome could lead to integrated understanding of the multifaceted regulatory mechanisms gatekeeping PSC identity transitions from pluripotency to early tri-lineage differentiation. In parallel to these exploratory screens, phosphorylation of serine/threonine kinases (such as mTORC1 target S6K1) can be inhibited to determine the functional cell fate consequences of blocking these signaling pathways.

Lastly, though we characterized glutamine-starved then repleted ectoderm cells with residual pluripotency and blocked ectoderm specification, their comprehensive identity profile remains to be clarified. As noted in Chapter 7, this cell population exhibits equivalent functional profiles in

viability, bioenergetics, proliferation, protein synthesis, and cell cycle but not downstream cell identity. We observed no alternative lineage differentiation on these impaired ectoderm cells of interest, with nonsignificant changes in endoderm and mesoderm biomarker expression in glutamine-starved compared to non-starved cells. Furthermore, it is unknown what biochemical alterations occurring during the 14-hour glutamine starvation period on Day 0 are sufficient to cause downstream specification impairments at Day 5. Accordingly, a key next step will be to perform transcriptional and chromatin profiling to gain more conclusive insight on expression patterns underlying transient glutamine starvation during the initiation and termination of ectoderm differentiation. Specifically, utilization of single cell RNA sequencing will be most informative since high heterogeneity is expected in these populations (Blakeley et al., 2015; Liu et al., 2018; Luecken and Theis, 2019; Tyser et al., 2021; Wang and Navin, 2015). Data from assay for transposase-accessible chromatin using sequencing (ATAC-Seq) will provide additional insight on potential altered chromatin landscapes associated with glutamine availability during the defined period of differentiation induction (Grandi et al., 2022). Combined, these proposed future directions will likely produce impactful information on how nutrient specificity, differentiation kinetics, and intracellular signaling ultimately influence PSC fate outcomes, and potentially reveal transferable knowledge on early human embryo development.

While the conclusions described in this thesis are promising, three study limitations temper this excitement. First, transient glutamine absence likely does not occur during *in vivo* embryo development. Thus, while experimental glutamine starvation was a useful tool to identify temporal nutrient dependencies of the tri-lineage cell types, this condition does not mirror endogenous regulation and limits our conclusions on *in vivo* processes. Second, we report transcriptional data suggesting correlative *in vitro* and *in vivo GLS1*, *GLS2*, and *GLUL* expression signatures may reflect similar tri-lineage glutamine synthesis versus consumption

dependencies during human gastrula development (Lu et al., 2022; Tyser et al., 2021). Though these datasets are in good agreement, transcript levels may not equate to protein abundance and activity. Therefore, this correlation between human embryo tissue and hPSC-derived cells represents a testable hypothesis for future detailed work rather than a definitive conclusion. Third, nutrient concentration levels used in general *in vitro* culture systems are supra-physiologic; thus, further work may be necessary to determine the physiologic concentrations sufficient to elicit glutamine-dependent cell fate decisions (Cantor et al., 2017).

In conclusion, this thesis marks the beginning of countless future investigations on nutrients acting as a signaling molecule to enable differential coordination of early pluripotency exit and cell specification commitment. For instance, additional nutrient specificities (other amino acids/sugars) and influence of manipulating glutamine gatekeeping enzymes on cell fate decisions remain to be uncovered. These findings hold profound promise in providing tighter control and mastery over the production of high-quality hPSC derivatives for disease modeling, regenerative cell therapies, and ultimately clinical usage.

REFERENCES

Blakeley, P., Fogarty, N.M., Del Valle, I., Wamaitha, S.E., Hu, T.X., Elder, K., Snell, P., Christie, L., Robson, P., and Niakan, K.K. (2015). Defining the three cell lineages of the human blastocyst by single-cell RNA-seq. Development *142*, 3613.

Cantor, J.R., Abu-Remaileh, M., Kanarek, N., Freinkman, E., Gao, X., Louissaint, A., Jr., Lewis, C.A., and Sabatini, D.M. (2017). Physiologic Medium Rewires Cellular Metabolism and Reveals Uric Acid as an Endogenous Inhibitor of UMP Synthase. Cell *169*, 258-272 e217.

Carey, B.W., Finley, L.W., Cross, J.R., Allis, C.D., and Thompson, C.B. (2015). Intracellular alpha-ketoglutarate maintains the pluripotency of embryonic stem cells. Nature *518*, 413-416.

Chi, F., Sharpley, M.S., Nagaraj, R., Roy, S.S., and Banerjee, U. (2020). Glycolysis-Independent Glucose Metabolism Distinguishes TE from ICM Fate during Mammalian Embryogenesis. Dev Cell.

Cliff, T.S., Wu, T., Boward, B.R., Yin, A., Yin, H., Glushka, J.N., Prestegaard, J.H., and Dalton, S. (2017). MYC Controls Human Pluripotent Stem Cell Fate Decisions through Regulation of Metabolic Flux. Cell Stem Cell *21*, 502-516 e509.

Grandi, F.C., Modi, H., Kampman, L., and Corces, M.R. (2022). Chromatin accessibility profiling by ATAC-seq. Nature Protocols.

Johnson, M.O., Wolf, M.M., Madden, M.Z., Andrejeva, G., Sugiura, A., Contreras, D.C., Maseda, D., Liberti, M.V., Paz, K., Kishton, R.J.*, et al.* (2018). Distinct Regulation of Th17 and Th1 Cell Differentiation by Glutaminase-Dependent Metabolism. Cell.

Liu, D., Wang, X., He, D., Sun, C., He, X., Yan, L., Li, Y., Han, J.J., and Zheng, P. (2018). Single-cell RNA-sequencing reveals the existence of naive and primed pluripotency in pre-implantation rhesus monkey embryos. Genome Res *28*, 1481-1493.

Lu, V., Dahan, P., Ahsan, F.M., Patananan, A.N., Roy, I.J., Torres, A., Jr., Nguyen, R.M.T., Huang, D., Braas, D., and Teitell, M.A. (2019). Mitochondrial metabolism and glutamine are essential for mesoderm differentiation of human pluripotent stem cells. Cell Res *29*, 596-598.

Lu, V., Roy, I.J., and Teitell, M.A. (2021). Nutrients in the fate of pluripotent stem cells. Cell Metab.

Lu, V., Roy, I.J., Torres, A., Jr., Joly, J.H., Ahsan, F.M., Graham, N.A., and Teitell, M.A. (2022). Glutamine-dependent signaling controls pluripotent stem cell fate. Dev Cell.

Luecken, M.D., and Theis, F.J. (2019). Current best practices in single-cell RNA-seq analysis: a tutorial. Mol Syst Biol *15*, e8746.

Marsboom, G., Zhang, G.F., Pohl-Avila, N., Zhang, Y., Yuan, Y., Kang, H., Hao, B., Brunengraber, H., Malik, A.B., and Rehman, J. (2016). Glutamine Metabolism Regulates the Pluripotency Transcription Factor OCT4. Cell Rep *16*, 323-332.

Oburoglu, L., Tardito, S., Fritz, V., de Barros, S.C., Merida, P., Craveiro, M., Mamede, J., Cretenet, G., Mongellaz, C., An, X., *et al.* (2014). Glucose and glutamine metabolism regulate human hematopoietic stem cell lineage specification. Cell Stem Cell *15*, 169-184.

Tohyama, S., Fujita, J., Hishiki, T., Matsuura, T., Hattori, F., Ohno, R., Kanazawa, H., Seki, T., Nakajima, K., Kishino, Y., *et al.* (2016). Glutamine Oxidation Is Indispensable for Survival of Human Pluripotent Stem Cells. Cell Metab *23*, 663-674.

Tyser, R.C.V., Mahammadov, E., Nakanoh, S., Vallier, L., Scialdone, A., and Srinivas, S. (2021). Single-cell transcriptomic characterization of a gastrulating human embryo. Nature *600*, 285-289.

Vardhana, S.A., Arnold, P.K., Rosen, B.P., Chen, Y., Carey, B.W., Huangfu, D., Fontaine, C.C., Thompson, C.B., and Finley, L.W.S. (2019). Glutamine independence is a selectable feature of pluripotent stem cells. Nat Metab *1*, 676-687.

Wang, Y., and Navin, N.E. (2015). Advances and applications of single-cell sequencing technologies. Mol Cell *58*, 598-609.

Yang, P., Humphrey, S.J., Cinghu, S., Pathania, R., Oldfield, A.J., Kumar, D., Perera, D., Yang, J.Y.H., James, D.E., Mann, M., *et al.* (2019). Multi-omic Profiling Reveals Dynamics of the Phased Progression of Pluripotency. Cell Syst *8*, 427-445 e410.

Yu, Y., Newman, H., Shen, L., Sharma, D., Hu, G., Mirando, A.J., Zhang, H., Knudsen, E., Zhang, G.F., Hilton, M.J., *et al.* (2019). Glutamine Metabolism Regulates Proliferation and Lineage Allocation in Skeletal Stem Cells. Cell Metab.